Influence of Vertical Steel Reinforcement on the Behaviour of Edge Restrained Reinforced Concrete Walls

Muhammad Kashif Shehzad

Submitted in accordance with the requirements for the degree of
Doctor of Philosophy

The University of Leeds
School of Civil Engineering

August, 2018

The candidate confirms that the work submitted is his own, except where work which has formed part of jointly-authored publications has been included. The contribution of the candidate and the other authors to this work has been explicitly indicated below. The candidate confirms that appropriate credit has been given within the thesis where reference has been made to the work of others.

The work presented in Chapters 3, 4 and 6 of this thesis has appeared in the following publication;
Shehzad, M.K and Forth, J.P 2017. 'Imposed loading effects on reinforced concrete walls restrained at their base'. Accepted for publication in the Journal of Structures and Buildings.

The candidate was responsible for experimental investigation, collection and analysis of the data. The guidance at each step of the work and in preparation of manuscript was provided by the co-author.

The work presented in Chapter 5 of this thesis has appeared in the following publication;
Shehzad, M.K and Forth, J.P 2018. 'Influence of transverse reinforcement on the cracking behaviour of reinforced concrete panels subjected to uniaxial tension'. Proceedings of the 12th Fédération Internationale du béton (fib) International PhD Symposium 2018 being held at Prague, Czech Republic.

The candidate was responsible for experimental investigation, collection and analysis of the data. The guidance at each step of the work and in preparation of manuscript was provided by the co-author.

Acknowledgements

First and foremost, I owe the successful completion of this research to my **Gracious God** who granted me the wisdom, determination and strength to undertake this work.

My sincere gratitude and profound thanks to my esteemed advisor and mentor **Professor John P Forth**, who provided continuous support, guidance and motivation during each stage of my PhD and related research. I am highly indebted to him for his encouragement and motivation which kept me going through the thick and thin. This work would not have been possible without his dedicated and invaluable support. I am also thankful to my co-supervisors **Dr Nikolaos Nikitas** and **Dr Emilio Garcia-Taengua** for their valued input and advice.

I am extremely grateful to the technical staff **Mr Norman Harmon**, **Mr Peter Flatt**, **Mr Marvin Wilman**, **Mr Robert Clarke** and **Mr Stephen Holmes** at the George Earl Laboratory for their continued support and assistance in execution of the experimental work. My special appreciation to **Mr Peter** for his assistance and incredibly accurate work in preparation of test specimens. I would also like to thank all my fellow colleagues at University of Leeds for their support and encouragement throughout the research.

I wish to thank my superiors at the **Pakistan Army** for allowing me to undergo PhD studies and also to my supervisor and the **University of Leeds** for financially assisting in execution of research.

All of this would have remained a dream without the love and special prayers of the family members; my parents, an aunt more than a mother, two loving brothers, my very special and caring sister, my wife & three wonderful children. Lastly, I can't forget to thank the one(s) who brought happiness to my life and became an important part of my life.

I dedicate this thesis to the people dearest to me in this world;

MY BELOVED AUNT

MS PARVEEN AKHTER,

MY TWO BEAUTIFUL BUTTERFLIES

HIBA, ALIHA

AND

MY HANDSOME YOUNG SUPERSTAR

HASHAAM

who have been and will always be a source of happiness, inspiration and motivation for me

Abstract

Freshly cast concrete undergoes volume changes due to thermal and shrinkage mechanisms which can be restrained both internally and externally. Externally applied restraint can be either end, edge or a combination of the two. Tensile stresses are induced as a consequence of restraint of volume changes which often result in cracking particularly during early age. These are 'through' cracks and are of particular concern in liquid retaining structures, nuclear containment chambers, tunnels and basements where besides being aesthetically unpleasant, such cracks can also result in water leakage, ingress / discharge of harmful chemicals and corrosion of steel reinforcement. This calls for development of a clear understanding of the mechanism of cracking and the factors involved in restraint formation so that appropriate mitigation measures at the design and construction stage can be taken.

Currently available guidance is based on the end restraint cases and has been evolved from experimental and analytical investigations on axially reinforced prisms. In walls and slabs, reinforcement is present in both longitudinal and transverse directions and the influence of transverse reinforcement on cracking has not been analysed and incorporated in existing guidance. Critical review of previous research revealed that cracking behaviour of members subjected to edge restraint is very different from those under end restraint. Therefore, the need to undertake experimental investigation for determining the influence of major influencing factors like vertical steel dowels and members geometry was realized.

This research investigates the restraint of imposed strains in edge restrained members and in particular, experimentally illustrates the influence of vertical steel reinforcement between the restrained (wall) and the restraining (base slab) members on the mechanism of restraint development. The investigation constructed real scale reinforced concrete walls onto reinforced concrete bases and also illustrated why previous studies, which have mostly utilized steel members to restrain the imposed strain, are inappropriate for gaining an understanding of edge restraint as they fail to reflect the heat transfer between the wall and the base. Thickness of the tested walls was also varied in the tests to ascertain the influence of relative geometries of the two members on degree of restraint. Results revealed that the restraint significantly increased in the presence of vertical steel reinforcement. They also showed that

restraint increases with time due to the steel reinforcement and decreases in its absence. Moreover, in order to ascertain the significance of the transverse reinforcement, tests on reinforced concrete panels were performed. The panels were subjected to direct tension and the results indicate that when transverse reinforcement was present, the cracking load for the tested specimens decreased by 25 – 30 %, whereas the crack widths and number of cracks increased.

Due to paucity of time and the resources involved in experimental investigation, finite element analysis has been utilized to study the behaviour of walls subjected to combination of end and edge restraint. Parametric study was carried out to investigate the influence of combined restraint on the number and size of cracks and crack widths. By investigating walls of different aspect ratios, the domination of end restraint in higher parts of the walls having lower aspect ratios was found. Through finite element analysis the significance of correctly incorporating the real time boundary conditions of the restraining base slab was also identified.

Table of Contents

List of Figures

List of Tables

Chapter 1

Introduction

1.1 Background to the Research

Cracking in newly cast concrete subjected to restraint is a common phenomenon which is primarily attributed to the restraint of volume changes within the concrete. Immediately after casting and following peak hydration temperature, the concrete starts to exhibit volume change due to the concomitant processes of early age thermal contraction and shrinkage (both autogenous and drying). Concrete is not free to undergo these volume changes and some form of restraint to these volume changes is present in almost all practical scenarios. The restraint may be external and imposed by one or more of the adjoining members; internal and be from the steel reinforcement present in the concrete; or result from thermal gradients / differential thermal strains, particularly those occurring in mass concrete structures (Forth, 2014). Once the free volume change of the concrete is restrained, tensile stresses develop in the concrete which can lead to cracking, should the stresses exceed the tensile strength of the concrete. Cracks occurring due to the above mentioned phenomenon are mostly 'through cracks'. Design codes and construction practices present numerous measures to assist with the control of cracking; these include the lowering of the temperature during the hydration process, the provision of horizontal steel reinforcement, the provision of joints and the limiting of the length to height (L/H) ratio of each pour (Emborg et al., 1994; Bamforth, 2007).

External restraint is further categorized into two types; end and edge restraint. In practice, however, the situation gets more complex when a combination of edge and end restraint exists (Forth, 2014). The mechanism of cracking due to external end restraint has been researched in detail and the theory of cracking due to restrained volume changes was developed based on the behaviour of members subjected to end restraint (Evans et al., 1968; Gilbert, 1992). The developed cracking theory is primarily based on axially reinforced prisms. The situation, however, is quite different and complex in members reinforced in both longitudinal and transverse directions such as walls and slabs. Moreover, little research has been performed on the behaviour of

edge restrained members; most experimental research has been performed on reduced scale members with micro concrete and reduced bar diameters (Stoffers, 1978) or on mortar mixes (Kheder et al., 1990; Kheder, 1997; Kheder et al., 1994). Recently, Micallef (2017) conducted tests on full scale reinforced concrete walls subjected to a combination of flexure and edge restraint, where the restraint was imposed by a steel restraining base. The cracking theory based on end restraint is being applied for the design and analysis of edge restrained members as well. Interestingly, the research that has been performed on edge restraint, suggests that the effects of end and edge restraint are quite different from each other (Beeby and Forth, 2005; Bamforth, 2007).

The mechanism of cracking due to edge restraint involves two important parameters namely the magnitude of imposed loads and the degree of restraint. While considerable research and well developed guidance on estimation of volume change of concrete is available, the techniques for estimation of degree of restraint are not very well researched so far. In existing methods, the restraint estimation is primarily based on the relative stiffness of restrained and restraining members. However, findings and observations by some researchers (Kheder et al., 1990; Nilsson, 2003) indicate that there are other contributory factors which are not fully acknowledged in the currently available methods. Scarcity of experimental research on edge restraint, use of steel restraining base and micro concrete specimens appear to be few reasons for non-identification of all important parameters involved. An important influencing factor is the amount of vertical steel reinforcement dowels continuing from the restraining member into the restrained walls.

1.2 Problem Statement

A design based on currently available guidance on edge restraint can prove to be erroneous and misleading since the validity of existing cracking theory in such case is questionable. This calls for a clearer understanding about the major influencing factors in edge restraint and incorporation of the same in the design process. Presence of vertical steel dowels at the interface between restrained and restraining members can increase the interface shear thus preventing the joint slip and can also increase the stiffness of the restraining member. Moreover, it has also been reported to influence the crack spacing in edge restrained walls. Development of curvature in the

restraining base has an influence on the restraint formation and variation in the restrained wall and thus an experimental set up suitable to analyse this influence needs to be developed. There is also a need to evaluate the influence of transverse reinforcement in walls and slabs on the cracking behaviour.

1.3 Aim of Research

This research is aimed at identifying the influence of vertical steel reinforcement on the behaviour of edge restrained reinforced concrete walls by specifically focusing on the degree of restraint, number and width of cracks and the role of the edge restraining element. It also highlights the shortfalls of using the steel member as a restraining base for edge restrained reinforced concrete walls.

1.4 Objectives

The following objectives were set for this study:

1.4.1 Objective 1

Carry out a review of the current state of knowledge on the behaviour of reinforced concrete walls subjected to different forms of restraint and identify the shortfalls in existing techniques for predicting the response of edge restrained walls.

1.4.2 Objective 2

Conduct experimental investigations on edge restrained reinforced concrete wall specimens reinforced with varying amounts of vertical reinforcement to analyse the influence of vertical steel dowels on the degree of restraint.

1.4.3 Objective 3

Using reinforced concrete restraining base in the experimental investigations, ascertain the efficacy of the use of steel sections as restraining members in analysing the reinforced concrete walls under edge restraint.

1.4.4 Objective 4

Carryout experimental investigation on reinforced concrete panels subjected to uniaxial tension (simulating end restraint) to identify the influence of transverse steel

reinforcement on the prediction of cracking load, crack spacing and width in such members.

1.4.5 Objective 5

Using the finite element analysis, carry out a parametric study to ascertain the behaviour of reinforced concrete walls subjected to combined restraint and identify the influence of aspect ratio and type of restraint on the cracking behaviour.

1.4.6 Objective 6

Through finite element analysis and experimental investigation, analyse the influence of curvature development in the restraining members on the degree of restraint and cracking in reinforced concrete walls.

1.5 Research Strategy

In order to achieve the aim and objectives set for this research, the work was undertaken in following stages;

- **Stage 1**: In this stage the relevant research carried out by previous researchers was consulted to develop an understanding of the current state of knowledge and identify the aspects which require further work. This stage formed a significant part of the work and continued throughout the research.
- **Stage 2**: Having reviewed the existing guidance and identified the key aims of current work, in this stage the experimental investigation and the procedures were planned and designed. The experimental work was then executed and the results were gathered in this stage.
- **Stage 3**: This stage continued simultaneously with stage 2 and the results obtained from the experimental investigation were critically analysed to evaluate the parameters studied.
- **Stage 4**: In this stage the finite element modelling of the reinforced concrete walls was carried out. The results of experimental study were utilized to calibrate the models and parametric study was conducted to achieve an understanding about different aspects.

- **Stage 5**: After having conducted the experimental and numerical investigations and analysed the results obtained, in this stage thesis writing was undertaken.

1.6 Thesis Layout

Chapter 1 provides brief background of current research, highlights the problem statement and defines key aim and objectives of research.

Chapter 2 includes the review of the previous research related to this subject and presents details of the volume change mechanism of concrete. Different types of restraint and the behaviour of reinforced concrete members under each of these types are briefly discussed. Cracking mechanism in reinforced concrete members and the cracking theories presented by different researchers have been reviewed. Finally the experimental and analytical investigations on edge restrained members undertaken in the past have been analysed and the methods available for restraint estimation have been discussed.

Chapter 3 provides the details about the experimental program. Test set up, details of the test specimens and test procedure are explained in detail. Process of preparation, casting and curing of the test specimens has been illustrated. Mechanical properties of concrete obtained through tests on small specimens are also presented.

Chapter 4 contains the details about acquisition and analysis of the results from tests performed during experimental investigation. The results have been discussed in detail to analyse the influence of various parameters and their contribution towards fulfilment of set objectives. Comparison of the obtained results with currently available guidelines has also been carried out.

Chapter 5 includes the details about uniaxial tensile tests on reinforced concrete panels. Significance of these tests has been highlighted from the previously undertaken research. Details of the tested specimens, test set up and procedure are explained in detail. Finite element models of the tested specimens are also presented and compared to the experimental findings. Results of the experimental and numerical investigations have been analysed and discussed in detail.

Chapter 6 provides the details of finite element analysis carried out during this research. Procedure used for preparation of models, constitutive models employed for modelling the behaviour of materials and the analysis details are included. Correlation of the finite element models with the tested specimens is established. Parametric study on walls of varying aspect ratios subjected to edge and combined restraint is also presented.

Chapter 7 includes the key conclusions drawn from this study and recommendations for future research on the subject.

Chapter 2

Literature Review

2.1 Introduction

Cracking in newly cast concrete subjected to restraint is a common phenomenon which is primarily attributed to the restraint of volume changes within the concrete. The mechanism of cracking due to restraint involves two important parameters namely the magnitude of volume changes also termed as the imposed loads and the degree of restraint. In order to correctly understand and analyse the complex problem posed by the restraint of volume changes, it is important to first understand the mechanism involved and the factors influencing the above mentioned parameters. The risk of early age cracking involves three important factors; temperature and shrinkage development, development of material properties of concrete and the restraint conditions.

In this chapter the composition of volume changes and guidelines available for their prediction or estimation have been presented. Development of the mechanical properties of concrete with age and the influence of temperature development due to hydration on these properties is also discussed. This chapter also includes the review of different types of restraint imposed onto the newly cast reinforced concrete walls and their behaviour under each type of restraint. The mechanism involved in generation of tensile stresses in concrete due to restraint of imposed loads and formation of cracks is discussed along with measures proposed in the literature for prevention and mitigation of the risk of cracking.

2.2 Volume Change Mechanisms

Volume change implies an increase or decrease in the volume and, for convenience, the magnitude of volume change is generally stated in linear rather than volumetric units. Most commonly, the subject of concrete volume change deals with linear expansion and contraction due to temperature development and moisture loss. Freshly mixed concrete remains plastic for a relatively short period of time. During this period, changes in its volume can occur due to cement hydration, water evaporation, thermal change and absorption. Temperature development gives rise to thermal

contraction whereas the moisture loss is manifested in the form of shrinkage. Previous research indicates that the thermal movements are far greater than the shrinkage movements during the early age and are the major source of cracking (Evans et al., 1968; Bamforth, 1982). Both of these mechanism are discussed in detail below.

2.2.1 Temperature Development

As a result of the exothermic process of cement hydration, considerable amount of heat (up to 35 joules per gram of cement (De Larrard et al., 1994)) is generated in the newly cast concrete. The rate and magnitude of heat generation is directly related to the chemical composition, fineness and particle size distribution of the cement and the water to cement or binder ratio used in the mix (Breugel, 1998). Heat generated per unit volume of concrete is a material property whereas the heat loss from concrete is dependent upon the formwork used, exposed surface area of concrete and the ambient temperature of the surroundings. The rate of heat generation is initially far greater than that of heat loss and therefore the concrete temperature rises. With time the rate of heat generation is considerably reduced and the rate of heat loss becomes more prominent. Due to this reason the concrete temperature starts to drop after reaching a certain peak value and contraction is caused in concrete mass. The concrete tends to expand due to increase in temperature and starts to contract when the temperature starts to drop below the peak value. According to Bamforth (2007), a rise in excess of 20°C in temperature poses considerable risk of early age thermal cracking in a concrete member cast against another member. The rise in temperature of concrete depends on its heat generation capacity which is influenced by the following factors (Bamforth, 2007);

- Cement content and type
- Types and sources of cementitious materials
- Other concrete constituents and mix proportions that influence the thermal properties of the concrete
- Section thickness
- Formwork type and insulation
- Concrete placing temperature
- Ambient conditions

- Active forms of temperature control such as internal cooling pipes.

2.2.2 Thermal Drop

Thermal strain in the concrete can be calculated as the product of thermal drop and the coefficient of thermal expansion of concrete. The concrete temperature starts to drop after reaching a peak during hydration until the ambient value is reached. The temperature may drop to a value even lower later during its life due to decrease in environmental temperature. Thermal drop can be classified as early age and long term for the purpose of determining the risk of cracking. Bamforth (2007) recommended early age and long term thermal drop to be calculated separately and then used in the estimation of restrained strain. The early age thermal drop is calculated from the difference between peak temperature attained by concrete during hydration and the ambient temperature. Whereas the long term thermal drop is taken as the maximum variation in ambient temperature during a year.

Various models based on the heat diffusion and heat transfer are available for modelling and estimation of the early age thermal drop. Calculation of thermal drop takes into account the placing temperature of the concrete, the maximum temperature rise and the specified ambient temperature. CIRIA C660 (2007) provides the graphs and data for estimation of the early age temperature drop for different types and contents of cement and formwork used. Thermal drop is more when plywood formwork is used and lesser in the case of steel formwork primarily because plywood acts as a better insulator than the steel and the rate of heat dissipation is lower in the case of former. Value of early age thermal drop increases with the increase in section thickness as well as the cement content in the concrete mix. When part of cement is replaced by the cementitious materials like ground granulated blast furnace slag (GGBS) and fly ash, the thermal drop is reduced as compared to that obtained with CEM I. Figure 2.1 shows the temperature drop values for CEM I concrete in relation to the section thickness and the cement content separately for the steel and plywood formworks. In the UK values of long term thermal drop may normally be taken as 20°C for concrete cast in summers and 10°C for winter casting (Bamforth, 2007). The long term temperature drop may be ignored if both restrained and the restraining members are subject to the same environmental conditions.

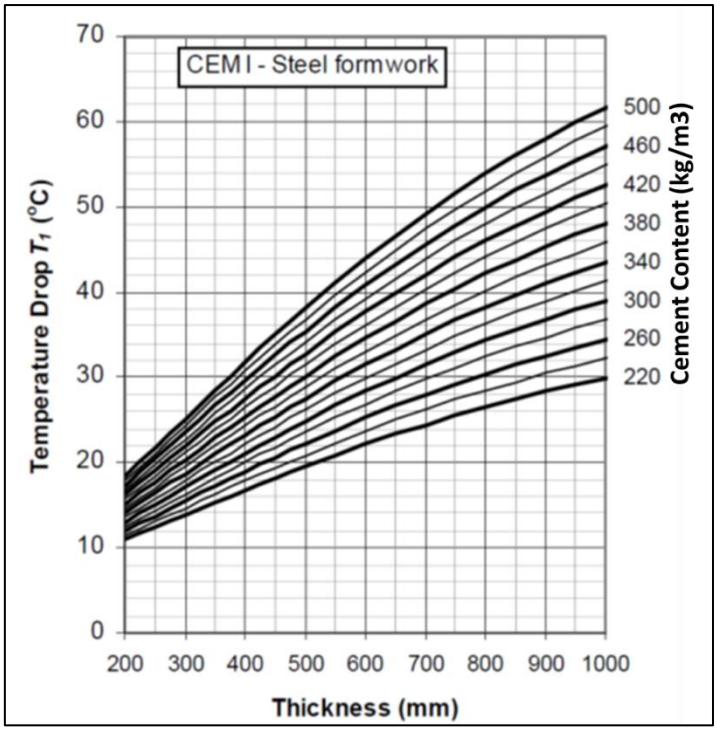

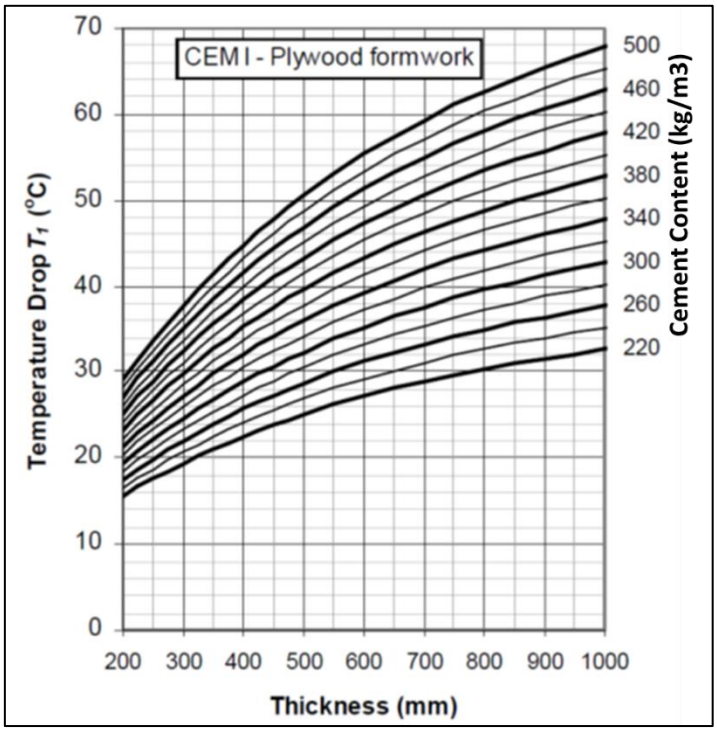

Figure 2.1. Temperature drop for concrete members cast in steel and plywood formwork as modified from (Bamforth, 2007).

2.2.3 Coefficient of Thermal Expansion

The coefficient of thermal expansion α_c is a measure of the strain change per unit temperature change. In general, the coarse aggregate forms the 60 – 75 % of the

volume of concrete and therefore, the coefficient of thermal expansion of concrete is greatly influenced by the type of aggregate used. Value of α_c ranges from 5x10^{-6} to 15 x 10^{-6} /°C for hardened concrete depending mainly on the type of aggregate used; however, there is no consensus among the researchers about the value of thermal coefficient of hardening concrete (Bosnjak, 2000). The coefficient of thermal expansion of concrete is approximately equal to the volumetrically weighted average of the coefficients of its ingredients (Walker et al., 1952; Mitchell, 1953) and is primarily attributed to the coefficient of expansion of the aggregate used. Miao et al. (1993) observed that the coefficient of thermal expansion for a concrete with Dolomite limestone aggregate reduced from 24 x 10^{-6} at 7 hours after casting to 10 x 10^{-6} at 10 hours and thereafter remained constant. Byfors (1980) also reported that the coefficient of thermal expansion decreases rapidly a few hours after mixing reaching a value of 12 x 10^{-6} in 8 hours. Researchers (Emborg, 1989; Gutsch, 1998) found that the coefficient of thermal expansion is different from that during contraction. Browne (1972) proposed the design values of coefficients of thermal expansion for different types of aggregates as given in Table 2.1. BS EN 1992-1-1 (2004) recommends a value of 10 x 10^{-6} to be used as coefficient of thermal expansion in the UK in the absence of accurately determined values through tests.

Table 2.1. Coefficients of thermal expansion (Browne, 1972)

Coarse aggregate/ rock group	**Thermal expansion coefficient (microstrain/°C)**		
	Rock	**Saturated Concrete**	**Design Value**
Chert or flint	7.4–13.0	11.4–12.2	12
Quartzite	7.0–13.2	11.7–14.6	14
Sandstone	4.3–12.1	9.2–13.3	12.5
Marble	2.2–16.0	4.4–7.4	7
Siliceous limestone	3.6–9.7	8.1–11.0	10.5
Granite	1.8–11.9	8.1–10.3	10
Dolerite	4.5–8.5	Average 9.2	9.5
Basalt	4.0–9.7	7.9–10.4	10
Limestone	1.8–11.7	4.3–10.3	9
Glacial gravel	-	9.0–13.7	13
Lytag (coarse and fine)	-	5.6	7
Lytag coarse and natural fines	-	8.5–9.5	9

2.2.4 Thermal Conductivity of Concrete

Thermal conductivity is a measure of the ability of a material to conduct heat and is defined as the ratio of the rate of heat flow to the temperature gradient. It is one of the important parameters in predicting the temperature variation and heat flow during the hydration, however, the information available on thermal conductivity of concrete at early ages is very limited. Thermal conductivity is greatly influenced by the aggregate type and content, density of concrete and the moisture content whereas the age of concrete is hardly influential except for the very early age (less than 2 days) (Kim et al., 2003). The value of thermal conductivity for normal strength concrete ranges between 1.2 – 3.0 W/m.K (Breugel, 1998). The value of thermal conductivity of concrete slightly reduces during the early age due to loss of moisture content and density of concrete (Brown et al., 1970). However, Byfors (1980) did not notice any significant change in the thermal conductivity of concrete with age.

2.2.5 Specific Heat of Concrete

Specific heat is defined as the ratio of the amount of heat required to raise the temperature in a unit mass of the material by unit degree to the amount of heat required to raise the temperature of the same mass of water by unit degree. For normal strength concrete the specific heat capacity depends on the density of concrete, water content and temperature and its value varies between 0.89 – 1.15 kJ/kgK (Breugel, 1998; Brown et al., 1970). Type and quantity of coarse aggregate, however, does not greatly influence the specific heat of concrete (Neville, 1995). Increase in specific heat of normal strength concrete with increase in temperature and moisture content was reported by Khan et al. (1998). De Schutter et al. (1995) found the specific heat to reduce linearly with the degree of hydration.

2.2.6 Shrinkage in Concrete

Shrinkage can be termed as the reduction in volume of concrete associated with chemical changes and exchange of moisture from the concrete. Total shrinkage in a concrete mass can be classified as chemical, autogenous, drying, carbonation and plastic shrinkage and it is normally difficult to segregate one from the other. Various shrinkage mechanisms are operating at different stages of the life of a concrete member, however; those of more significance in analysing the behaviour of

members under restraint are autogenous and drying shrinkage. Different forms of shrinkage are explained below:

- **Chemical Shrinkage**: It is the reduction in absolute volume of solids and liquids in concrete as a consequence of cement hydration. The net volume of hydrated cement products is less than the total volume of cement and water before hydration. Chemical shrinkage continues to occur at a microscopic scale as long as cement hydrates. It is important to understand that the volume change occurring due to chemical shrinkage is mostly internal and is not visibly witnessed in the form of reduction in external volume of concrete.
- **Autogenous Shrinkage**: Autogenous shrinkage is the macroscopic volume reduction of concrete caused by cement hydration without the exchange of moisture from concrete to the surroundings. In contrast to chemical shrinkage which is an internal volume change, the autogenous shrinkage is an external volume change which can be measured. The macroscopic volume reduction of autogenous shrinkage is much less than the absolute volume reduction of chemical shrinkage because of the rigidity of the hardened paste structure. During hardening of concrete, a number of capillaries are formed which accommodate the unused water. This internally stored water is consumed by cement particles in the hydration process and thereby a reduction in total volume of concrete occurs which is referred to as self-desiccation of concrete and is also considered part of autogenous shrinkage (Tazawa, 2014). Although autogenous shrinkage has been researched since long, however, it had been assumed that it will occur in concretes with very low water cement ratios typically below 0.40 (Pigeon et al., 2005). The phenomenon of change in volume due to chemical and autogenous shrinkage is illustrated in Figure 2.2.

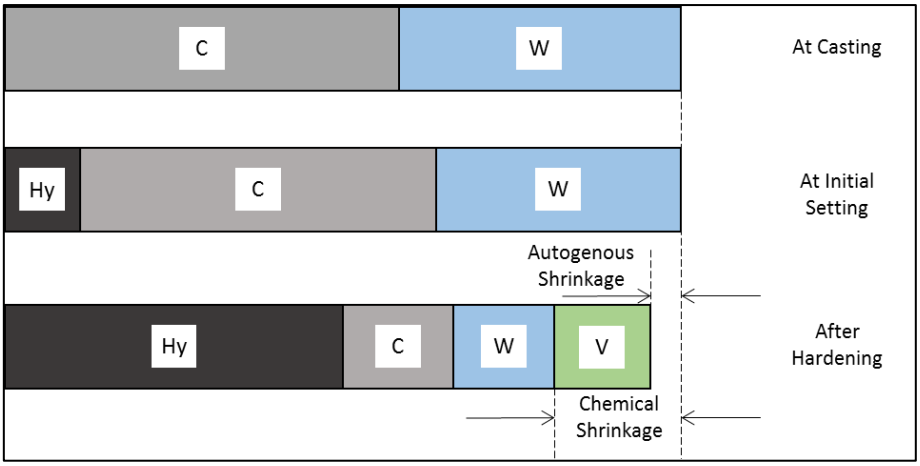

Figure 2.2. Chemical and autogenous shrinkage processes (Tazawa, 2014): C=unhydrated cement; W=unhydrated water; Hy=hydration products; V=voids

- **Plastic Shrinkage**: It refers to the volume changes occurring during the very first hours while the concrete is still fresh in the liquid and skeleton formation stages. It is usually observed in the form of plastic shrinkage cracks occurring before or during finishing. Plastic shrinkage results from the rapid evaporation of moisture from the surface that exceeds the bleeding rate. Plastic shrinkage cracking can be controlled by minimizing surface evaporation through use of fogging, wind breaks, shading, plastic sheet covers, wet burlap and plastic fibres.
- **Carbonation**: It is the process in which the cement paste in the hardened concrete reacts with moisture and carbon dioxide in the air and results in the formation of calcium carbonate. Carbonation causes slight shrinkage and reduction in pH value which can cause corrosion of the steel reinforcement (Neville, 1995). Carbonation affects the durability of the structure in long term (in order of many years) and is not of significance during the early age of concrete members.
- **Drying Shrinkage**: Drying shrinkage occurs due to loss of moisture to the surroundings and is a long term phenomenon. It depends on the temperature and relative humidity of the surroundings, exposed surface area of the concrete member and the water cement ratio. In the assessment of early age cracking risk, drying shrinkage is normally not included and it is perceived to be of more significance in the long term. The rate of drying shrinkage is more in small mass of concrete compared to the larger mass, however, the shrinkage process continues for longer duration in the case of latter. Members with higher volume

to surface area ratio experiences lower shrinkage (Mindess, 1981). Curing can also reduce the rate and amount of ultimate shrinkage caused due to drying.

2.3 Unrestrained or Free Strain Estimation

Restraint of volume change in concrete is directly linked to the magnitude or the degree of restraint which is defined as the ratio of the strain restrained from occurring to the free or unrestrained strain which could have occurred in a member in the absence of restraint. In order to ascertain the degree of restraint imposed on to a member, the knowledge of the unrestrained or free strain likely to occur in a member is important. Free volume change is a combination of the thermal and shrinkage components and it is difficult to segregate these two mechanisms. Two approaches can be adopted for ascertaining the free volume change occurring in a member. First approach is that a member of the size of the restrained member is cast without any steel reinforcement and is allowed to freely slide without any external restraint. Such approach had been adopted in the past by researchers (Stoffers, 1978)while working on small scale reinforced concrete walls. Micallef (2017) used 1000 mm long specimens with a cross section similar to the tested walls to ascertain the free thermal and drying shrinkage strain for the edge restrained walls. This approach becomes difficult to employ in the case of tests on full scale reinforced concrete members as despite all possible efforts some level of restraint remains unpreventable and the control specimens for free volume change measurement do not remain absolutely free from the restraint.

Second approach is to ascertain the thermal and shrinkage strain separately and combine them to get the free strain. This approach is more suited for the full scale members and had been adopted by Kheder et al. (1994). In adopting this approach, the thermal strain can be calculated from the measured thermal drop in the reinforced concrete wall and the coefficient of thermal expansion of concrete. Small size specimens like prisms, which do not exhibit the influence of thermal contraction, can be used to investigate the shrinkage strain for the concrete used. The data obtained from concrete prisms can then be employed to ascertain the free or unrestrained shrinkage strain for the tested members using the size ratio of both members.

2.3.1 Thermal Strain Calculation

Thermal strain can be worked out as a product of the temperature drop and the coefficient of thermal expansion of concrete. The temperature drop can be experimentally obtained for any part of the member by monitoring the temperature development using thermocouples. Coefficient of thermal expansion of concrete can be measured experimentally or estimated in the light of existing data for a particular type of coarse aggregate used as explained in the previous section. Thermal strain for early age and long term can then be calculated from the following equation;

$$\varepsilon_{th} = \alpha_c . \Delta T$$

where;

ε_{th} = Thermal strain

α_c = Coefficient of thermal expansion of concrete

ΔT = Temperature drop

2.3.2 Shrinkage Estimation Models

Estimation or prediction of shrinkage likely to occur in any concrete member is a complex phenomenon. Based on the research data, various models have been developed by different researchers for estimating the shrinkage strain in concrete. These models are adopted by different codes and although these are not meant to be truly predictive as they do tend to provide an upper bound value of shrinkage, yet they can provide a reasonable estimate of shrinkage strain. Gedam et al. (2010) carried out an experimental investigation for prediction of creep and shrinkage in high performance concrete and compared four models i.e. ACI model, CEB FIP 1990 model, Bazant-Baweja B3 model and the GL2000 model. They concluded that the CEB model gives better shrinkage prediction than the remaining models. The models available in different codes for prediction of shrinkage are discussed below:

2.3.2.1 CEB FIP 2010 Model

In CEB FIP Model code 2010 the total shrinkage, $\varepsilon_{cs}(t, t_s)$ is taken as the sum of autogenous shrinkage, ε_{cas} and drying shrinkage, $\varepsilon_{cds}(t, t_s)$ and is given as under;

$$\varepsilon_{cs}(t, t_s) = \varepsilon_{cas}(t) + \varepsilon_{cds}(t, t_s)$$

The autogenous shrinkage component $\varepsilon_{cas}(t)$ may be estimated by means of the notional autogenous shrinkage coefficient $\varepsilon_{cas0}(f_{cm})$ and the time function $\beta_{as}(t)$;

$$\varepsilon_{cas}(t) = \varepsilon_{cas0}(f_{cm}).\beta_{as}(t)$$

and,
$$\varepsilon_{cas0}(f_{cm}) = -\alpha_{as}\left[\frac{f_{cm}/_{10}}{6+\frac{f_{cm}}{10}}\right].10^{-6}$$

$$\beta_{as}(t) = 1 - \exp(-0.2\sqrt{t})$$

where;

f_{cm} = The mean compressive strength at the age of 28 days in MPa

α_{as} = Coefficient dependent on the type of cement

t = Concrete age in days

The drying shrinkage $\varepsilon_{cds}(t, t_s)$ is calculated by means of the notional drying shrinkage coefficient $\varepsilon_{cds0}(f_{cm})$, the coefficient $\beta_{RH}(RH)$, taking into account the effect of the ambient relative humidity and the function $\beta_{ds}(t - t_s)$ describing the time-development as under:

$$\varepsilon_{cds}(t, t_s) = \varepsilon_{cds0}(f_{cm}).\ \beta_{RH}(RH).\beta_{ds}(t - t_s)$$

and,

$$\varepsilon_{cds0}(f_{cm}) = [(220 + 110\alpha_{ds1}).exp(-\alpha_{ds2}f_{cm})].10^{-6}$$

$$\beta_{RH} = -1.55[1 - (\frac{RH}{100})^3] \quad for\ 40 \le RH < 99\% .\beta_{s1}$$

$$\beta_{RH} = 0.25 \quad for\ RH \ge 99\% .\beta_{s1}$$

$$\beta_{ds}(t - t_s) = (\frac{(t - t_s)}{0.035.h^2 + (t - t_s)})^{0.5}$$

$$\beta_{s1} = (\frac{35}{f_{cm}})^{0.1} \le 1.0$$

where;

$\alpha_{ds1}, \alpha_{ds2}$ = Coefficients dependent on the type of cement

RH = The relative humidity of the ambient atmosphere, in %

h = $2A_c / u$ is the notional size of member, in mm; with A_c as the cross section, in mm² and u as the perimeter of the member in contact with the atmosphere, in mm

t = Concrete age, in days

t_s = Concrete age at the beginning of drying, in days

$(t - t_s)$ = Duration of drying, in days

2.3.2.2 Eurocode Model

According to BS EN 1992-1-1 (2004), autogenous shrinkage is specifically important when new concrete is cast against the hardened concrete. It describes total shrinkage (ε_{cs}) as a sum of autogenous shrinkage (ε_{ca}) and drying shrinkage (ε_{cd}):

$$\varepsilon_{cs} = \varepsilon_{ca} + \varepsilon_{cd}$$

During early age, the autogenous shrinkage is more important and may be calculated as under:

$$\varepsilon_{ca}(t) = \beta_{as}(t)\varepsilon_{as}(\infty)$$

where 't' is time, in days and;

$$\varepsilon_{ca}(\infty) = 2.5(f_{ck} - 10)10^{-6}$$

$$\beta_{as}(t) = 1 - \exp(-0.2t^{0.5})$$

Development of drying shrinkage with time can be calculated as under;

$$\varepsilon_{cd}(t) = \beta_d(t, t_s).k_h.\varepsilon_{cd0}$$

The terms $\beta_d(t, t_s)$, k_h and ε_{cd0} can be calculated from the following expressions;

$$\beta_d(t, t_s) = \left(\frac{(t - t_s)}{(t - t_s) + 0.04\sqrt{h_0^3}}\right)^{0.5}$$

$$\varepsilon_{cd0} = \left[(220 + 110\alpha_{ds1}).exp\left(-\alpha_{ds2}\frac{f_{cm}}{f_{cm0}}\right)\right].10^{-6}.\beta_{RH}$$

$$\beta_{RH} = -1.55\left[1 - \left(\frac{RH}{RH_0}\right)^3\right]$$

where;

t = The age of the concrete at the moment considered, in days

t_s = The age of the concrete (days) at the beginning of drying shrinkage normally taken from the end of curing

h_0 = the notional size of member *(2A_c / u)*, in mm; where A_c is the concrete cross section, in mm² and *u* is the perimeter of that part of the cross section which is exposed to drying

f_{cm} = the mean compressive strength of concrete in MPa

f_{cm0} = 10 MPa

α_{ds1} = coefficient which depends on the type of cement; 3 for cement class S, 4 for cement class N, 6 for cement class R

α_{ds2} = coefficient which depends on the type of cement; 0.13 for cement class S, 0.12 for cement class N, 0.11 for cement class R

RH = the ambient relative humidity, in %

RH_0 = 100 %

2.3.2.3 ACI Model

The model initially introduced by Branson et al. (1971) is available in the ACI 209.2R-08 (2008) after slight modifications introduced by the ACI committee. Using this model, the development of shrinkage strain with time can be predicted from the ultimate shrinkage strain. The shrinkage strain $\varepsilon_{sh}(t, t_c)$ at the age of concrete 't' (days), measured from the start of drying at 't_c' (days), is calculated from the following equation;

$$\varepsilon_{sh}(t, t_c) = \left(\frac{(t - t_c)^{\alpha}}{f + (t - t_c)^{\alpha}}\right).\varepsilon_{shu}$$

where; $(t - t_c)$ is the time from the end of curing. f and α are considered constants for a given member shape and size that define the time-ratio part. Value of α is taken as 1 and f is calculated (in SI units) using the volume to surface area ratio (V/S) as given below;

$$f = 26.0e^{[1.42*10^{-2}\left(\frac{V}{S}\right)]}$$

ε_{shu} is the ultimate shrinkage strain which, for standard conditions and 40% relative humidity, can be assumed to be 780 microstrain in the absence of experimental data. The ultimate shrinkage strain can also be predicted from the data obtained on shrinkage development for a certain duration of time. Prediction of ultimate shrinkage strain has been discussed in section 2.3.2.6 in detail.

For conditions other than the standard conditions, the value of ultimate shrinkage strain is required to be corrected by multiplying with various correction factors as explained below.

- Factor for curing, γ_{tc} is applicable if the curing time, 't_c' differs from seven days moist curing and can be calculated as under:

$$\gamma_{sh,tc} = 1.202 - 0.2337\log(t_c)$$

- For relative humidity of more than 40%, the correction factor for relative humidity, $\gamma_{sh,RH}$ should be calculated for the relative humidity, h (in decimals) as under;

$$\gamma_{sh,RH} = 1.40 - 1.02\text{h for } 0.4 \leq \text{h} \leq 0.8$$

$$\gamma_{sh,RH} = 3.00 - 3.0\text{h for } 0.8 \leq \text{h} \leq 1.0$$

- Correction factor for the size of the member, $\gamma_{sh,V/S}$ can be calculated in terms of the volume-surface ratio (V/S), for members with V/S ratio other than 38 mm according to the following equation;

$$\gamma_{sh,V/S} = 1.2e^{(-0.00472\left(\frac{V}{S}\right))}$$

- Correction factors $\gamma_{sh,s}, \gamma_{sh,\psi}, \gamma_{sh,c}$ and $\gamma_{sh,\alpha}$ are applicable for the composition of concrete to include the influence of slump (s), ratio of fine aggregate (ψ), cement content (c) and air content (α) respectively and can be calculated from the following equations;

$$\gamma_{sh,s} = 0.89 + 0.00161s$$

$$\gamma_{sh,\psi} = 0.30 + 0.014\psi \; for \; \psi \leq 50\%$$

$$\gamma_{sh,\psi} = 0.90 + 0.002\psi \; for \; \psi > 50\%$$

$$\gamma_{sh,c} = 0.75 + 0.00061c$$

$$\gamma_{sh,\alpha} = 0.95 + 0.008\,\alpha \geq 1.0$$

2.3.2.4 Bazant-Baweja B3 Model

This model for prediction of shrinkage and creep was proposed by Bažant et al. (1995) and is included in the ACI 209.2R-08 (2008). The model is applicable for normal strength concrete prepared with Portland cement (CEM 1) only. The effect of concrete composition and design strength on the model parameters is the main source of error in this model (ACI 209.2R-08, 2008). The model is restricted to the concrete subjected to service stress range only and cured for a minimum of one day. The average shrinkage strain $\varepsilon_{sh}(t, t_c)$ in a concrete section at the age of *t* (days) measured from the start of drying t_c (days) can be calculated as under;

$$\varepsilon_{sh}(t, t_c) = -\varepsilon_{sh\infty}.k_h.S(t - t_c)$$

where; $\varepsilon_{sh\infty}$ is the ultimate shrinkage strain, k_h is the relative humidity factor, $S(t - t_c)$ is the time function and $(t - t_c)$ is the time from the end of the initial curing. The ultimate shrinkage strain can be either obtained from the experimental data or calculated from the following equation using the modulus of elasticity E_{cm};

$$\varepsilon_{sh\infty} = -\varepsilon_{s\infty}\left(\frac{E_{cm607}}{E_{cm(t_c+\tau_{sh})}}\right)$$

here, E_{cmt} and $\varepsilon_{s\infty}$ can be calculated as under;

$$E_{cmt} = E_{cm28}\left(\frac{t}{4 + 0.85t}\right)^{0.5}$$

$$\varepsilon_{s\infty} = -\alpha_1\alpha_2[0.019w^{2.1}f_{cm28}^{-0.28} + 270].10^{-6}$$

where;

w = The water content, in kg/m^3

f_{cm28} = The mean compressive strength at 28 days in MPa

α_1, α_2 = Constants related to the cement type and curing conditions

τ_{sh} = The shrinkage half time, in days

The time function $S(t-t_c)$ for shrinkage development can be calculated from;

$$S(t-t_c) = tanh\sqrt{\frac{(t-t_c)}{\tau_{sh}}}$$

The size dependence of shrinkage is obtained using the volume to surface area ratio (V/S) as under;

$$\tau_{sh} = 0.085t_c^{-0.08}f_{cm28}^{-0.25}[2k_s(^V/_S)]^2$$

where; k_s is the cross section shape correction factor.

2.3.2.5 GL2000 model

This model was introduced by Gardner et al. (2001), later modified slightly by Gardner (2004) and is also included in the ACI 209.2R-08 (2008) for prediction of creep and shrinkage in concrete. It is simple and easy to use and is primarily intended to be used in the design offices. Shrinkage strain, $\varepsilon_{sh}(t,t_c)$ can be calculated from the following equation;

$$\varepsilon_{sh}(t,t_c) = \varepsilon_{shu}.\beta_h.\beta(t-t_c)$$

where;

ε_{shu} = Ultimate shrinkage strain

β_h = Coefficient to account for the effect of humidity

$\beta(t-t_c)$= Coefficient to account for the time of drying

The ultimate shrinkage strain can be calculated from the 28 days compressive strength, f_{cm28}in MPa and the coefficient k, representing the type of cement, as under;

$$\varepsilon_{shu} = 900k(\frac{30}{f_{cm28}})^{0.5}.10^{-6}$$

The coefficient for effect of humidity for a given relative humidity (in decimals), β_h is given by;

$$\beta_h = (1 - 1.18h^4)$$

The coefficient for time of drying, $\beta(t-t_c)$ is calculated using the volume to surface area ratio (V/S) in mm, by;

$$\beta(t-t_c) = \left(\frac{(t-t_c)}{(t-t_c) + 0.12(V/S)^2}\right)^{0.5}$$

2.3.2.6 Prediction of Ultimate Shrinkage Strain

Ultimate shrinkage strain can be predicted using the empirical equation given in various models described above. However, a more reliable prediction of ultimate shrinkage can be obtained by extrapolating the shrinkage strain observed in small specimens during short term tests. Extrapolation based on short term test results, if performed after appropriate qualification, can lead to a significant improvement of the predicted ultimate shrinkage (Ojdrovic et al., 1996). Since the majority of shrinkage strain occurs in small size specimens within 28 days, an equation was proposed by Meyers et al. (1972) to predict the ultimate shrinkage strain ε_{shu} from the shrinkage strain $\varepsilon_{sh(t)}$ at any time *t*. The proposed equation is as under;

$$\varepsilon_{shu} = \varepsilon_{sh(t)} \div \left(\frac{t}{35+t}\right)$$

Another convenient mathematical expression for prediction of ultimate creep strain was proposed by Ross et al. (1989). It is based on the hyperbolic curve and can also be used to predict the ultimate shrinkage strain in concrete. The Ross hyperbolic equation expresses creep, *c* for time *t* using following relationship;

$$c = \frac{t}{a+bt}$$

where; a and b are the constants obtained experimentally.

When the time t approaches infinity, then the equation becomes $c = \frac{1}{b}$ meaning that $\frac{1}{b}$ is the limiting value of strain. According to Neville (1995) when *t*/*c* is plotted against *t*, a straight line of slope *b* is obtained, and the intercept of the *t*/*c* axis is equal

to constant *a*. Inverse of *b* provides the ultimate value of creep or shrinkage strain of concrete.

2.4 Mechanical Properties of Concrete

2.4.1 Compressive Strength

Compressive strength is a fundamental property particularly for specifying the class of concrete. It can be determined by tests on small specimens (cubes or cylinders) of different sizes at different ages. The method of compressive strength testing is quite easy and is commonly employed for correlation with other properties of concrete like tensile strength and modulus of elasticity. Detailed procedure for testing of specimens to determine the compressive strength of concrete is specified in BS EN 12390-3 (2009). According to BS EN 1992-1-1 (2004) the compressive strength obtained from the cylinders is approximately 80 – 85% of that obtained by using cubes. The compressive strength obtained at the age of 28 days (f_{cm}) can be used to determine the value of compressive strength $(f_{cm(t)})$ at any time (t) using following equation given in BS EN 1992-1-1 (2004);

$$f_{cm(t)} = \beta_{cc(t)} . f_{cm}$$

where; (s) is a coefficient given by the type of cement and coefficient for effect of age of concrete $(\beta_{cc(t)})$ is given as;

$$\beta_{cc(t)} = \exp[s\left(1 - \left(\frac{28}{t}\right)^{0.5}\right)]$$

2.4.2 Tensile Strength

Tensile strength is a key factor in the cracking behaviour of reinforced concrete members and gains more significance in members subjected to restraint. Determination of tensile strength in the laboratory can be done using the direct (uniaxial tensile strength tests) or indirect (splitting or flexural strength tests). Procedure for determination of tensile strength of concrete in the laboratory is specified in BS EN 12390-6 (2009). No reliable and standardized methods of testing concrete specimens under direct tension are available. Infact, research (Wee et al., 2000) has shown that the direct tension tests have some inherent disadvantages which are mentioned in Section 2.6.1 below. Different correlations between the

uniaxial and splitting tensile strength of concrete have been specified in different guidelines (BS EN 1992-1-1, 2004; Model Code, 2010; Byfors, 1980). According to BS EN 1992-1-1 (2004) the uniaxial tensile strength is 90% of the splitting tensile strength. Development of tensile strength during early age of concrete is faster than the compressive strength (Kanstad et al., 1999; Kanstad et al., 2003). According to BS EN 1992-1-1 (2004), tensile strength $(f_{ctm(t)})$ at any time (t) can be calculated from the tensile strength obtained at the age of 28 days (f_{ctm}) using following equation;

$$f_{ctm(t)} = (\beta_{cc(t)})^{\alpha} . f_{ctm}$$

here; α = 1 for $t < 28$ days and α = 2/3 for $t \geq 28$ days

2.4.3 Modulus of Elasticity

Determination of the static modulus of elasticity of concrete is essential in the members subjected to restraint for estimation of tensile strain capacity. Like the tensile strength, modulus of elasticity also develops at a higher rate than the compressive strength of concrete. However, BS EN 1992-1-1 (2004) relates the modulus of elasticity using the compressive strength of concrete. It specifies following relationship for estimation of modulus of elasticity $(E_{cm(t)})$ at any time (t) from the modulus of elasticity at the age of 28 days (E_{cm});

$$E_{cm(t)} = \left({f_{cm(t)}}/{f_{cm}} \right)^{0.3} . E_{cm}$$

2.4.4 Fracture Energy

Three modes of fracture in materials can be found depending on the type of loading; tensile, shear or tearing. Mode 1 describes the fracture mechanism under tension. Fracture energy is defined as the energy required to open unit area of crack surface. It is a material property which is a function of the aggregate size and compressive strength and does not depend on the size of the member. No specific expression for estimation of fracture energy of concrete exists in BS EN 1992-1-1 (2004). Model Code (2010) provides following equation for estimation of fracture energy (G_f) of concrete;

$$G_f = 73\, {f_{cm}}^{0.18}$$

2.5 Behaviour of Reinforced Concrete Members under Restraint

When concrete is free to undergo the volume change, no stresses are induced and the concrete mass will initially expand and then shrink as a result of the expansion and contraction introduced by thermal and moisture effects. However, in almost all practical cases concrete is not free to exhibit the volume changes and some form of restraint to these changes is always imposed either internally or externally. Restraint, in simple words, can be termed as the mechanism which tends to inhibit, suppress or limit the free strain or volume change in concrete. Restrained strain increases in direct proportion to the magnitude of volume change and the degree of restraint. Restraint may be imposed on to a concrete member in various ways and therefore, its effects and corresponding response of the member also varies.

2.5.1 Types of Restraint

Reinforces concrete members can be subjected to different types of restraint. Basing on the location of adjoining members, section thickness and steel reinforcement provided, restraint can be classified into following types (Concrete Society Technical Report, 2008);

2.5.1.1 External Restraint

External restraint is imposed on to a newly cast member by its pre-existing adjoining members. It can be further categorized into following types based on the location of restraining members as shown in Figure 2.3:

- **End Restraint**: This form of restraint occurs when a new member is cast between two existing members such that both its ends are in contact with the existing members e.g. a suspended slab cast between two walls or columns.
- **Edge Restraint**: It is also referred to as base restraint and occurs when the base or the edge of a member is restrained by an already hardened member. Typical example of edge restraint is a cantilever wall restrained at its base by the foundation slab.
- **Combined Restraint**: In some cases, a concrete member can be subjected to a combination of end and edge restraint. In members subjected to combined restraint, the edge restraint will be dominant close to the base however, moving

away from the base, the effect of edge restraint continues to diminish and influence of end restraint becomes more prominent (Beeby and Forth, 2005). A simple example of such case is an infill wall panel cast between pre-existing panels on both ends and the base.

- **Surface Restraint**: When concrete topping is cast onto a precast substrate, the contraction of fresh concrete may be restrained by existing mass of concrete. Thus the tensile stresses would develop in the topping which may lead to formation of cracks.

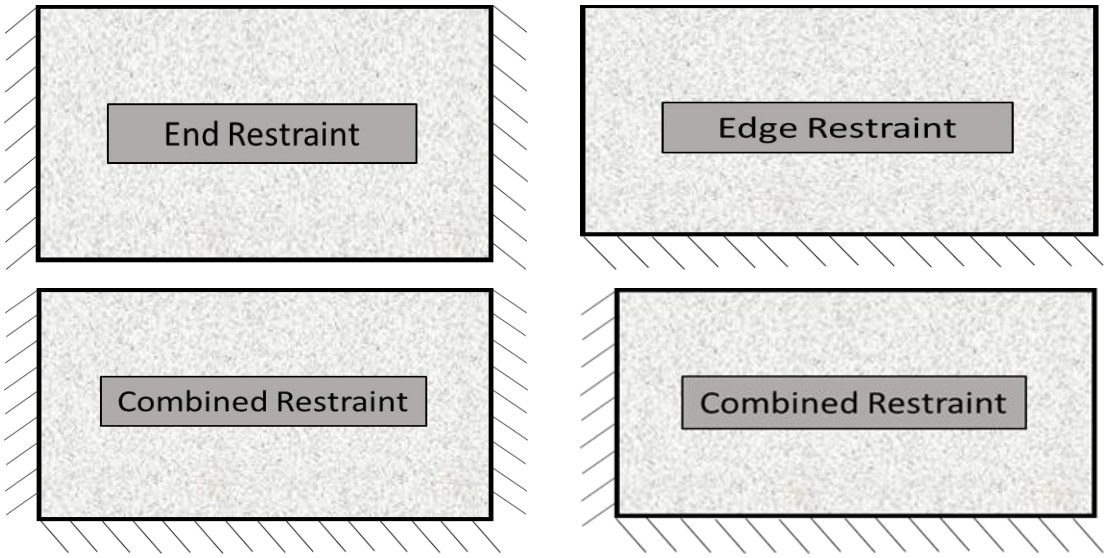

Figure 2.3. Types of external restraint (Concrete Society Technical Report, 2008)

2.5.1.2 Internal Restraint

A reinforced concrete member can also be restrained internally because of following mechanisms;

- Steel reinforcement present inside the member does not undergo the volume change like concrete and therefore restrains its free movement.
- Thermal differential can be created in concrete members having large section thickness (generally greater than 500 mm). In such members, the concrete surface starts to contract after hydration while the core temperature is still higher and thus the core restrains the surface contraction.
- In the case of concrete structures partially buried in the ground or bridge decks in which top surface of the slab is subjected to higher temperature than the bottom surface, a thermal gradient can also occur and pose internal restraint.

2.5.2 Behaviour under End Restraint

End restraint is thought to be uniformly acting in all parts of the restrained member. Initially Evans et al. (1968) presented a theory according to which all cracks in a member would form at once when the tensile strength is exceeded. Gilbert (1992) explained the cracking behaviour of members fully restrained at their ends. With an increase in contraction the restraining force in the member increases gradually generating tensile stress in the member until the tensile strength of concrete is exceeded and the first crack forms. Gilbert (1992) and Nejadi et al. (2004) developed methods to predict the number, spacing and width of cracks in a fully restrained member by using an approach based on principles of mechanics. Their work indicates that cracking in restrained members can be highly variable even in identical specimens. It was concluded that by application of a deterministic model, cracking behaviour cannot be predicted with great accuracy.

Because of the inherent variation of tensile strength, the first crack would form at the location where tensile strength in a member is the lowest. With the formation of the crack, the tensile force in the entire member is reduced and the stress in concrete at the crack location is transferred to the steel reinforcement. At some distance away from the crack, the stress is regained by concrete due to bond action but it remains below the tensile strength. With further increase in contraction, the tensile force and tensile stress again increases in the member until another crack is formed. The process of crack formation depicted in Figure 2.4 below, goes on until all possible cracks have formed and further increase in restrained strain results in widening of existing cracks. This is called the stabilised cracking stage and a restrained strain of the order of 1000 microstrain is required to reach this stage (Beeby and Forth, 2005).

The formation of first crack results in reduction of the stiffness and tensile stress in the entire member and with further increase in contraction, the width of the formed crack increases and so does the tensile stress in the member. It can be stated that the formation of a crack in end restrained member has a global effect since the crack results in reduction of the stress and stiffness of entire member. In end restrained members, the crack width is a function of the tensile strength of concrete and the amount of steel reinforcement present in the member. The restrained strain does not influence the crack width and is only significant in relation to the occurrence of cracking

and the number of cracks formed in the member (Bamforth, 2007). The crack width just before formation of each new crack will be slightly higher than the width at the time of formation of each previous crack (Beeby and Forth, 2005).

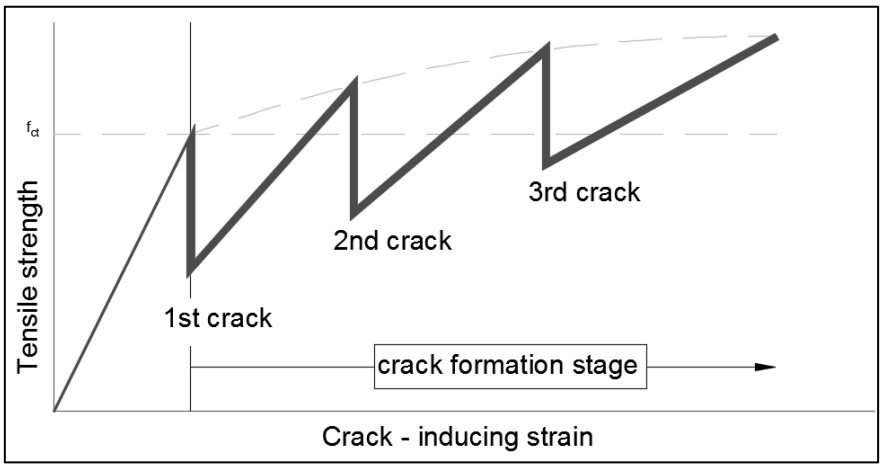

Figure 2.4. Schematic illustration of crack formation in end restrained members (Bamforth, 2007)

2.5.3 Behaviour under Edge Restraint

Little research has been performed on the behaviour of edge restrained members. Most of the experimental research has been performed on reduced scale members with micro concrete and reduced bar diameters (Stoffers, 1978) or on mortar mixes (Kheder et al., 1990; Kheder, 1997; Kheder et al., 1994). Recently, Micallef (2017) conducted tests on full scale reinforced concrete walls subjected to a combination of flexure and edge restraint, where the restraint was imposed by a steel restraining base. Moreover, in the works undertaken on edge restraint, the behaviour of restraining base has not been noticed. This is because in most of the research, steel members had been used to impose edge restraint on to the reinforced concrete walls (Stoffers, 1978; Micallef et al., 2017). The research that has been performed, suggests that the effects of end and edge restraint are quite different from each other (Beeby and Forth, 2005; Bamforth, 2010) . Unlike the end restraint, edge restraint is not uniform and varies along the height and length of the member. The degree of restraint is maximum at the base and reduces along the height of the wall (Kheder, 1997). With an increase in contraction in the wall, the restrained strain is maximum at the joint between the restrained and restraining members and decreases upwards along the height. The restraining member has a closing effect on the base of the wall which restricts the cracks from opening (Bamforth, 2007). The crack occurs when the

restrained strain exceeds the tensile strength, however, in this case the stress is relieved locally within the vicinity of the crack. Further cracks may form anywhere in the member where the stress remains unrelieved. The crack width in the case of edge restrained members is a function of the degree of restraint and not the tensile strength of concrete. The steel reinforcement acts to control or limit the crack widths and this can result in the formation of secondary cracks in between the primary cracks (Kheder et al., 1994; Bamforth, 2007).

Development of curvature in the restraining member also has a significant influence on the behaviour of edge restrained members. Due to contraction in the wall, warping may occur in the ends of the restraining base slab. Linear elastic investigations by Schleeh (1962) revealed that the development of curvature in the restraining member has a significant effect on the tensile stresses induced due to restrained movements. In such a case, top of the wall may undergo compression thereby restricting the height of the cracks. This, in other words, means that the crack widths and the extent of cracking are also related to the curvature development. Stoffers (1978) conducted tests on edge restrained reinforced concrete walls and analysed the effect of curvature in the base slab on the cracking in the walls. He found that when the base slab is permitted to curve, the effect of base in distribution of cracks is reduced. Stoffers (1978) presented the curvature theory and developed expressions for calculation of curvature based on the equilibrium of forces between wall and slab. It can be deduced that the case where curvature is prevented from occurring presents a more rigid base and the extent of cracking and degree of restraint is increased.

Beeby and Forth (2005) explained cracking in base restrained walls by considering cracking zones adjacent to a primary crack, which depend on the wall height. The areas of the wall close to a primary crack can be divided into three zones; A, B and C as is illustrated in Figure 2.5. Authors believed that no further cracks are likely to occur in Zone A. No new cracks are expected to occur in zone B as well, however, cracks initiating in zone C may pass into zone B. These cracks will be smaller in width and expected to close prior to reaching the boundary of zone A. However, new cracks may initiate in zone C since the stress relief is local in nature. Cracks occurring beyond distance 2H will be new primary cracks whereas, those occurring within this distance will be secondary cracks.

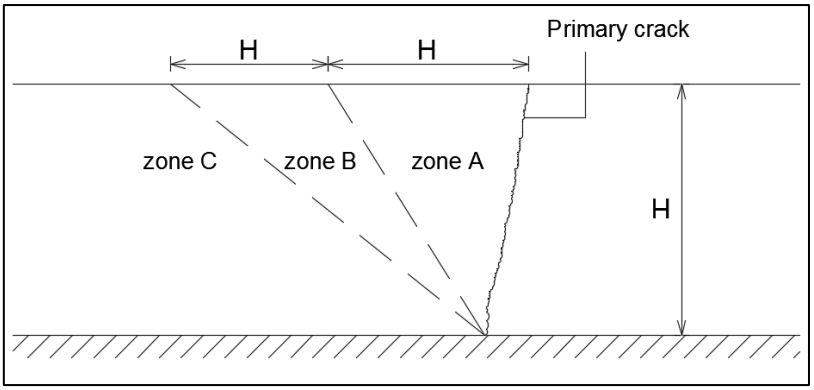

Figure 2.5. Illustration of cracking zones near a primary crack (Beeby and Forth, 2005)

2.5.4 Differences between End and Edge Restraint

Following are the fundamental differences between the behaviour of edge and end restrained members;

- End restraint is uniform throughout the member whereas the edge restraint is maximum at the base and minimum near the top of the wall.
- Stress relief and reduction in the stiffness of the member is global in the case of end restraint while it occurs locally in the vicinity of crack in edge restraint.
- Crack width is a function of tensile strength and steel reinforcement in end restrained members while in the case of edge restraint it is proportional to the degree of restraint.
- Newly formed cracks in the case of edge restrained members are independent of already existing cracks but this is not true for end restrained members.
- Crack spacing and thus the crack width is significantly greater in the case of end restraint compared to the edge restrained members. This is because of the fact that in the case of edge restraint, the restraint itself acts to limit the deformation at each crack location. While in the end restraint, the deformation at the crack is limited only by the reinforcement and the stress that is transferred to the reinforcement from the concrete (Bamforth, 2007).
- In edge restrained members, part of the load is transferred to the restraining base and also the base has a closing action on the cracks in the wall and therefore the maximum crack width does not occur at the location of maximum restraint rather at some point higher in the wall (Bamforth, 2007).

2.5.5 Behaviour under Combined Restraint

Edge and end restraints are two limiting forms of restraint, however, in many practical cases a member may be subjected to a combination of edge and end restraint. The behaviour of members under combined restraint has not been studied in detail so far and therefore the guidance on the design of members under such type of restraint is not available in the codes of practice (Forth, 2014). A hypothetical variation of different forms of restraint in a member subjected to combined restraint was proposed by Forth (2014) as given in Figure 2.6. According to which the edge restraint is dominant in the parts of member close to the base whereas at higher locations the end restraint becomes more pronounced. Generally adopted approach for combined restraint is to design the members according to the end restraint conditions, however, Micallef et al. (2017) conducted tests on walls subjected to combined restraint and concluded that such members be designed in accordance with the provisions for edge restraint. Al-Gburi (2014) carried out numerical modelling on structural members under different combinations of restraint and found that the critical or maximum restraint occurs at a height equal to 0.2 times the length of the member.

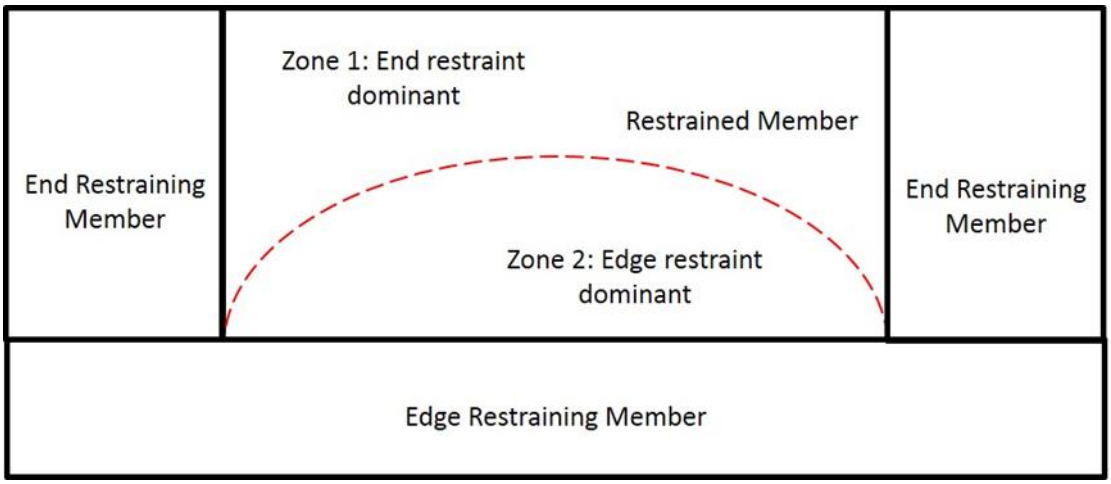

Figure 2.6. Hypothetical variation of restraint in members subjected to combined restraint (Forth, 2014)

2.6 Mechanism of Cracking

Restrained strain (ε_r) is the part of free strain (ε_{free}) which is restrained from occurring in a member due to restraint. Amount of restrained strain is proportional to the degree of restraint imposed (R). It is the restrained strain which produces the tensile stresses in the concrete member. Once the magnitude of restrained strain (ε_r)

exceeds the tensile strain capacity (ε_{ctu}) of concrete, cracking occurs. Bamforth (2007) defined risk of cracking in a member as the ratio of the restrained strain (ε_r) to the ultimate tensile strain capacity (ε_{ctu}) of the concrete. Upon cracking, part of the restrained strain is relieved which is called the crack inducing strain (ε_{cr}) and is exhibited as crack width. This crack inducing strain is equal to the restrained strain less the mean residual tensile strain capacity in concrete after cracking and is exhibited by the member as crack width. The process of crack initiation for both end and edge restraint member is identical; however, their post cracking behaviour is quite different.

2.6.1 Tensile Strain Capacity of Concrete

The tensile strain capacity of concrete can be defined as the maximum tensile strain that the concrete can endure without formation of a continuous crack. Estimation of tensile strain capacity is not easy since it can vary under different types of stress. In order to estimate the tensile strain capacity, both direct and indirect tensile strength tests had been used in the past. Direct tension tests were employed by Hughes et al. (1965), Dunstan (1981), Nianxiang et al. (1989) and Wee et al. (2000). Whereas Houghton (1976), Houk et al. (1970) and Thomas et al. (1995) used the indirect or flexural strength tests to ascertain tensile strain capacity. Hunt (1971) conducted tests on fully restrained prisms to estimate tensile strain capacity of concrete. Tasdemir (1996) reported that under direct tension, the tensile strain capacity can be predicted using tensile strength and static modulus of elasticity of concrete and the relationship is not dependent on the mix composition, age, specimen size and testing technique provided notched specimens are not used for the tests. Direct tension tests were reported to have certain drawbacks which include non-uniformity of stress, introduction of eccentricity and stress concentration near the ends of tested specimens. Indirect tensile strength tests can be more conveniently used for estimation of the tensile strain capacity (ε_{ctu}) from the tensile strength (f_{ct}) and modulus of elasticity of concrete (E_c) using following equation (Houghton, 1976);

$$\varepsilon_{ctu} = {f_{ct}}/{E_c}$$

Fracture mechanism of concrete is different under various states of stress. The tensile strain capacity should be calculated judiciously depending on the state of stress

in concrete. Limiting tensile strain under uniaxial compression was found to lie between 300 – 500 microstrain, in flexural strength tests it ranges between 150 – 200 microstrain whereas in direct tension tests between 100 – 140 microstrain (Wee et al., 2000). Tasdemir (1996) found that the value of tensile strain capacity obtained from the ratio of tensile strength to the modulus of elasticity represents a lower bound value. The stresses caused in the concrete due to early age thermal and shrinkage effects represent sustained loading. Tasdemir (1996) proposed a linear relationship between the tensile strain capacity (ε_{ctu}) and the ratio of tensile strength (f_{ct}) to the modulus of elasticity (E_c) of concrete as under;

$$\varepsilon_{ctu} = [1.01\left({f_{ct}}/{E_c}\right) + 8.4].\,10^{-6}$$

Bamforth (2007) therefore indicated that the tensile capacity of concrete increases due to creep relaxation and a reduction in the failure stress due to the sustained loading. In order to incorporate these effects, value of tensile strain capacity obtained from above equation by Tasdemir (1996) should be multiplied by a factor of 1.23 to account for the effect of creep relaxation and sustained loading. Suggested factor is based on a C30/37 concrete and for other concrete classes (in the range of 20 – 60 MPa), the tensile strain capacity calculated above should be adjusted by multiplying with following factor;

$$0.63 + \left({f_{c,cube}}/{100}\right)$$

2.6.2 Estimation of Restrained Strain and Crack Inducing Strain

While the restrained strain is the amount of strain restrained from occurring, the crack inducing strain is the component of restrained strain which is relieved on occurrence of a crack and is exhibited as crack width. Crack inducing strain can be calculated from the difference between restrained strain and the amount of residual tensile strain capacity of concrete. After cracking, the average value of residual strain in concrete can be assumed to be half of the tensile strain capacity and then crack inducing strain (ε_{cr}) can be given as (Bamforth, 2007);

$$\varepsilon_{cr} = \varepsilon_r - 0.5\varepsilon_{ctu}$$

BS EN 1992-1-1 (2004) and BS EN 1992-3 (2006) describe crack inducing strain as the average strain in steel less the average residual strain in concrete after cracking and can be termed as $(\varepsilon_{sm} - \varepsilon_{cm})$. This phenomenon is graphically illustrated in Figure 2.7. Different expressions have been given for estimation of crack inducing strain under end and edge restraint. In end restraint, the crack inducing strain is a function of the tensile strength of concrete and the ratio of horizontal steel reinforcement. The restraining force generated in such members is a sum of the force in steel and that in concrete. From the compatibility of forces, the expression for estimating the crack inducing strain and crack width was derived by Beeby (1990) which is part of the Eurocode 2. Expression M1 of BS EN 1992-3 (2006) describes the crack inducing strain for end restraint conditions as;

$$(\varepsilon_{sm} - \varepsilon_{cm}) = [0.5\alpha_e k_c k f_{ct,eff}(1 + 1/(\alpha_e \rho)]/E_s$$

where;

α_e = Modular ratio (E_s/E_c)

ρ = Reinforcement ratio

$f_{ct,eff}$ = Mean tensile strength of concrete

E_s = Modulus of elasticity of steel

k_c, k = Coefficients as defined in section 7.3.2 of BS EN 1992-1-1

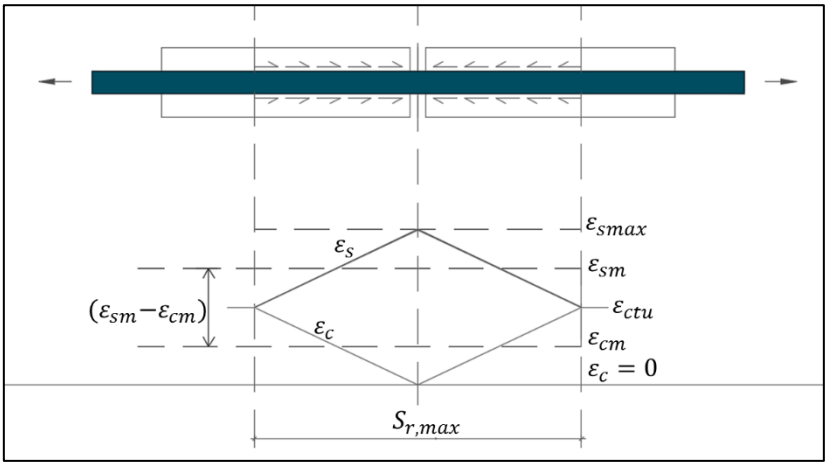

Figure 2.7. Schematic illustration of the strain variation near crack

Unlike end restraint, cracking under edge restraint is a function of the restrained strain and not the tensile capacity of concrete. Crack spacing is also influenced by the

restraining base and steel reinforcement. Expression M3 of BS EN 1992-3 (2006) describes the restrained strain under edge restraint conditions as under;

$$\varepsilon_r = R_{ax}\varepsilon_{free}$$

Where R_{ax} is the degree of axial restraint and ε_{free} is the magnitude of free or unrestrained strain likely to occur in the absence of restraint. According to Bamforth (2007), crack inducing strain for edge restraint can be worked out as under;

$$(\varepsilon_{sm} - \varepsilon_{cm}) = R_{ax}\varepsilon_{free} - 0.5\varepsilon_{ctu}$$

2.6.3 Crack Spacing

Axially reinforced tension members have been used by researchers (Beeby, 1979; Beeby, 2005; Gilbert, 1992) to evolve the relationships for crack spacing. In a member subjected to direct tension, the formation of first crack transfers the entire stress to steel bar at the location of crack. Moving away from the crack, stress in concrete starts to increase and the stress in steel bar starts to decrease. At some distance (S_0) from the crack location, the stress in steel and concrete is regained to the level that existed prior to cracking. The same happens on formation of second or any subsequent cracks as is indicated in Figure 2.8. The distance (S_0) is often referred to as the transfer length and is instrumental in determination of maximum crack spacing in a member. There has not been a consensus among researchers on crack width prediction as different design codes adopt different theories for crack width predictions (Beeby, 1979; Carino, 1995). These theories are based on the anticipated behaviour at the interface between steel reinforcement and concrete on occurrence of a crack. Three theories i.e. ‘Slip’ theory, ‘No Slip’ theory and a combination of Slip and No Slip theory have been stated by researchers (Hughes et al., 1988; Beeby, 2005; Carino, 1995) for determination of the post cracking behaviour at the steel concrete interface. These theories are briefly explained below;

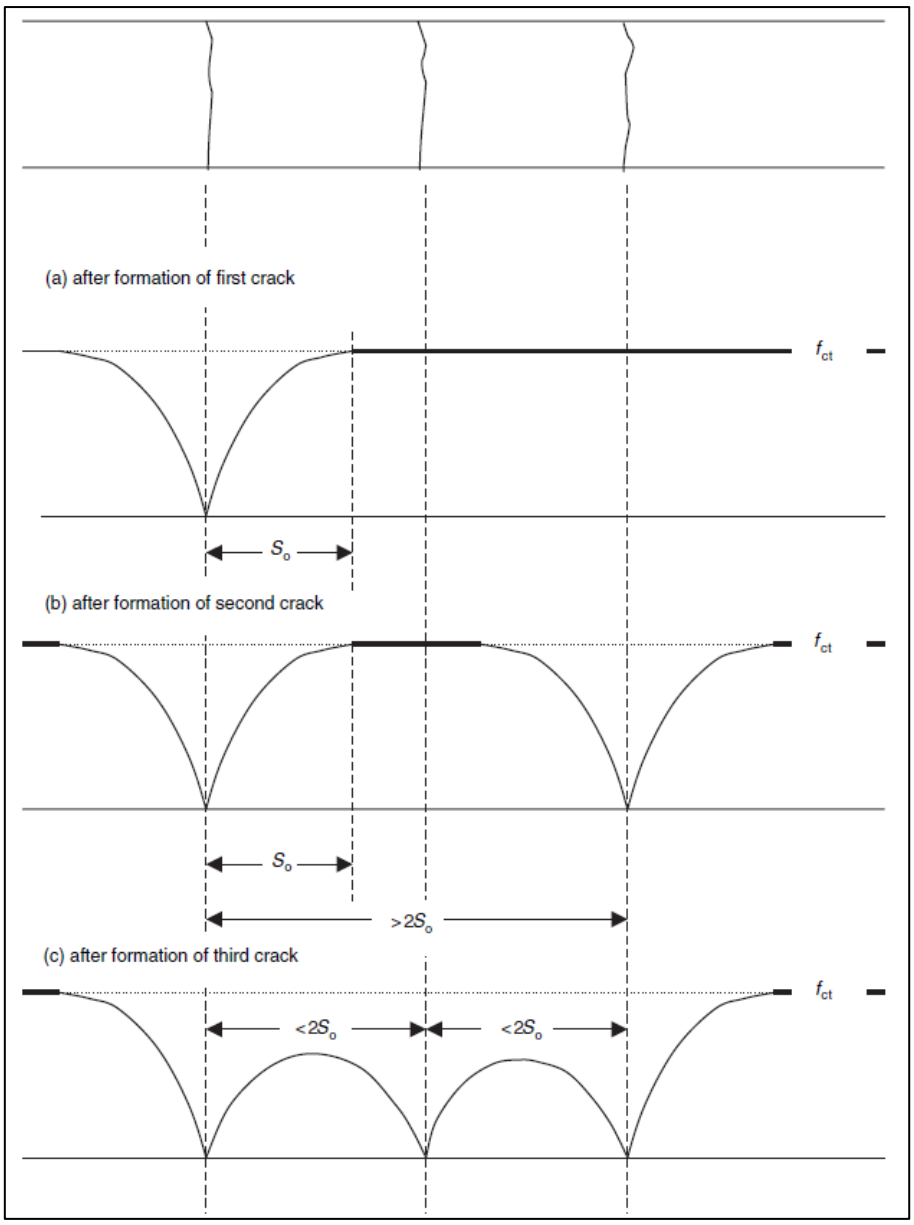

Figure 2.8. Stress distribution in axially reinforced concrete member under direct tension on cracking (Beeby, 2005)

- **Slip Theory**: This theory was presented by Saliger (1936) and it assumes total bond failure at each crack location and considers that plane sections remain plane after cracking. Splitting along the steel reinforcement bar occurs and a relative slip of concrete occurs on both sides of the crack. The slip occurs on each side of the crack for a distance called transfer length (S_0) as indicated in Figure 2.9 and the distribution of forces between concrete and steel interface is dictated by the bond strength (f_b). By equating the forces in concrete and steel bar, the distance (S_0) over which the transfer of stress between concrete and steel reinforcement occurs can be calculated as under;

$$S_0 = C_1 \frac{f_{ct}}{f_b} \frac{\emptyset}{\rho}$$

Here C_1 is a constant depending on bond stress distribution and is obtained experimentally, f_{ct} is the tensile strength of concrete, $\emptyset$ is the diameter of steel bar and ρ is the steel reinforcement ratio. According to Slip theory, the crack spacing is directly proportional to the ratio of bar diameter to steel reinforcement ratio ($\frac{\emptyset}{\rho}$).

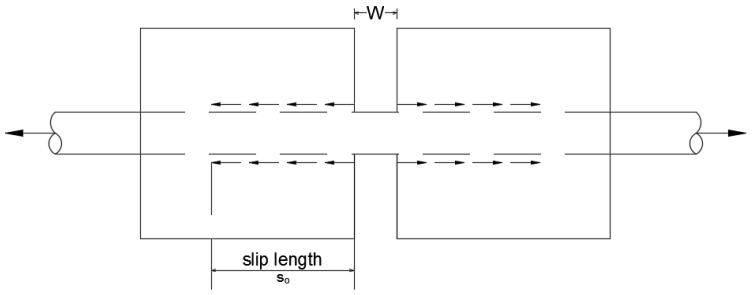

Figure 2.9. Illustration of the Slip theory (Carino, 1995)

- **No Slip Theory**: This theory is based on the work by Base et al. (1966) in which various parameters were evaluated for their influence on the crack widths. According to No Slip theory the transfer length, (S_0) is thought to be dependent on the distance to the concrete surface from the surface of steel reinforcement bar or in other words, the concrete cover (c). No slip and debonding is thought to occur at the interface between steel and concrete as indicated in Figure 2.10. The transfer length is given as under;

$$S_0 = C_2 . c$$

Here, C_2 is a constant to be determined experimentally.

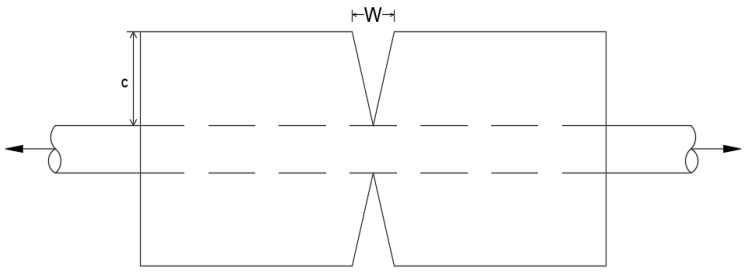

Figure 2.10. Illustration of the No Slip theory (Carino, 1995)

- **Combination of Slip and No Slip Theory**: The behaviour at the interface of steel and concrete is a combination of the above two theories (Beeby, 1979) as indicated in Figure 2.11. According to this theory, the debonding does occur at the interface but is limited by the interlocking mechanism between concrete and reinforcement lugs which is also responsible for formation of internal or secondary cracks. Beeby (1979) declared the stress transfer length (S_0) to be a function of both concrete cover (c) and the ratio of bar diameter to steel reinforcement ratio $(\frac{\emptyset}{\rho})$. Stress transfer length according to this theory can be given as;

$$S_0 = C_3 c + C_4 \frac{\emptyset}{\rho}$$

Here, C_3 and C_4 are experimentally obtained non-dimensional constants.

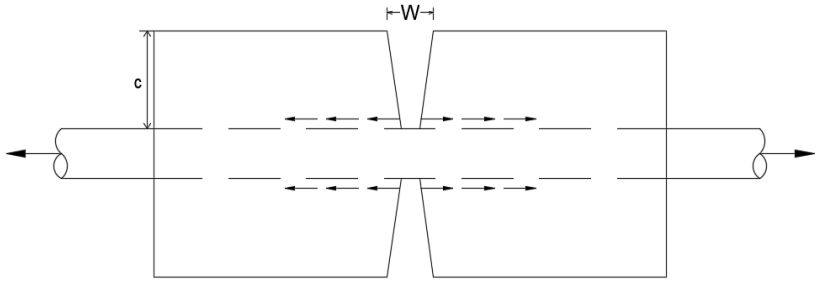

Figure 2.11. Representation of the combination of Slip and No Slip theory (Carino, 1995)

The above mentioned equation was incorporated in BS EN 1992-1-1 (2004) and the expression for maximum crack spacing as under;

$$S_{max} = k_3 c + k_1 k_2 k_4 \frac{\emptyset}{\rho_{c,eff}}$$

where;

c = concrete cover from the surface of concrete to the surface of steel bar

k_1= coefficient taking account of bond properties of bonded reinforcement, taken as 0.8 for high bonded bars and 1.6 for bars with plain surface (like prestressing tendons),

k_2= coefficient which takes account of distribution of strain, taken as 0.5 for bending and 1.0 for pure tension,

k_3, k_4 = coefficients found in National Annex and values are 3.4 and 0.425 respectively.

$\rho_{c,eff} = \frac{A_s}{A_{c,eff}}$ and $A_{c,eff}$ is calculated using $h_{c,eff}$ which is taken as lesser of 250 mm, $h/2$ or $2.5(c + \emptyset/2)$ as per Section 7.3.2 of BS EN 1992-1-1 (2004)

Beeby (2005) carried out critical analysis of the classical theory for prediction of crack spacing basing on experimental data available. Although it was initially thought that the only variable affecting crack spacing is the factor $(\emptyset/\rho)$, Beeby had shown that no particular relationship between the crack spacing and $(\emptyset/\rho)$ existed. However, concrete cover appears to be a comparatively more influential factor in determining crack spacing than $(\emptyset/\rho)$. Its validity is more to the flexural cracking than cracking due to direct tension. Inclusion of cover in the above mentioned equation of Eurocode has served the purpose to some extent.

Above discussion indicates that considerable amount of work has been done for understanding the factors determining crack spacing in end restrained members, however, the factors influencing the crack spacing in edge restrained members are different. Stoffers (1978) was the first to consider the mechanism of cracking in edge or base restrained walls. He related the crack spacing with the wall height and believed that cracks are spaced at 1 to 1.5 times the height of wall. Researchers (ACI Committee 207, 2007; Kheder et al., 1990; Stoffers, 1978) believed that an unreinforced wall restrained at its base will develop full height cracks spaced at 1 to 2 times the height of wall. Provision of horizontal reinforcement in the wall will prevent the cracked faces from moving apart just like the restraining base. It tends to reduce the spacing of cracks since the reinforcement enables the concrete to reach its tensile capacity within a shorter distance. Superimposing the role of reinforcement and the restraining base, Kheder (1997) presented following formula for minimum spacing of primary cracks:-

$$S_{min} = k\rho H/(\rho H + k\emptyset)$$

Where k = 0.57, 0.68, and 0.85 for deformed, indented, and plain steel reinforcement respectively. For secondary cracks, the crack height (Y) should be used in above expression instead of the wall height (H). Based on the experimental evidence; Kheder et al. (1994) also believed that no crack appears within a distance

equal to the wall height, from the free edge of the member. Whereas earlier in BS 8007 (1987), it was suggested that no crack is formed with in 2.4 m of the free edge of a member and the same approach was later adopted in BS EN 1992-3 (2006). Bamforth (2010) also stated that the spacing is mainly influenced by the element geometry (height of member being the critical factor) and reinforcement plays a secondary role in this. Crack spacing is influenced by the combined effects of the restraining base and the steel reinforcement. It is to be noted that in the existing guidelines, the influence of degree of restraint on crack spacing has not been evaluated.

2.6.4 Prediction of Crack Widths

Different approaches are available in various guidelines and codes of practice for calculation of crack widths. There is a consensus among the researchers (ACI Committee 207, 2007; Stoffers, 1978; Bamforth, 2007; Kheder et al., 1990) that the crack width in edge restrained walls varies along the height of the wall and location of maximum crack width varies with the aspect ratio of the walls. According to BS 8007 (1987), crack width is estimated by multiplying crack spacing, S_{max} with the effective strain, ε i.e. $w_{max} = S_{max}\varepsilon$. The effective strain, ε is the strain due to thermal and shrinkage effects less the residual average tensile strain in concrete, as given in equation;

$$\varepsilon = \varepsilon_{te} + \varepsilon_{cs} - 0.5\varepsilon_{ult}$$

where;

ε_{te} = Thermal contraction

ε_{cs} = Total shrinkage strain

ε_{ult} = Ultimate concrete tensile strain

BS 8007 (1987) specified a value of 200 microstrain as ultimate concrete tensile strain (ε_{ult}) and 100 microstrain as the total shrinkage strain (ε_{cs}) which implies that effective strain is actually equal to the thermal contraction (ε_{te}). It further specified that for immature concrete, coefficient of thermal expansion (α) may be reduced to half of its value for mature concrete. This resulted in the expression for maximum crack width under short term effects to be;

$$w_{max} = 0.5S_{max}\alpha T_1$$

It is from above expression that BS 8007 (1987) considered the degree of restraint for immature concrete in a member restrained at its ends to be 0.5. Based on the later research (Beeby 2005) which highlighted the importance of concrete cover and steel reinforcement on crack spacing and width, and also the fact that the crack width is proportional to the crack inducing strain, instead of effective strain for calculation of crack width, the expression for crack width included in BS EN 1992-1-1 (2004) takes into account these aspects. The crack width is obtained as the difference between extension of reinforcement over the spacing and that of the concrete between the cracks (Beeby, 2005). According to BS EN 1992-3, maximum crack width (w_{max}) for both flexural and early thermal and shrinkage cases at the surface of member is estimated by multiplying the maximum crack spacing (S_{max}) with the crack inducing strain ($\varepsilon_{sm} - \varepsilon_{cm}$);

$$w_{max} = S_{max}(\varepsilon_{sm} - \varepsilon_{cm})$$

Model Code (2010) provides an expression for crack width estimation which is apparently based on the Slip theory since it does not include the influence of concrete cover. Model Code (2010) equation for crack width prediction in members subjected to direct tension is as under;

$$w_{max} = \frac{f_{ctm}\phi}{2\tau_{bm}\rho}(\varepsilon_{sm} - \varepsilon_{cm})$$

where; τ_{bm} is the mean bond strength between reinforcing bar and concrete.

ACI Committee 207 (2007) recommends that following expression derived for flexural members by Gergely et al. (1968) may be used for members subjected to axial tension as well;

$$w_{max} = 0.076\sqrt[3]{(d_c A)}Rf_s 10^{-3}$$

Reasonable correlation is observed by the use of above expression (ACI Committee 207, 2007) however, a slightly different equation for members under axial tension is also presented in ACI Committee 224.2R (1997) according to which the maximum crack width is given as;

$$w_{max} = 0.10 f_s \sqrt[3]{d_c A} * 10^{-3}$$

where;

w_{max} = maximum crack width at the surface

d_c = cover measured to the centre of bar (inches)

A = average effective concrete area around a reinforcing bar ($2d_c$ x spacing)

R = distance from neutral axis to the tensile face divided by distance from neutral axis to steel

f_s = calculated steel stress (ksi)

Stoffers (1978) found that the maximum crack width in the case of rigid or non curving restraining members occurs at the top of the walls while for restraining base slabs allowed to curve, the maximum crack width lies at some height above the base slab. However, the basic equation proposed for crack width calculation is as under;

$$w_k = (\frac{\phi f_y^2}{4 f_b E_s})(\frac{1-\rho}{1+\left(\frac{E_s}{E_c}-1\right)\rho})$$

Kheder (1997) presented a concept of change in restraint, in base restrained walls, before cracking (R_b) and after cracking, (R_a). It was confirmed that crack width at any level in the wall is proportional to the tensile strain relieved in the process of cracking. In other words, the crack width depends on the difference of restrained volume change before and after cracking. It was also found that maximum width of crack does not occur at the base rather at a height equal to approximately 10% of the wall length. The change in restraint (R_b - R_a) depends on the aspect ratio of wall, and the point in the wall at which the crack is being considered. Using the finite element analysis, Kheder (1997) presented idealized diagrams to calculate the restraint factors and change in restraint. Following equation was proposed for calculation of maximum crack width in reinforced concrete walls subjected to edge restraint;

$$w_{max} = S_{max}[k_1(R_b - k_2 R_a)\varepsilon_v - {}^{\varepsilon_{ult}}/_2]$$

where;

k_1 = 0.60, a factor to consider the effect of creep in concrete

k_2 = 0.80, a factor to consider any slippage between wall and base

ε_v = Total free volume change.

2.6.5 Cracking Pattern

The information on the extent and orientation of cracks under different forms of restraint is not found in most of the codes and guidance available. Annexure M to BS EN 1992-3 (2006) provides the patterns of cracking likely to be encountered under restrained contraction which are given in Figure 2.12. Despite providing the likely orientation of cracks at different points in the wall, it is also suggested that no crack is formed with in a distance of 2.4 meters from the free edge of a member. Kheder et al. (1994) believed that no crack appears within a distance equal to the wall height, from the free edge of the member. The restraining base has a closing action on the cracks forming in the wall. The crack width is not maximum at the point of maximum restraint mainly because of two reasons; firstly, the base acts to prevent the cracks from opening and secondly, quite a lot of heat is transferred from the wall to the base slab near the joint between two members and therefore the thermal strain is lesser at this point (Bamforth, 2007).

Pattern of cracks formed under end and edge restraint are different. In edge restrained members, the cracks initiate close to the base slab and propagate upwards. However, the location of maximum crack width occurs at some height above the base (Stoffers, 1978; Kheder, 1997). In members having large aspect ratios, the maximum crack width is likely to occur at the top of the wall in the case where the base slab is prevented from curvature (Stoffers, 1978). According to Kheder et al. (1994); (Kheder, 1997) and Bamforth (2010) the maximum crack width is seen to occur at a height approximately 10% of the length of member. The ratio between restraints at the location of maximum crack width location and at the joint was found to have an almost constant value of 0.78 for different aspect ratios (Bamforth, 2007).

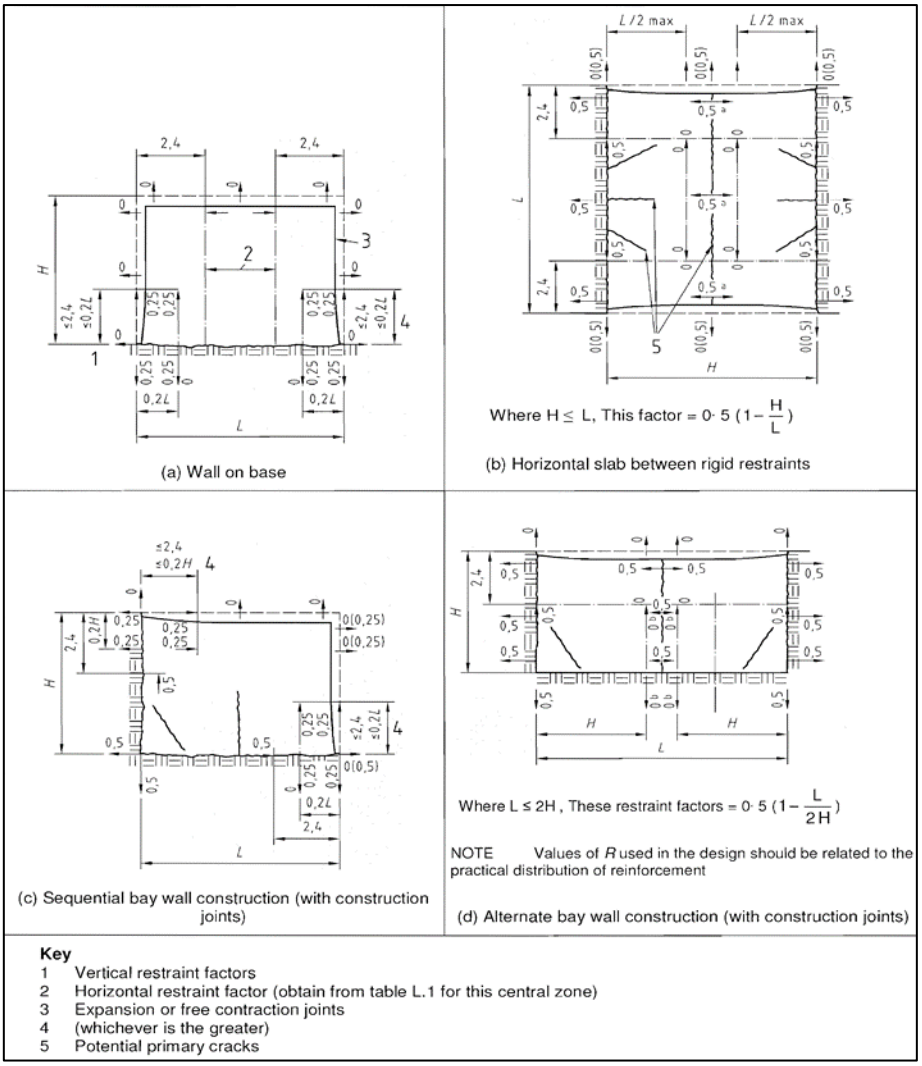

Figure 2.12. Illustration of cracking patterns for members subjected to various types of restraint (BS EN 1992-3, 2006)

2.7 Estimation of Degree of Restraint

Cracking under end restraint is a function of tensile strength, however, in edge restraint the degree of restraint is a primary factor as the restrained and crack inducing strain is a direct consequence of the degree of restraint. Correct estimation of the restraint factors by identifying the factors involved and ascertaining their contribution towards restraint formulation is important. Two aspects in this regard are particularly important; the degree of restraint at the joint between restrained and restraining members, and the variation of restraint at different points along the length and height of the restrained member. There is a consensus among researchers in this field that the degree of restraint is maximum at the joint between the restrained and restraining member along the centreline of the wall, and it reduces over the height and length of

the wall (Carlson et al., 1988; Kheder, 1997; Nilsson, 2003; Bamforth, 2007; Stoffers, 1978). However, Micallef (2017) noticed that the maximum value of restraint may exist at some point above the mid height of the wall, although this may be influenced by the test procedure that was adopted. Brief details of the experimental and analytical work carried out in the past and the guidance available for estimation of restraint factors is given in the following paragraphs.

2.7.1 ACI Method

ACI Committee 207 (2007) report provides a method for calculation of restraint factor primarily based on the relative axial rigidity of the two members. Guidance on the estimation of edge restraint was included in ACI 207.2R-73 (1973) for the first time. The guidance contained in the report was based on the measurements of the structural behaviour of Norris and Hiwassee Dams (Technical Monograph No 67 of Tennessee Valley Authority, 1950) and on the work pertaining to drying shrinkage of large concrete members by Carlson (1937). The restraint factors and their variation along the height of a concrete structure were derived from above mentioned works and published by the US Bureau of Reclamation in 1965 as “Control of Cracking in Mass Concrete Structures” in Engineering Monograph No 34 (Townsend, 1965). The graphs included in this monograph indicated the restraint variation at the centreline, 1/4th and 1/10th of the concrete span or length of the member. This information later adopted by ACI Committee 207 in 1973 has remained unchanged since then in all subsequent ACI reports. The ACI method provides an equation for calculation of the restraint factor at the joint location as under;

$$R_j = \frac{1}{1 + \frac{A_g}{A_F}\frac{E_c}{E_F}}$$

where;

A_g = Gross area of concrete cross section

A_F = Cross sectional area of foundation or other restraining member

E_c = Modulus of elasticity of restrained member concrete

E_F = Modulus of elasticity of foundation or restraining element

The degree of restraint calculated at the joint varies along the height of wall and the restraint at any height (h) in the wall can be calculated based on the length to height ratio $(L\ /\ H)$ of the wall using following equations;

$$K_R = [(L\ /\ H - 2)/(L\ /\ H + 1)]^{h/H} \qquad for\ {}^{L}/_{H} \geq 2.5$$

$$K_R = [(L\ /\ H - 1)/(L\ /\ H + 10)]^{h/H} \qquad for\ {}^{L}/_{H} < 2.5$$

The restraint variation for walls with different length to height ratios was worked out and is given in ACI Committee 207 (2007) report. The calculated restraint factors indicate that the loss of restraint along height is less in walls with higher aspect ratios. Figure 2.13 shows the restraint profiles according to the ACI method;

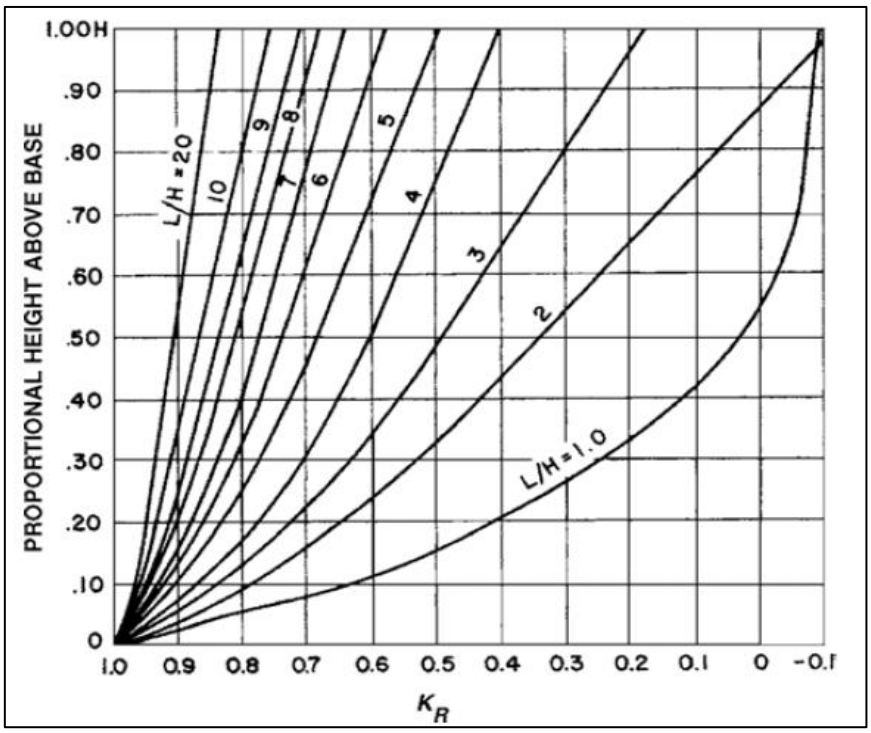

Figure 2.13. Degree of restraint at the wall centreline for different aspect ratios (ACI Committee 207, 2007)

The ACI Committee 207 (2007) report primarily includes the thermal effects and relates more to the mass concrete structures. The volume changes associated with the moisture loss are not taken into account in this report. Another important aspect to note here is that this guidance is based on construction of dams or in other words the massive concrete structures cast on the rock foundation. Because of the way ACI method has evolved, two observations can be made; firstly, the role of internal restraint

was not segregated and thus the adequacy of the application of the findings to thinner sections of concrete needs to be evaluated and secondly, unlike the walls or slabs cast onto existing concrete members, the construction of dams on the rock foundations did not have the continuing steel reinforcement between the two members. Therefore, the slip at the interface or the restraint of slip due to steel dowels is not incorporated in the method.

2.7.2 Eurocode Method

The guidance on estimation of degree of edge restraint is provided in Annexure L to BS EN 1992-3 (2006) and has been adopted from BS 8007 (1987). In the BS 8007 (1987) approach, the effective restraint is assumed to be taken as half of the total restraint to incorporate the influence of internal creep. The restraint linearly varies from zero at the free end to the maximum value of 0.5 at a distance of 2.4 meters from the free end. No cracking is anticipated in this region as found out by Deacon (1973) from observations on different wall segments. This approach is primarily based on approximations and observations on concrete walls and slabs. In BS EN 1992-3 (2006) the degree of moment restraint is recommended to be taken as 1. No detailed method for estimation of restraint factors is provided.

2.7.3 CIRIA C660 Approach

The axial restraint factor for a wall cast on the base slab is expected to vary between 0.3 and 0.7 and therefore a value of 0.5 is suggested by the code for most cases. However, a difference in restraint of 0.1 from this mean value will affect the level of restrained strain by 20% and therefore a more rigorous estimation of restraint factors is necessary (Bamforth, 2007). In CIRIA C660 (2007) the approach adopted in ACI method has been presented and it is stated that due to rapid increase in the modulus of elasticity of concrete, the degree of restraint is likely to reduce with time. A coefficient (K_1) to incorporate the influence of creep has been provided which has a value of 0.65 for both early age and long term analysis. The effective width of restraining slab for calculation of the relative areas of new and old member becomes difficult in some cases. Bamforth (2007) recommended that the relative area may be calculated in proportion to the relative thicknesses, h_n and h_o of the new and old members respectively according to the following principles;

- For a wall cast at the edge of a slab, $A_n/A_o = h_n/h_o$
- For a wall cast remote from the edge of a slab, $A_n/A_o = h_n/2h_o$
- For a slab cast against an existing slab, $A_n/A_o = h_n/h_o$

2.7.4 Work by Schleeh and Stoffers

Schleeh (1962) studied the linear elastic behaviour of walls under edge restraint and analysed the stress distribution along the wall height. Assuming total fixity of the wall edge due to base slab, the restraint factors for walls of varying aspect ratios were worked out. He was the first to identify the influence of curvature in the restraining base on stress distribution in the wall. It was found that if the restraining member is rigid enough not to develop any curvature, the stress variation along the height will be less which in other words means that the effect of restraint in the higher parts of the wall would be relatively more compared to the case where the base can curve. When the base is allowed to develop curvature, the top fibres of the wall might undergo compression as well. Thus it can be conveniently deduced that flexibility of the restraining member influences the restraint variation and crack widths in a wall. Stoffers (1978) presented the curvature theory and developed expressions for both curved and non-curved cases. He stated that the curvature in the base slab can be used as a crack controlling measure and also that the amount of steel reinforcement in the wall can be reduced in the higher parts of the wall since the stress is lesser there. Work by both researchers did not, however, describe the mechanism of restraint formulation or its influencing factors.

2.7.5 Work by Kheder

Kheder conducted experimental and analytical investigations (Kheder et al., 1990; Kheder et al., 1994; Kheder, 1997) on the cracking behaviour of edge restrained reinforced concrete walls. He stated that the restraint at the joint can be influenced by roughness of concrete surface, relative volume change between base and wall, amount of steel reinforcement dowels and the rigidity of base slab. Concept of change in restraint before and after cracking was introduced for calculation of crack widths. Idealized diagrams for change in restraint in walls of different aspect ratios have been presented by Kheder (1997). He analysed the influence of vertical steel dowels on restraint using quite low percentages (0.15 and 0.5%) of steel reinforcement and

concluded that the dowels slightly influenced the distribution of cracks or the crack spacing. From his work, it can be deduced that crack spacing in edge restrained walls is influenced by the restraining base or in other words, the magnitude of restraint imposed has an impact on the crack spacing.

2.7.6 Analytical and Numerical Investigations

Numerous researchers have conducted analytical and numerical investigations on the early age cracking in edge restrained walls. Nilsson (2003) highlighted the significance of accuracy in determination of degree of restraint in identifying the risk of cracking. He developed a semi analytical technique based on the compensation plane method using the linear elastic theory for determination of restraint factors and their variation in walls cast on a slab. The developed expressions (given below) incorporate the correction factors for slip at the joint, boundary restraint and resilience;

$$\gamma_R = \delta_{res}\delta_{slip} - \gamma_R^t - \gamma_R^{ry} - \gamma_R^{rz}$$

where;

δ_{res} = high wall effect, resilience

δ_{slip} = slip in joint effect

γ_R^t = translational restraint part

γ_R^{ry} = rotational restraint part for rotation around the *y*-axis (the vertical axis)

γ_R^{rz} = rotational restraint part for rotation around the *z*-axis (the horizontal, transverse axis)

Al-Gburi et al. (2012) conducted finite element modelling of different forms of restraint to ascertain the location of critical restraint and estimation of risk of cracking. Focus of most of the finite element studies has been the cracking behaviour and not the estimation of degree of restraint. Kianoush et al. (2008), Pettersson et al. (2001a) and Pettersson et al. (2001b) used finite element analysis to study the development of cracks and crack widths in reinforced concrete walls under edge restraint. Klemczak et al. (2013) carried out a comparative study of three methods of restraint estimation (ACI, Eurocode and Nilsson methods) and concluded that; the Eurocode approach is useful only when assuming that the restraining member does not deform; the ACI approach is simple and easy to use with results being similar to those obtained from

numerical analysis, however, the approach focuses mainly on the volume changes due to thermal effects, since it has been developed for mass concrete; the method given by Nilsson (2003) is quite complex and a little difficult to use - also, its application is limited and only applicable to wall elements having aspect ratios of less than 5.

2.7.7 Review of the Presented Methods / Works

Critical review of the work presented above reveals that the factors involved in the mechanism of restraint formulation have not been fully identified and incorporated in the available methods. One important reason for this may be the use in previous experimental investigations of a steel member as the restraining base; although this may simulate edge restraint, the behaviour of the concrete base in terms of thermal contraction, heat transfer and the role of steel dowels cannot realistically be depicted by the steel members. In most practical cases, a wall is cast onto an existing concrete member and a certain amount of vertical steel reinforcement is present at the joint. As of yet, the contribution of this reinforcement in defining the degree of restraint cannot be assessed from the existing research / the existing design guidance expressions. Moreover, majority of the work has focussed on the restraint effects during early age and the influence of restraint during long term is not ascertained. No experimental evidence of change in restraint with time has been provided by researchers in the past, however, Micallef (2017) did find that the restraint increased with time, proposing that this was due to the reduction of wall stiffness after cracking.

2.8 Conclusions

The review of previous research presented in this chapter was aimed at identifying the gaps in current state of knowledge regarding the behaviour of reinforced concrete members under edge restraint. Guidance for estimation of thermal drop and various shrinkage estimation models available in different codes / guidelines have been evaluated. Cracking theories presented by researchers in the past and techniques available for prediction of crack spacing and crack width have been analysed. The behaviour of members under end, edge and combined restraint have been evaluated and compared to identify the differences between edge and end restraint. Methods available in different codes for estimation of degree of restraint are also reviewed. Previous experimental research on edge restrained members have

also been consulted to understand the identified contributory factors which influence the degree of restraint. Based on the shortfalls or the gaps identified in the guidance available on the behaviour of edge restrained members, the experimental methodology was developed which is presented in Chapter 3. From the reviewed literature, following important conclusions highlighting the gaps in the current state of knowledge can be drawn;

- Methods for estimation of degree of restraint do not incorporate all contributory factors influential in formation of restraint. Major factors influencing the edge restraint mechanism include relative volume change between wall and base, vertical steel dowels at the joint, geometry of the members, concrete strength, wall height and the length to height ratio of the walls.
- Considerable amount of steel reinforcement continuing from the restraining base to the wall is always present, however, its influence on degree of restraint, crack spacing and crack width has not been analysed in the experimental research in detail. Use of steel sections for imposing restraint do not realistically depict the contribution of steel dowels.
- Previous experimental research on edge restrained reinforced concrete utilized steel members for imposing edge restraint. However, in practice the reinforced concrete walls or members are cast against an existing concrete member. In order to correctly understand the behaviour of the two members, there is a need to develop the experimentally methodology where in both restrained and restraining members are built using concrete thus simulating a scenario more similar to the real time cases.
- Due to contraction in the wall, the restraining base slab can develop the curvature. Due to this phenomenon, the influence of restraint is reduced. This indicates that a scenario where the base slab is prevented against warping represents a more severe case of edge restraint and therefore the experimental methodology developed to understand the behaviour of edge restrained walls should incorporate the mechanism for clamping the base slab to the floor.
- Degree of restraint at the interface between restrained and restraining members is independent of the wall aspect ratio. However, its variation along the wall height is dependent on the wall height and the length to height ratio

of the wall. In order to clearly observe the variation of degree of restraint along the wall height, it is important to select the wall height which can distinctly manifest the variation between the surface strains at the top and bottom of the wall.

- When CEM I cement is used in concrete, the amount of heat generated is more compared to the cements partly replaced with other supplementary materials. Thus use of CEM I provides an extreme case as far as the temperature development and thermal strain is concerned. The experimental methodology developed to study the degree of restraint in walls should, therefore utilize a concrete mix with CEM I.

Chapter 3

Experimental Program

3.1 Introduction

This chapter describes the methodology of the experimental work carried out to develop a better understanding of the behaviour of reinforced concrete walls restrained along their edge. The rationale for selection of the specimen geometries and mix design is provided. The details of the tested specimens including concrete cover, steel reinforcement provided in both restrained and the restraining elements and mechanism adopted for prevention of curvature in the restraining base are discussed. Tests carried out for obtaining the mechanical properties of the materials used, instrumentation employed for gathering the desired data and the procedure adopted for the tests are also described.

In order to investigate the influence of vertical steel reinforcement on the mechanism of degree of restraint, an experimental research programme looking at the behaviour of edge restrained reinforced concrete walls has been undertaken. The experimental study primarily considers tests on four reinforced concrete walls cast onto previously constructed and hardened reinforced concrete bases. In addition to the vertical steel reinforcement, the wall thickness was also varied in the tests to analyse the influence of the relative geometry of both members on the degree of restraint. During the period of testing, the average temperature in the laboratory varied between 14 and 24°C, and the average relative humidity ranged between 46 and 62%.

3.2 Aims of Experimental Work

This experimental program was aimed at developing a better understanding of the behaviour of edge restrained reinforced concrete walls with the focus on following objectives:

- Determining the role of the vertical steel reinforcement dowels extending from the base into the walls on the mechanism / development of restraint.
- Identifying the importance of using a reinforced concrete base in order to correctly understand the phenomenon of edge restraint.

- Analysing the influence of the relative geometry of the restrained and restraining members on the degree of restraint
- Understanding the initiation and development of cracks due to restraint of imposed strains during early age and long term.
- Evaluating the influence of wall thickness on temperature drop.

3.3 Important Design Considerations

Very few experimental studies on the cracking behaviour of edge restrained walls are available in the literature. In the process of designing the specimens and the experimental set up, it was deemed important to implement the following design considerations;

- In order to impose the restraint to the bottom edge of the wall, the base slab should be cast first, cured and allowed to develop its mechanical properties for a period of 28 days and then the wall should be cast on to it.
- The length of the walls should be sufficient to allow the development of at least two primary cracks according to the guidance on crack spacing available in the currently available literature (Stoffers, 1978; Kheder et al., 1994).
- The concrete mix should be designed using the CEM I as it provides the maximum heat of hydration and therefore would provide sufficiently large thermal drop. Moreover, a realistic value of water to cement ratio (commonly used in concrete mixes) should be adopted.
- The walls should be sufficiently high to allow any variation in restraint over the height of the wall to materialise (Stoffers, 1978; Kheder et al., 1994).
- The base should be prevented from developing curvature due to the shrinkage and thermal contraction occurring in the wall.
- The thermal drop in the walls, from peak temperature to ambient should be large enough to cause an appropriate amount of imposed strain normally encountered in the construction practices.

3.4 Test Set Up

As part of this experimental investigation, four walls were tested and each test continued for a period of 12 weeks. In each test, reinforced concrete wall was cast

onto an already cast and hardened reinforced concrete base. In phase 1, the reinforced concrete base slab was cast and cured for up to 14 days. In phase 2, once the slab was at least 28 days old, the wall was cast onto it. The base slab was cast and allowed to develop its material properties for a period of 28 days. By this time, the concrete in the base slab had hardened and hence, the existing slab imposed a restraint to the volume changes occurring in the newly cast wall. The walls had a length to height ratio (L/H) of 4, which is representative of the range of commonly used aspect ratios in practice. In first two tests, the walls had a larger cross sectional area (240000 mm^2) than that of the base slab (204000 mm^2) whereas in the last two tests, the cross sectional area of the walls (160000 mm^2) was lesser than that of the base slab (204000 mm^2). The test set up adopted for the experimental investigation is shown in Figure 3.1.

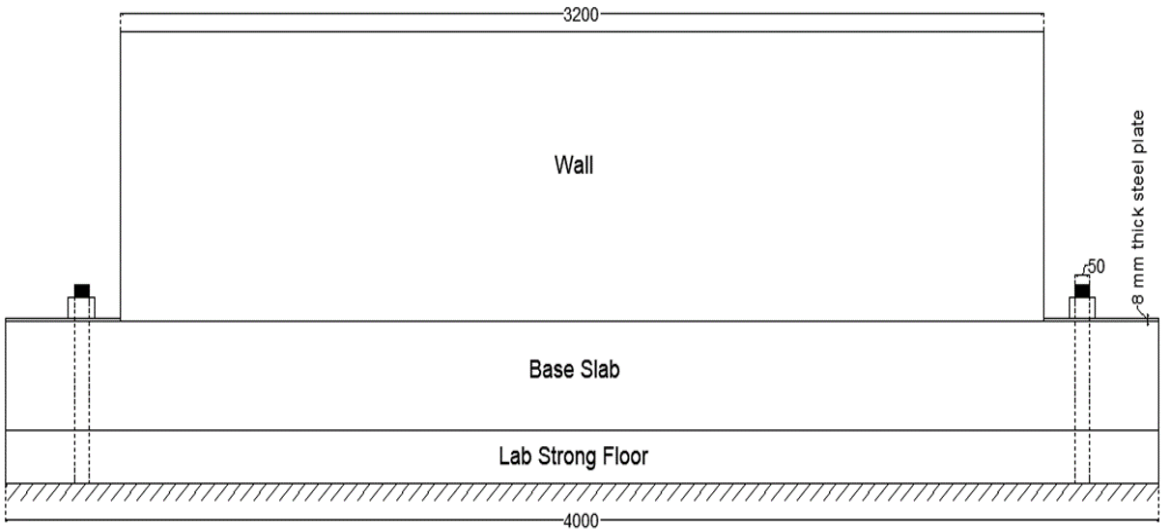

(a)

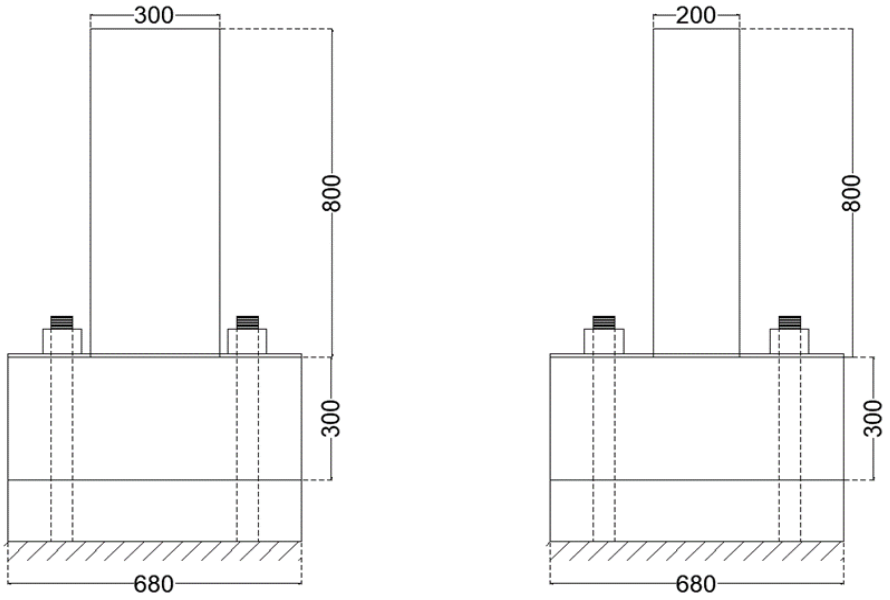

(b)

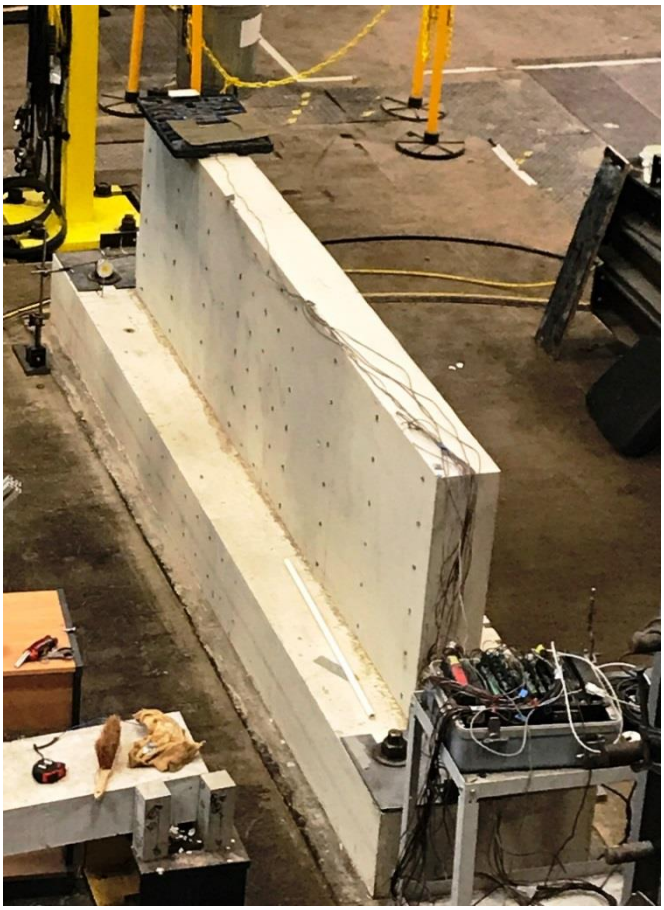

(c)

Figure 3.1. The test set up: (a) Elevation of the test specimens; (b) cross section of the test specimens; (c) a view of the tested specimen

The strains and temperatures in both the wall and slab were monitored for a period of eight weeks after the wall had been cast. Concrete surface strains were measured using DEMEC gauges, while temperatures were monitored using K type exposed welded tip thermocouples. For these tests, it was decided to prevent the development of curvature in the base slab, hence, both ends of the slab were clamped to the strong floor of the laboratory using two-off 50 mm diameter steel studs as shown in Figure 3.1. An 8 mm thick steel plate was also placed on top of the slab ends to distribute the force applied by tightening the nuts. The upward deflection at the slab ends was monitored using analogue deflection gauges at both ends of the base.

3.5 Design of Specimens

In previously available experimental investigations, Stoffers (1978) and (Micallef, 2017) used steel members as restraining base to impose the restraint on newly cast reinforced concrete walls. The choice of steel members was made in these studies because the steel was not prone to time dependent changes like creep and shrinkage and also it facilitated the data analysis. However, in this investigation it was deemed necessary to adopt a reinforced concrete restraining element primarily because it represents the real time problem of restraint induced cracking. Moreover, the obtained results are indicative of the fact that the volume changes occurring in the newly cast wall have an influence on the volume change of the restraining base which should be essentially incorporated in the estimation of the degree of edge restraint.

Preliminary calculations based on the guidance on crack spacing available in BS EN 1992-3 (2006), CIRIA C660 (2007) and recommendations of Stoffers (1978) indicated that for the development of at least two primary cracks, the wall length should be kept as 3000 mm. Another influencing factor in deciding the dimensions of base slab and the wall was the layout of the laboratory strong floor. The wall height of 800 mm was selected so that the variation of restraint along the height of wall can be clearly noticed. Moreover, it was planned that a length to height ratio within a range commonly adopted (between 2 and 8) in concrete pours on the site should be adopted. The selected length and height of the walls resulted in a length to height ratio of 4. Width of the base slab was also slightly influenced by the location of the strong floor studs, however, CIRIA C660 (2007) recommendations for effective slab width were incorporated. It was decided that the wall thickness should be kept within a range

where the internal restraint due to thermal differential between the core and the surface of the wall does not become significant. Moreover, the thickness and height of the wall was selected so as to provide a vertical steel reinforcement ratio close to 1% and 1.5% in test 2 and 4 respectively. The wall thickness in the case of test 1 and 2 was 300 mm and in test 3 and 4 it was reduced to 200 mm. Wall thickness was reduced to analyse the influence of the relative geometry of the members on axial rigidity and the degree of restraint. The dimensions of both wall and slab for each test are indicated in Figure 3.1 above.

The details of the concrete cover and the reinforcement provided in the wall as well as in the base slab for each test are shown in Figure 3.2. The base slab was reinforced, on both top and bottom faces, longitudinally with 12 mm diameter steel reinforcement bars spaced at 100 mm and in the lateral direction with 8 mm diameter steel reinforcement bars spaced at 200 mm. In the test 1 and 3, the walls had no vertical steel reinforcement which meant that there were no dowels at the wall – slab joint. In test 2 and 4, 16 mm diameter steel reinforcement bars spaced at 150 mm were used as the vertical steel reinforcement in the walls. In all tests, the walls were reinforced horizontally with 10 mm diameter steel reinforcement bars with a spacing of 180 mm in each face.

For identification purposes, the specimens were assigned a code ‘T#X’ comprising two parts. First part ‘T#’ indicates the test number e.g. T1 denotes Test 1. The second part ‘X’ indicates the element i.e. base slab (denoted by letter ‘B’) or wall (denoted by letter ‘W’). For instance, ‘T2W’ indicates the wall from test 2 and ‘T4B’ represents the base slab from test 4.

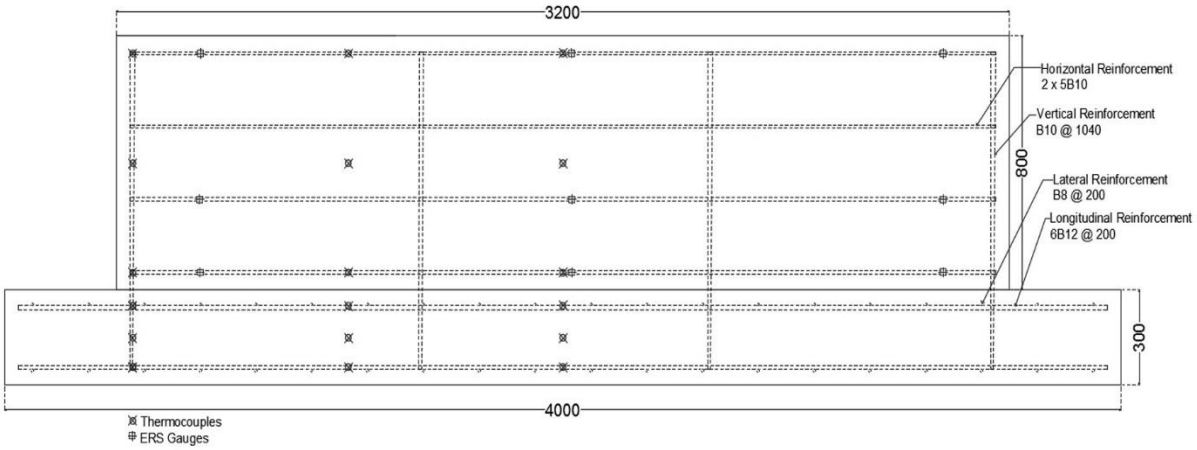
3200
Horizontal Reinforcement
2 x 5B10
Vertical Reinforcement
B10 @ 1040
800
Lateral Reinforcement
B8 @ 200
Longitudinal Reinforcement
6B12 @ 200
300
4000
Thermocouples
ERS Gauges

(a)

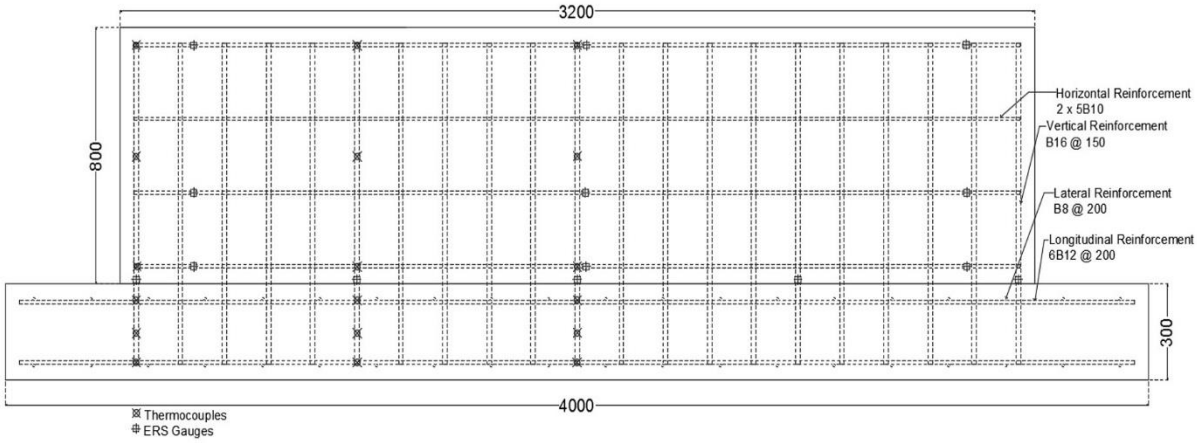
3200
800
Horizontal Reinforcement
2 x 5B10
Vertical Reinforcement
B16 @ 150
Lateral Reinforcement
B8 @ 200
Longitudinal Reinforcement
6B12 @ 200
300
4000
Thermocouples
ERS Gauges

(b)

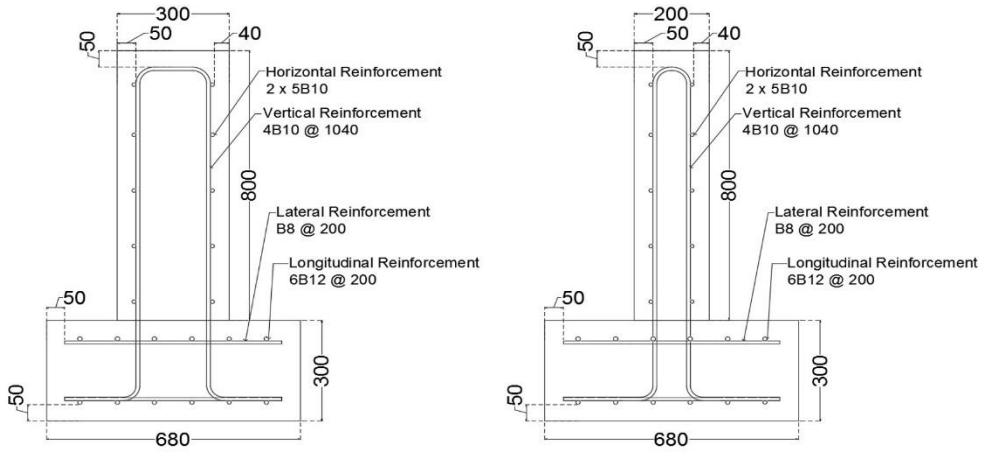
300
50
40
50
Horizontal Reinforcement
2 x 5B10
Vertical Reinforcement
4B10 @ 1040
800
Lateral Reinforcement
B8 @ 200
Longitudinal Reinforcement
6B12 @ 200
50
50
300
680
200
50
40
50
Horizontal Reinforcement
2 x 5B10
Vertical Reinforcement
4B10 @ 1040
800
Lateral Reinforcement
B8 @ 200
Longitudinal Reinforcement
6B12 @ 200
50
50
300
680

(c)

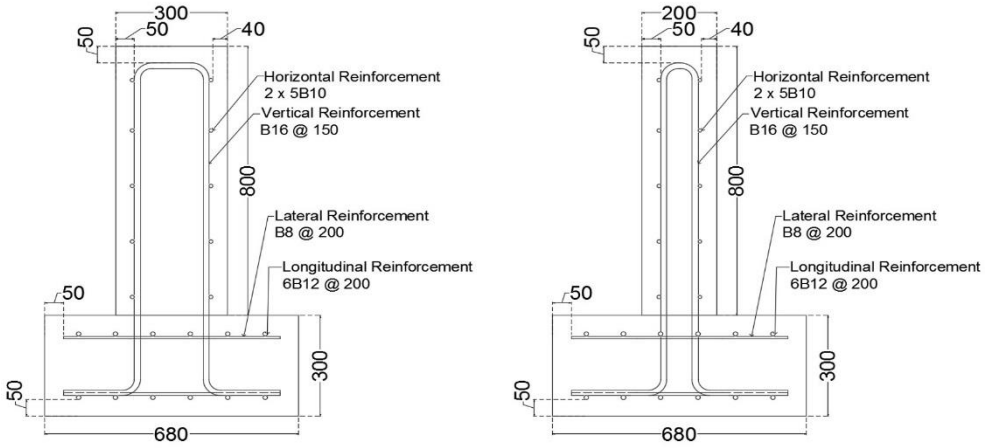

(d)

Figure 3.2. Details of steel reinforcement and cover: (a) Longitudinal Section of Test 1 and 3; (b) Longitudinal Section of Test 2 and 4; (c) Cross Section of Test 1 and 3; (d) Cross Section of Test 2 and 4

3.6 Material Properties and Instrumentation

3.6.1 Concrete Mix Design

Concrete mix for the tests was designed according to the European mix design standards and in accordance with the (BS EN 206, 2013). Casting of each reinforced concrete element in a test i.e. wall or slab, required approximately one cubic meter of concrete. Design strength of 40 MPa and slump class S2 was selected for the concrete mix. A water to cement ratio (*w/c*) of 0.45 was specified for the mix. The mix composition is given in Table 3.1. The cement used in this work was CEM I (52.5 N) conforming to the requirements of BS EN 197-1 (2011). Naturally occurring limestone crushed aggregate obtained from Horton quarry site with a maximum aggregate size of 20 mm was used. The sand used in this work was obtained from Wakefield quarry site. Owing to the quantity of concrete required for casting of each element, it was decided to get one cubic meter of ready-mixed concrete from Hanson Concrete, Leeds according to the mix composition specified. Moreover, a trial mix was also prepared at the University of Leeds laboratory before the start of the first test and the strength and shrinkage properties were later compared to those obtained from the ready mixed concrete used in the test 1 and 2. Comparison of compressive strength and shrinkage obtained from the trial mix and the ready mixed concrete is given in Figure 3.3. It was

found that the ready mixed concrete displayed higher compressive strength and more shrinkage strain than the trial mix prepared at the laboratory.

Table 3.1. Composition of the concrete mix

Ingredients	Quantity (kg/m^3)
Cement (CEM I)	385
Water	175
Fine Aggregate	730
Coarse Aggregate	1364
Admixture (VS1000)	1.93

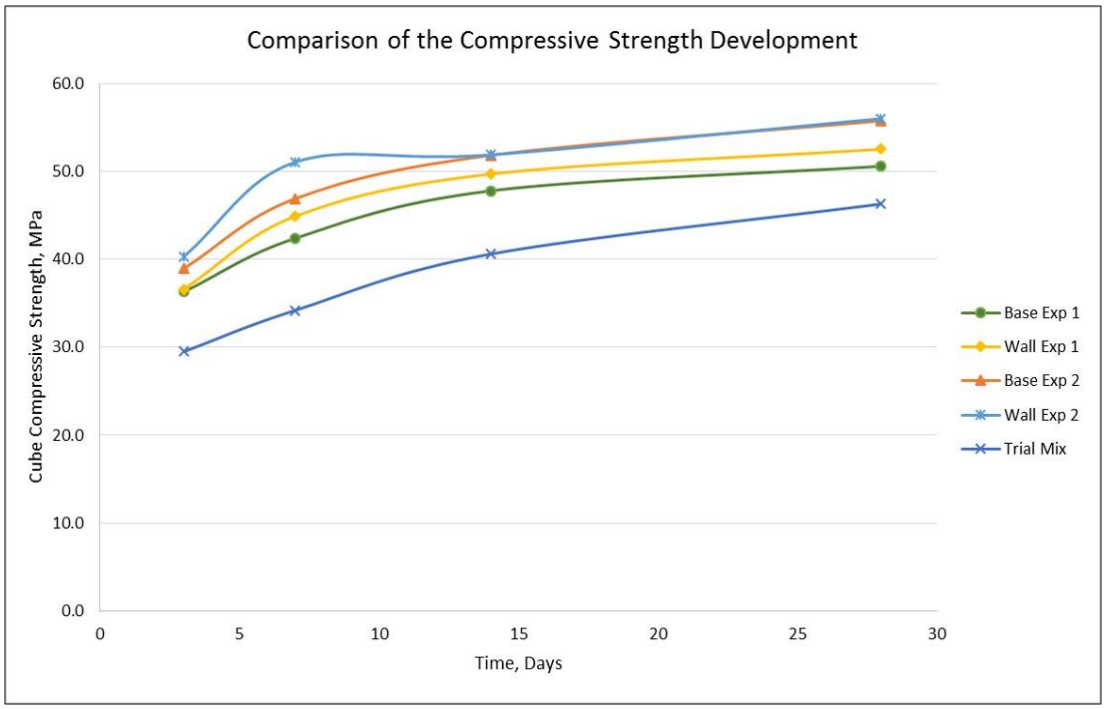

(a)

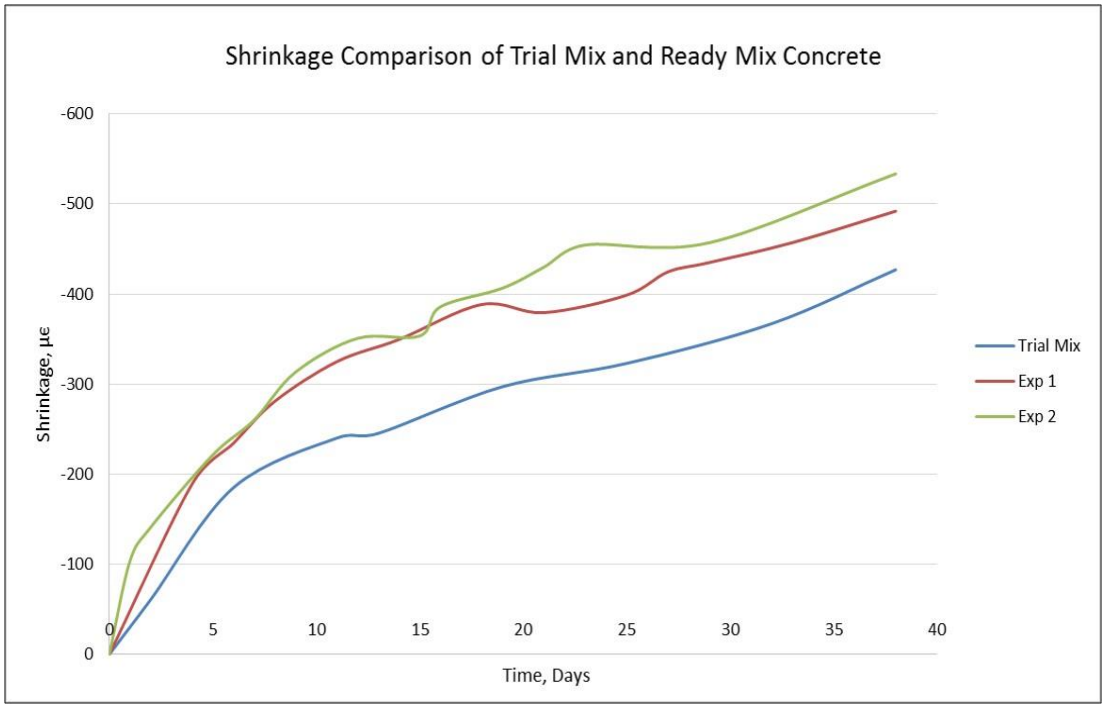

(b)

Figure 3.3. Comparison of the concrete properties obtained from ready mix concrete and the trial mix prepared at the laboratory: (a) Compressive strength; (b) Shrinkage strain

3.6.2 Environmental Conditions at the Laboratory

Tests were conducted inside the laboratory at the University of Leeds. The temperature and the relative humidity in the laboratory were recorded during the test durations and was later incorporated in the calculation of shrinkage using different shrinkage prediction models. The comparison of the measured shrinkage from the concrete prisms and the predicted shrinkage using different models is given in Chapter 4. The ambient temperature and the relative humidity recorded in the laboratory near the test specimens is given in Figure 3.4 below.

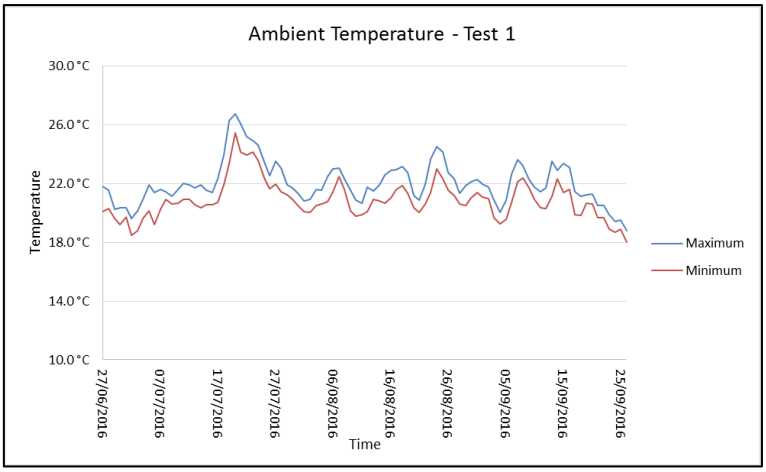
Ambient Temperature - Test 1
30.0 °C
26.0 °C
22.0 °C
18.0 °C
14.0 °C
10.0 °C
Temperature
27/06/2016
07/07/2016
17/07/2016
27/07/2016
06/08/2016
16/08/2016
26/08/2016
05/09/2016
15/09/2016
25/09/2016
Time
Maximum
Minimum

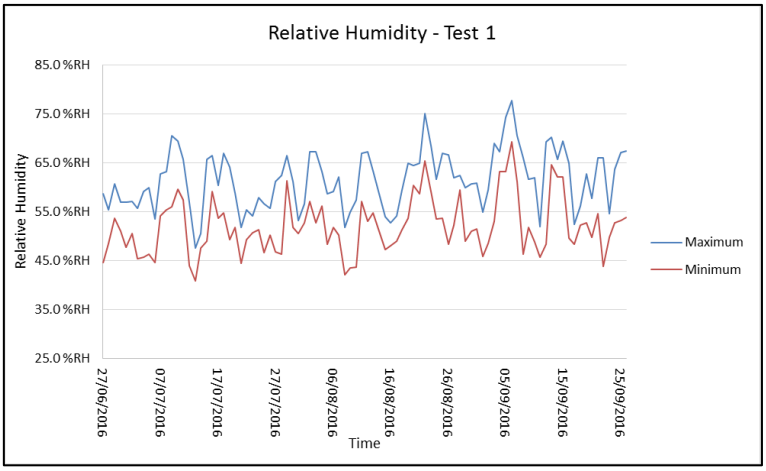
Relative Humidity - Test 1
85.0 %RH
75.0 %RH
65.0 %RH
55.0 %RH
45.0 %RH
35.0 %RH
25.0 %RH
Relative Humidity
27/06/2016
07/07/2016
17/07/2016
27/07/2016
06/08/2016
16/08/2016
26/08/2016
05/09/2016
15/09/2016
25/09/2016
Time
Maximum
Minimum

(a)

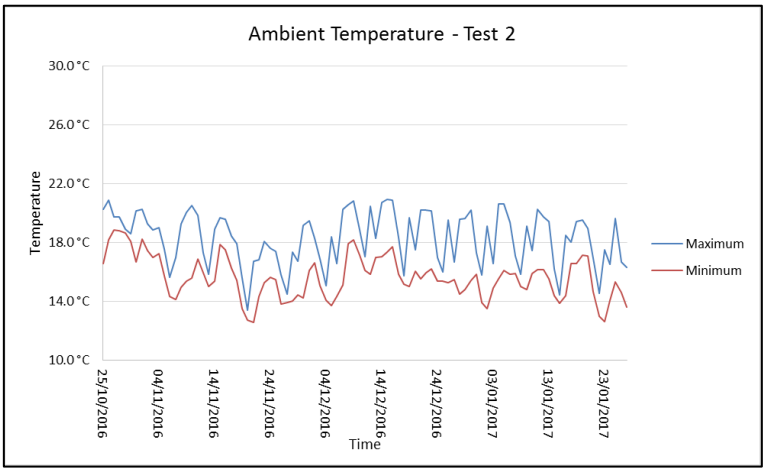
Ambient Temperature - Test 2
30.0 °C
26.0 °C
22.0 °C
18.0 °C
14.0 °C
10.0 °C
Temperature
25/10/2016
04/11/2016
14/11/2016
24/11/2016
04/12/2016
14/12/2016
24/12/2016
03/01/2017
13/01/2017
23/01/2017
Time
Maximum
Minimum

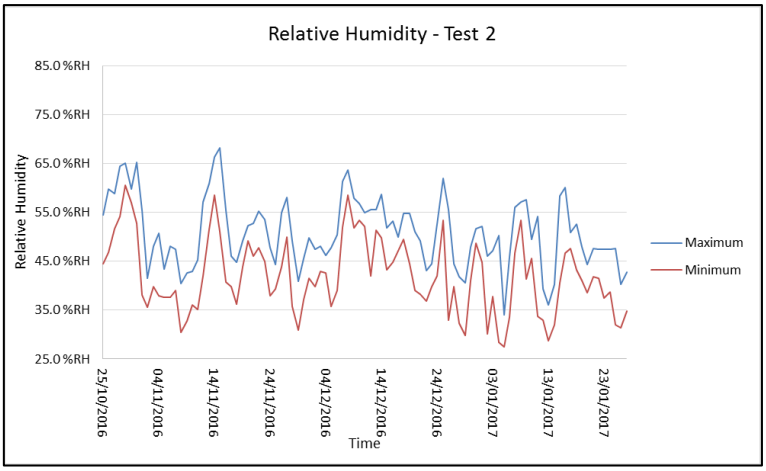
Relative Humidity - Test 2
85.0 %RH
75.0 %RH
65.0 %RH
55.0 %RH
45.0 %RH
35.0 %RH
25.0 %RH
Relative Humidity
25/10/2016
04/11/2016
14/11/2016
24/11/2016
04/12/2016
14/12/2016
24/12/2016
03/01/2017
13/01/2017
23/01/2017
Time
Maximum
Minimum

(b)

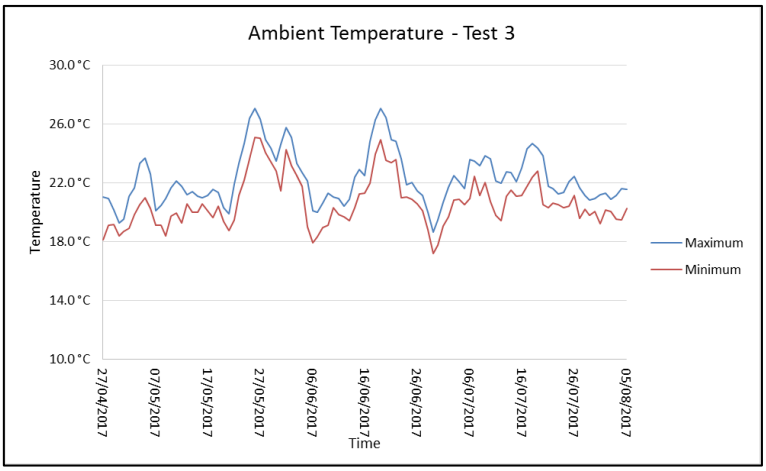
Ambient Temperature - Test 3
30.0 °C
26.0 °C
22.0 °C
18.0 °C
14.0 °C
10.0 °C
Temperature
27/04/2017
07/05/2017
17/05/2017
27/05/2017
06/06/2017
16/06/2017
26/06/2017
06/07/2017
16/07/2017
26/07/2017
05/08/2017
Time
Maximum
Minimum

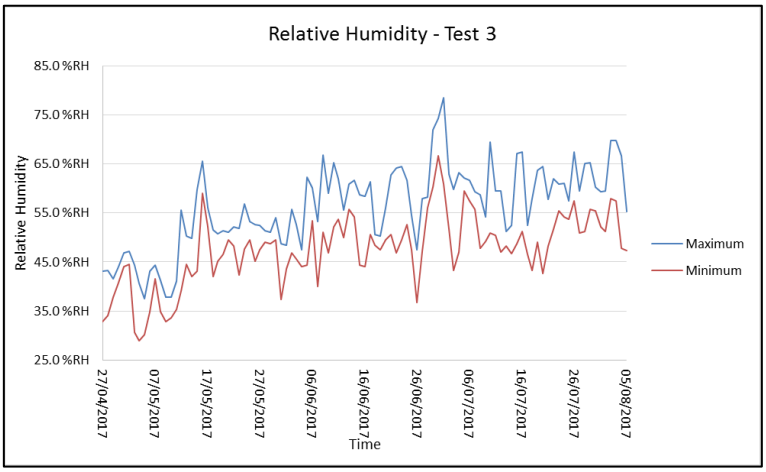
Relative Humidity - Test 3
85.0 %RH
75.0 %RH
65.0 %RH
55.0 %RH
45.0 %RH
35.0 %RH
25.0 %RH
Relative Humidity
27/04/2017
07/05/2017
17/05/2017
27/05/2017
06/06/2017
16/06/2017
26/06/2017
06/07/2017
16/07/2017
26/07/2017
05/08/2017
Time
Maximum
Minimum

(c)

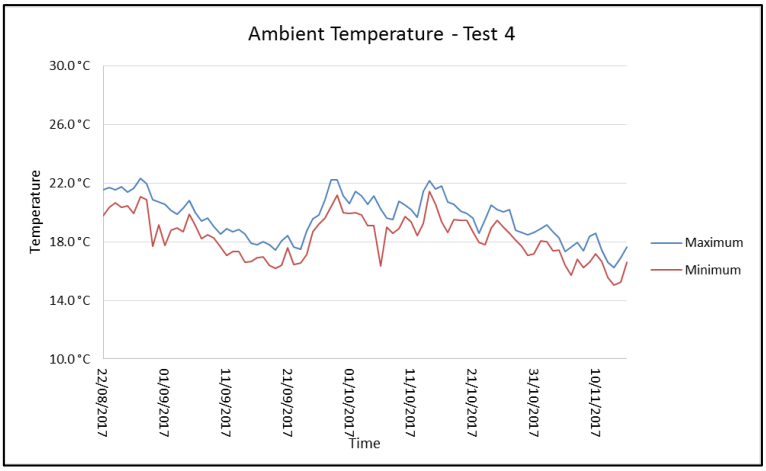

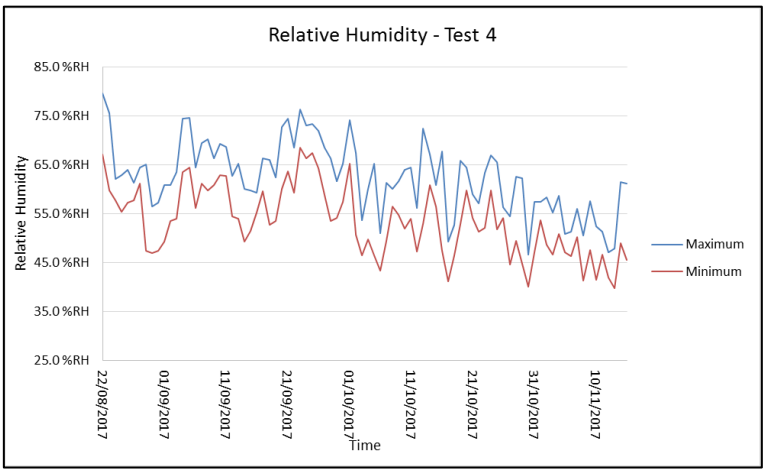

(d)

Figure 3.4. Ambient temperature and relative humidity recorded during the tests at the laboratory: (a) Test 1; (b) Test 2; (c) Test 3; (d) Test 4

3.6.3 Concrete Properties

The compressive strength, splitting tensile strength and the modulus of elasticity of each batch of concrete were determined in the laboratory. All the specimens were moist cured inside a curing room (99% relative humidity). The samples were tested to obtain the compressive strength of concrete according to the procedure specified in BS EN 12390-3 (2009). Before testing, the surface of the samples was wiped clean and the specimens were left to dry for at least 4 hours in the laboratory. The load was increased at a constant rate of 3 kN/sec and the failure loads were recorded (Pictures of the tests are shown in Figure 3.5). From the failure loads, the cube and cylinder strengths were calculated. The compressive strength of each concrete mix was determined using 100 mm cubes at 3, 7, 14 and 28 days. Figure 3.6

shows the development of compressive strength with time for each batch of concrete. The cylinder compressive strength and modulus of elasticity of each mix were also obtained using 150 x 300 mm cylinders at the age of 28 days. Average cylinder compressive strength obtained for each batch of concrete is given in Table 3.2.

Figure 3.5. Cube tests for compressive strength

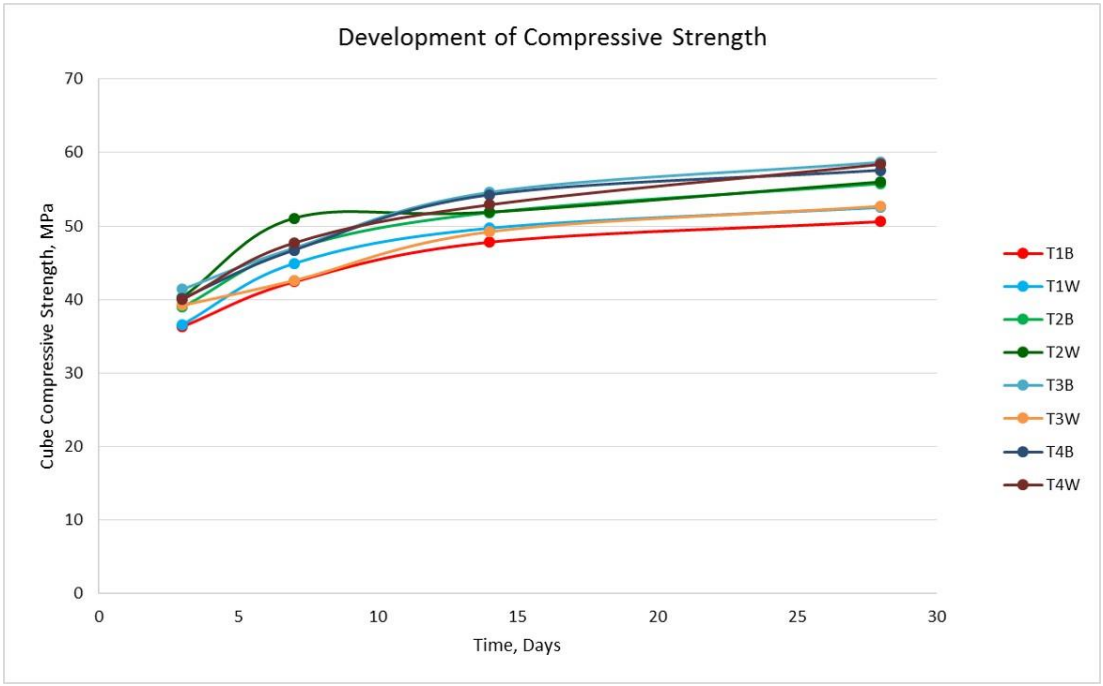

Figure 3.6. Development of the cube compressive strength

Table 3.2. Cylinder compressive strength of the concrete

Concrete Batch	28 Days Cylinder Compressive Strength (MPa)
T1B	40.5
T1W	42.0
T2B	44.6
T2W	44.8
T3B	43.3
T3W	40.0
T4B	48.6
T4W	46.4

To determine the direct tensile strength of concrete, concrete bobbins (75 x 365 mm) were used. Indirect tensile strength of concrete was obtained using the splitting tensile strength test on 150 x 300 mm cylinders (Test pictures are given in Figure 3.7). A compressive load was applied along the cylinder length as specified by BS EN 12390-6 (2009). The specimen was initially fixed in a special jig which ensured the sample was correctly located and the load was applied at two points along the circumference of the cylinders. After the samples were placed in the testing machine, the compressive load was applied at a constant rate of 0.2kN/sec until failure and the failure load (P) was recorded. The tensile splitting strength (f_{spt}) was calculated in MPa using the following equation:

$$f_{spt} = 2\ P\pi\ L\ D$$

where; L and D are the length and diameter of the test specimen in mm, respectively.

Figure 3.7. Splitting tensile strength test

Figure 3.8 shows the development of indirect or splitting tensile strength with time for each batch of concrete. The direct strength tests were also carried out using the bobbins at the age of 28 days as shown in pictures given in Figure 3.9. The direct strength obtained was compared to the indirect strengths and the comparison along with the variation between them is given in Table 3.3. BS EN 1992-1-1 (2004) suggests that direct or axial tensile strength should be taken as 90% of the splitting tensile strength whereas the data in Table 3.3 indicates that the direct tensile strength

obtained is approximately 68% of the splitting strength. Although determination of direct tensile strength has its inherent inaccuracies as highlighted in Section 2.6.1, yet it appears that the factor of 0.9 as suggested by the Eurocode is perhaps too high.

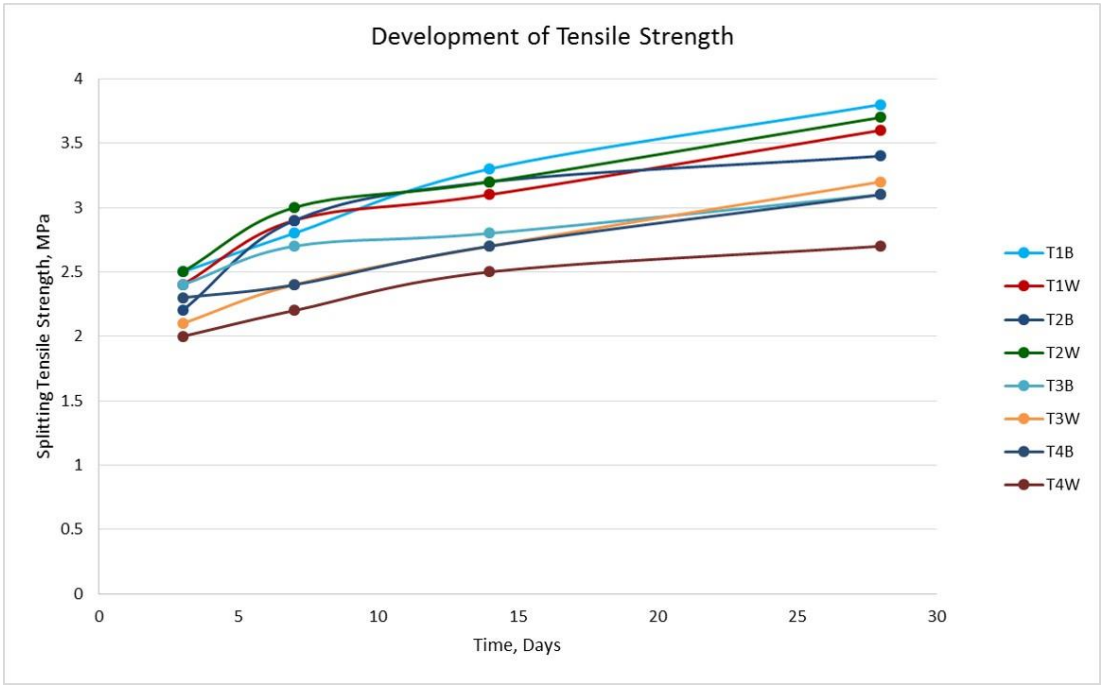

Figure 3.8. Development of the tensile strength of concrete

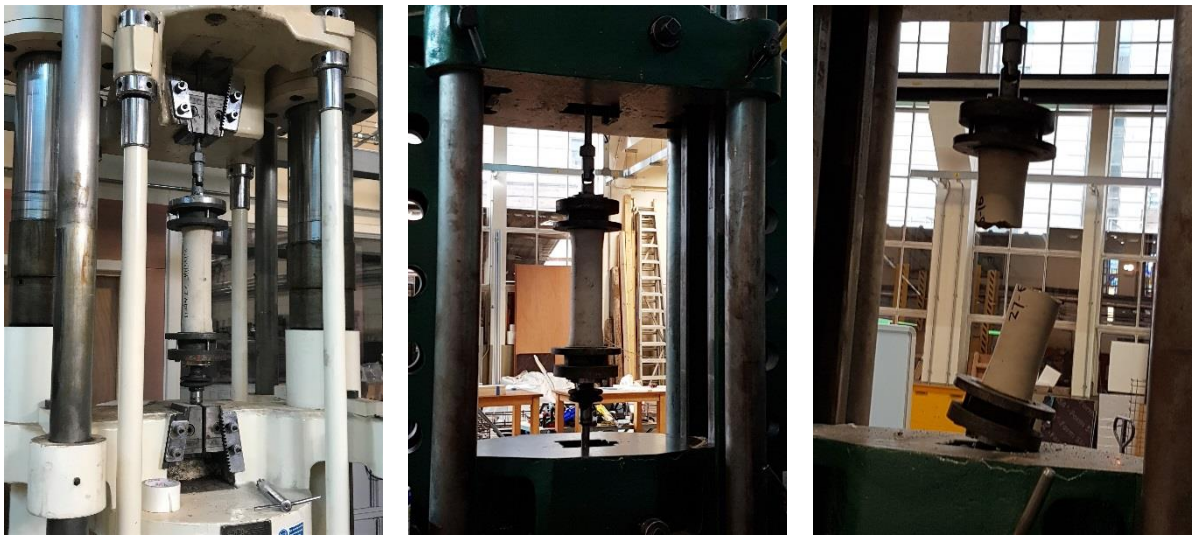

Figure 3.9. Tests on concrete bobbins for direct tensile strength

Table 3.3. Comparison of splitting and direct tensile strength

Concrete Mix	Splitting Tensile Strength (MPa)	Direct Tensile Strength (MPa)	Variation (%)
T1B	3.8	2.8	26.3
T1W	3.4	2.1	38.2
T2B	3.6	1.9	47.2
T2W	3.7	2.5	32.4
T3B	3.1	1.9	38.7
T3W	3.2	2.2	31.3
T4B	3.1	2.0	35.5
T4W	2.7	1.6	40.7

Four concrete prisms (75 mm x 75 mm x 200 mm) as shown in Figure 3.10 were used to obtain the free shrinkage for each batch of concrete. In all cases, these prisms were cured under the same environmental conditions as their respective wall and slab elements. DEMEC studs were fixed on two opposite faces of each prism and the measurements were taken using 150 mm DEMEC gauge. The prisms were stored next to the tested walls to provide similar temperature and humidity conditions as applicable for the tested walls. Average value of the shrinkage measured from four prisms was taken as the shrinkage strain for a particular batch of concrete.

Figure 3.10. Concrete prisms for shrinkage

Modulus of elasticity of concrete was obtained for each batch of concrete through tests on 150 x 300 mm cylinders at the age of 28 days. Top surface of all the cylinders was coated with plaster of Paris and a circular steel plate was placed over it to ensure smooth application of the load. Electric resistance strain (ERS) gauges of 60 mm gauge length were installed on the concrete surface at two points along the circumference of the cylinders. Pictures of the tested specimens are shown in Figure 3.11. The cylinders were tested to failure under compressive load applied at a rate of 3 kN/sec. The modulus of elasticity was calculated for each batch of concrete according the following equation and the values are given in Table 3.4.

$$E_c = (\sigma_2 - \sigma_1)/(\varepsilon_2 - 50 * 10^{-6})$$

where; σ_2 is the stress corresponding to 40% of the failure load, σ_1 is the stress corresponding to a longitudinal strain of 50×10^{-6} and ε_2 is the longitudinal strain due to an applied stress of σ_2.

Figure 3.11. Test on concrete cylinders for modulus of elasticity

Table 3.4. Experimentally obtained modulus of elasticity of concrete

Concrete Batch	28 Days Modulus of Elasticity (MPa)
T1B	32158
T1W	30363
T2B	31508
T2W	29495
T3B	32174
T3W	31179
T4B	31559
T4W	30683

3.6.4 Steel Reinforcement

Steel reinforcement bars of different diameters were used in the experimental investigation. Tests on three 16 mm diameter steel reinforcement bars were carried out to evaluate the yield strength and the ultimate tensile strength of steel reinforcement used. ERS gauges were installed on the reinforcement bars to monitor the strain occurring in the bars due to the applied tensile load. The stress strain relationship was obtained for the tested steel bars and the average yield strength was found to be 512 MPa.

3.6.5 Instrumentation

During each test, concrete surface strains, temperature development in the concrete members, strain occurring in steel reinforcement bars, the ambient temperature, relative humidity and crack widths were monitored.

Surface strains on both the wall and base were measured immediately after removal of the formwork using the 150 and 400 mm DEMEC gauges. The DEMEC

arrangement used in the tests is shown in Figure 3.12. DEMECs were installed on both faces of the walls immediately after removal of the formwork.

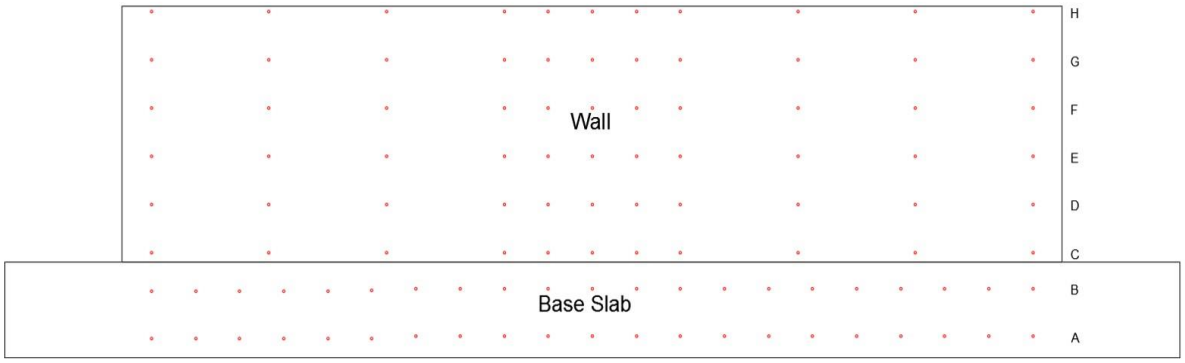

Figure 3.12. Layout of the DEMECs installed on concrete surface

The temperature development in both wall and slab were monitored using the K type welded tip thermocouples installed at different locations over the height and length of both members as shown in Figure 3.13 below. Owing to symmetry, temperatures were only monitored in one quarter of each member.

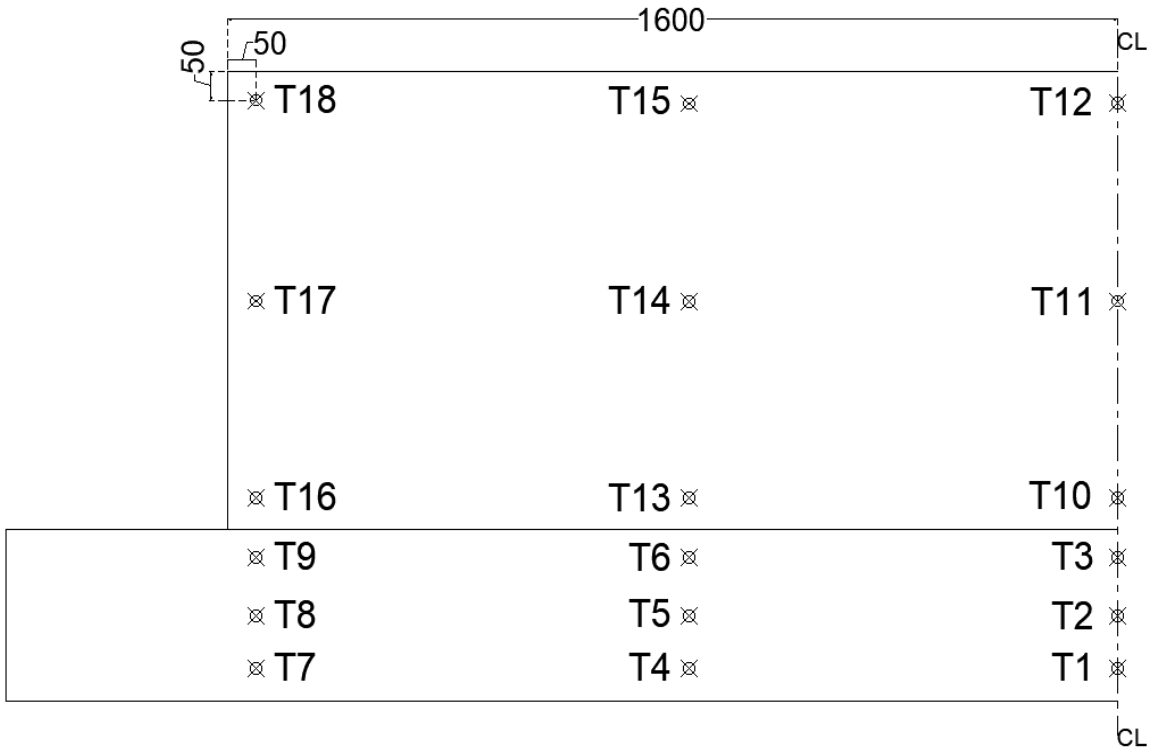

(a)

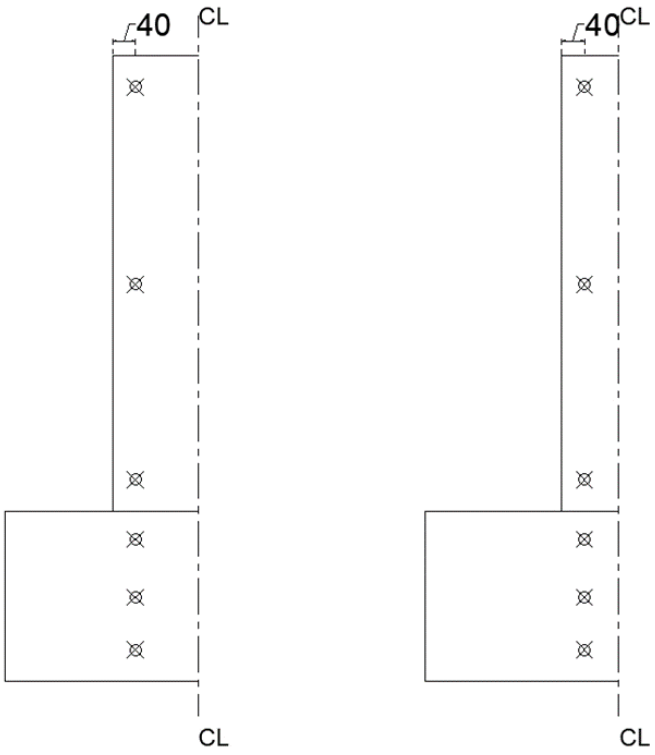

(b)

Figure 3.13. Location of the thermocouples installed in the wall and base slab: (a) Elevation; (b) Cross section.

ERS gauges were also installed on selected steel bars, as indicated in Figure 3.2 above, to monitor the strains occurring in the steel reinforcement bars. After installation of the ERS gauges on the steel bar, the continuity test was performed to ascertain the functionality of these gauges. On occurrence of cracks in the tested walls, the crack widths were measured using the portable microscope having a magnification power of 40 and a precision of $\pm$0.02 mm.

3.7 Preparation, Casting and Curing of Specimens

3.7.1 Preparation

Although the base slab and the wall were cast in two phases for each test, the steel reinforcement for both elements was prepared and fixed prior to the start of the test i.e. before casting the base slab. For the base slab, steel reinforcement was provided in two layers (top and bottom) and the spacers of 50 mm depth were used to provide concrete cover. The vertical steel reinforcement for the wall was then placed and tied to the bottom layer of the slab reinforcement. Vertical steel reinforcement bars

used in the tests were cut and bent according to the shape code 23 of BS 8666:2005 as shown in Figure 3.14. Top bent up ends of the vertical steel bars from both faces were overlapped and tied together. The horizontal steel reinforcement of 10 mm diameter for the wall was then tied to the vertical bars. Figure 3.15 shows the shape of vertical steel reinforcement used in the test 2 and 4.

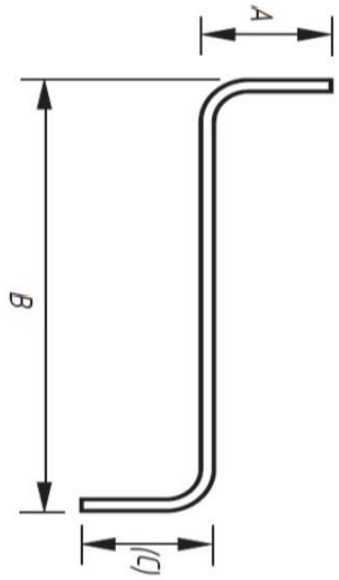

Figure 3.14. Shape of the vertical steel bars used in the test (Shape code 23 of 8666:2005)

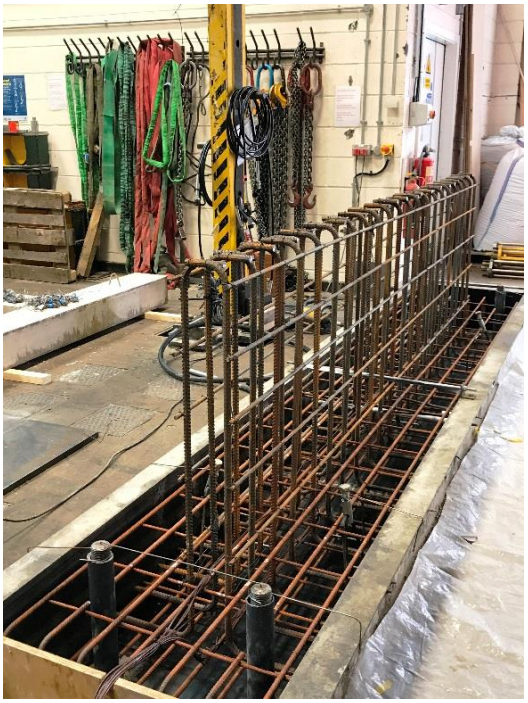

Figure 3.15. Steel reinforcement used in test 4

In order to prevent the curvature development in the base slab after casting of the wall, two-off 50 mm diameter steel studs were attached to the laboratory strong floor (as shown in Figure 3.16) prior to the placing of formwork and the steel

reinforcement. The formwork for the base slab was then prepared and installed. The thermocouples were installed for monitoring the temperature development in the base slab. Thermocouples for the wall were installed after casting of the base slab and prior to assembling of the formwork for the wall.

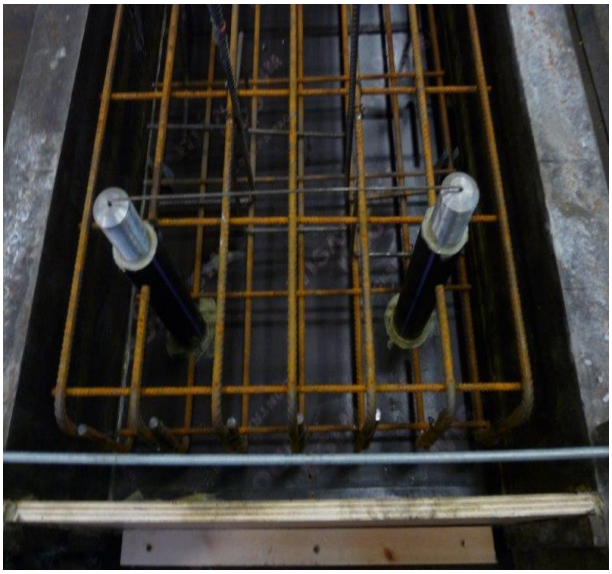

Figure 3.16. Steel studs used for clamping the base slab

16 mm thick plywood formwork supported by the timber and steel box sections was used for the wall. Plywood formwork was preferred over steel formwork since the former helps in achieving a greater temperature drop than the latter. The formwork had to be strong enough to sustain the weight of the concrete placed and for that purpose prior calculations were carried out. The formwork used in the experimental work for construction of the walls is shown in Figure 3.17. The wall formwork was insulated with 50 mm thick polyisocyanurate (PIR) thermal insulation sheets (which have a thermal conductivity of 0.022 W/m.K) to prevent heat loss to the atmosphere.

Figure 3.17. Formwork used for casting of the walls

3.7.2 Casting

Each test required casting of the base slab and the wall elements in two different phases. Ready mixed concrete for casting of each element was obtained from Hanson Concrete Leeds and poured manually. The concrete was compacted using the vibrating pokers to avoid the risk of honeycombing and to achieve similar density of concrete throughout the member. Particular care was taken to avoid segregation and bleeding of concrete due to excessive vibration. The top surface of the base slab was levelled using the trowels. The part of the slab where wall had to be cast in the second phase of the test was roughened up to give a rough concrete surface at the

interface between the wall and the base slab. Casting process of the base slab is illustrated in Figure 3.18.

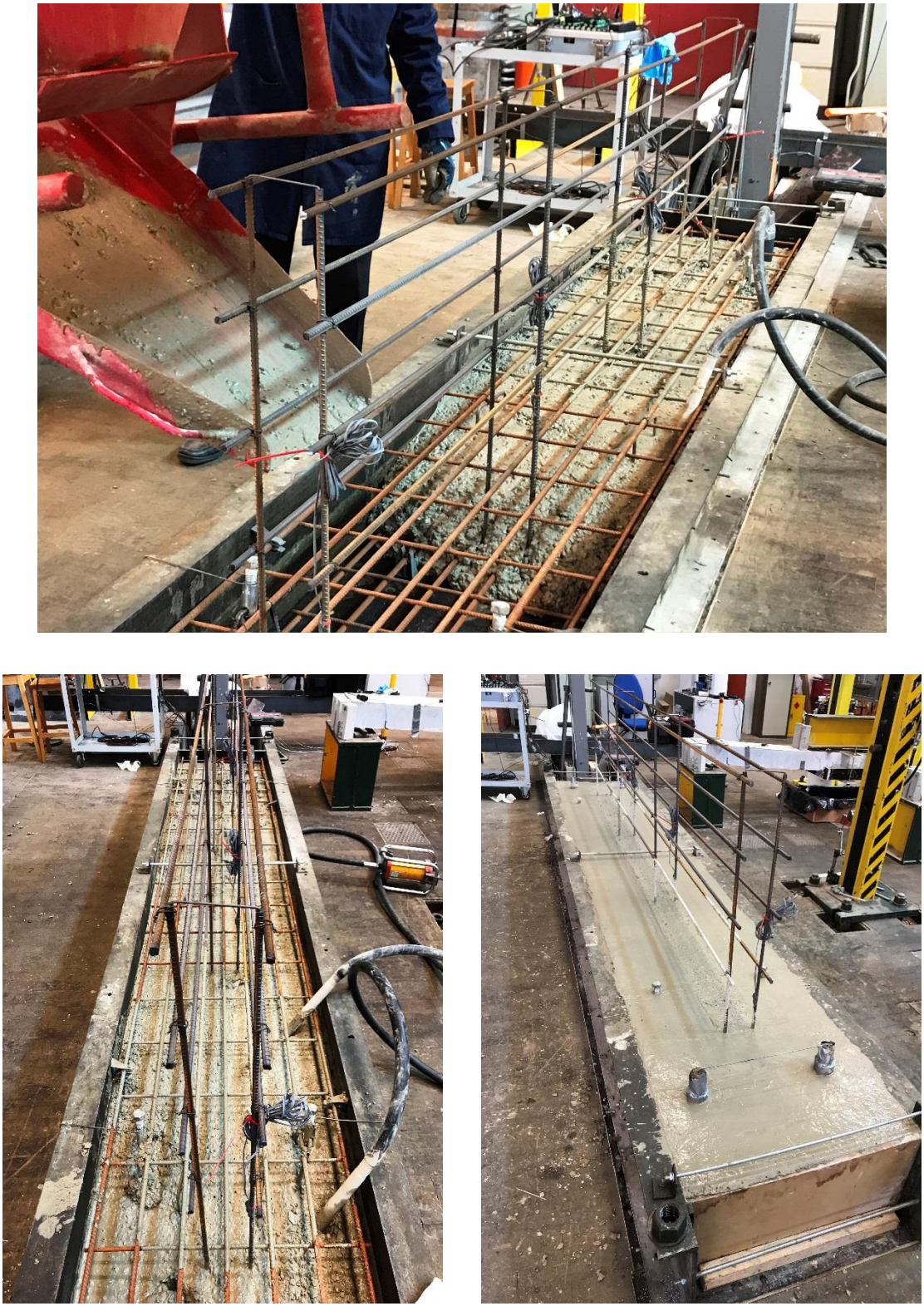

Figure 3.18. Casting of the base slab

After 28 days of casting of the base slab, the wall was cast. The concrete was poured in the formwork using the hopper and compacted through vibrating pokers. After casting, the top surface of the wall was levelled and was covered with PIR sheets to prevent heat loss from the top. Slump test was carried out for each batch of concrete according to the BS EN 12350−2: 2009 (2009) and the results of slump test are presented in Table 3.5. From each batch of concrete, 12 cubes (100 x 100 x 100 mm), 18 cylinders (150 x 300 mm), 4 prisms (75 x 75 x 200 mm) and 3 bobbins (75 x 365 mm) were also cast for conducting tests to obtain the material properties of the concrete used. The moulds were filled with concrete in layers and compacted using a vibrating table. After casting, the specimens were covered with polyethylene sheets to prevent moisture loss and left to dray for one day.

Table 3.5. Measured slump values of concrete mixes

Concrete Batch	Slump (mm)
T1B	80
T1W	75
T2B	85
T2W	90
T3B	95
T3W	90
T4B	105
T4W	85

3.7.3 Curing

In the case of base slab, the formwork was removed 48 hours after casting. The base slab was then cured for two weeks using the wet hessian cloth as shown in Figure 3.19 and was kept covered with the polyethylene sheets to prevent moisture loss to the atmosphere. The wall formwork in the first test was removed 48 hours after casting.

From the temperature profile obtained in the first test, it was realised that the peak temperature was reached by the concrete in less than 20 hours after casting and by the time of formwork removal (48 hours), quite a lot of thermal drop had already occurred and thus in the other three tests, the formwork was removed less than 24 hours after casting. In order to maximize the early age thermal contraction and shrinkage the wall was not cured after the removal of the formwork. Specimens for concrete material properties were unmoulded after 24 hours of casting. The prisms used for monitoring the shrinkage in concrete were stored next to each element under the same curing and environmental conditions. All other specimens were placed in the curing room and cured under 99% relative humidity conditions.

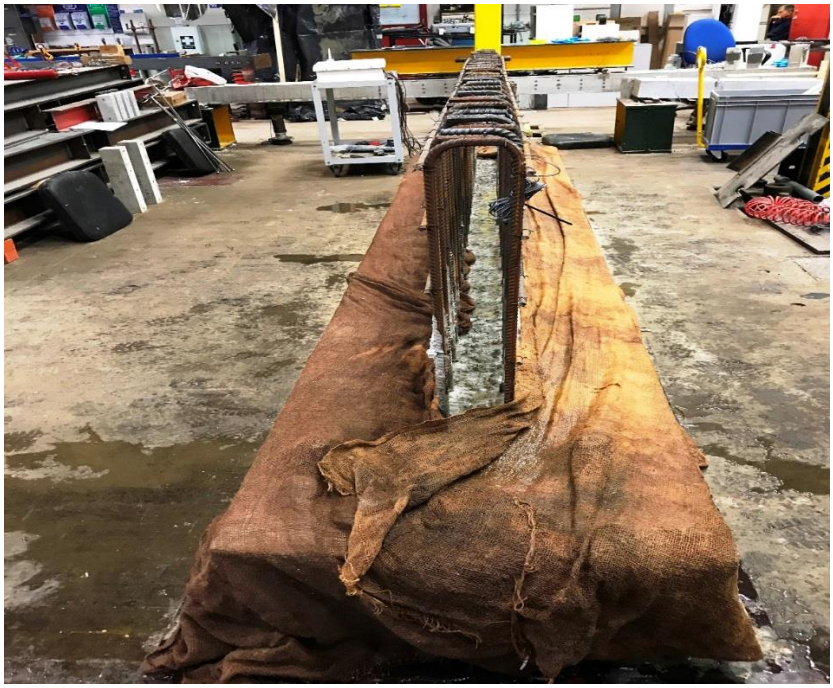

Figure 3.19. Curing of the base slab

3.8 Test Procedure

Surface strain monitoring started immediately after the removal of formwork and continued for the entire duration of test. First the formwork was removed from one face of the wall and installation of the DEMEC studs was started. After installation on one face was finished, then the formwork from second face was removed followed by installation of DEMEC studs. The shrinkage of the wall was recorded at six different levels along the wall height as indicated in Figure 3.12 above. 150 mm DEMEC grid was used in the central part of the wall and 400 mm grid was used towards the free ends. This was done to reduce the time required for installation of studs and recording of strains. Installation of the DEMEC studs on each face was completed in 2 to 3 hours. After installation of the DEMEC studs on one face, the first readings were taken and then the studs were installed on the second face and readings taken again. During the initial two weeks, the readings were taken daily, in the next two weeks, readings were taken twice a week and thereafter, once in a week throughout the monitoring period. Prior to casting of the wall, DEMEC studs on the base slab were also fixed and the shrinkage in the base slab was monitored to ascertain the variation in shrinkage of slab before and after casting of the wall.

For temperature monitoring, the thermocouples were already installed and connected to the data logger before casting. Thus the temperature development in the concrete was monitored right from the beginning. Temperature recordings were logged every 15 minutes using the data logger. Ambient temperature and relative humidity were also monitored throughout the duration of each test. Temperature values at the time of first DEMEC reading were taken as the reference for calculation of the thermal drop. Thermal strain was calculated as a product of the thermal drop and the coefficient of thermal expansion. The ERS gauges installed on the steel reinforcement bars were also connected to the data logger and the readings were recorded automatically at 15 minutes intervals.

In these tests, it was decided to prevent / limit the development of curvature in the base slab due to contraction occurring in the wall and to do that, the clamping mechanism as mentioned above was used. Immediately prior to the removal of wall formwork, the bolts were checked to ensure that the base slab was uniformly in contact with the floor. Analogue deflection gauges were installed on each exposed end of the base slab and the upward deflection was monitored. A constant value on these deflection gauges was maintained throughout the test by tightening the nuts whenever any upward deflection was detected during the test period. This adjustment was performed a maximum of 3 times during the test and the maximum upward deflection observed during any test was 0.05 mm.

Detailed monitoring of the wall for detection of cracks in each wall was carried out every day using a magnifying glass. On occurrence of the cracks, crack propagation with time was recorded. Crack widths were measured perpendicular to the crack using a portable microscope with a magnification power of 40 and a precision of ±0.02 mm. The crack widths at different points along each crack were measured and the maximum crack width was then determined.

3.9 Summary

This chapter provides details of the experimental methodology adopted in the tests carried out as part of this research. Testing program was aimed at identifying the influence of vertical steel dowels and relative axial rigidity of the members on degree of restraint, ascertaining the efficacy of using steel sections as restraining members

and observing the cracking behaviour of the walls. Testing rationale for the experimental investigation is presented. Test set up for four edge restrained reinforced concrete wall specimens are described. Details of the geometry and steel reinforcement provided in the base slab and wall for all tests is presented. Vertical steel reinforcement and the wall thickness were the parameters varied during the tests to establish their influence. Tests carried out to determine the mechanical properties of concrete are also described. Instrumentation used in the test specimens to observe the temperature and surface strain development is also presented. Finally the casting, curing and monitoring procedures are described in detail. Results obtained from these tests are presented and discussed in Chapter 4.

Chapter 4

Experimental Results and Discussion

4.1 Introduction

The results of the tests conducted on four reinforced concrete walls restrained along their edges are presented and discussed in this chapter. For each test, the development of temperature at different points along the length and height of both wall and base slab due to hydration process is included. Surface strains observed during the tests are presented and the restrained strain is calculated from the difference between free strain and the measured values. Comparison of the shrinkage prediction models used for calculation of the unrestrained or free shrinkage strain of concrete is also included. The degree of restraint for each test is calculated from the restrained strain and the variation of restraint with time is also analysed.

Parameters considered in this research were the vertical steel reinforcement and the axial rigidity of restrained and restraining elements to ascertain how they influence the development of edge restraint. These parameters have been critically analysed and discussed and a comparison is drawn between the degree of restraint experimentally determined and that calculated from the existing analytical expressions available in different guidelines / codes. CIRIA C660 (2007) guidelines on estimation of the tensile strain capacity of concrete under sustained loading conditions have also been evaluated and discussed in the light of obtained results. The development and propagation of cracks and measured values of crack widths are also presented.

4.2 Temperature Development

Concrete temperature started to rise immediately after casting due to the hydration process. Temperatures were recorded close to the surface of the walls at different locations as given in Chapter 3 (Figure 3.13). The temperature profile observed in both the wall and the base for each test are presented in Figure 4.1. The vertical dotted lines in Figure 4.1 depict the time of formwork removal. A sharp decline in temperature can be seen in all tests on removal of the formwork. In the case of first test, the formwork was removed 48 hours after casting while in all other tests it was removed after 24 hours. The influence of this on the temperature profile is obvious in

Figure 4.1 where the post peak temperature drop is more gradual in the case of test 1. In order to ascertain the thermal drop for calculation of thermal strain, the temperature at the time of formwork removal was taken as a reference and the difference between this value and the ambient temperature provided the thermal drop. First DEMEC readings were taken after removal of the formwork and were used as a reference for calculation of the measured surface strain at different times during the test. Free volume change or strain was calculated as a sum of the thermal strain and shrinkage strain. The measured surface strain was subtracted from the free strain (calculated as mentioned above) to obtain the restrained strain. Finally the degree of restraint was calculated as a ratio of restrained to free strain. In doing so, by taking the temperature at the time of removal of formwork as a reference, the free strain calculation was independent of the formwork removal time and thus was not likely to influence the test. Peak temperature along the wall centreline was reached after 15 to 18 hours of casting in all tests. After that the temperatures within the concrete started to drop and reached close to the ambient value. In all tests the temperature dropped to ambient value after 72 to 80 hours from initial casting. Temperature drop remained gradual except at the time of formwork removal. Significant heat flow from the wall to the base slab was observed in all tests. Maximum temperature reached in the wall close to the free end was relatively less than that at the centreline along the wall length. Near the free edge, the maximum temperature occurred at the mid height of the walls and was quite similar to the temperatures recorded near the top of the walls. However, temperatures observed in the wall close to the joint between the wall and the base were significantly lower than those at the higher locations in the wall. Peak temperature reached by the concrete varied with the wall thickness. With a wall thickness of 300 mm, the maximum temperature reached in test 1 was 55.4°C and in test 2 it was 50.5°C; both of these values occurred near the top of wall along the wall centreline. When the wall thickness was reduced to 200 mm, the maximum temperature recorded in test 3 was 48.8°C and in test 4 it was 42.2°C; like the first two tests these values were recorded near the top of wall along the wall centreline.

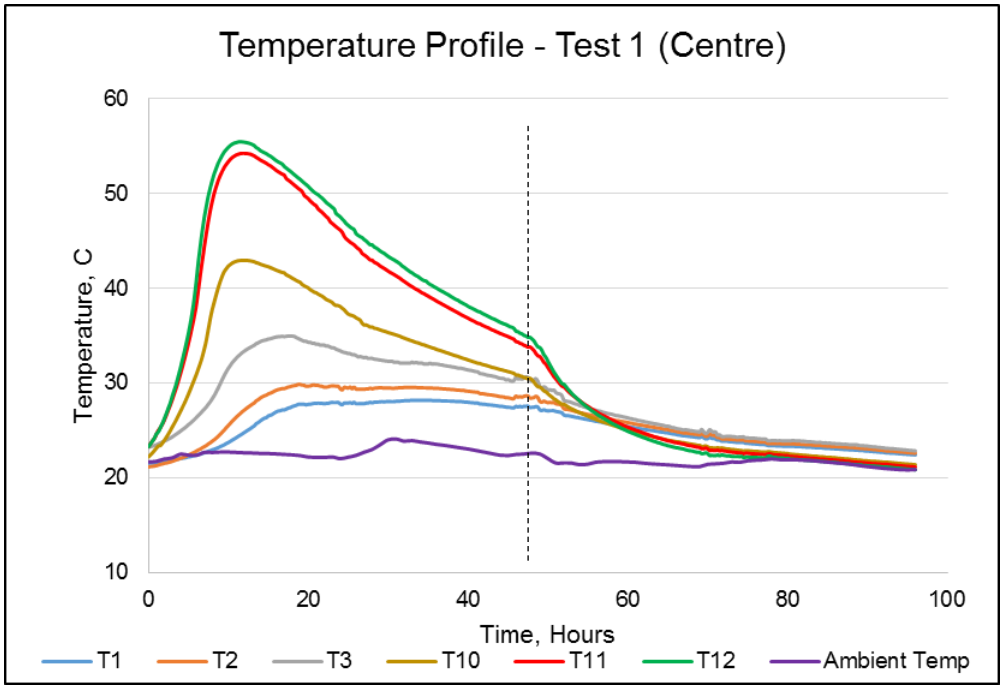
Temperature Profile - Test 1 (Centre)
Temperature, C
60
50
40
30
20
10
0
20
40
60
80
100
Time, Hours
T1
T2
T3
T10
T11
T12
Ambient Temp

(a)

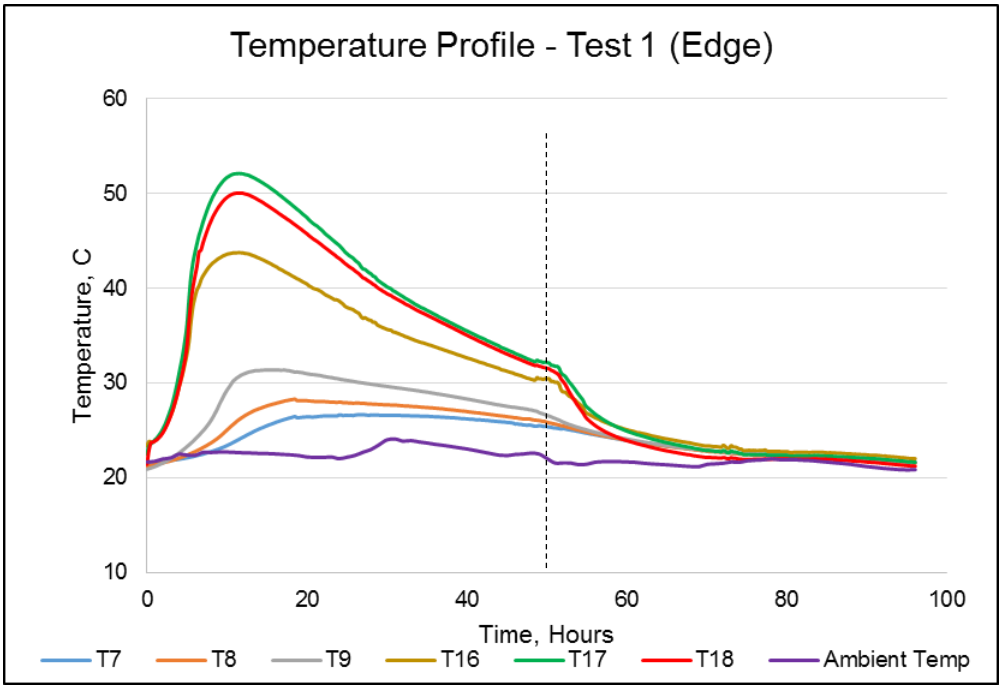
Temperature Profile - Test 1 (Edge)
Temperature, C
60
50
40
30
20
10
0
20
40
60
80
100
Time, Hours
T7
T8
T9
T16
T17
T18
Ambient Temp

(b)

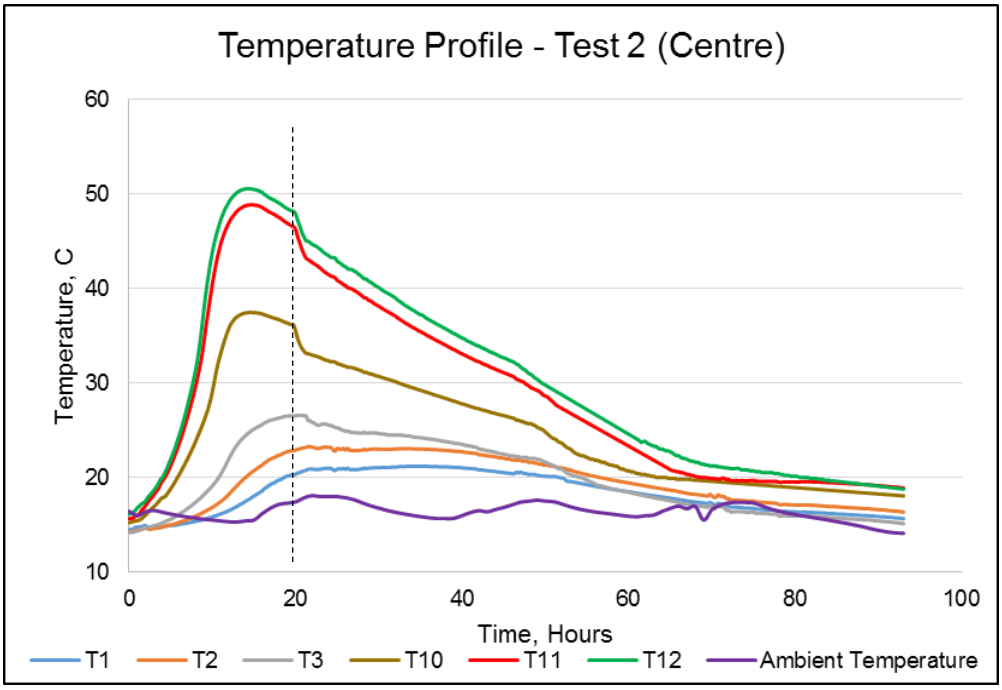
Temperature Profile - Test 2 (Centre)
Temperature, C
60
50
40
30
20
10
0
20
40
60
80
100
Time, Hours
T1
T2
T3
T10
T11
T12
Ambient Temperature

(c)

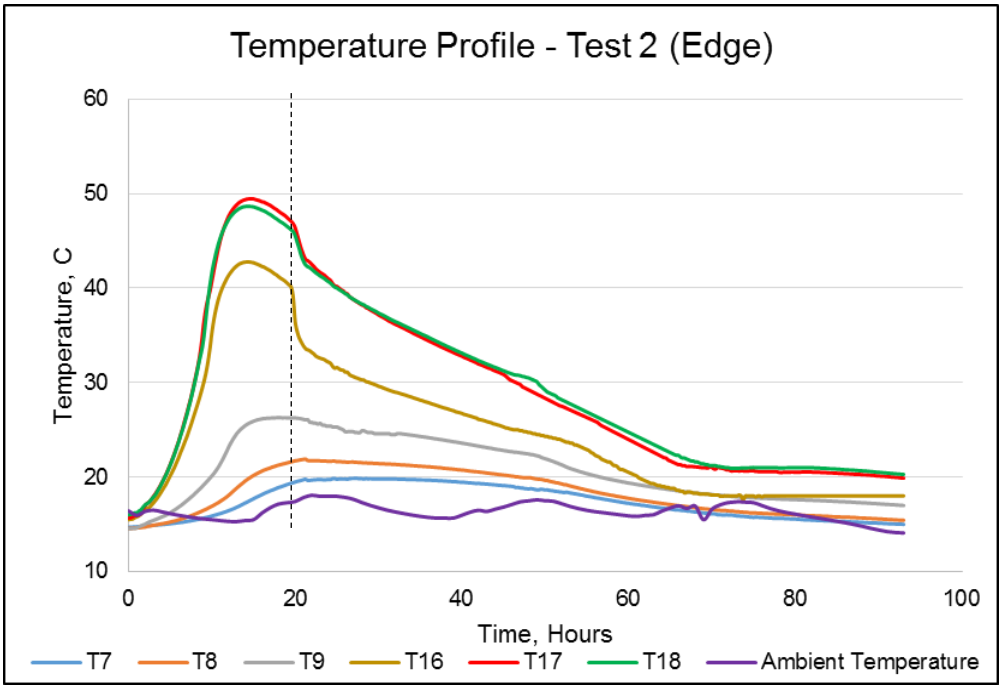
Temperature Profile - Test 2 (Edge)
Temperature, C
60
50
40
30
20
10
0
20
40
60
80
100
Time, Hours
T7
T8
T9
T16
T17
T18
Ambient Temperature

(d)

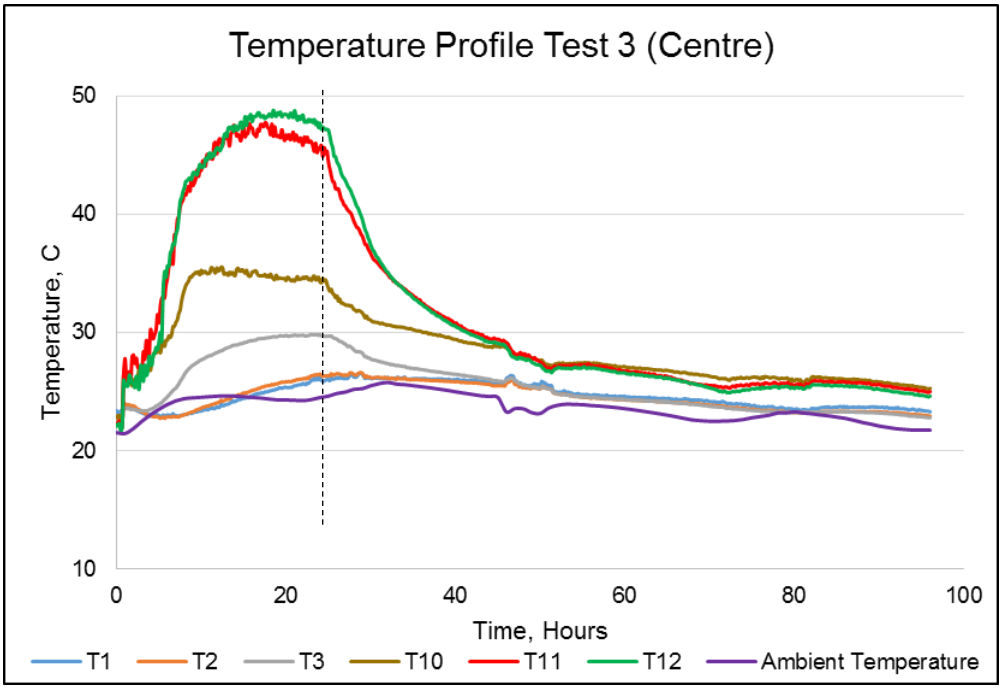
Temperature Profile Test 3 (Centre)
50
40
30
20
10
Temperature, C
0
20
40
60
80
100
Time, Hours
T1
T2
T3
T10
T11
T12
Ambient Temperature

(e)

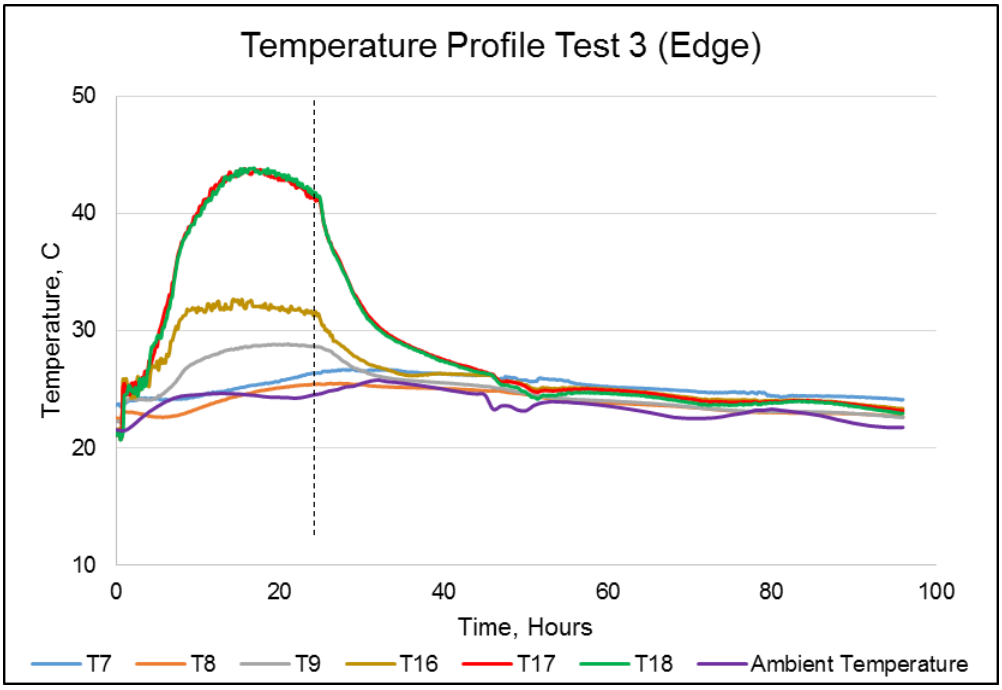
Temperature Profile Test 3 (Edge)
50
40
30
20
10
Temperature, C
0
20
40
60
80
100
Time, Hours
T7
T8
T9
T16
T17
T18
Ambient Temperature

(f)

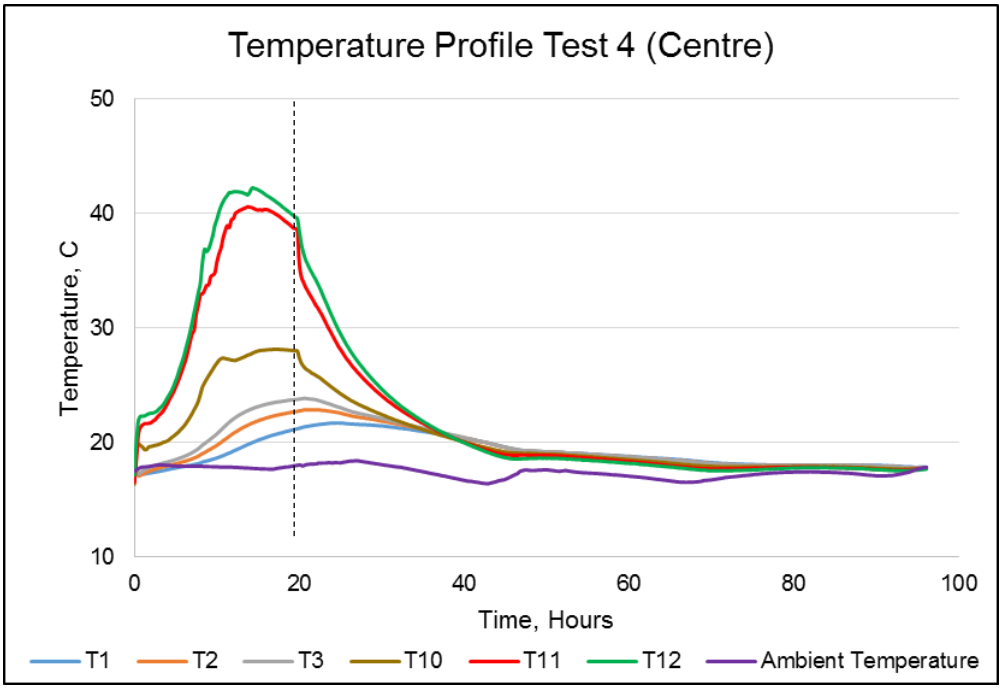

(g)

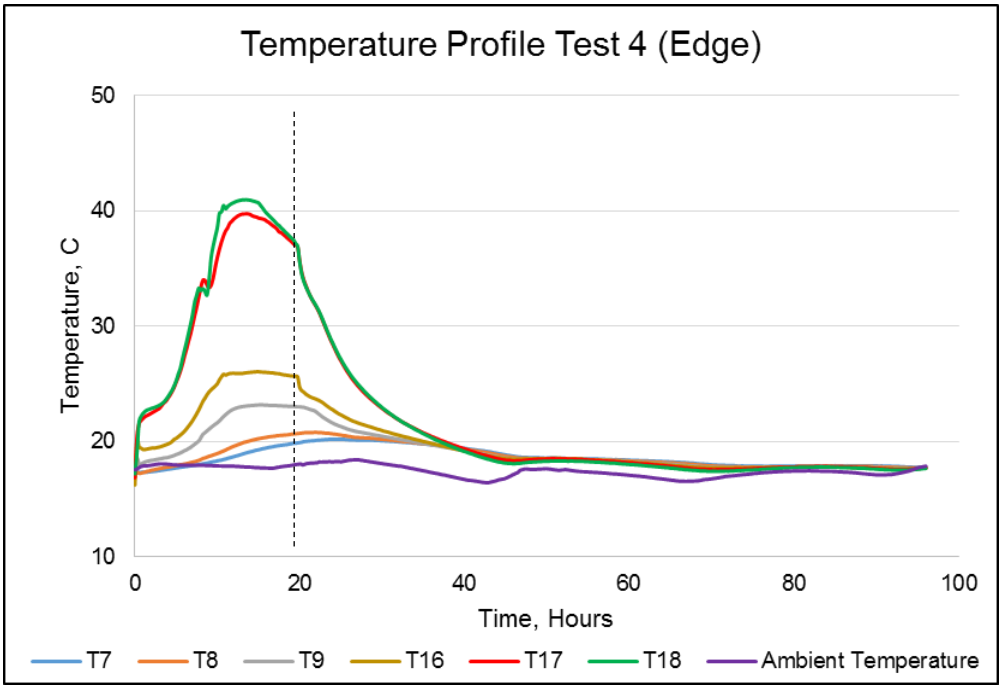

(h)

Figure 4.1. Temperature development after casting of the wall: (a) Test 1 Centre; (b) Test 1 Edge; (c) Test 2 Centre; (d) Test 2 Edge; (e) Test 3 Centre; (f) Test 3 Edge; (g) Test 4 Centre; (h) Test 4 Edge

The temperature drop from the peak to the ambient temperature in the test1 and test 2 was almost the same. Similarly, test 3 and test 4 walls had an approximately

similar thermal drop. The temperature drop at the centre of the wall was 33.5°C in test 1 and 33.3°C in test 2. The temperature drop at the centre of the wall in test 3 was 25.4°C and in test 4 it was 25.0°C. The temperature drop obtained from CIRIA C660 (2007) for a 300 mm thick wall, having a cement content of 380 Kg/m^3 is 30°C and the same for a 200 mm thick wall is 23°C. It can be seen that in both cases, the experimentally obtained thermal drop is more than the values given in CIRIA C660 (2007). Thus guidance contained in CIRIA C660 (2007) appears to be slightly conservative in estimation of the temperature drop for calculation of restrained strain and design of edge restrained reinforced concrete walls. Due to increase in the wall temperature during hydration, a rise in temperature in the base was also observed; this was greater close to the joint with the wall and lesser towards the bottom of the base, near the floor. This clearly indicates that a significant amount of heat is transferred from the wall to the base in the region of the joint. Moreover, it is also obvious that more heat flows to the adjoining concrete members and less to the surrounding atmosphere. Transfer of heat to the base slab entails additional volume change on to it and has a bearing on the behaviour of the restraining slab as well as on the calculation of degree of restraint. This aspect is discussed in detail in Section 4.5 below. This phenomenon is also in line with the observations of Bamforth (2007) who predicts that this heat loss is the reason that the maximum crack width occurs at some height above the joint.

4.3 Surface Strain Measurement

Strain occurring in concrete was measured and monitored through DEMECs installed on the wall and slab surfaces as mentioned in Chapter 3. Since previously available literature and the guidance on the subject indicates that the degree of restraint as well as the risk of cracking is more in the middle region of the wall and comparatively lesser towards its free ends, it was therefore decided to use DEMEC grids of two different gauge lengths. Accordingly, 150 mm gauge length was used in the central part of the walls and 400 mm gauge length was used towards the free ends. This was done to economize on time and yet monitoring the strains in the critical region in greater detail. Since on removal of formwork, lot of heat escaped and therefore it was felt necessary to complete the DEMEC installation and take the first readings as early as possible. Installation of the DEMEC studs started immediately on removal of

the formwork from one face of the wall. The DEMEC installation process was started from the centre of the wall and proceeded outwards. The process was completed in 2 hours on first face. First readings were taken after one hour (mainly on the DEMECs installed in the central part of the wall) and then after two hours the readings on the entire first face of the wall were taken. After that the same procedure was repeated for the second face of the wall. The readings were taken at six different levels along the wall height on both faces. The first readings were taken as a reference for calculating the strain for each of the subsequent readings. For the purpose of strain measurement and for calculation of degree of restraint, wall was divided into three parts. The central 1600 mm part and the two 800 mm edge parts. Average of the strains observed on both faces was taken as the measured strain. The strain profile of the walls at the bottom, mid height and top were plotted against the wall length and are shown in Figures 4.2, 4.3, 4.4 and 4.5 for each test. In Figures 4.3 and 4.5, the peaks in the strain variation demonstrating positive strain or expansion at different locations indicate the occurrence of cracks and the increase in strain manifested as crack width.

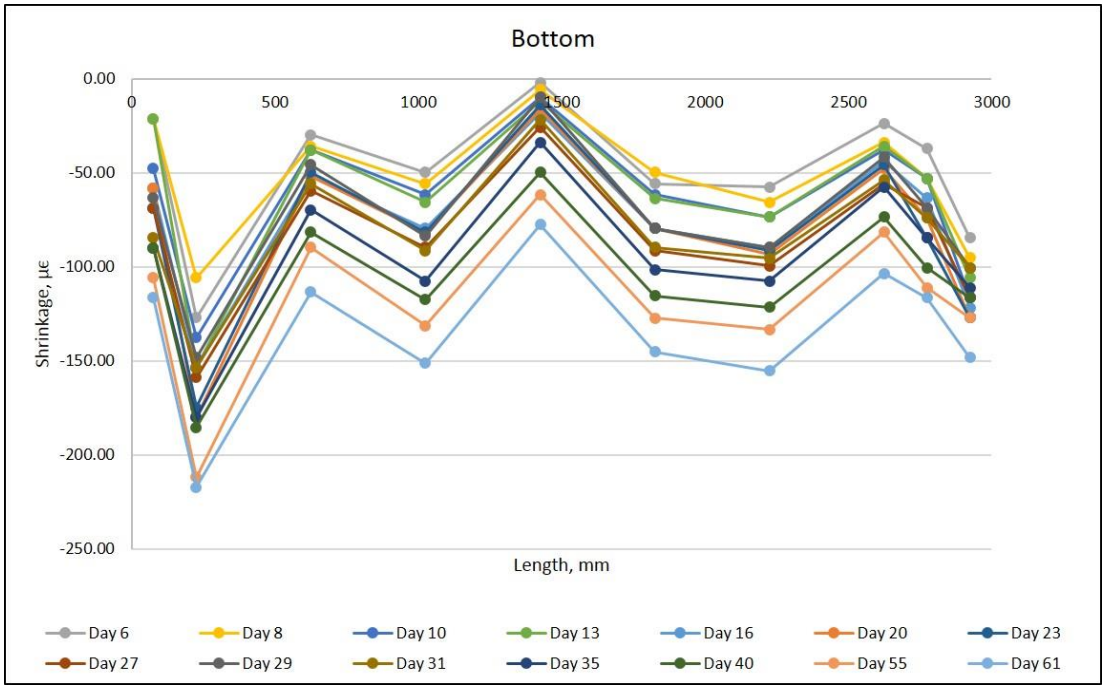

(a)

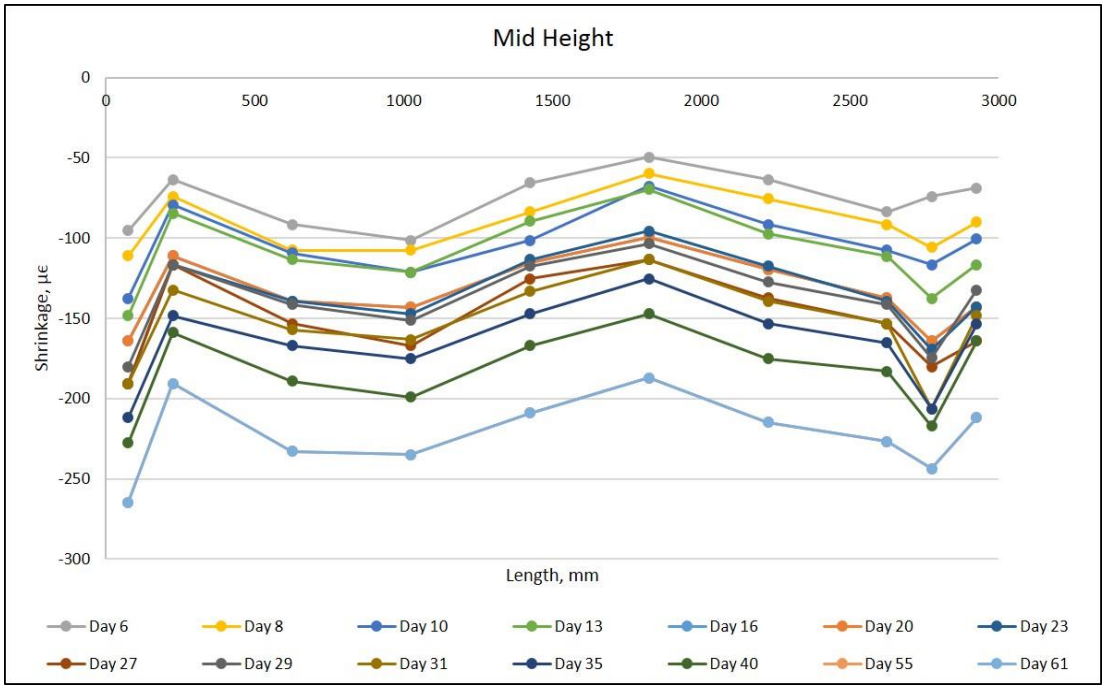

(b)

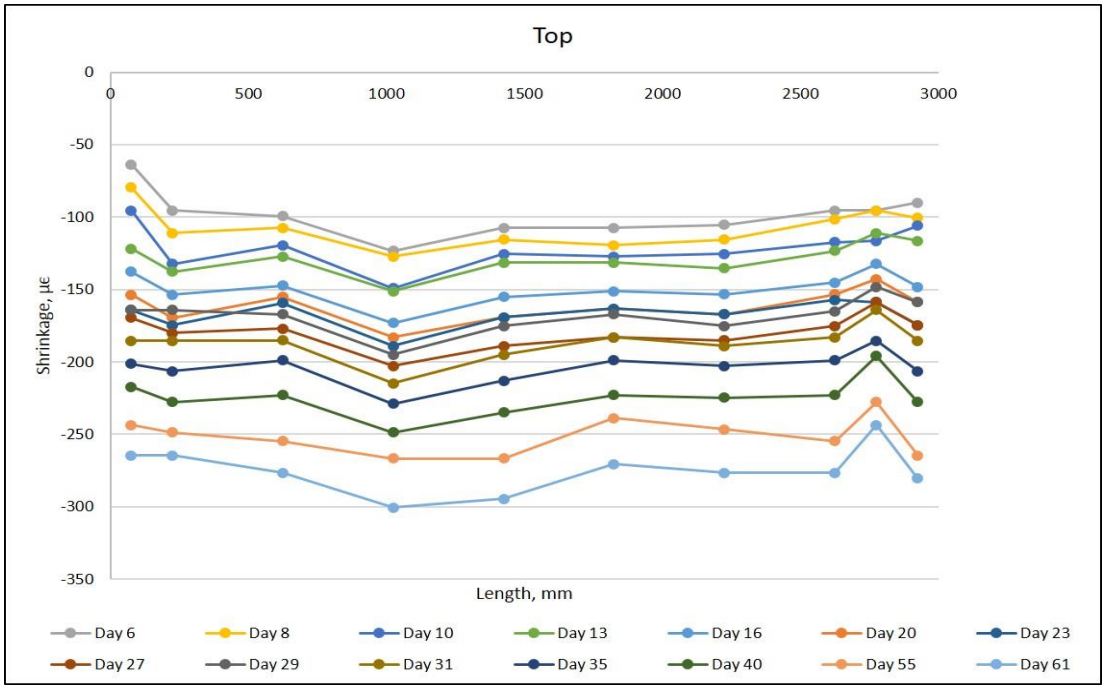

(c)

Figure 4.2. Measured surface strains in T1W: (a) Bottom of the wall; (b) Mid Height of the wall; (c) Top of the wall

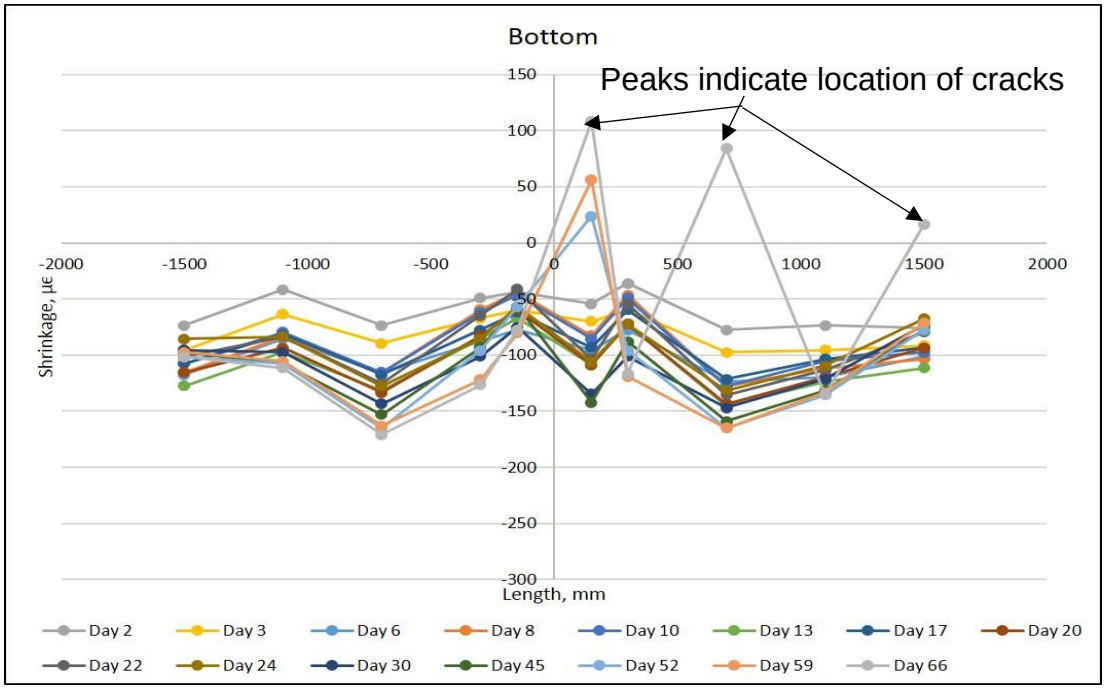
Bottom
Peaks indicate location of cracks
150
100
50
0
-50
-100
-150
-200
-250
-300
-2000
-1500
-1000
-500
0
500
1000
1500
2000
Shrinkage, με
Length, mm
Day 2
Day 3
Day 6
Day 8
Day 10
Day 13
Day 17
Day 20
Day 22
Day 24
Day 30
Day 45
Day 52
Day 59
Day 66

(a)

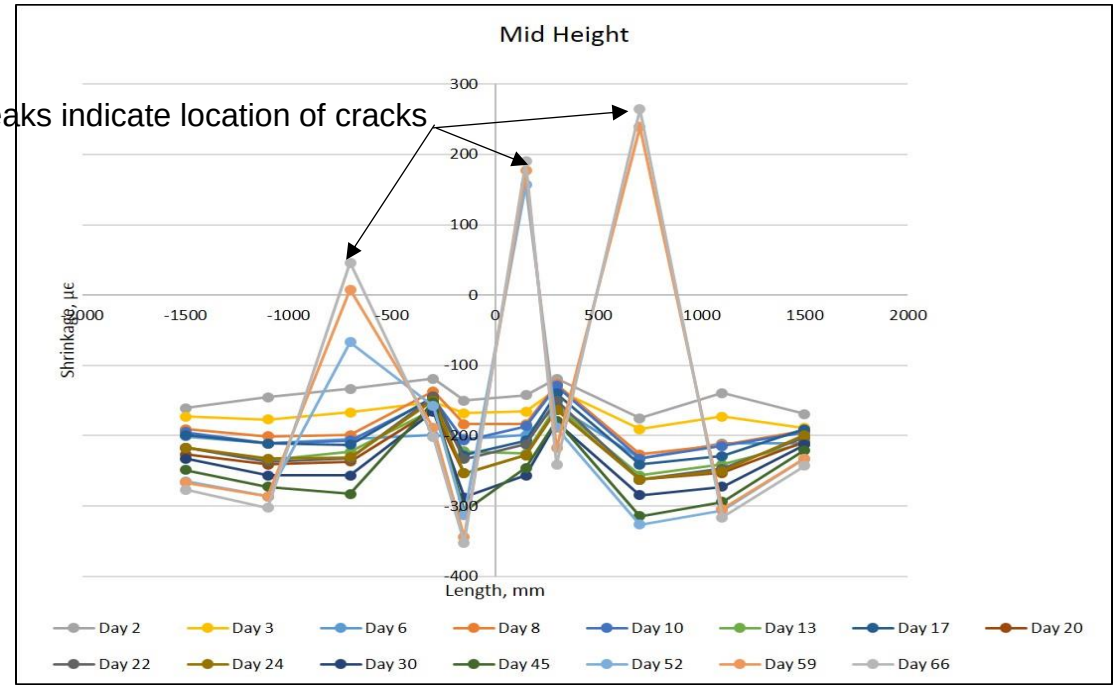
Mid Height
Peaks indicate location of cracks
300
200
100
0
-100
-200
-300
-400
-2000
-1500
-1000
-500
0
500
1000
1500
2000
Shrinkage, με
Length, mm
Day 2
Day 3
Day 6
Day 8
Day 10
Day 13
Day 17
Day 20
Day 22
Day 24
Day 30
Day 45
Day 52
Day 59
Day 66

(b)

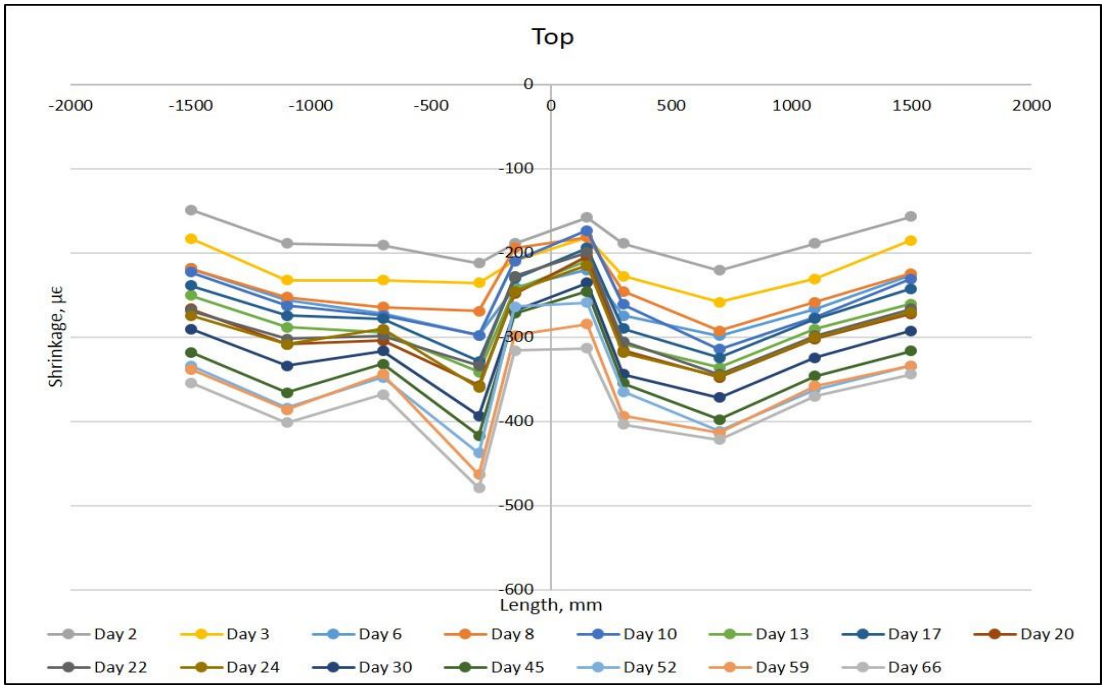

(c)

Figure 4.3. Measured surface strains in T2W: (a) Bottom of the wall; (b) Mid Height of the wall; (c) Top of the wall

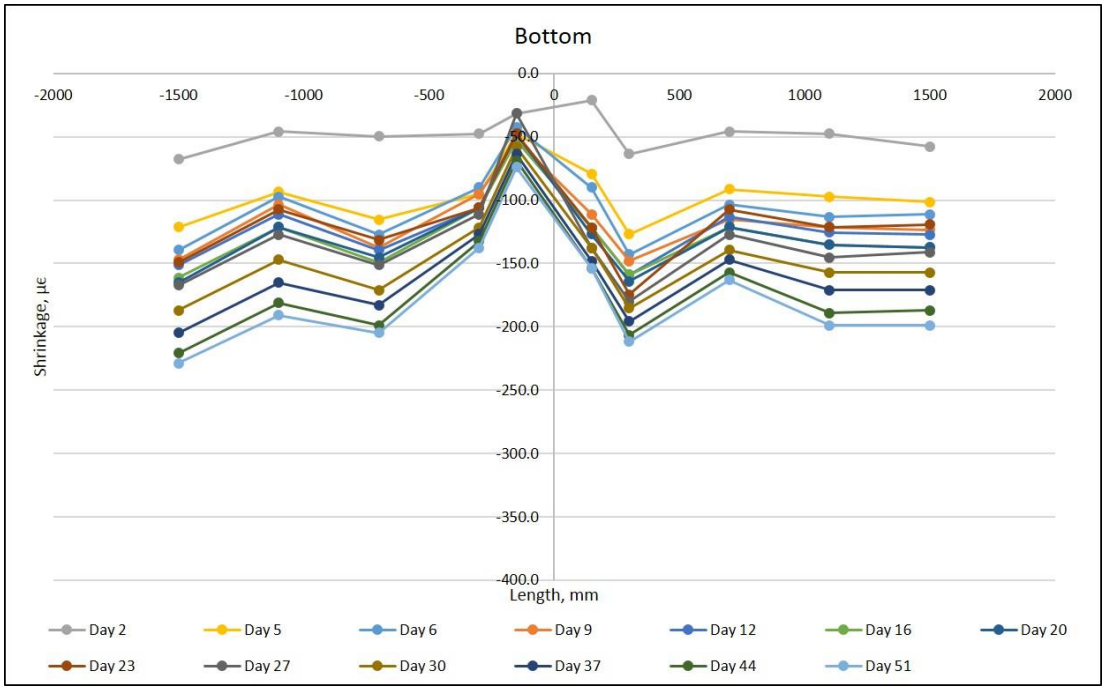

(a)

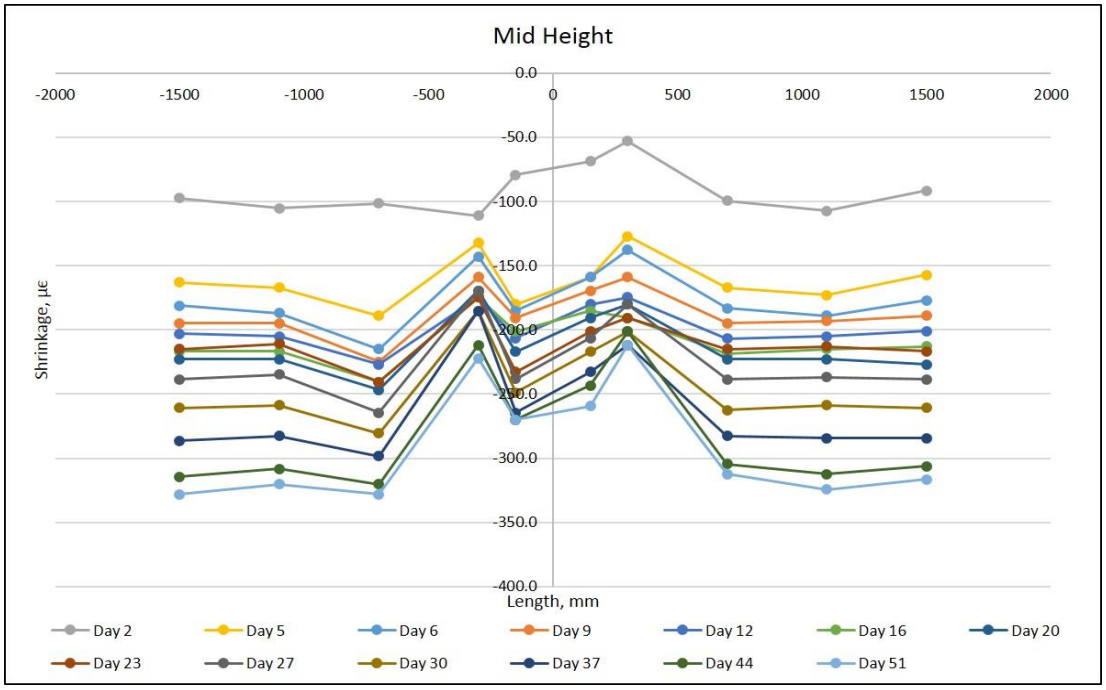

(b)

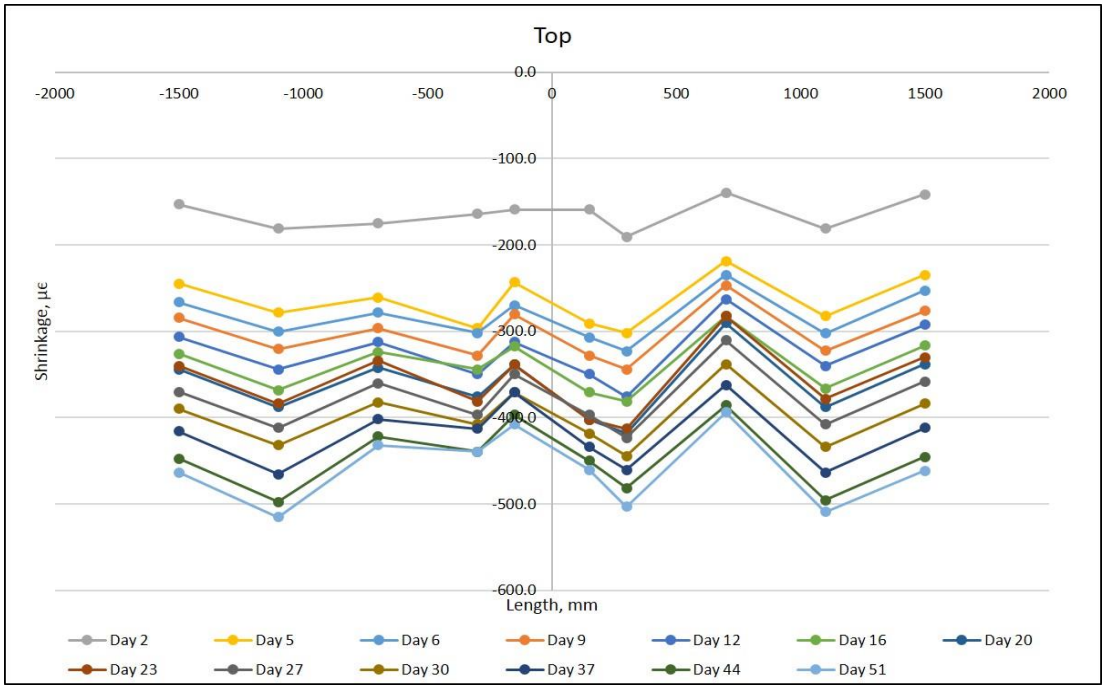

(c)

Figure 4.4. Measured surface strains in T3W: (a) Bottom of the wall; (b) Mid Height of the wall; (c) Top of the wall

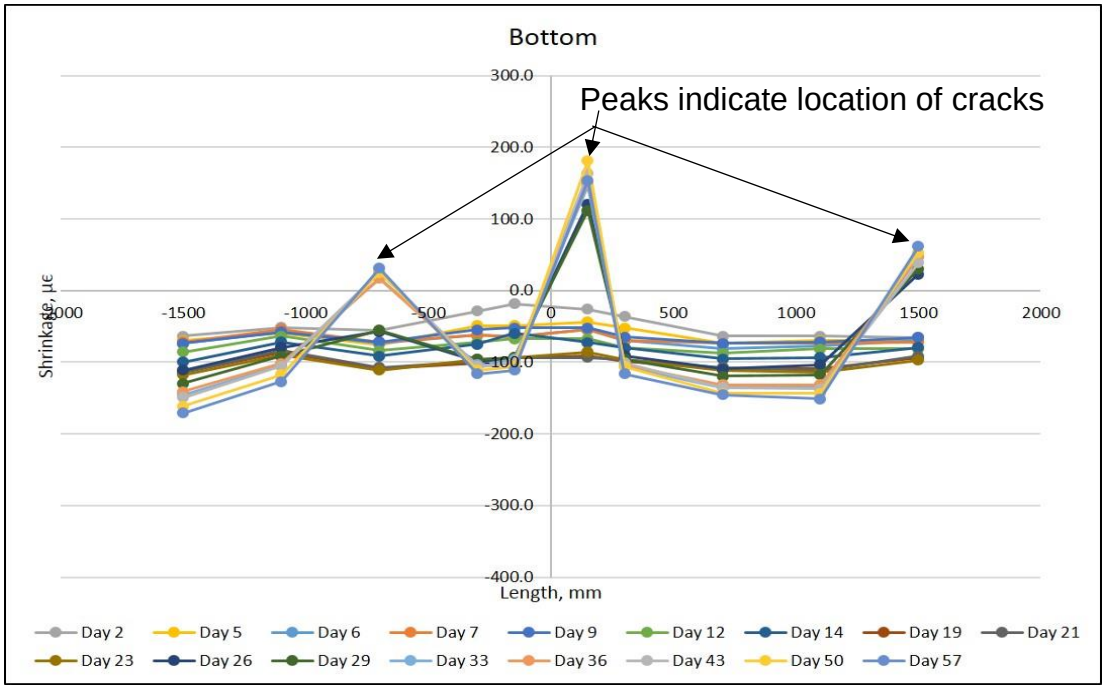
Bottom
Peaks indicate location of cracks
300.0
200.0
100.0
0.0
-100.0
-200.0
-300.0
-400.0
-2000
-1500
-1000
-500
0
500
1000
1500
2000
Shrinkage, με
Length, mm
Day 2
Day 5
Day 6
Day 7
Day 9
Day 12
Day 14
Day 19
Day 21
Day 23
Day 26
Day 29
Day 33
Day 36
Day 43
Day 50
Day 57

(a)

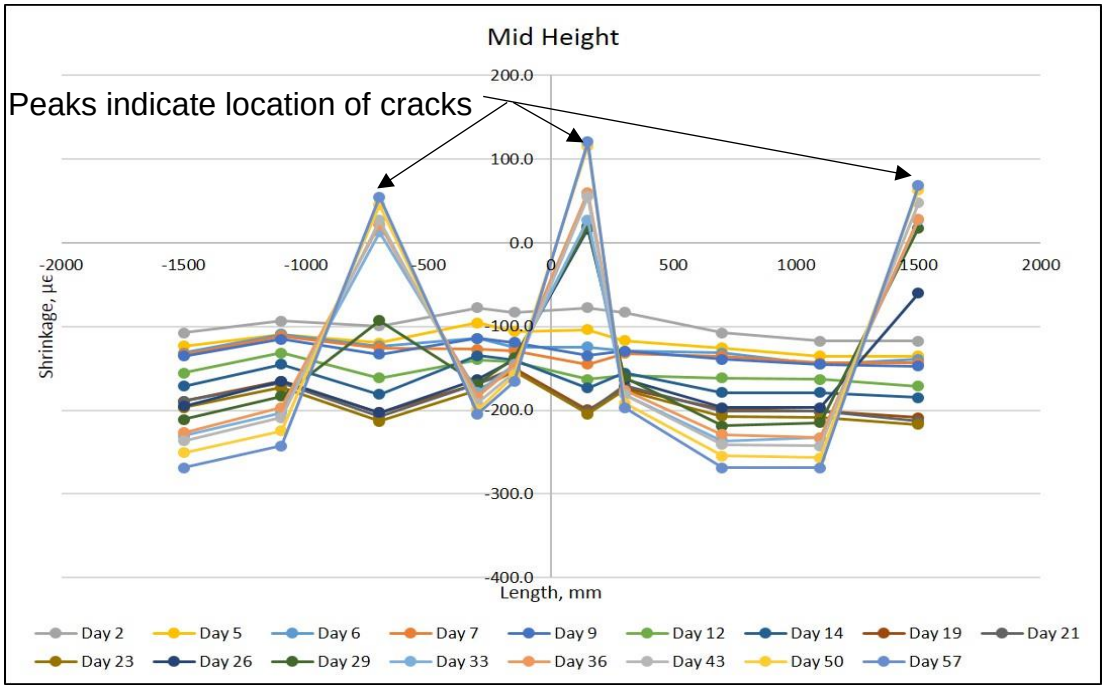
Mid Height
Peaks indicate location of cracks
200.0
100.0
0.0
-100.0
-200.0
-300.0
-400.0
-2000
-1500
-1000
-500
0
500
1000
1500
2000
Shrinkage, με
Length, mm
Day 2
Day 5
Day 6
Day 7
Day 9
Day 12
Day 14
Day 19
Day 21
Day 23
Day 26
Day 29
Day 33
Day 36
Day 43
Day 50
Day 57

(b)

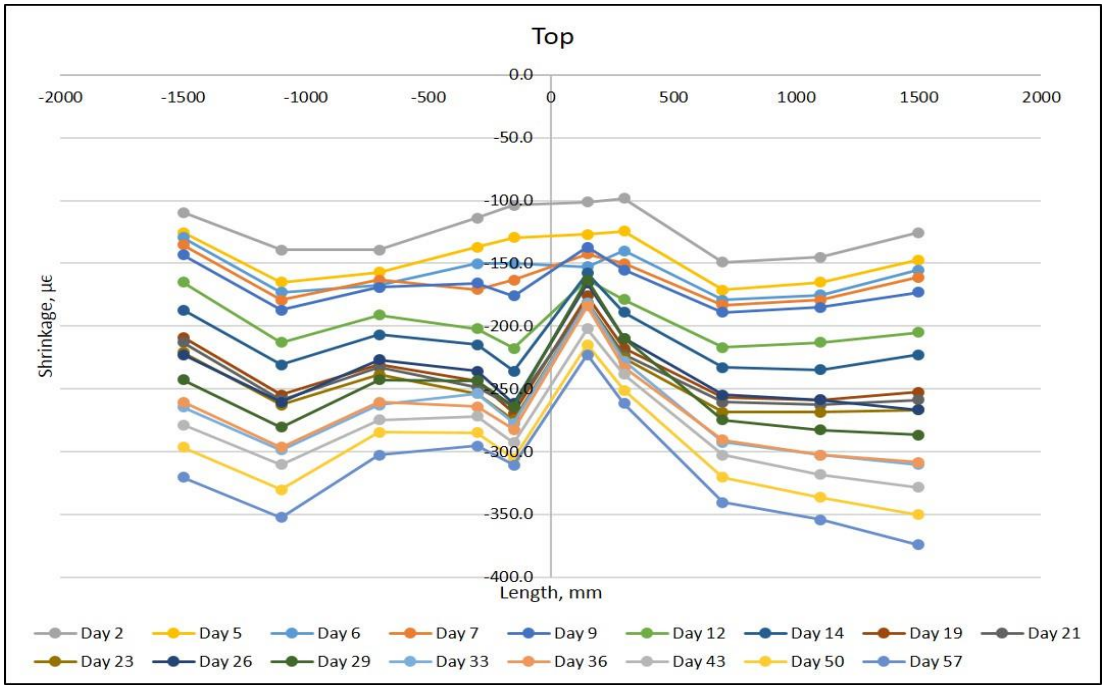

(c)

Figure 4.5. Measured surface strains in T4W: (a) Bottom of the wall; (b) Mid Height of the wall; (c) Top of the wall

From the measured strain profiles, the variation of surface strain along the height of the wall in the centre and edge parts was also drawn. For this purpose, the strain variation along height in the central 1600 mm part, and each of the edge 800 mm parts was calculated and then an average of both the edges was taken. This variation of the observed surface strains along the wall height for each test is shown in Figures 4.6, 4.7, 4.8 and 4.9. It was observed that the surface strain close to the base slab was minimum and that near the top of the wall was the maximum in all the walls. With time, the surface strain increased and this increase was lesser close to the base and more near the top.

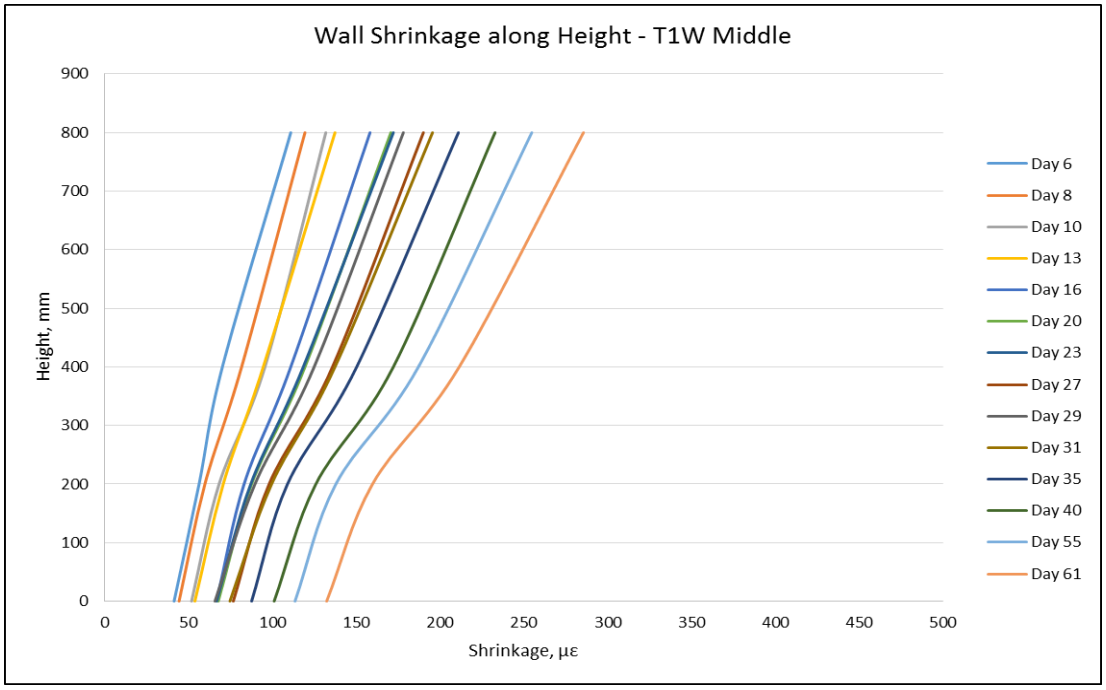

(a)

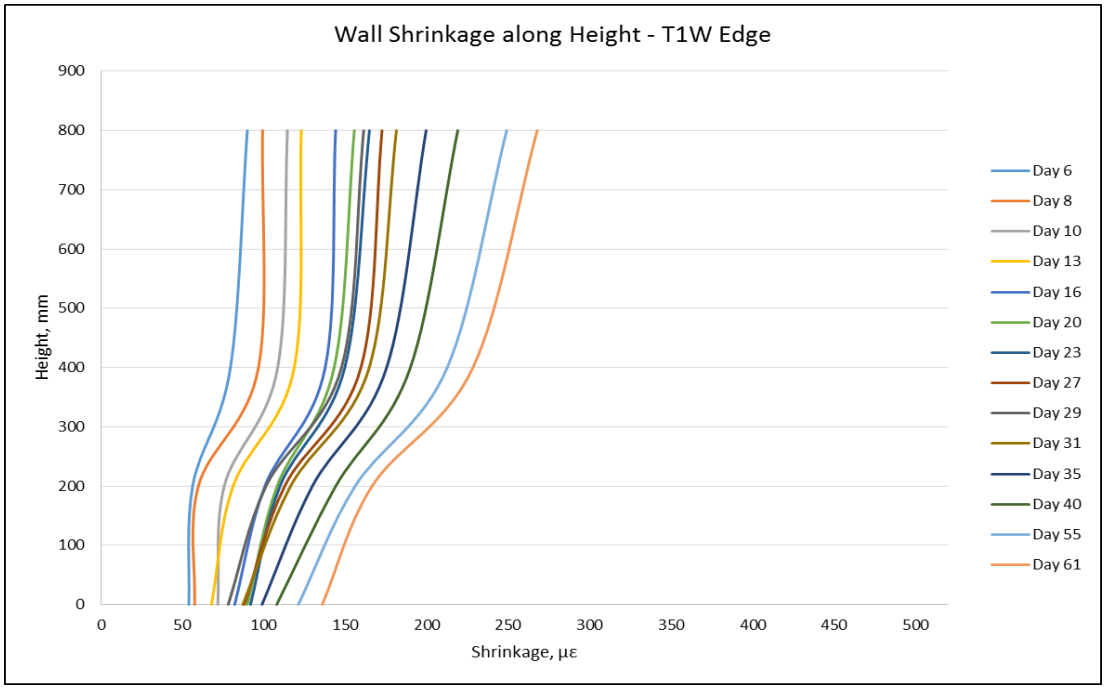

(b)

Figure 4.6. Variation of surface strain along height: (a) Test 1 Middle; (b) Test 1 Edge

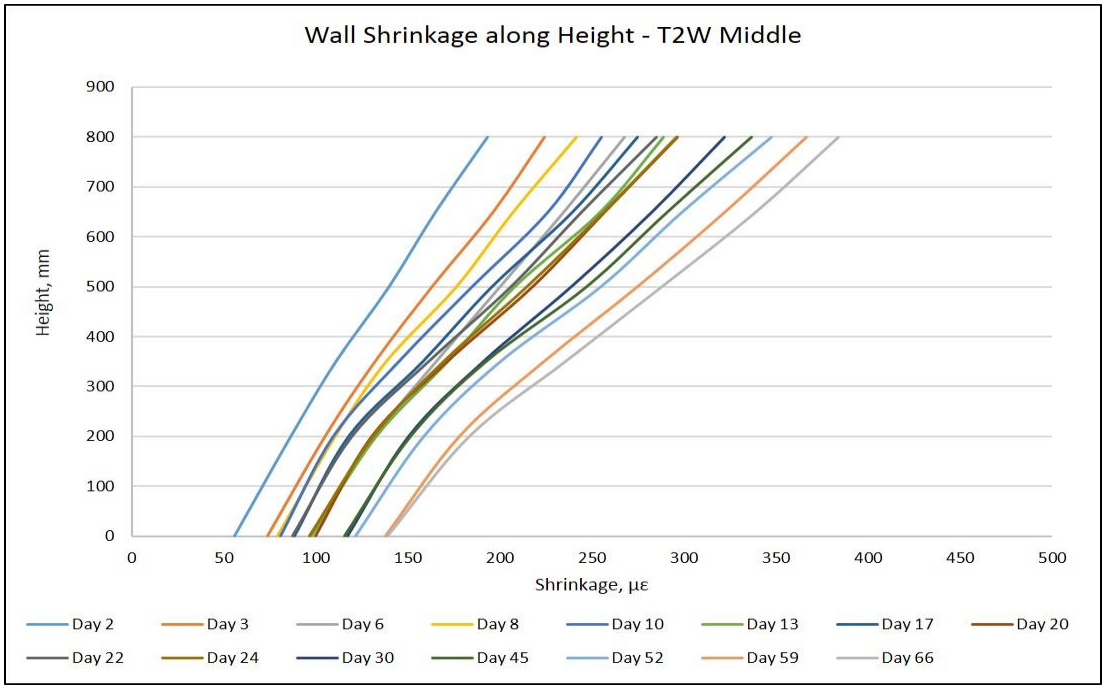

(a)

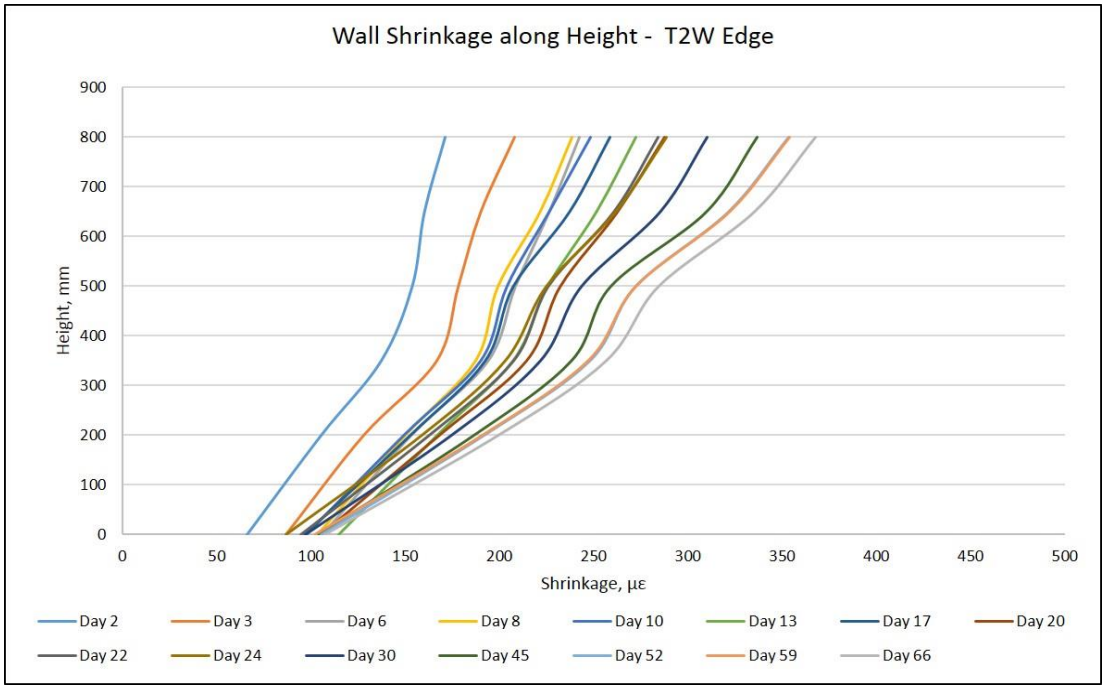

(b)

Figure 4.7. Variation of surface strain along height: (a) Test 2 Middle; (b) Test 2 Edge

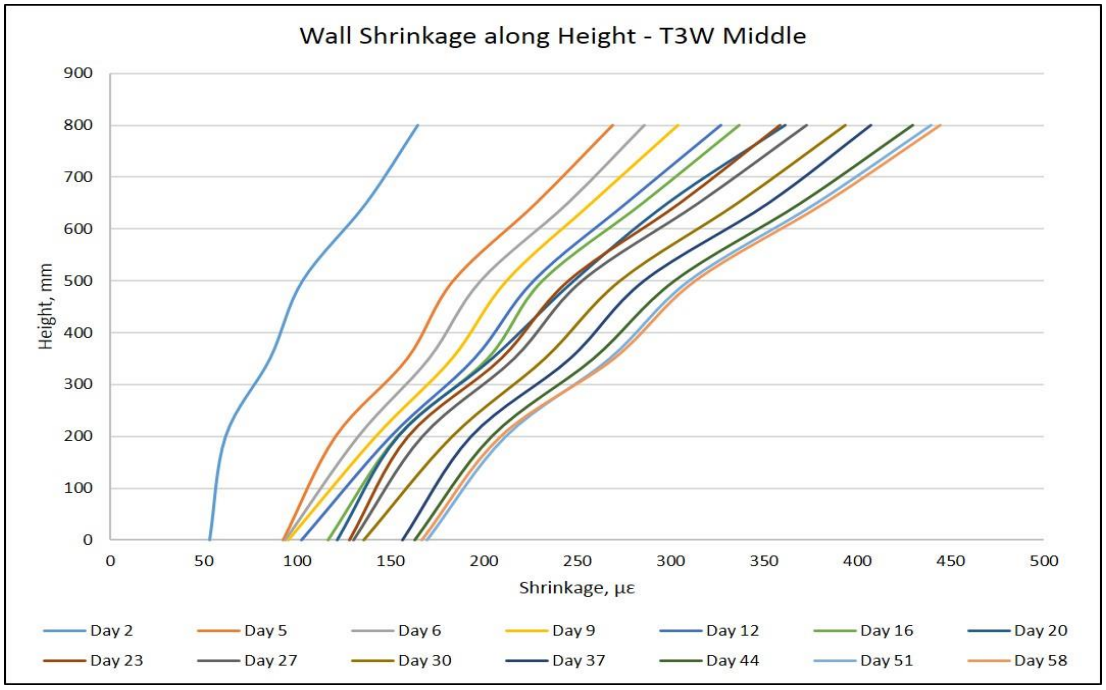

(a)

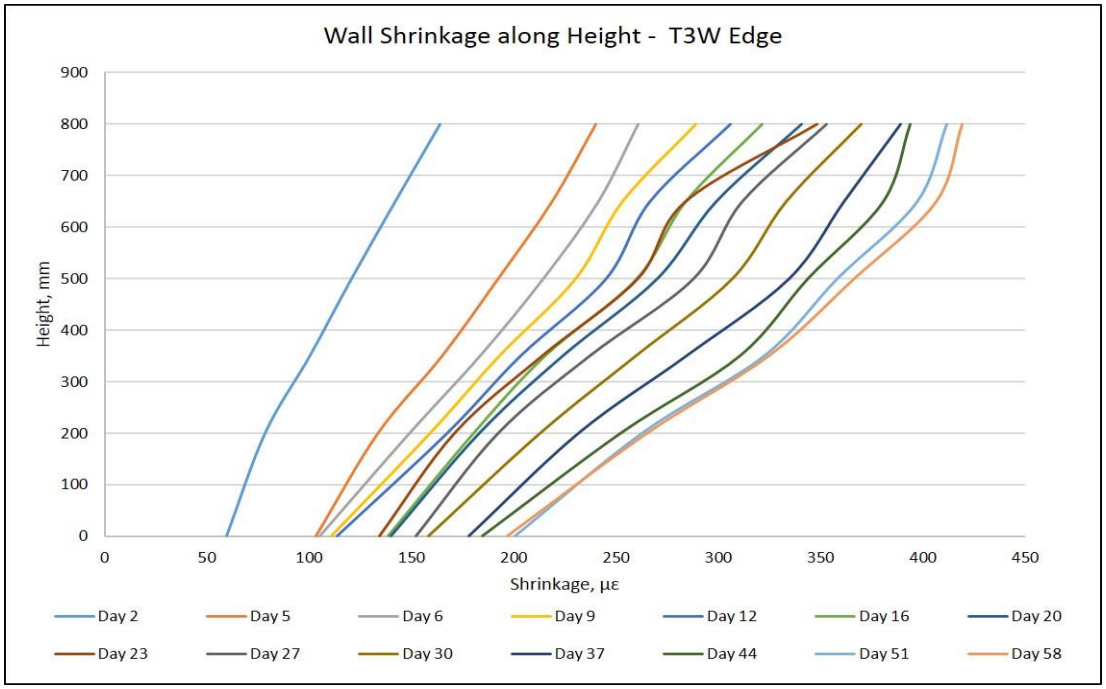

(b)

Figure 4.8. Variation of surface strain along height: (a) Test 3 Middle; (b) Test 3 Edge

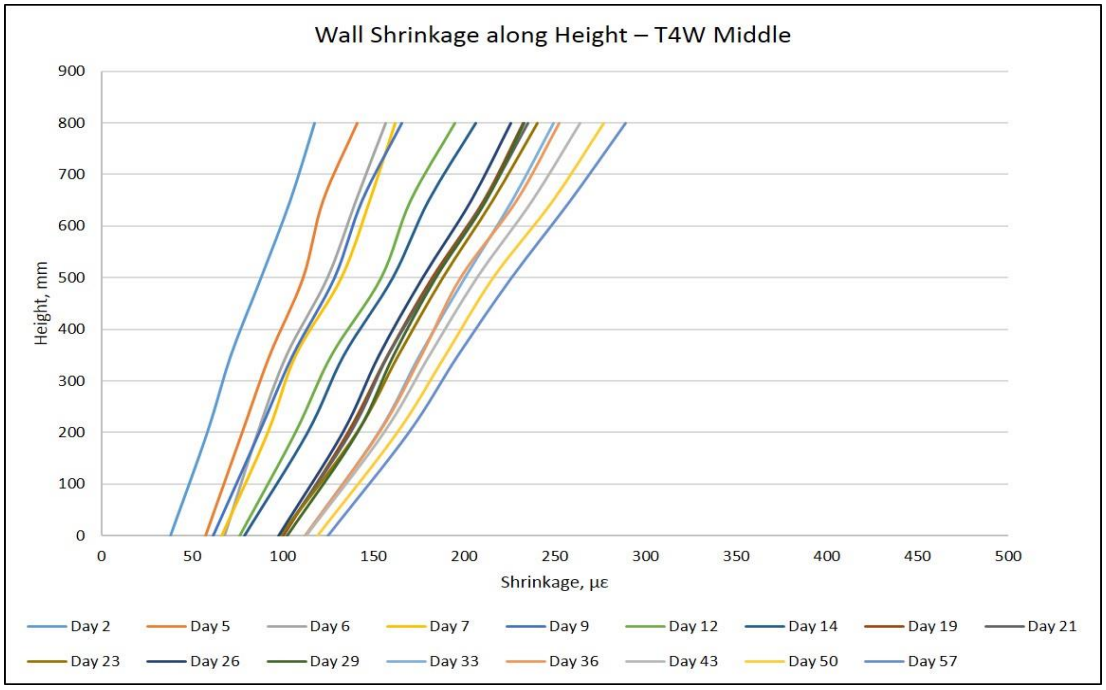

(a)

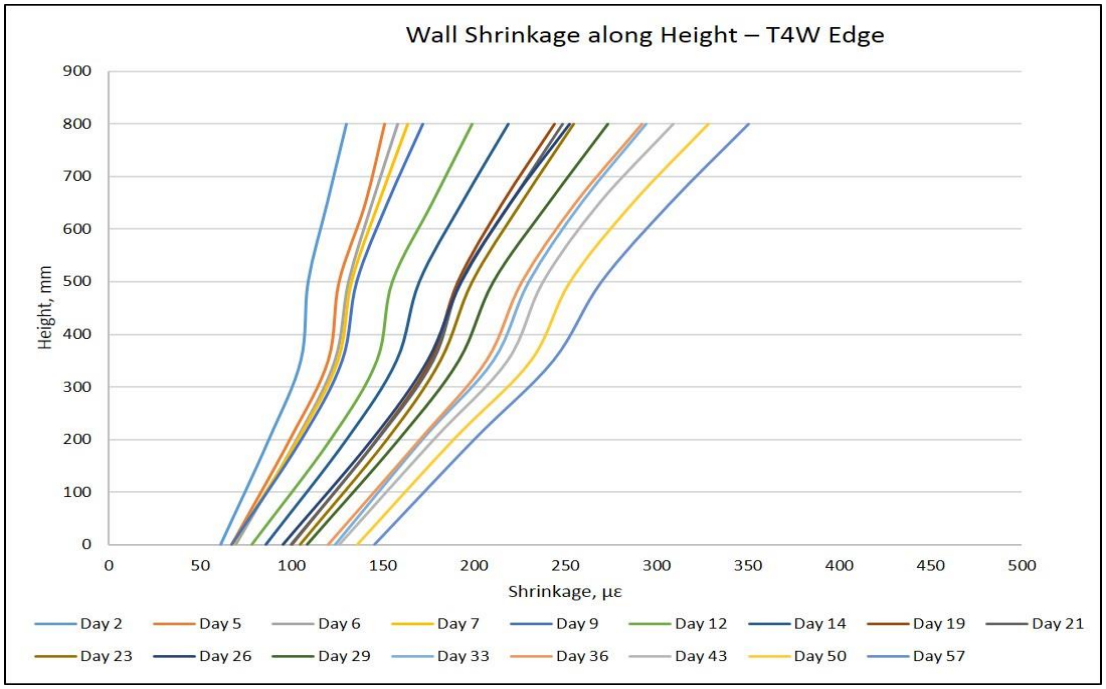

(b)

Figure 4.9. Variation of surface strain along height: (a) Test 4 Middle; (b) Test 4 Edge

4.4 Unrestrained Shrinkage and Thermal Strain

As mentioned in Chapter 3, the unrestrained or free strain in a wall is a combination of the shrinkage strain and the thermal strain. Measurement of free shrinkage strain in a wall of the size of tested specimens is extremely difficult. This is because of the fact that some degree of restraint would always be present even in a free to slide wall. The shrinkage and thermal strain calculation was carried out as mentioned in the following paragraphs.

4.4.1 Unrestrained Shrinkage Comparison and Estimation

To measure the free shrinkage strain, four prisms were cast from each batch of concrete. The prisms were stored close to the tested walls and were therefore subjected to similar temperature and relative humidity. The shrinkage strain was measured on two faces of each prism using a 150 mm DEMEC gauge. First readings were taken as the reference values and from the subsequent readings, the shrinkage strain was calculated. The DEMEC readings on the prisms were taken throughout the test duration. The average of four prisms was calculated and taken as the free shrinkage strain for a particular batch of concrete. Since the prisms were very small in size (compared to the walls) and because of their small volume to surface area ratio, the influence of any type of internal or external restraint in these specimens was unlikely.

Theoretically the development of shrinkage with time was predicted for the tested prisms according to four different models. The actual environmental conditions i.e. temperature and relative humidity, compressive strength and curing time was used as input variables. The shrinkage was predicted according to the CEB FIP 2010 model, the Eurocode model, ACI model and Bazant-Baweja B3 model given in ACI 209.2R-08 (2008). For ACI and Bazant-Baweja B3 model, the ultimate shrinkage strain was predicted from the experimentally obtained data using the Ross hyperbolic method as explained in Section 2.3.2. The shrinkage strain measured from the concrete prisms was compared to the shrinkage predicted by the above mentioned shrinkage prediction models and the comparison for each batch of concrete is given in Figure 4.10. From Figure 4.10, it can be seen that the experimentally observed unrestrained shrinkage observed in all tests was most accurately predicted by Model Code 2010.

The ACI and Bazant-Baweja B3 model predicted quite low values of shrinkage in comparison to those observed experimentally. The Eurocode model prediction was also close to the experimental values however, as the codes are meant to provide slightly conservative values, it slightly over estimated the experimentally obtained shrinkage behaviour. From the stated comparisons, it was decided to calculated the unrestrained shrinkage strain for the tested walls using the method given in Model Code (2010). Using the concrete properties and the notional size of the wall and base, the unrestrained shrinkage for both elements was estimated using the Model Code (2010) for the calculation of the restraint factors.

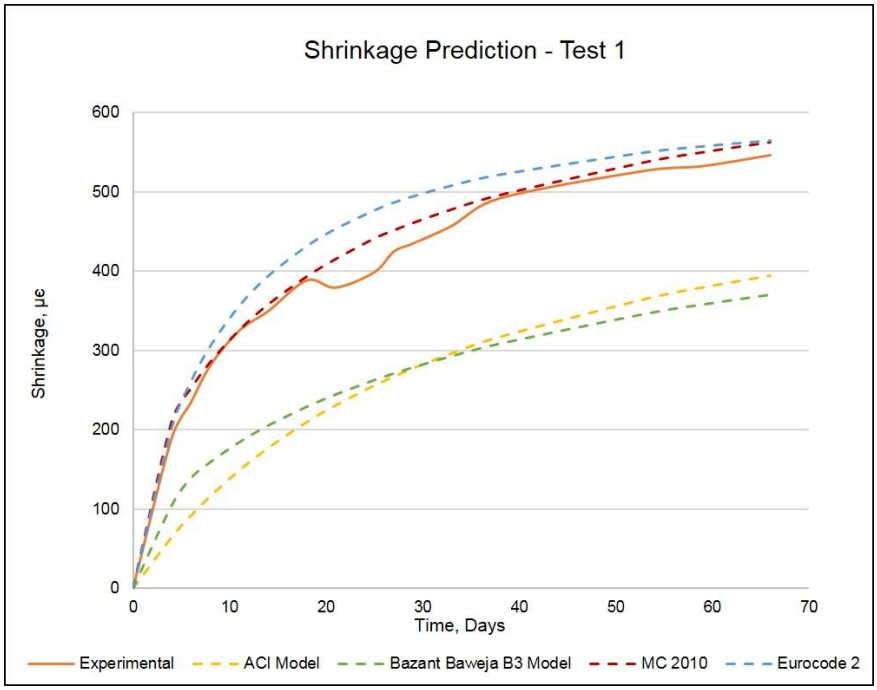

(a)

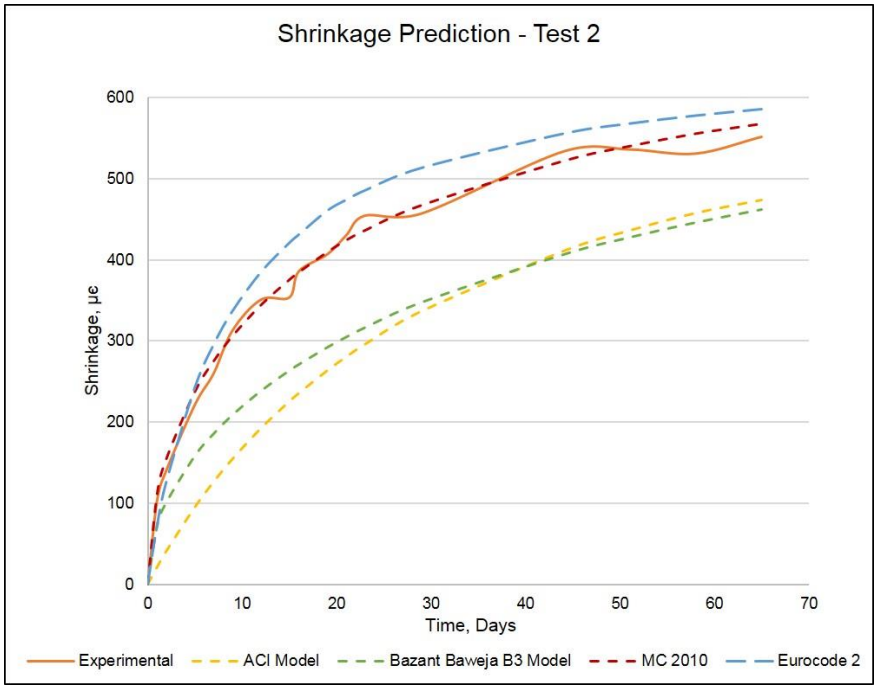
Shrinkage Prediction - Test 2
Shrinkage, με
600
500
400
300
200
100
0
0
10
20
30
40
50
60
70
Time, Days
Experimental
ACI Model
Bazant Baweja B3 Model
MC 2010
Eurocode 2

(b)

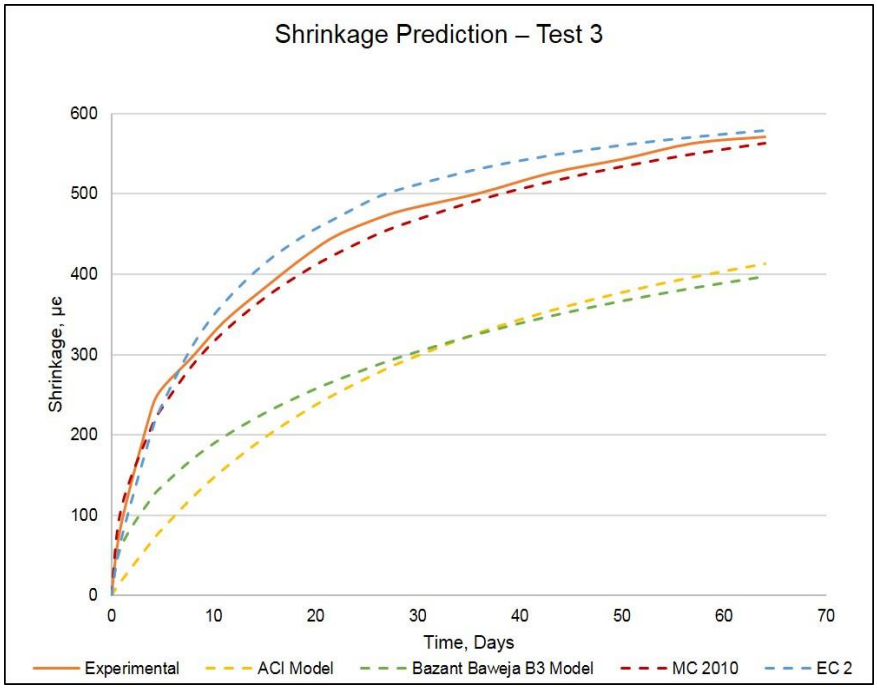
Shrinkage Prediction – Test 3
Shrinkage, με
600
500
400
300
200
100
0
0
10
20
30
40
50
60
70
Time, Days
Experimental
ACI Model
Bazant Baweja B3 Model
MC 2010
EC 2

(c)

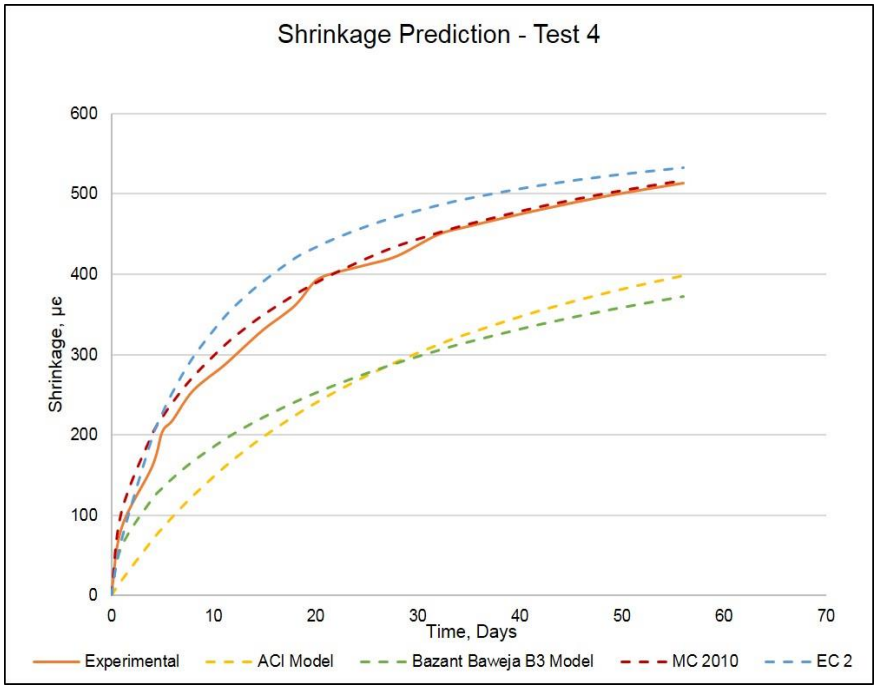

(d)

Figure 4.10. Comparison of predicted and measured shrinkage on prisms: (a) Test 1; (b) Test 2; (c) Test 3; (d) Test 4

4.4.2 Calculation of Thermal Strain

The thermal strain was calculated by multiplying the thermal drop measured by the thermocouples with the coefficient of thermal expansion of the concrete. The coefficient of thermal expansion of concrete (α_c) was not measured experimentally, however, a comparative analysis of the influence of different values of coefficient of thermal expansion on the degree of restraint calculation was carried out using three values i.e. α_c = 9, 10 and 11 $\mu\varepsilon/℃$. This comparison is presented in Section 4.6.3. From this comparison, it was found that the degree of restraint slightly increased with an increase in the value of α_c, however, the variation of restraint over the height and with time remained similar. It was, therefore, decided to use the value of α_c = 10 $\mu\varepsilon/℃$ as recommended by BS EN 1992-1-1 (2004) and Bamforth (2007) in CIRIA 660 when siliceous limestone aggregate is used. The sum of the thermal and shrinkage strain gave the free or unrestrained strain in the wall which was used to calculate the restrained strain and the degree of restraint.

4.5 Influence of Wall on the Shrinkage in Base

In practice, the edge restraint is imposed by an already constructed reinforced concrete element and that is why it was felt important to use a reinforced concrete restraining base. When the wall is cast onto an existing base slab, the transfer of heat from new to old member takes place. This coupled with the ongoing shrinkage mechanism entails an influence on the shrinkage behaviour of the base slab. In order to ascertain and monitor this phenomenon, shrinkage occurring in the base slab before and after construction of the wall was monitored during each test.

The development of shrinkage in the base slab was monitored through the DEMECs installed on both longitudinal faces of the base slab. The DEMECs were installed at two levels along the thickness of the base slab after the curing period ended. 150 mm DEMEC gauge was used for taking the readings. The first readings were taken at the end of the curing period (14 days after casting of the slab) and taking these as a reference, the development of shrinkage in the slab with time was calculated from each of the subsequent readings. In test 3, the wall could not be cast exactly 28 days after casting of the base slab and therefore the monitoring period was more (20 days) in this case which can be seen in Figure 4.11 (c) below. Just like the wall, average of the shrinkage measured on each face was taken.

To estimate the free shrinkage for the base slab, four prisms (75 x 75 x 200 mm) were cast from the concrete used for casting the base slab. Development of shrinkage with time was monitored using these prisms and was compared to the four shrinkage prediction models (as mentioned above in Section 4.4.1). The free shrinkage which would have occurred in the base slab in the absence of any form of restraint was estimated using the Model Code (2010).

The shrinkage measured on both faces of the base slab was averaged and the ratio of measured shrinkage to the free shrinkage was calculated. This ratio was calculated for each of the readings taken prior to casting of the wall. The ratio provided the fraction of free strain which was exhibited by the base slab. To extrapolate the shrinkage behaviour of the base slab prior to casting of the wall, average of the calculated ratios / fractions was taken. Based on the observed shrinkage in the base prior to casting of the wall, the shrinkage strain likely to occur in the base in the

absence of wall was extrapolated by multiplying the calculated average fraction with the free shrinkage strain. A comparison of the measured shrinkage strain, predicted free shrinkage strain and the extrapolated shrinkage strain for the base slab was drawn in each test. This comparison is given in Figure 4.11 for each test.

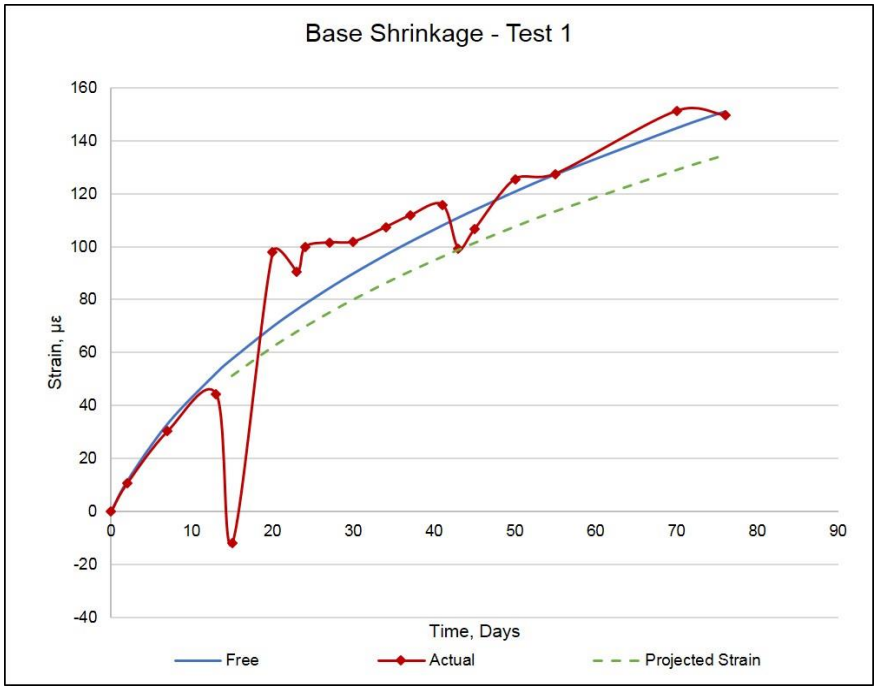

(a)

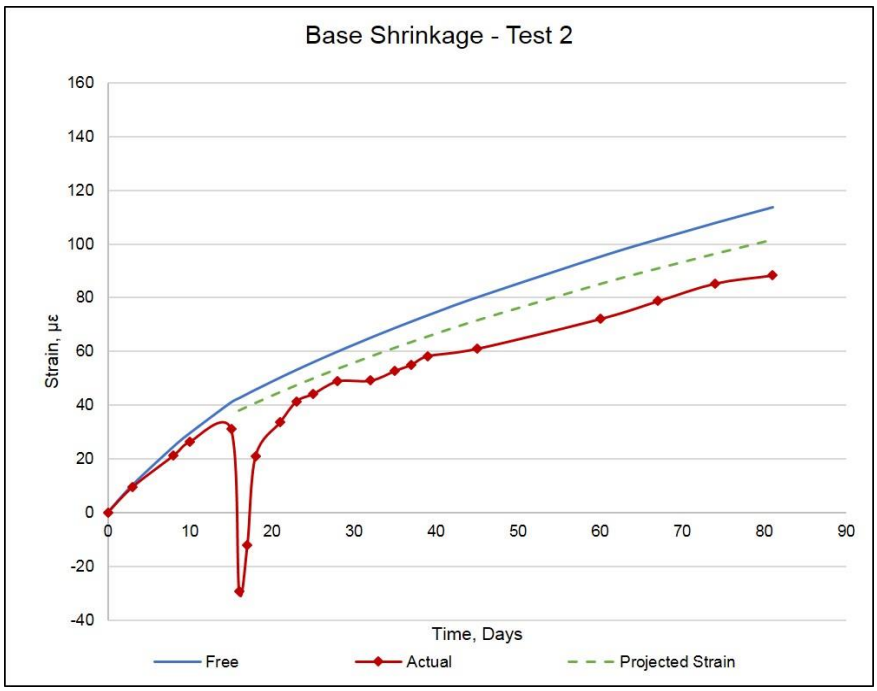

(b)

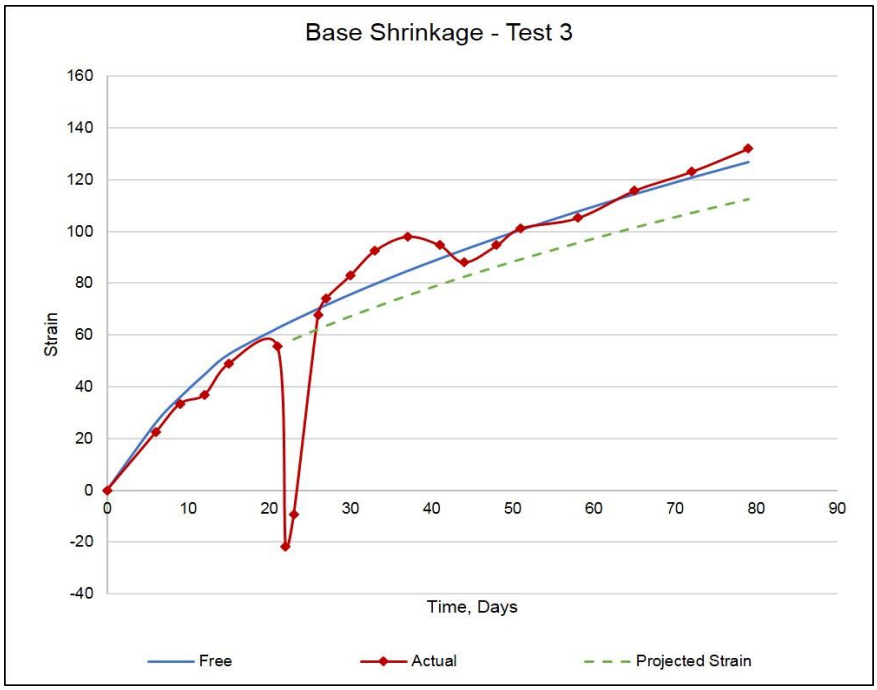

(c)

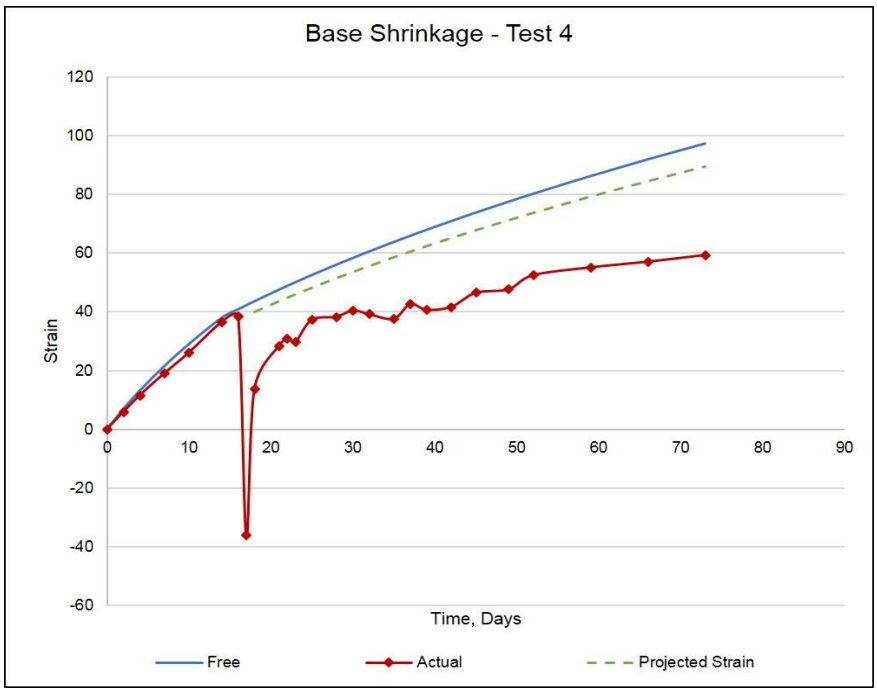

(d)

Figure 4.11. Influence of the wall on the shrinkage development in base slab: (a) Test 1; (b) Test 2; (c) Test 3; (d) Test 4

From these results it is obvious that the volume changes occurring in the newly cast wall influences the volume change in the base slab. This occurs primarily due to the flow of heat from wall to the base during the hydration process. Monitoring of the temperatures in the wall and the base indicates that a large portion of the heat generated in the bottom part of the wall flows into the base slab. Immediate effect is an expansion of the base slab which can be noticed in Figure 4.11 and it is followed by the contraction when the wall concrete starts to cool down. In the absence of steel dowels at the interface between the wall and slab, an additional amount of strain is imposed on to the base slab as the experimentally obtained strain profile deviates and goes beyond the projected strain profile. The heat generated by the wall after casting meant that the base also underwent thermal changes along with the wall and an expansion in the base was observed after the wall was cast followed by a subsequent contraction (see Figure 4.11). It was noticed that in test 1 and 3, the base exhibited more strain than was anticipated from its behaviour before the wall was cast whereas in test 2 and 4, the induced volume change in the base was restrained due to the presence of the vertical steel reinforcement.

By reducing the wall thickness in test 3 and 4, two cases of relative axial rigidity of the restrained and restraining members were studied. The base slab in test 3 and 4 had relatively more axial rigidity (ratio of the cross sectional area of the base to that of the wall was more) compared to that in test 1 and 2. From Figure 4.11, it can also be noticed that the additional strain was more when the base had a smaller cross section than the wall (Test 1) and was comparatively lesser when the base cross sectional area was larger than that of the wall (Test 3). Similarly, in test 4, the measured values of strain deviate more from the extrapolated strain curve as compared to test 2. This implied that the inhibited or restrained strain was lesser when the base had a smaller cross section than the wall (Test 2) and was comparatively more when the base cross sectional area was larger than that of the wall (Test 4). Although the amount of additional or restrained strain varies in both cases, yet it is evident that the phenomenon is primarily influenced by the presence or absence of the steel reinforcement at the interface between the wall and base.

It can, therefore, be inferred from the results that the steel dowels enhance the stiffness and thus the restraint imposed by the base on the wall. This interaction

between the base and the wall is clearly difficult to quantify when steel members are used as a restraining base; yet it is extremely important. The restrained strain at the bottom of the wall is the combination of the restrained strain calculated for the wall and the restrained strain in the base. Therefore, in the experimental evaluation of the degree of restraint, it is important to take into account the strain restrained from occurring in the base slab in order to correctly ascertain the degree of restraint imposed on the wall. The presence of the steel reinforcement at the joint has clearly increased the stiffness of the base slab. However, currently available guidance for the estimation of the restraint factor does not incorporate this steel reinforcement ratio. The amount of vertical steel reinforcement present at the joint between the restrained and the restraining members is therefore an important contributory factor towards the formulation of restraint and needs to be incorporated within the design guidance.

4.6 Degree of Restraint

4.6.1 Calculation of the Degree of Restraint

Degree of restraint was calculated for the edge and centre parts of the wall in each test from the exhibited strain on the wall surface. Degree of restraint is regarded as the ratio of restrained strain to unrestrained or free strain. The unrestrained or free strain was taken as the sum of thermal strain (calculated from the thermal drop) and the shrinkage strain (calculated according to the Model Code (2010)). From the experimentally observed shrinkage strain on the wall surface and the additional strain imposed or restrained in the base slab (as explained in Section 4.5 above), the restrained strain was calculated as under:

$$\varepsilon_r = \varepsilon_{free} - \varepsilon_{measured} + \Delta\varepsilon_{base}$$

where; ε_r is the restrained strain, ε_{free} is the unrestrained or free strain, $\varepsilon_{measured}$ is the measured surface strain on the tested specimens and $\Delta\varepsilon_{base}$ is the additional strain imposed or restrained in the base slab due to the wall.

The restrained strain was calculated at three points along the wall height i.e. bottom, middle and top levels. Accordingly the degree of restraint was calculated for these three levels and the variation of degree of restraint along the wall height was

plotted. From the restrained strain and the free strain, the degree of restraint (R_{ax}) at any particular time was calculated using the following equation.

$$R_{ax} = {\varepsilon_r}/{\varepsilon_{free}}$$

4.6.2 Estimation of Restraint Factor According to Different Existing Guidelines

For the purpose of drawing a comparison between the experimentally obtained values of the degree of restraint to theoretically predicted values, the degree of restraint according to various available guidelines was calculated for the tested walls. The restraint profiles for a wall with similar aspect ratio and member sizes were calculated according to the ACI Committee 207 (2007), BS EN 1992-3 (2006) and the work carried out by Stoffers (1978) and Schleeh (1962). In the case of ACI method, the degree of restraint was calculated according to expressions given in Section 2.7.1 and the experimentally obtained values of the moduli of elasticity for both wall and the base elements was used. BS EN 1992-3 (2006) method provides a constant value of the degree of restraint along the height of wall. The restraint factor according to the work of Stoffers (1978) and Schleeh (1962) was calculated from their experimental findings for a wall with aspect ratio of 4.

4.6.3 Influence of the Coefficient of Thermal Expansion on the Degree of Restraint

As mentioned previously, the coefficient of thermal expansion was not measured in the laboratory experimentally for this study. Limestone crushed aggregate was used in all the tests. Based on the recommendations contained in CIRIA C660 (2007) and BS EN 1992-1-1 (2004), the value of coefficient of thermal expansion was selected as 10 $\mu\varepsilon/℃$. However, a comparative analysis of the influence of the value of coefficient of thermal expansion on the calculation of degree of restraint was carried out during the study and is illustrated in Figure 4.12 for one of the tests.

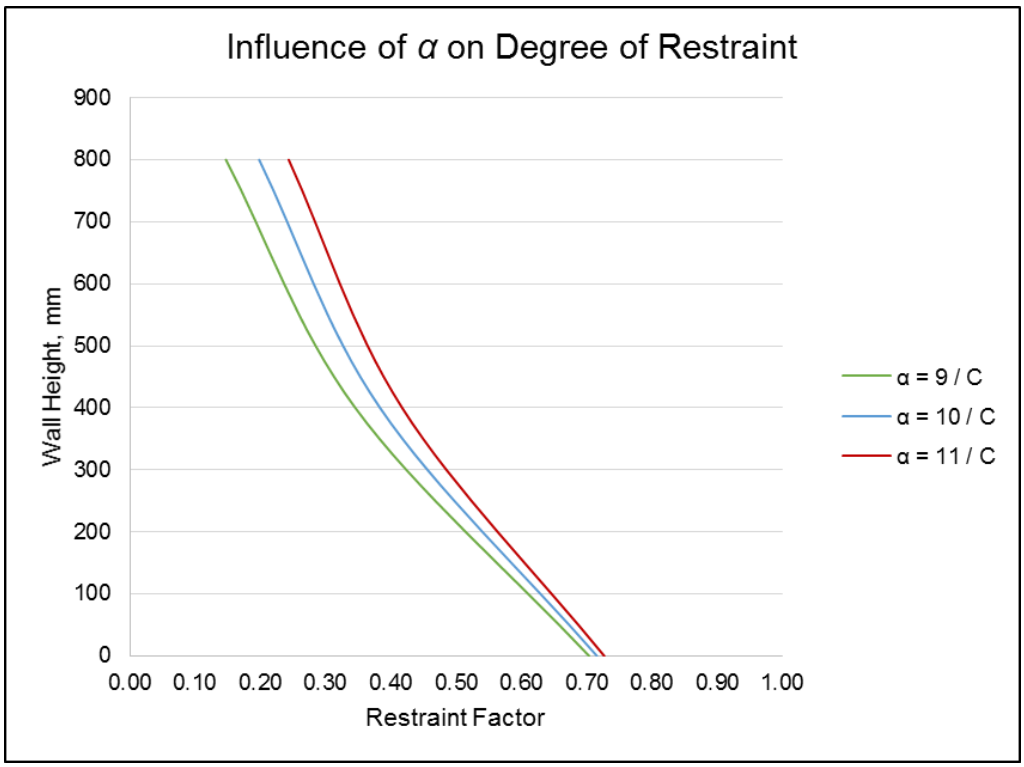

Figure 4.12. Influence of coefficient of thermal expansion on the degree of restraint

Three different values of the coefficient of expansion of concrete i.e. 9, 10 and 11 $\mu\varepsilon/℃$ were used in this analysis. It was noticed that the increase in the value of coefficient of thermal expansion slightly increased the calculated value of degree of restraint. However, the variation of degree of restraint along the height of wall remained constant. This indicated that the choice of coefficient of expansion did not affect the calculation of restraint factors much. Therefore, use of 10 $\mu\varepsilon/℃$ as coefficient of thermal expansion in the light of above mentioned design guidance was considered justified.

4.6.4 Variation of Degree of Restraint along Wall Height

Comparison of the stated restraint factors and the variation of restraint over the height of the wall for each of the tested walls is given in Figures 4.13 to 4.16. The restraint at the edge and middle regions of the wall has been compared to the predicted values. The restraint factors calculated for each of the wall in the first week after casting and at the end of the monitoring period have been compared. From the comparison it can be seen that the restraint is greater in the middle section of the wall and lower near the free ends. The experimentally obtained values of restraint vary considerably from the predicted values. For test 1 and 3 (no vertical steel at the joint

between wall and base) the degree of restraint is less, whilst in test 2 and 4 (vertical steel present) the restraint is greater.

It is also obvious from the test results that due to the presence of the vertical steel reinforcement, the degree of restraint significantly increased at the joint between the two members. In test 1 and 2, the wall and base slab had the same geometry and the only factor varied was the vertical steel reinforcement. The degree of restraint at the bottom of the wall in test 1 was 0.39 and in test 2 (by providing 0.9% vertical steel reinforcement) the restraint factor increased up to 0.57 (an increase of 46%) during the first week after casting. Similarly in test 3, the degree of restraint imposed by the base slab was 0.40 and in test 4 (by providing 1.4% vertical steel reinforcement) it increased to 0.67 (an increase of 67.5%) at the end of first week. By reducing the wall thickness from 300 mm in test 1 to 200 mm in test 3 where in both walls no vertical steel reinforcement was present, the degree of restraint did not change much. It was 0.39 in test 1 (300 mm wall thickness) and 0.40 in test 3 (200 mm wall thickness). This highlights the fact that the vertical steel dowels play a more significant role in increasing the restraint rather than the relative geometry of the two members.

From these results it is also important to note that increasing the size of the base slab relative to wall had a very little impact on the increase in restraint factor. Whereas, increasing the steel reinforcement at the joint between the wall and base slab significantly changed the degree of restraint imposed. Moreover, when the vertical steel reinforcement was present (test 2 and 4), the degree of restraint at the joint location increased with time whereas in its absence (test 1 and 3), a decrease in the restraint values with time was witnessed. This aspect has been discussed in more detail in section 4.6.4 below.

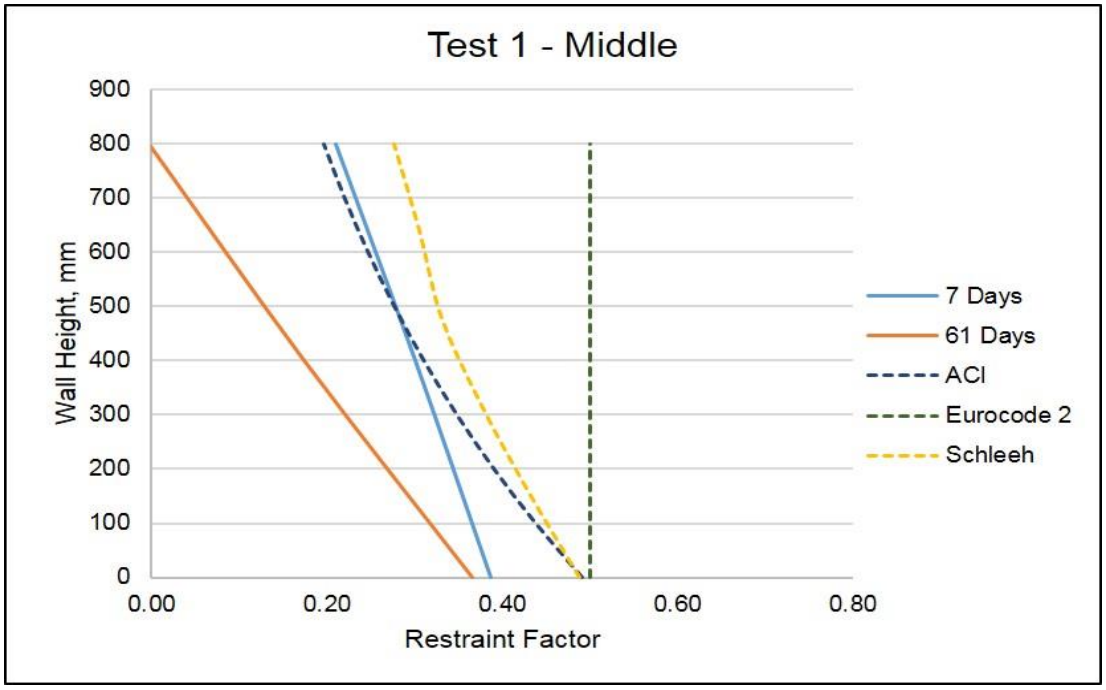

(a)

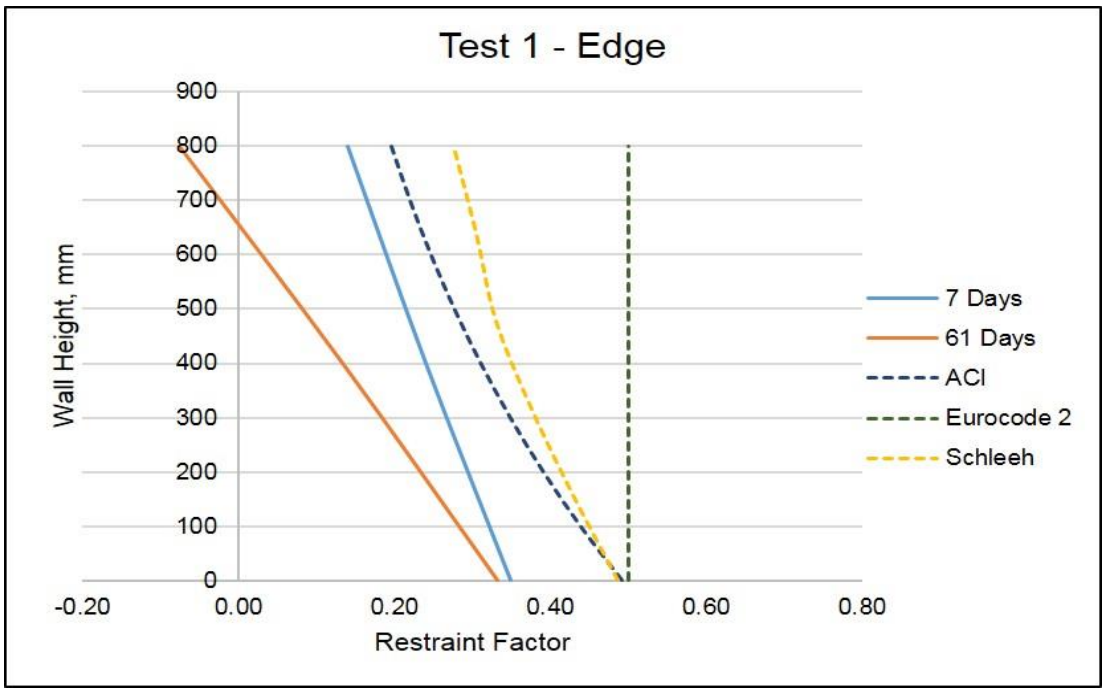

(b)

Figure 4.13. Variation of the degree of restraint along height and its comparison to the theoretically calculated values for T1W: (a) Middle; (b) Edge

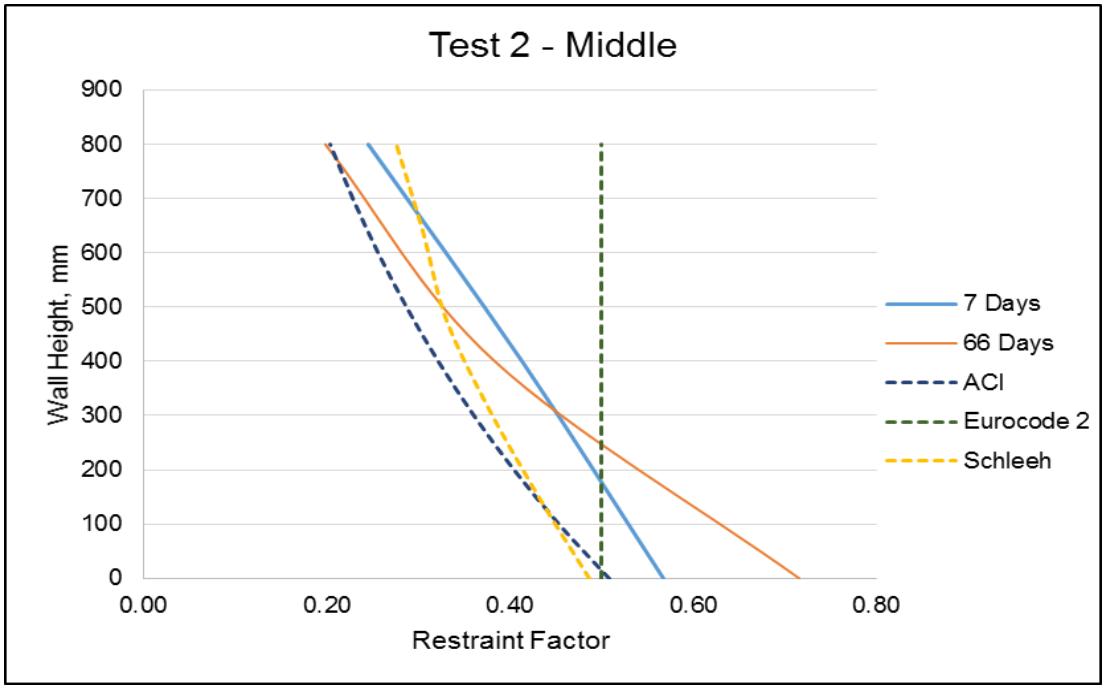

(a)

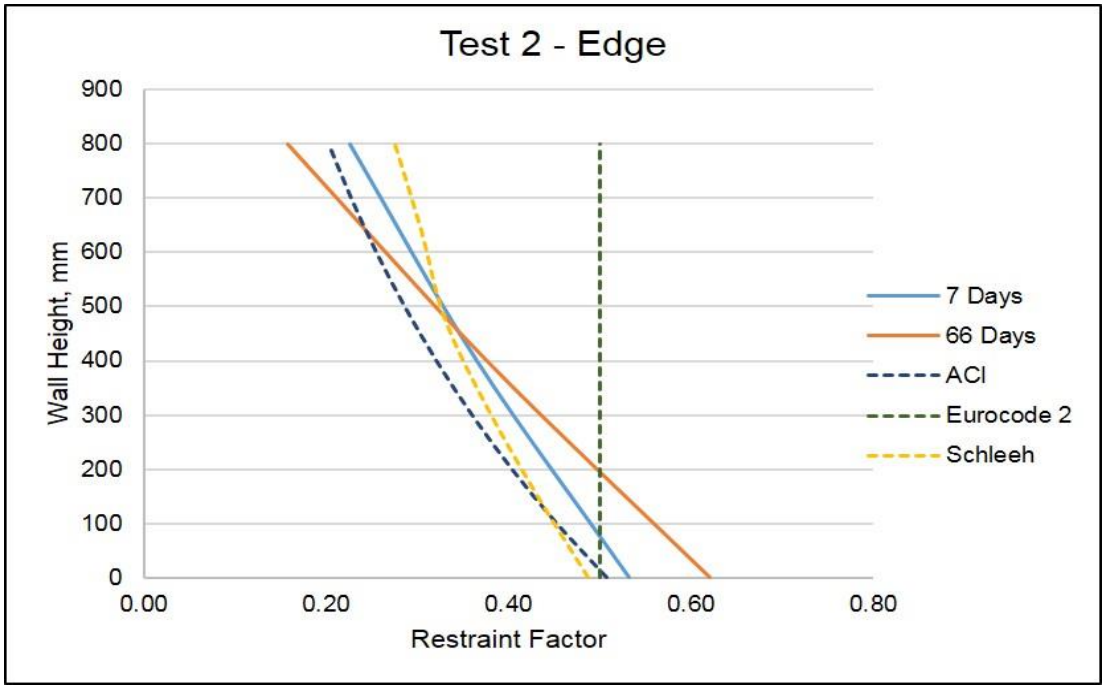

(b)

Figure 4.14. Variation of the degree of restraint along height and its comparison to the theoretically calculated values for T2W: (a) Middle; (b) Edge

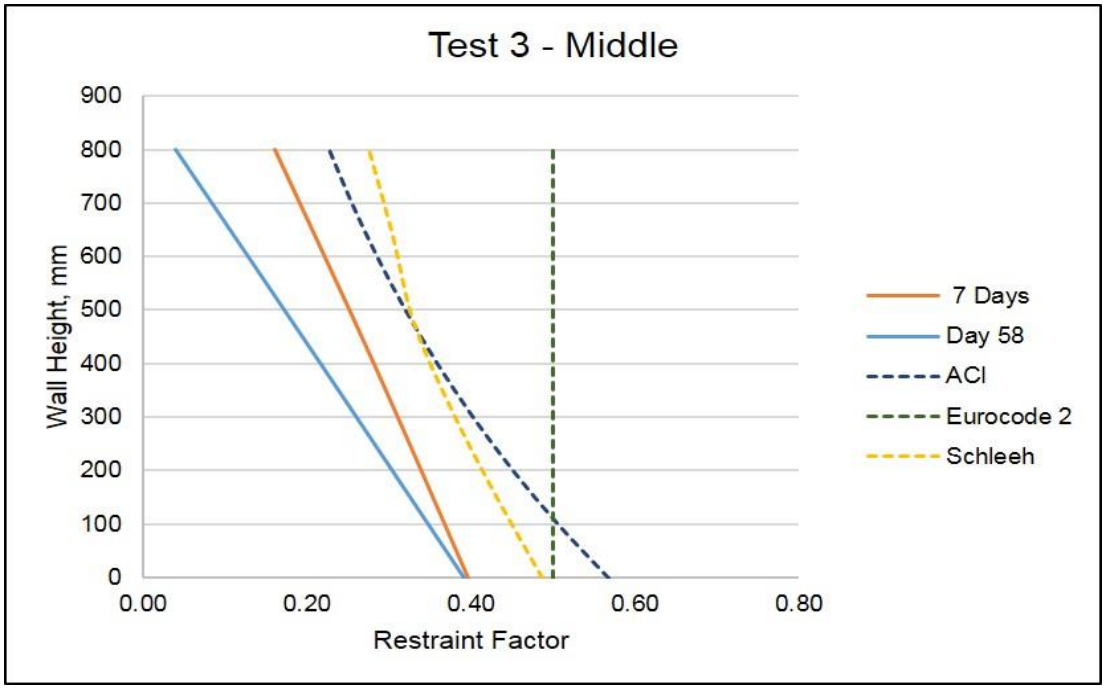

(a)

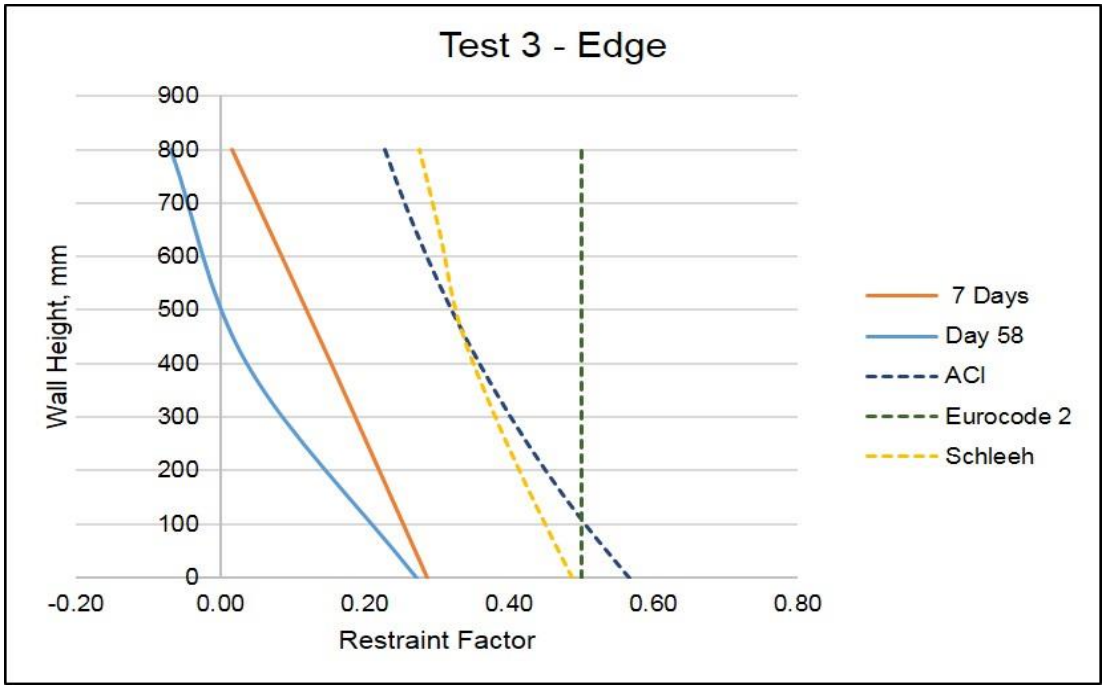

(b)

Figure 4.15. Variation of the degree of restraint along height and its comparison to the theoretically calculated values for T3W: (a) Middle; (b) Edge

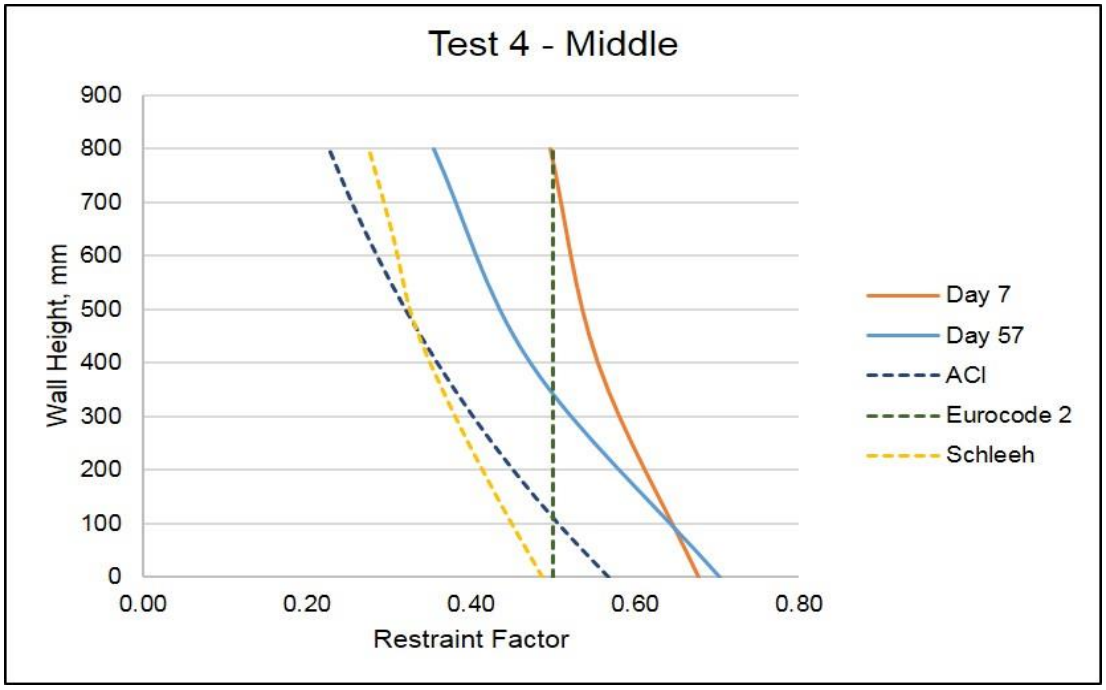

(a)

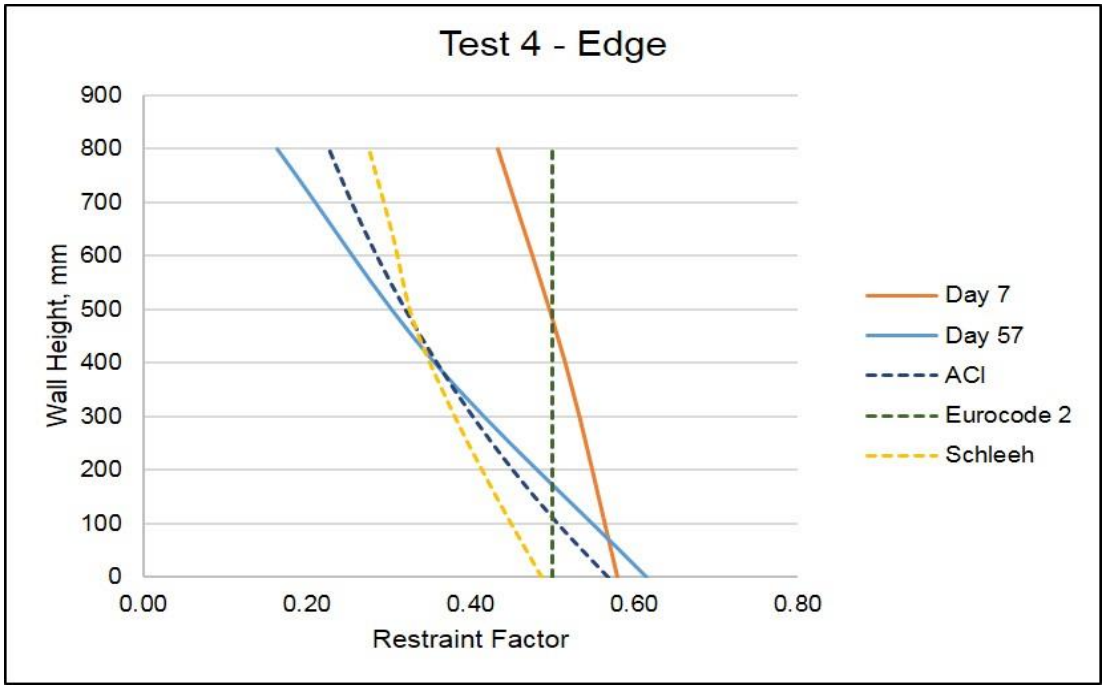

(b)

Figure 4.16. Variation of the degree of restraint along height and its comparison to the theoretically calculated values for T4W: (a) Middle; (b) Edge

Figures 4.13 to 4.16 also indicate that the experimentally measured restraint decreases over the height of the wall. Degree of restraint being maximum at the joint

between the restrained and restraining members and minimum at the top of the wall. This decrease in restraint over the height of wall has also been mentioned by other researchers (Bamforth, 2007; Stoffers, 1978; Kheder, 1997; Nilsson, 2003; Carlson et al., 1988). Although Micallef (2017) observed that the restraint is maximum at some point above the mid height of the wall and decreases towards the top and bottom of the wall. When compared to the predicted restraint profiles, considerable difference between the experimental and theoretical values was noticed. The variation between the experimental and predicted restraint factors at the joint and along the height of wall indicates that the existing methods of restraint estimation do not take into account all contributory factors.

It can also be seen that the variation of restraint over the height of wall is affected by the presence of vertical steel reinforcement. With time, the restraint over the height of wall decreases. In test 1 and 3, there was a significant loss of restraint over the height, whereas in test 2 and 4, the loss of restraint was comparatively lower. Previously (Micallef, 2017; Bamforth, 2007), it was believed that the loss of restraint over the height of a member is dependent on the height and aspect ratio of the members. However, these tests indicate that the amount of vertical steel reinforcement present in the wall also appears to contribute significantly to the degree of restraint at different points over the height and length of the wall.

From Figures 4.13 to 4.16, it can also be seen that there is a change (reduction) in the gradient of the degree of restraint close to the top of the wall (middle section). It is thought that by preventing the base slab from curling, even though very little force was needed to do this, this may have induced a slight amount of tension near the top of the wall effectively reducing the restraint at this point.

4.6.5 Variation of Restraint with Time

The variation in the calculated degree of restraint at the joint with time was analysed and is shown in Figure 4.17 for each of the tested walls. In test 1 and 3, the degree of restraint decreased with time while in test 2 and 4 it increased. The increase and decrease in restraint with time was more pronounced in test 1 and 2 as compared to test 3 and 4. Experiments by Micallef (2017) on edge restrained reinforced concrete walls also revealed an increase in restraint with time. Micallef (2017) attributed the

increase in restraint to the loss of wall stiffness due to the occurrence of cracks. However, in the current study presented here, the degree of restraint increased with time in the presence of vertical steel dowels even when the wall did not exhibit any cracks (See Figures 4.17(b) and 4.17(d)). Also, even when cracks began to form; after 51 days in test 2 and after 23 days in test 4, there was no change to the gradient of increasing restraint with time. This highlights the fact that the increase in restraint with time is attributed to the steel reinforcement dowels at the interface between the wall and base.

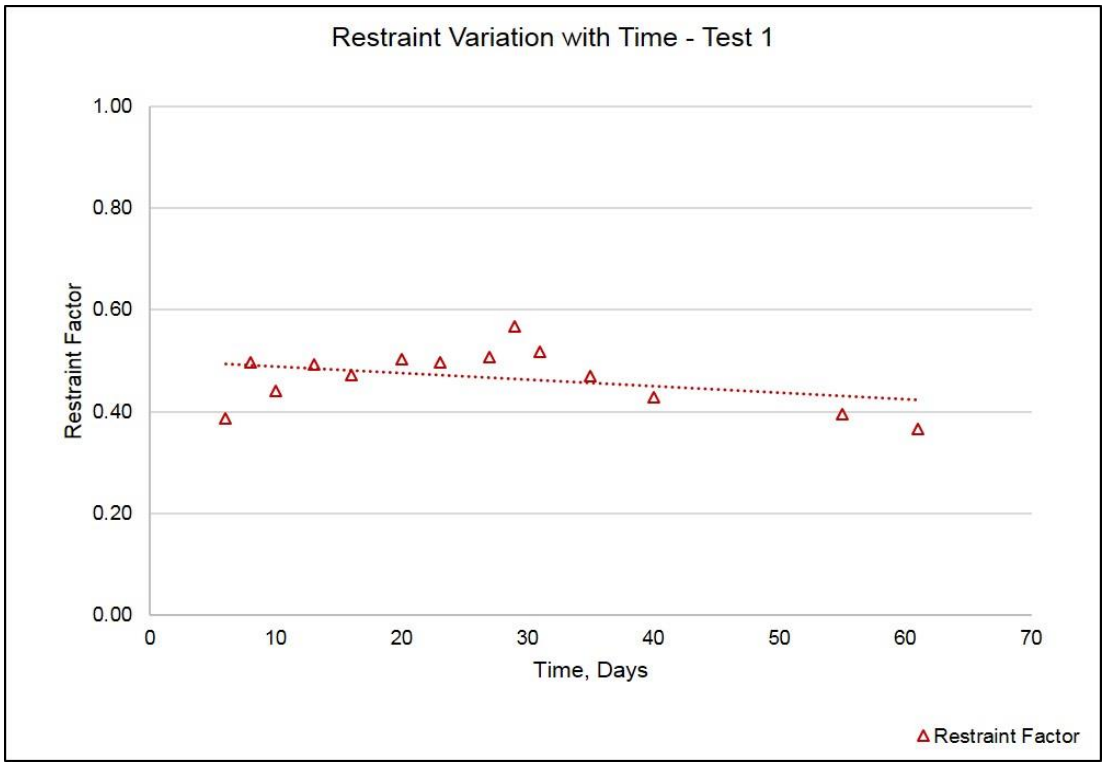

(a)

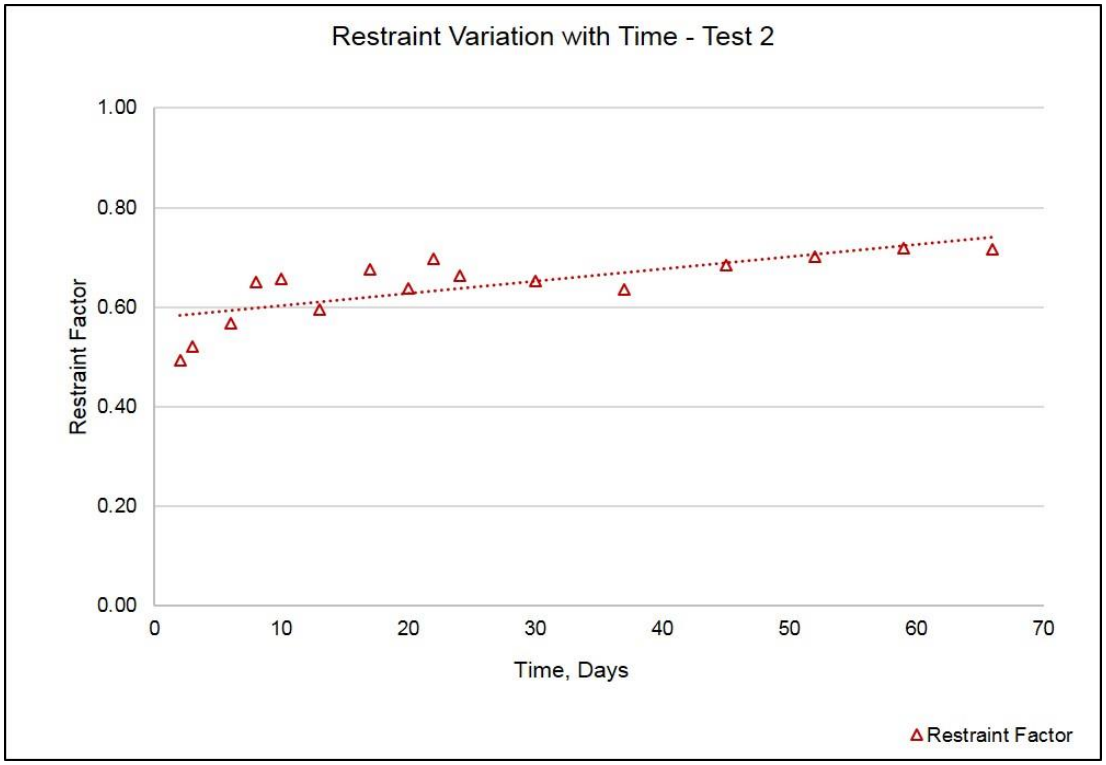
Restraint Variation with Time - Test 2
1.00
0.80
0.60
0.40
0.20
0.00
Restraint Factor
0
10
20
30
40
50
60
70
Time, Days
Restraint Factor

(b)

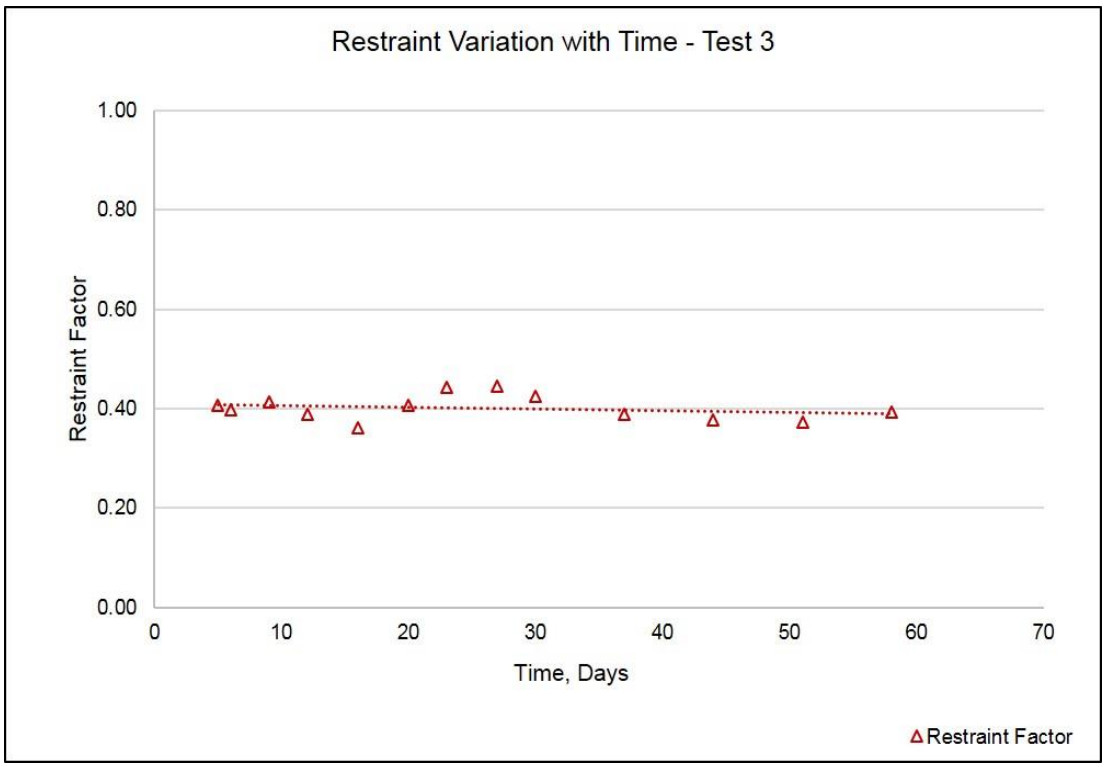
Restraint Variation with Time - Test 3
1.00
0.80
0.60
0.40
0.20
0.00
Restraint Factor
0
10
20
30
40
50
60
70
Time, Days
Restraint Factor

(c)

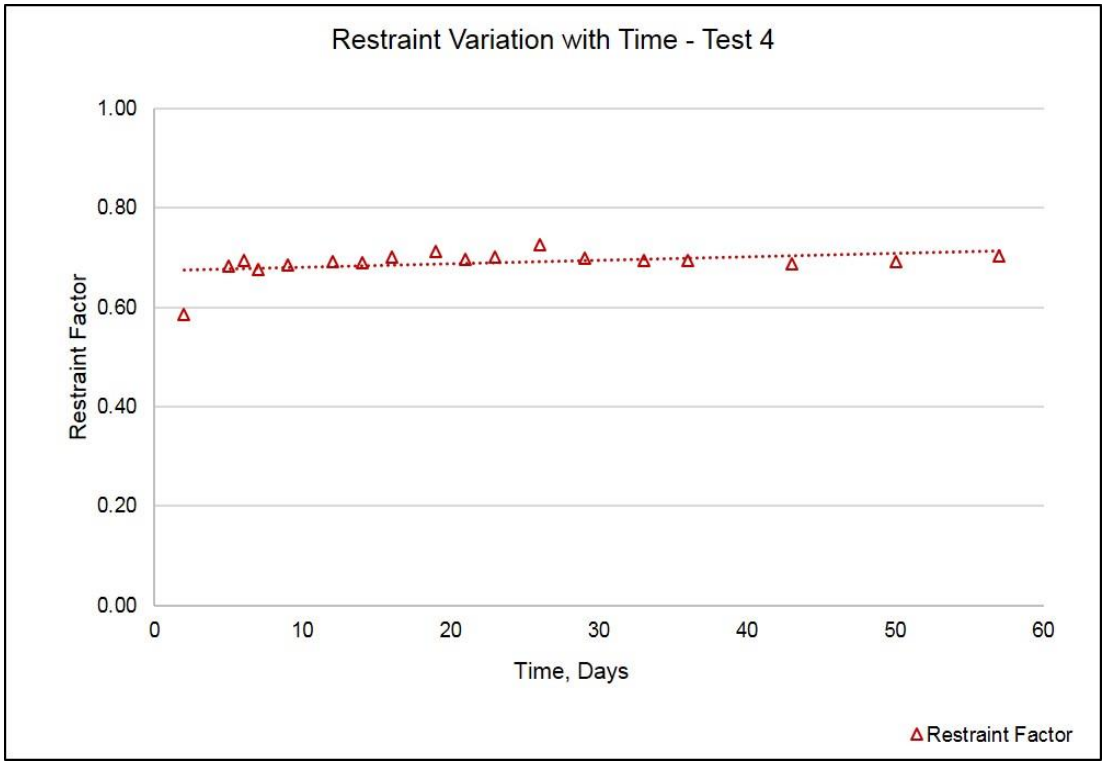

(d)

Figure 4.17. Variation of the degree of restraint with time: (a) Test 1; (b) Test 2; (c) Test 3; (d) Test 4

It is thought that the vertical reinforcement dowels provide an increased restraint to the ongoing shrinkage in both members and thus increase the value of the restraint factor. The restrained strain in the base slab increases due to the steel bars and further augments the restrained strain present at the bottom of the wall. Moreover, the slip at the interface between the old and new member is also prevented by the steel reinforcement dowels. All of these factors contribute towards the increase in degree of restraint. In the absence of vertical reinforcement dowels (test 1 and 3), the time dependent shrinkage occurred without this restraint and the degree of restraint decreased with time.

From these experimental results it can be seen that the degree of restraint decreased with time when $\rho_v = 0$ (test 1 and 3) and increased when $\rho_v = 0.9\%$ (test 2). This implies that within this range of vertical steel reinforcement, the degree of restraint may still decrease with time even if some amount of vertical steel reinforcement is present. Further investigation is, therefore, required into the effect of vertical steel reinforcement ratio.

4.7 Comparison of the Restrained Strain and Tensile Strain Capacity of Concrete

Cracks initiate in the reinforced concrete members when the restrained strain in the concrete exceeds the tensile strain capacity of concrete. Development of the restrained strain in each of the tested walls with time was compared to the development of tensile strain capacity of the concrete. In order to calculate the tensile strain capacity of concrete, the experimentally obtained values of tensile strength and modulus of elasticity of concrete were used. Tensile strain capacity was calculated as a ratio of the tensile strength to the modulus of elasticity of concrete. The development of strength and modulus of elasticity was estimated using the Eurocode expressions.

According to Tasdemir (1996) the value of tensile strain capacity calculated from the ratio of tensile strength to the modulus of elasticity of concrete represents a lower bound value. The stresses generated in the concrete due to early age thermal and shrinkage effects represent a sustained loading. Bamforth (2007) in CIRIA C660 suggested that the tensile strain capacity of concrete increases due to creep relaxation and a reduction in the failure stress due to the sustained loading. Tensile strain capacity for the concrete used in each test was also calculated according to the recommendations in CIRIA C660 (2007) as explained in detail in Section 2.6.1 and compared to the restrained strain. The comparison of the restrained strain with the tensile strain capacity for each test is given in Figure 4.18.

From Figure 4.18, it can be seen that the restrained strain in test 1 remained below the tensile strain capacity of concrete, calculated as a ratio of tensile strength to modulus of elasticity and was exceeded after 20 days in the case of test 3. But in both of these tests no cracking in the walls was observed during the monitoring period. In the case of test 2 and 4, the tensile strain capacity calculated from the ratio of tensile strength to the modulus of elasticity is exceeded during the first week after casting. However, in these tests also, no cracking was observed during this time.

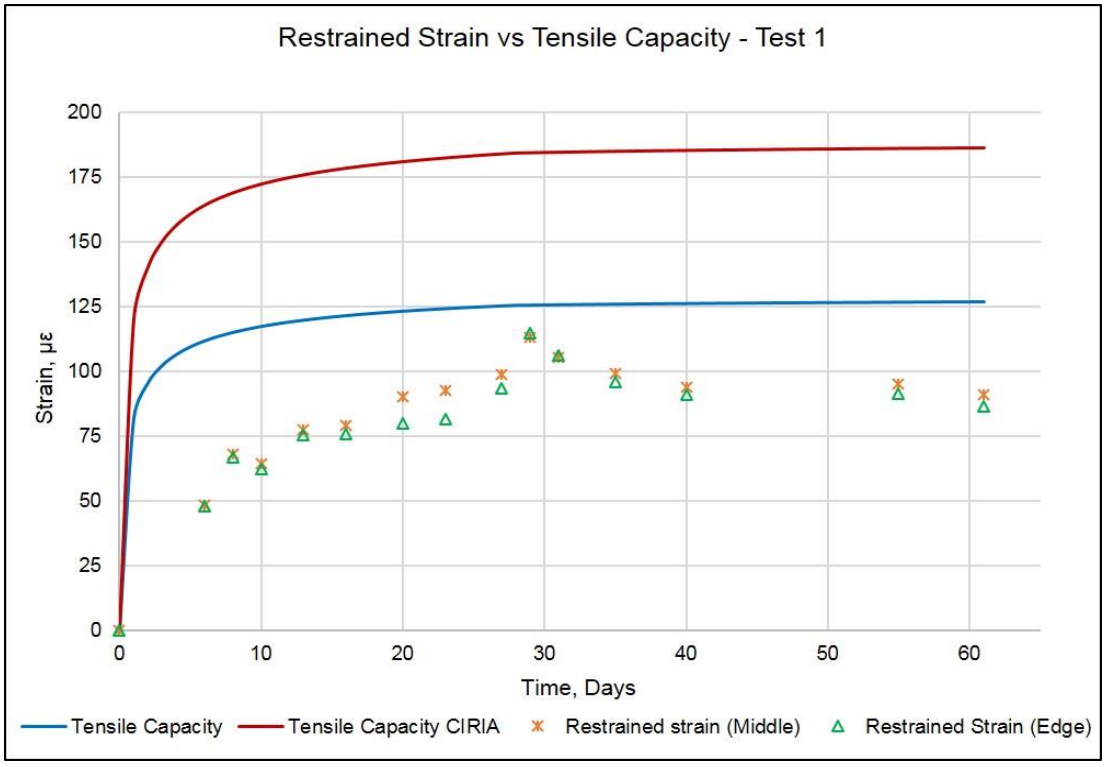
Restrained Strain vs Tensile Capacity - Test 1
Strain, με
Time, Days
Tensile Capacity
Tensile Capacity CIRIA
Restrained strain (Middle)
Restrained Strain (Edge)

(a)

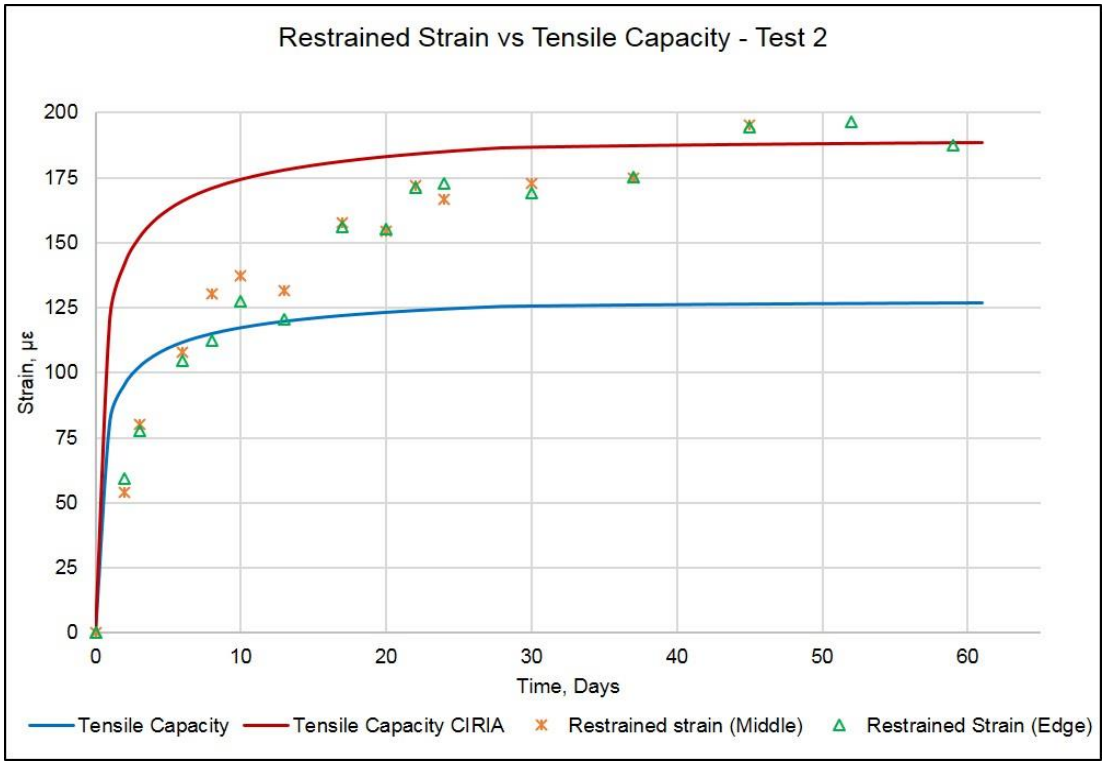
Restrained Strain vs Tensile Capacity - Test 2
Strain, με
Time, Days
Tensile Capacity
Tensile Capacity CIRIA
Restrained strain (Middle)
Restrained Strain (Edge)

(b)

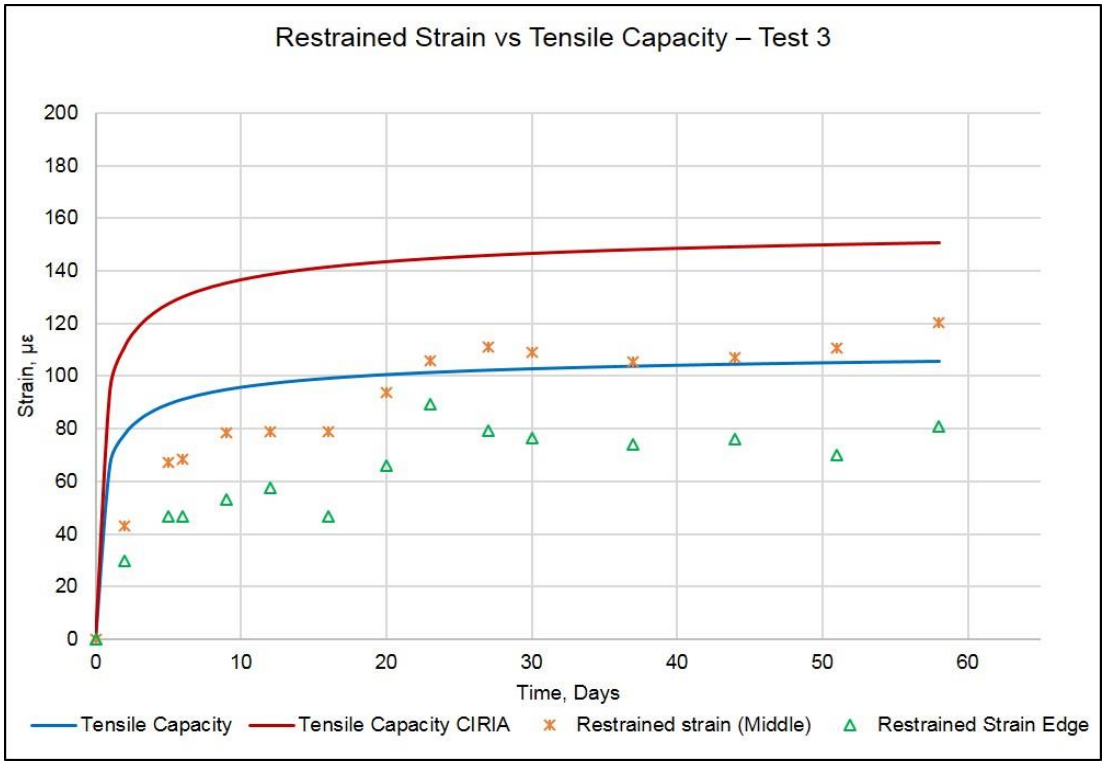

(c)

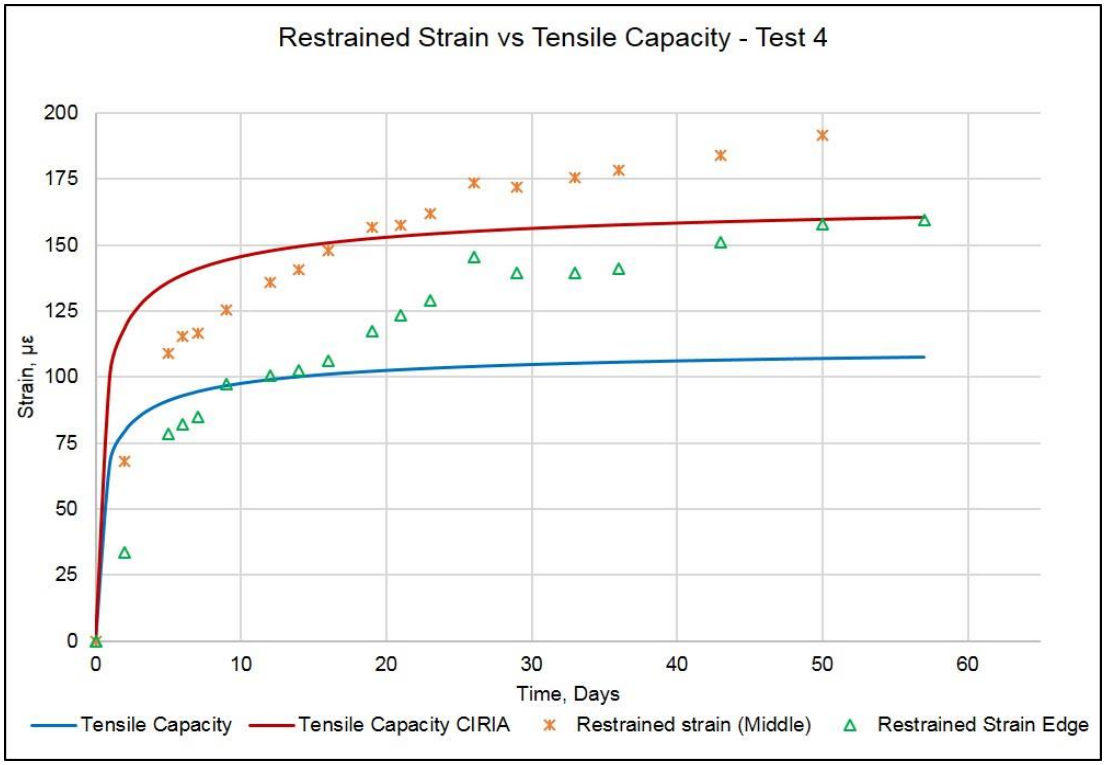

(d)

Figure 4.18. Comparison of the experimentally calculated restrained strain with tensile strain capacity of concrete: (a) Test 1; (b) Test 2; (c) Test 3; (d) Test 4

Figure 4.18 also compares the restrained strain with the tensile strain capacity calculated on the basis of the CIRIA C660 (2007) recommendations. The comparison for test 2 revealed that the restrained strain in the middle part of the wall exceeded the tensile strain capacity of the concrete 45 days after casting. The first crack in the wall T2W was observed 51 days after casting. Similarly in the case of test 4, the restrained strain exceeded the tensile strain capacity of concrete after 19 days and the first crack in this case occurred 23 days after casting.

The comparison given in Figure 4.18 reveals that the tensile strain capacity calculated as the ratio of the tensile strength to the modulus of elasticity of concrete does not realistically predict the tensile capacity for members subjected to restraint of imposed loads. The development of tensile strain capacity calculated based on the CIRIA C660 (2007) recommendations quite closely resembles the experimental observations. Therefore, it is concluded that Eurocode 2 underestimates the development of the tensile strain capacity of the concrete and that the recommendations in CIRIA C660 (2007) for predicting the tensile strain capacity of the concrete are more reasonable. Although since the predicted crack was 4 - 6 days earlier than the crack observed during the test, this suggests that the theory for tensile strain capacity, though appropriate, still needs some fine tuning.

4.8 Observed Cracking

Monitoring of the tested walls to check the appearance of any cracks was started after removal of the formwork and continued throughout the test duration. The walls were inspected for any possible cracks using the magnifying glass. Moreover, sudden change in the DEMEC values and the calculated strain were also monitored and provided evidence of the crack formation. On occurrence, the cracks were marked and numbered and their propagation with time was noted. Crack widths were measured along the height of the crack using the portable microscope. Variation of the crack widths with time was also monitored.

4.8.1 Initiation of Cracking

At the start of this investigation, based on overall current theory, cracking due to the restraint of early age thermal and shrinkage imposed strains could be expected in the walls only a few days after casting. However, in the case of T1W and T3W, no

cracks appeared during the entire duration of the test. In T2W, no cracks were observed during early ages, however, with the passage of time and with an increase in the magnitude of restrained strain the first crack occurred 51 days after casting. The first crack formed on both faces of the walls at almost the same location along the length. The crack did not start at the joint, rather at 200 mm above the joint. It then propagated upwards and downwards over the wall height.

In T4W again no cracks appeared during the initial few weeks. Later, as the restrained strain increased and exceeded the tensile capacity of concrete, first crack was observed after 23 days of casting. This crack also appeared on both faces of the wall at almost similar location. The crack did not initiate at the joint between the wall and base slab, rather at 230 mm above the joint. Although it is generally perceived that cracking due to restrained volume changes is primarily caused by the restraint of early age thermal contraction, in this study it was apparent that the increase in restrained strain is continuous and drying shrinkage can also play an important role in the occurrence of cracks.

4.8.2 Cracking Pattern

After the appearance of first crack, the walls were monitored for another four weeks during which time further cracks were formed. In the case of T2W, four other small cracks appeared at different locations in the wall during the monitoring period. The location and orientation of the cracks at the end of first week and fourth week of the crack monitoring duration are shown in Figure 4.19. These cracks were numbered, on both faces, according to the sequence in which they appeared. Like the first crack, cracks 2 and 4 also started a distance above the joint location and then propagated upwards and downwards. However, crack 3 and 5 on face 1 and crack 3 on face 2 initiated close to the joint and then propagated upwards.

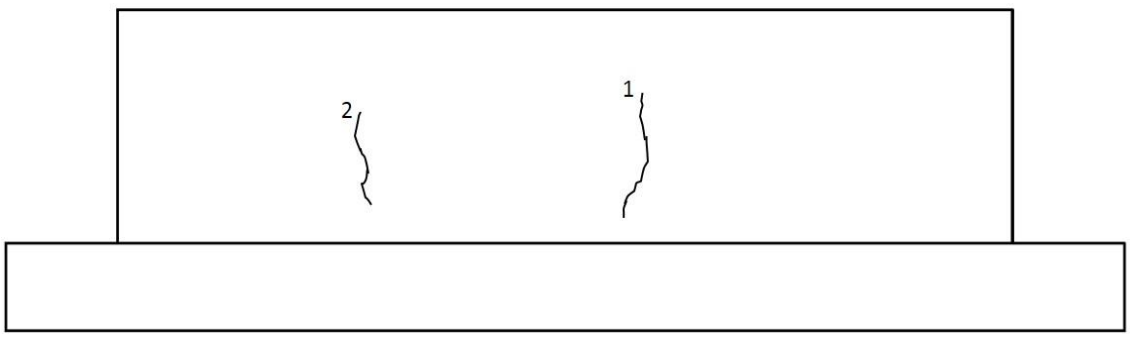

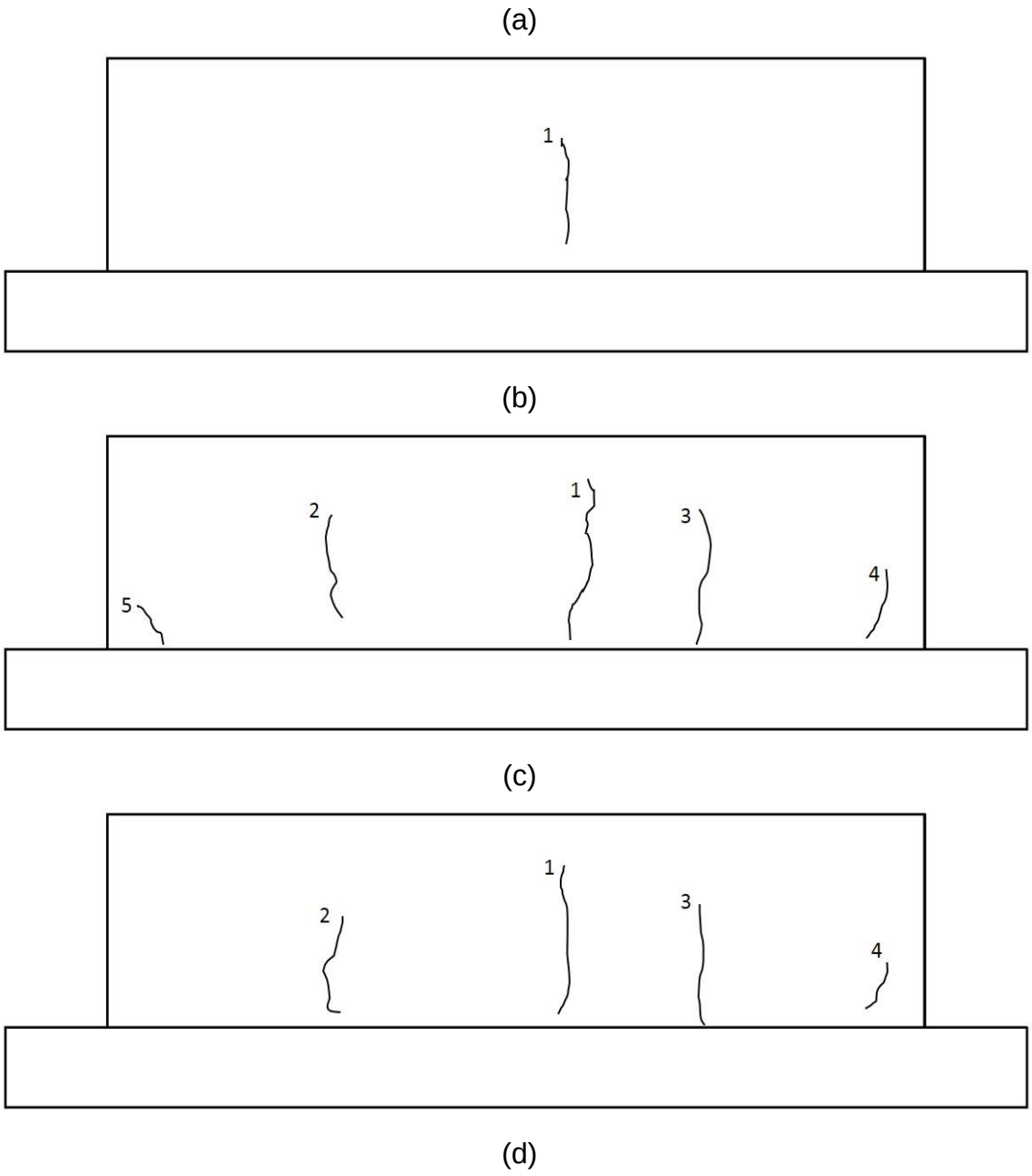

Figure 4.19. Observed cracking in the T2W: (a) face 1 during 1st week; (b) face 2 during 1st week; (c) face 1 during 4th week; (d) face 2 during 4th week

In T4W, three more cracks appeared at different locations in the wall after occurrence of the first crack. The cracking pattern observed in T4W is shown in Figure 4.20. In this test also, most of the cracks did not initiate at the joint, rather at some distance above it. Cracks 1, 3 and 4 all started at some distance above the joint location and then propagated upwards and downwards. Crack 2 also initiated slightly above the joint on face 1, however, on face 2 it initiated close to the joint and then propagated upwards.

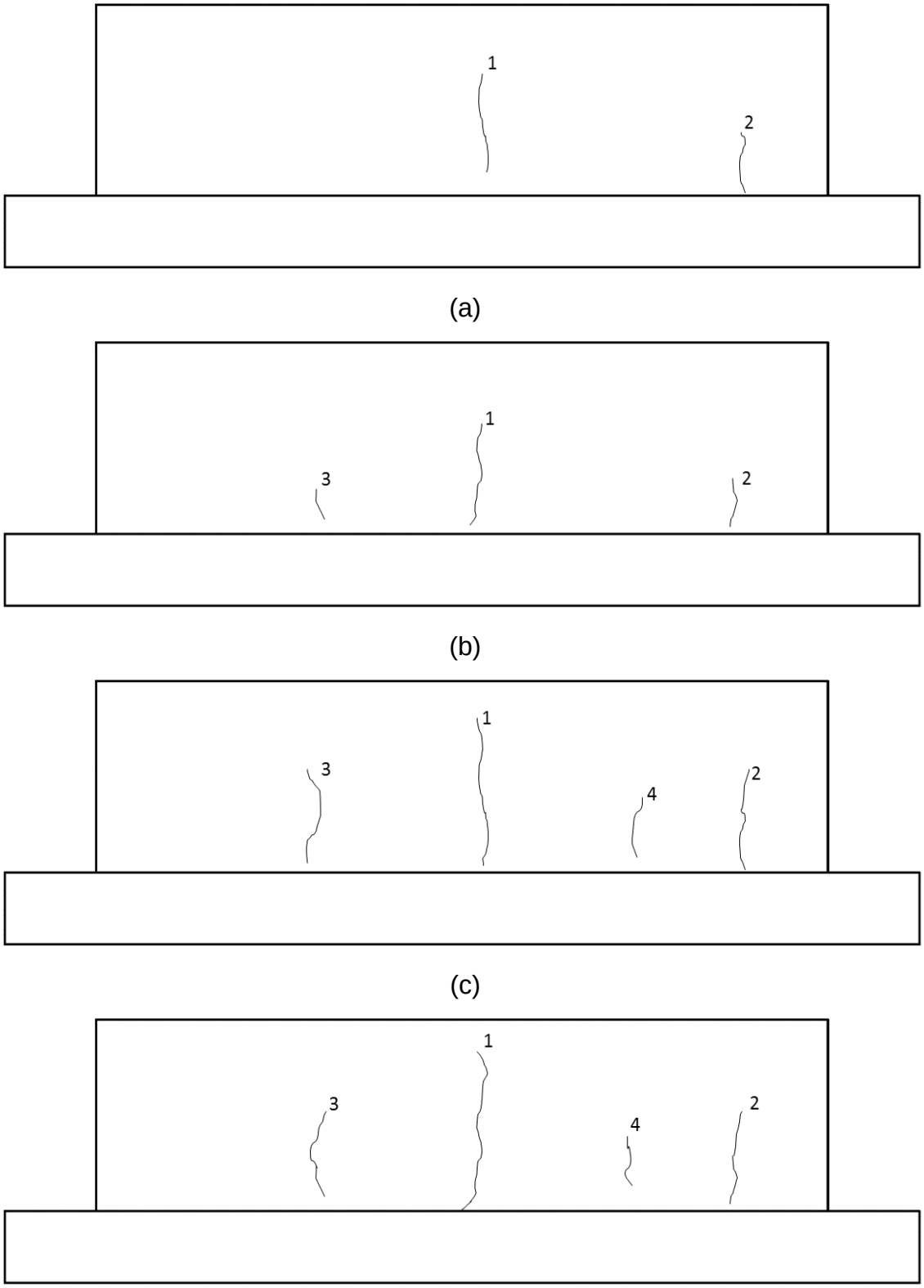

Figure 4.20. Observed cracking in the T4W: (a) face 1 during 1st week; (b) face 2 during 1st week; (c) face 1 during 4th week; (d) face 2 during 4th week

It was noticed that in both of the walls, most of the cracks did not initiate from the joint location where the degree of restraint was maximum. The fact that the cracks did not initiate at the joint can be attributed to the closing action of the base on the cracks as mentioned by Bamforth (2007). Moreover, the cracks observed in the walls did not propagate down to the joint between the wall and the restraining base and therefore the amount of load transferred to the base due to cracking could not be investigated.

4.8.3 Crack Widths

Crack widths at different locations along each crack were measured using the portable microscope. The exact points where the crack width measurements were taken were marked on the wall so that each time, the width of crack at the same location was measured. The number of points, at which the measurements were taken, varied for each crack depending on the height of the cracks. After appearance of the first crack in T2W and T4W, the development and propagation of cracks was monitored for a period of four weeks. An increase in crack width with time was noticed during the monitoring period.

Crack widths for each of the cracks at the end of first week and fourth week after initiation of cracking during test 2 and test 4 are shown in Figures 4.21 and 4.22, respectively. The maximum crack width in test 2 was observed in crack 1. It was 0.3 mm on face 1, occurring 390 mm above the joint, and 0.24 mm on face 2, occurring at 375 mm above the joint. In test 4 also, the maximum crack width was found in crack 1. The maximum crack width observed was 0.22 mm on face 1, which occurred at 320 mm above the joint, and 0.24 mm on face 2 at a height of 332 mm above the joint.

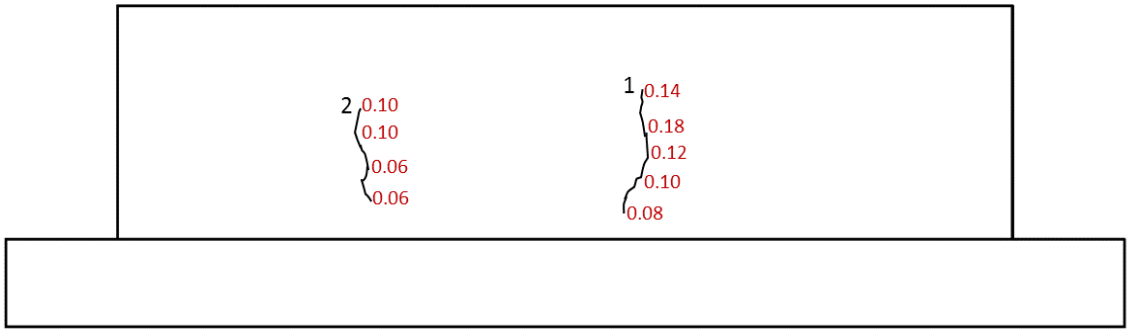

(a)

(b)

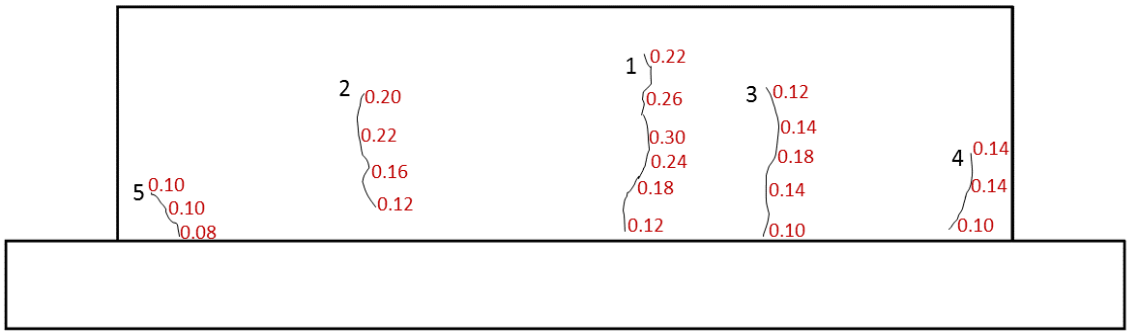

(c)

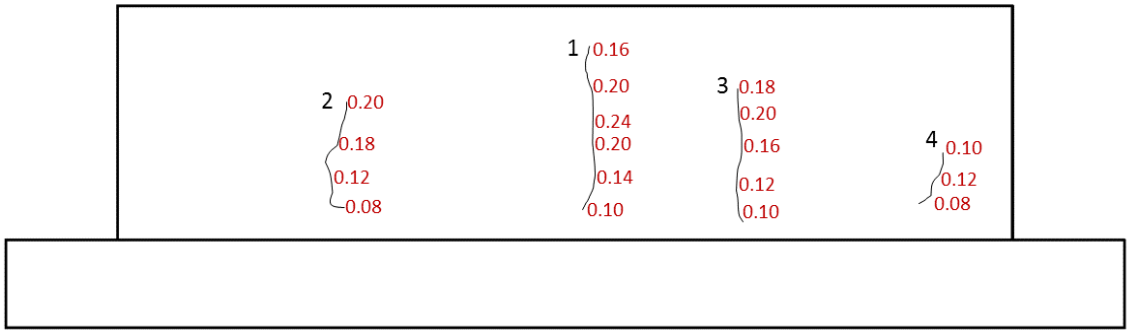

(d)

Figure 4.21. Crack widths observed in the T2W: (a) face 1 during 1st week; (b) face 2 during 1st week; (c) face 1 during 4th week; (d) face 2 during 4th week

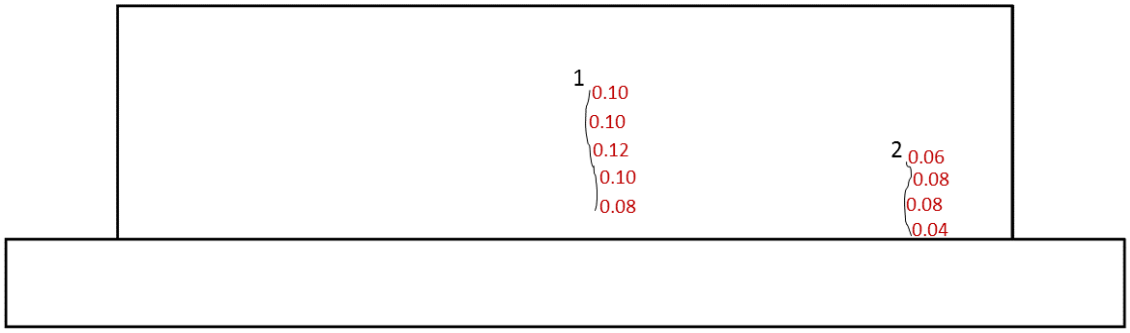

(a)

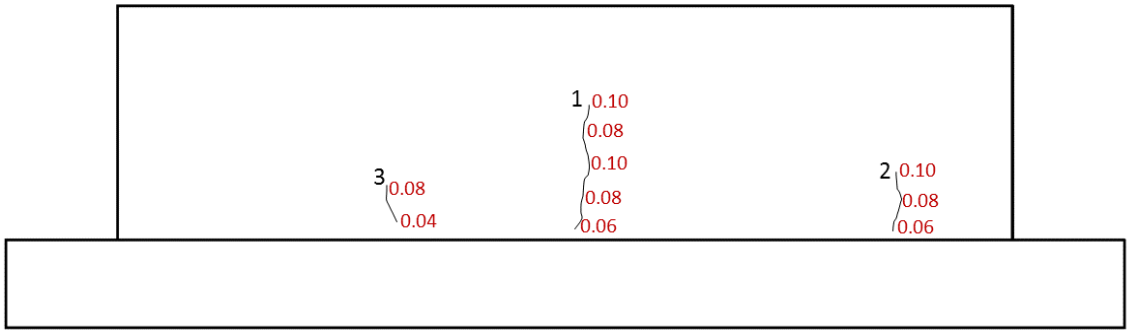

(b)

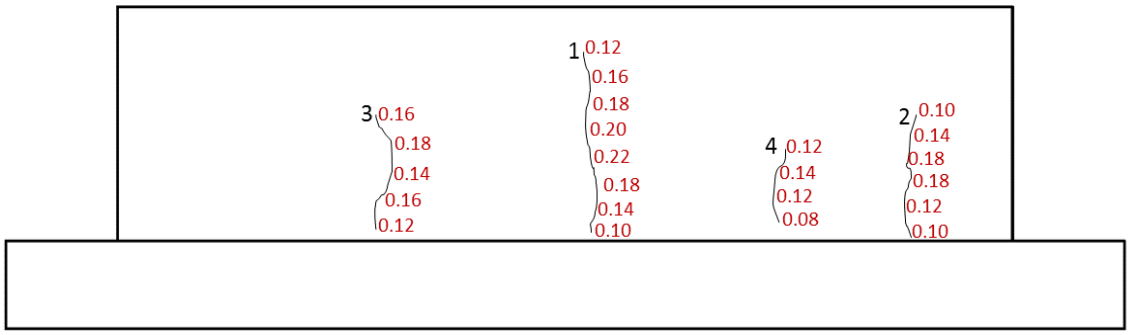

(c)

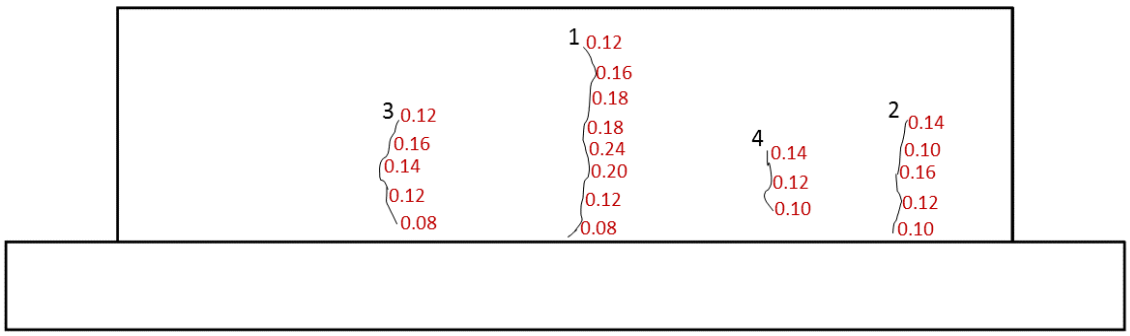

(d)

Figure 4.22. Crack widths observed in the T4W: (a) face 1 during 1st week; (b) face 2 during 1st week; (c) face 1 during 4th week; (d) face 2 during 4th week

According to the findings of different researchers (Kheder et al., 1994; Kheder, 1997; Bamforth, 2007), the maximum crack width in an edge restrained wall occurs at a height of approximately 10% of the length of the wall which in this case is equal to 320 mm. The maximum crack width in the tests occurred at a height between 10-12% of the wall length. In test 2, this maximum value of crack width was reached in the second week after the initiation of the first crack and thereafter remained constant for the remaining duration of the monitoring period. However, in the case of test 4, the value of maximum crack width kept on increasing with time and at the end of the monitoring period, the observed maximum value was noted.

Theoretically, the crack width was calculated using the expression given in BS EN 1992-1-1 (2004). This gave the value of maximum crack width for the tested wall to be (0.15 mm for test 2 and 0.13 mm for test 4), which is quite a lot less than the values obtained experimentally. It was also noticed that the calculated degree of restraint at the location of the maximum crack width was quite lesser than the degree of restraint at the bottom of the wall. In test 2 the degree of restraint at the point of initiation of the first crack was 0.55 and at the location of maximum crack width it was 0.39. However, the maximum value of the degree of restraint was 0.72 at the joint between the two members. Similarly in the case of test 4, the maximum value of degree of restraint at the joint was 0.70, at the point of initiation of crack it was 0.62 and at the location of maximum crack width the calculated restraint factor was 0.48. The above figures provide the ratio between restraint at the location of maximum crack width to that at joint to be 0.54 in test 2 and 0.69 in test 4. However, according to CIRIA C660 (2007), this ratio has a constant value of 0.78 in all cases; this was not found to be true in the tests carried out during this research. The occurrence of maximum crack width at some point higher in the wall and not at the location of maximum restraint confirms the closing action of the restraining base slab.

4.9 Summary

In this chapter the results obtained from tests on four edge restrained reinforced concrete walls have been presented and analysed. In first section, the results from thermocouples installed to monitor the temperature development in both wall and base are presented. It was found that quite a significant amount of heat was transferred to the base slab due to which the thermal drop was lesser near the bottom of the wall. At

mid-height the thermal drop was maximum and it slightly decreased near the top. Variation of temperature drop along the length of the walls was also monitored and was found to be maximum at the centre and minimum close to the ends. Maximum temperature recorded in 300 mm thick was more than that in 200 mm walls. Thermal drop observed in the tested specimens very slightly varied from the values presented in CIRIA C660 (2007).

Techniques used for monitoring the surface strain in both wall and base slab are described and the measured strains and their variation along the wall height are also presented. Unrestrained or free shrinkage measured using concrete prisms and its comparison with shrinkage prediction models (ACI, CEB FIP, Eurocode and Bazant-Baweja B3 models) was carried out. The CEB FIP model for shrinkage prediction was found to closely match the experimentally obtained shrinkage profiles. Accordingly, this model was used for estimation of unrestrained shrinkage in the wall and base slab.

Contraction in the wall was observed to influence the shrinkage profile of the restraining base slab. Measured shrinkage in the base slab was compared to the shrinkage profile before and after construction of the wall and influence of the wall was analysed. In test 1 and 3, the base slab experienced more shrinkage than it was undergoing before the construction of wall. Whereas in test 2 and 4, the observed shrinkage after casting the wall was less than that before the wall was cast. Restraint of the shrinkage in base slab is attributed to the vertical steel reinforcement and augments the degree of restraint imposed on the wall.

From the measured surface strain and free or unrestrained strain, the restrained strain and ultimately the degree of restraint was worked out. Comparison of the experimentally obtained restraint factors with that calculated using existing methods for restraint estimation was carried out and is presented in this Chapter. The degree of restraint was maximum at the bottom of the wall and reduced gradually along the height. Restraint was more in the central part of the wall and lesser near the edges. Degree of restraint significantly increased in the presence of vertical steel reinforcement; 46% in case of test 2 and 67.5% in case of test 4 when compared to the walls in test 1 and 3 respectively. Reduction in wall thickness alone did not change the degree of restraint much; the degree of restraint was 0.39 in test 1 (300 mm wall

thickness) and 0.40 in test 3 (200 mm wall thickness). This indicated that the vertical steel dowels are a major influencing factor in formation of restraint. Moreover, restraint increase with time in the presence of vertical steel and slightly decreased in their absence.

Tensile strain capacity of concrete was calculated according to the guidelines available in CIRIA C660 (2007) and compared to the restrained strain calculated for the tested specimens. The comparisons revealed that the estimation of tensile strain capacity using CIRIA guidance matched very closely to the experimentally observed behaviour.

Finally the observed cracking in the tested specimens is presented. No cracks were observed in test 1 and 3. In test 2 first crack appeared 51 days after casting and in test 4, 23 days after casting. It was found that most of the cracks did not initiate at the joint location rather at some height above it. Maximum crack width was also observed at a height approximately 10-12% of the wall length. Crack widths were measured at different locations along each crack and were seen to increase with time.

Chapter 5

Tests on Reinforced Concrete Panels under Uniaxial Tension

5.1 Introduction

The work presented in this chapter was aimed at confirming the influence of transverse steel reinforcement on the prediction of cracking behaviour in general, and the cracking load in particular, for reinforced concrete walls and slabs. The experimental methodology and results of direct tension tests on six reinforced concrete panels are described. The influence of transverse steel reinforcement on the cracking behaviour of these panels was analysed. Finite element analysis of these reinforced concrete panels using MIDAS FEA is also presented in this chapter.

The cracking mechanism of reinforced concrete members has been studied for many years. However, although a number of analytical and experimental investigations have been carried out, a consensus on predicting the cracking behaviour still does not exist. Most of the theories and experimental investigations on the subject have been based on concrete prisms reinforced axially with a steel bar and subjected to direct tension. The findings of these investigations have then been applied to all types of members by relating the tension zone around the steel reinforcement to the concrete in the analysed prisms.

Beeby (1979) carried out a comparison of the crack width prediction based on different codes available internationally and found significant variation among them. The observation is still valid despite a considerable amount of research undertaken since then on the subject. Cracking occurs when the tensile stress developed in the concrete exceeds its tensile capacity. Under direct tension, normally the entire section of the member cracks at once reducing the concrete stress at the crack location to zero and at this point the entire load is transferred to the steel reinforcement. The force required to cause a crack can be computed from the cross sectional area and tensile strength of concrete. Away from the crack, the transfer of applied stress from steel to concrete occurs through bond and at some distance from the crack location the concrete stress becomes unaffected by the crack. This distance on both sides of the crack is instrumental in defining the minimum and maximum crack spacing in a

member. Maximum crack width can then be calculated as a product of the maximum crack spacing and the difference of the average strain in the steel and concrete.

The theory mentioned above formed the basis of the cracking phenomenon in end restrained members and has been used for predicting their response. Gilbert (1992) described the cracking phenomenon in axially reinforced concrete prism restrained at its both ends. Prior to cracking, the strain in steel and concrete is the same due to equilibrium. The mechanism of development of first crack and stress transfer in end restrained axially reinforced concrete prisms is shown in Figure 5.1.

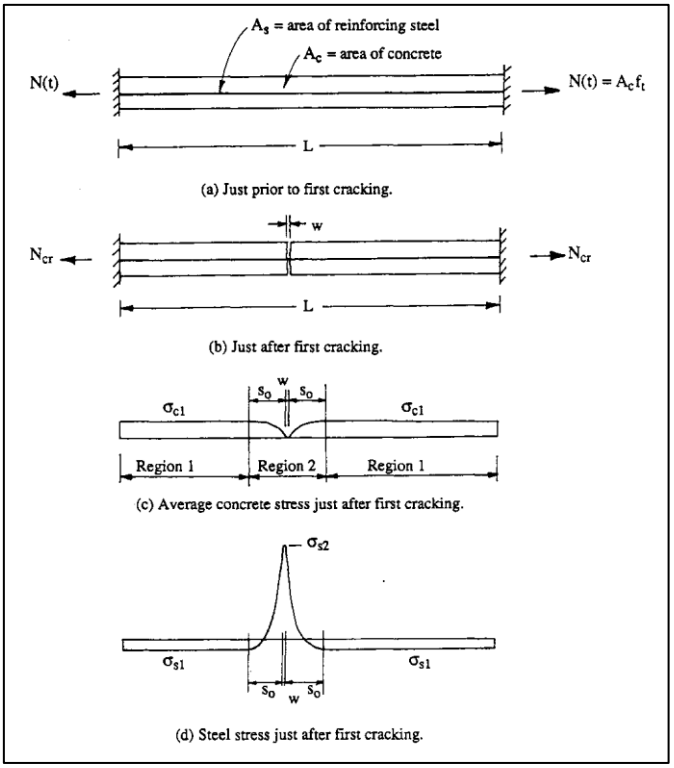

Figure 5.1. Development of first crack in end restrained prisms (Gilbert, 1992)

The force required to cause a crack in a member subjected to uniaxial tension can be calculated from the cross sectional area and the tensile strength of concrete. Expressions for prediction of the cracking load under direct tension are available in ACI Committee 224.2R (1997) and Model Code (2010). Both approaches are based on the theory defining the total force as the sum of forces in the steel and concrete, and therefore predict almost similar values for the cracking load. The ACI and Model code expressions are given below in Equation 5.1 and 5.2, respectively:

$$P_{cr} = (1 - \rho + \alpha_e \rho) A_g f_t' \tag{5.1}$$

$$P_{cr} = A_c f_{ctm}\left(1 + \alpha_e \rho_{s,eff}\right) \quad (5.2)$$

where;

P_{cr} = Cracking load

ρ = Steel reinforcement ratio

α_e = Modular ratio

$\rho_{s,eff}$ = Effective steel reinforcement ratio

A_g = Gross area of concrete

f_{ctm}/f_t' = Mean tensile strength of concrete

However, although, the maximum crack width in members subjected to direct tension can be calculated using the expressions available in the above two codes as well as BS EN 1992-1-1 (2004), the appraoches are based on different cracking theories and they thus predict quite different values. Expressions available in ACI Committee 224.2R (1997), Model Code (2010) and BS EN 1992-1-1 (2004) are given as Equation 5.3, 5.4 and 5.5, respectively:

$$w_{max} = 0.10 f_s \sqrt[3]{d_c A} * 10^{-3} \quad (5.3)$$

$$w_{max} = \frac{f_{ctm}\phi_s}{2\tau_{bm}\rho_s}(\varepsilon_{sm} - \varepsilon_{cm}) \quad (5.4)$$

$$w_{max} = (k_3 c + k_1 k_2 k_4 \frac{\phi}{\rho_{s,eff}})(\varepsilon_{sm} - \varepsilon_{cm}) \quad (5.5)$$

where;

w_{max} = Maximum crack width

f_s = Stress in steel reinforcement bar

d_c = Distance from centre of bar to extreme tension fibre

A = Cross section area of concrete

f_{ctm} = Mean tensile strength of concrete

ϕ_s = Diameter of the steel bar

τ_{bm} = Mean bond strength between reinforcing bar and concrete

ρ_s = Steel reinforcement ratio

ε_{sm} = mean strain in steel

ε_{cm} = mean strain in concrete

$\rho_{s,eff}$ = Effective steel reinforcement ratio

c = Concrete cover to the steel reinforcement

k_1 = Coefficient which takes account of bond properties

k_2 = Coefficient which takes account of distribution of strain

k_3, k_4 = Coefficients found in National Annex; values are 3.4 and 0.425 respectively

In members like reinforced concrete walls and slabs, steel bars in two perpendicular directions are provided. Therefore, suitability of the theory and expressions developed on the basis of axially reinforced prisms needs to be investigated, particularly in terms of the influence of the reinforcement perpendicular to the direction of applied load. Previously, Desayi et al. (1976) emphasized the importance of considering transverse reinforcement and developed analytical expressions for the determination of maximum crack width in two way reinforced concrete slabs which incorporated the influence of the transverse steel.

Rizkalla et al. (1983a) and Rizkalla et al. (1983c) conducted an experimental investigation into members subjected to uniaxial tension and, subsequently, analysed the role of transverse reinforcement. They found that the crack spacing was influenced by the transverse reinforcement. Beeby (1979) stated that the transverse reinforcement present in members can act as a 'crack former' and in certain circumstances can significantly influence the spacing and width of cracks. Both Leonhardt (1977) and Beeby (1979) proposed expressions for estimating the average surface strain in the concrete near the crack location. Rizkalla et al. (1983a) analysed these proposed expressions and suggested a modification to the equations proposed by Beeby (1979). Finally, Dawood et al. (2010) performed tests on thick reinforced concrete panels subjected to biaxial tension and developed an analytical model for predicting the crack spacing in such members.

5.2 Experimental Program

5.2.1 Introduction

In order to investigate the influence of transverse steel reinforcement, tests on six reinforced concrete panels were carried out at the University of Leeds. Four of the tested specimens were reinforced in both directions while the remaining two were reinforced only in the direction of the applied load. The uniaxial tensile load was applied to the specimens using the universal testing machine (UTM) and the cracking behaviour of the specimens was observed.

5.2.2 Test Specimens

The space available between the two ends of the UTM was a limiting factor on the physical size of the specimens. Therefore, the test specimens were 600 mm x 600 mm square concrete panels having a thickness of 100 mm. Details of specimen size, reinforcement and concrete cover are given in Figure 5.2. The specimens were cast from two different batches of concrete; one specimen without and two specimens with transverse reinforcement were cast from each batch.

Specimens were allocated a code for identification purposes comprising three parts. The first part of the code is a number depicting concrete batch one or two; the second part comprises the letter ‘S’ or ‘D’ and denotes the absence or presence of transverse reinforcement, respectively; and the third part is a number describing the specimen number in each category. Thus 1D2 indicates a specimen cast from batch one of concrete, reinforced in both longitudinal and transverse directions and the specimen number in this category is 2.

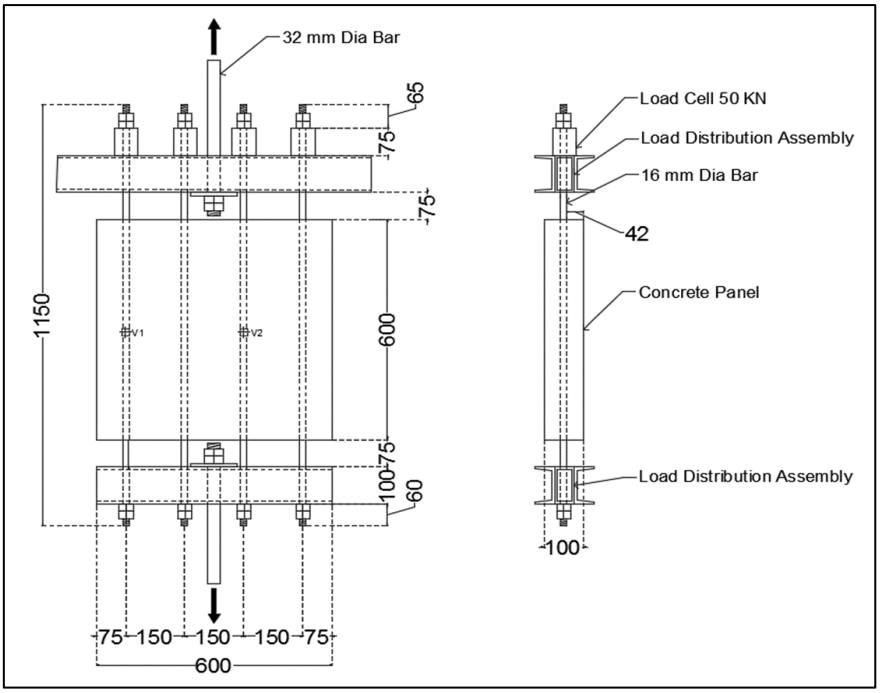

(a)

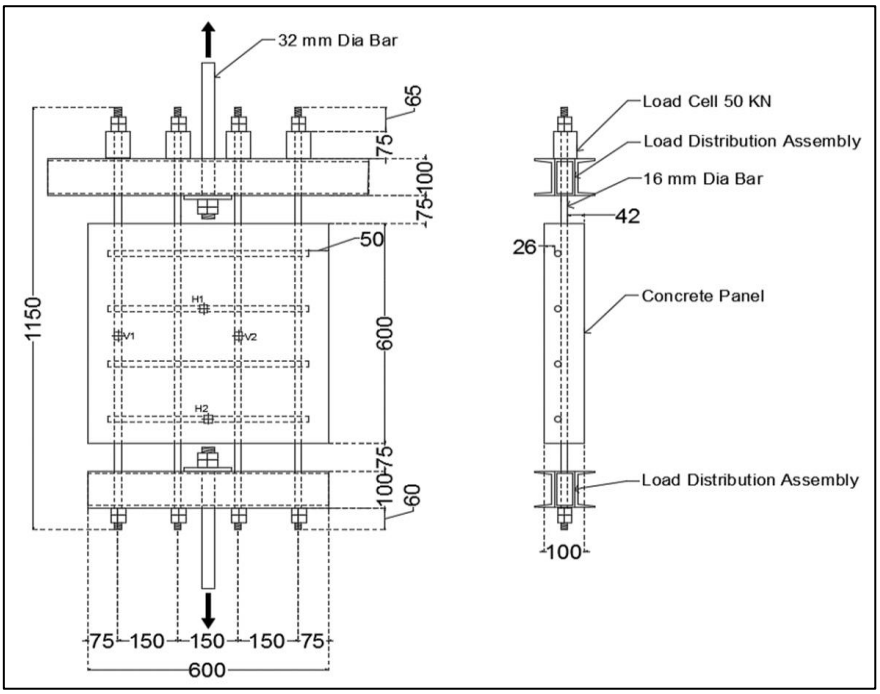

(b)

Figure 5.2. The test specimens: (a) Specimen reinforced in both directions; (b) Specimen reinforced in only one direction.

5.2.3 Test Set Up

The uniaxial load from the 1000kN capacity UTM was transmitted to the 16 mm steel reinforcement bars of the specimens using a specially designed load distribution assembly. The test set up is shown in Figure 5.3. The assemblies were sufficiently stiff to apply the load equally to all 16 mm bars. Load cells were attached to each reinforcement bar for adjustment so that the load variation remained within ±1 kN. The applied load was limited to 200 kN, in order to avoid the yielding of the steel bars. The load was transferred from the steel bars to the concrete via the bond between the two elements of the reinforced concrete composite.

Figure 5.3. The test set up.

5.2.4 Material Properties and Instrumentation

Specimens were cast from two different batches of concrete which had the same mix composition as for the concrete used in the tests on edge restrained walls (given in Chapter 3). The compressive strength, splitting tensile strength and the modulus of elasticity of each batch of concrete were determined in the laboratory by testing 150 x 300 mm cylinders at the age of 28 days. All the specimens were moist cured inside a curing room (99% relative humidity). Batch 1 concrete had a compressive strength of 40 MPa and a splitting tensile strength of 2.7 MPa, while the batch 2 concrete had a compressive strength of 46.4 MPa and a splitting tensile strength of 3.2 MPa.

As each batch was used to cast a comparative set of panels, the difference in physical strengths between the two batches did not affect the analysis of the panel results; rather, as it was the cracking pattern being investigated these differences provided further evidence for this review (see Section 5.3.1). In order to monitor the strain in the steel reinforcement bars, ERS gauges were installed on two bars in each direction. DEMEC studs were installed on the concrete surface and strains in the concrete were recorded during the test using the DEMEC gauge.

5.2.5 Preparation, Casting and Curing of Specimens

The concrete panels were cast in the moulds prepared in the laboratory using the 19 mm thick plywood and timber. ERS gauges were installed on the steel reinforcement bars and the bars were then placed in the moulds. The steel bars in the direction of applied loading were threaded and protruded out of the moulds. The moulds were checked for water tightness to prevent the leakage of cement mortar after casting.

At the time of casting, the moulds were placed on the vibrating table available in the laboratory. Concrete was poured in the moulds manually and the vibrating table was turned on. Because of the vibration, concrete was well compacted and the risk of honeycombing was avoided. After the moulds were filled with concrete, they were removed from the vibrating table and placed on a level surface.

After casting the specimens were kept covered for one day with polyethylene sheets and cured for one day. After that the specimens were removed from the moulds and placed in the laboratory. The specimens were then cured for 14 days using wet Hessian cloth.

5.2.6 Test Procedure

The load distribution assembly was attached to the test specimen prior to putting the specimen in the UTM. The load was gradually applied to the specimens at an approximate rate of 0.5 kN per second in increments of 20 kN. An equal load on all bars, within a variation of ±1 kN, was ensured during the test (Figure 5.4). After each increment of 20 kN, the DEMEC gauge readings were recorded and the appearance of any cracks was observed. On occurrence of a crack, the cracking load was noted, the alignment of each crack was marked and the crack widths were measured using the portable microscope. Application of the load was continued until a total load of 200 kN was achieved. The specimen was then unloaded and removed from the rig.

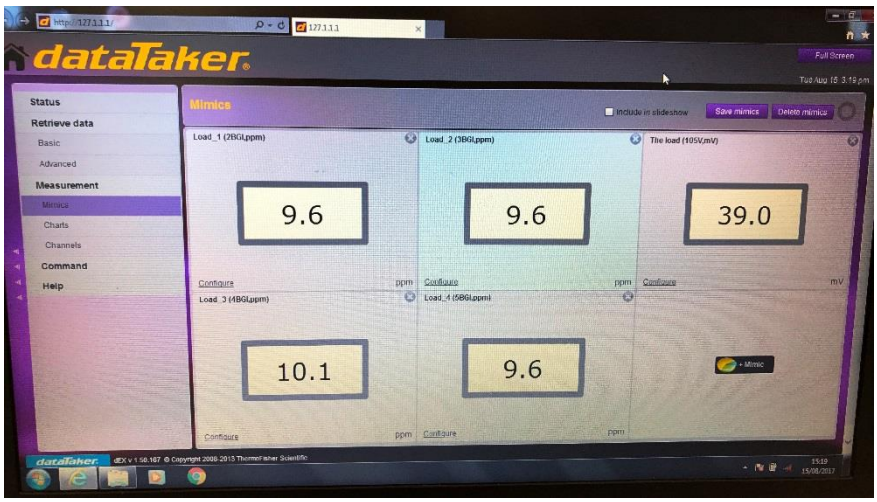

Figure 5.4. Monitoring of the loads transferred to steel bars.

5.3 Experimental results and Discussion

5.3.1 Cracking Load

Due to the composite behaviour of reinforced concrete, the bond stresses between the steel bars and the concrete enable a proportion of the tensile load applied to the bars to be transferred to the concrete. When the stress in the concrete exceeded its tensile strength capacity, cracks were formed. The cracking load for the specimens

was calculated using Equation 5.1 and 5.2; these are compared with the experimental load at which cracks were developed in the specimens - see Table 5.1.

From Table 5.1 it can be seen that all of the specimens cracked at a lower load than that predicted by the codes. The specimens having transverse reinforcement cracked at an even lower load compared to the specimens reinforced in only one direction. The tensile strength of the second batch of concrete was higher than that of the first batch; although this led to higher cracking loads for the batch 2 specimens, the pattern of crack development due to presence of transverse reinforcement remained the same and was therefore independent of the concrete tensile strength. On average the cracking load was reduced by 25 – 30% in the specimens containing transverse steel.

Table 5.1. Comparison of predicted and experimentally obtained cracking loads

Cracking Load (kN)					
Specimen	ACI	Model Code	1st Crack	2nd Crack	3rd Crack
1S1	154	156	142	-	-
1D1			90	110	-
1D2			106	118	-
2S1	186	189	161	-	-
2D1			136	180	192
2D2			120	151	-

5.3.2 Crack Spacing

The cracking patterns obtained in the tested specimens are given in Figure 5.5. Specimens 1S1 and 2S1 developed only one crack during the test; this occurred near the mid-span. Specimens 1D1, 1D2 and 2D2 each developed two cracks; specimen 2D1 had three cracks. It was noticed that in the case of the D- series tests, the cracks occurred almost at the location of the transverse reinforcement. This observation is in

line with the observation made by Beeby (1979), i.e. transverse reinforcement can act as a ‘crack former’. Similar observations were also made by Rizkalla et al. (1983c) and Rizkalla et al. (1983b) during their tests.

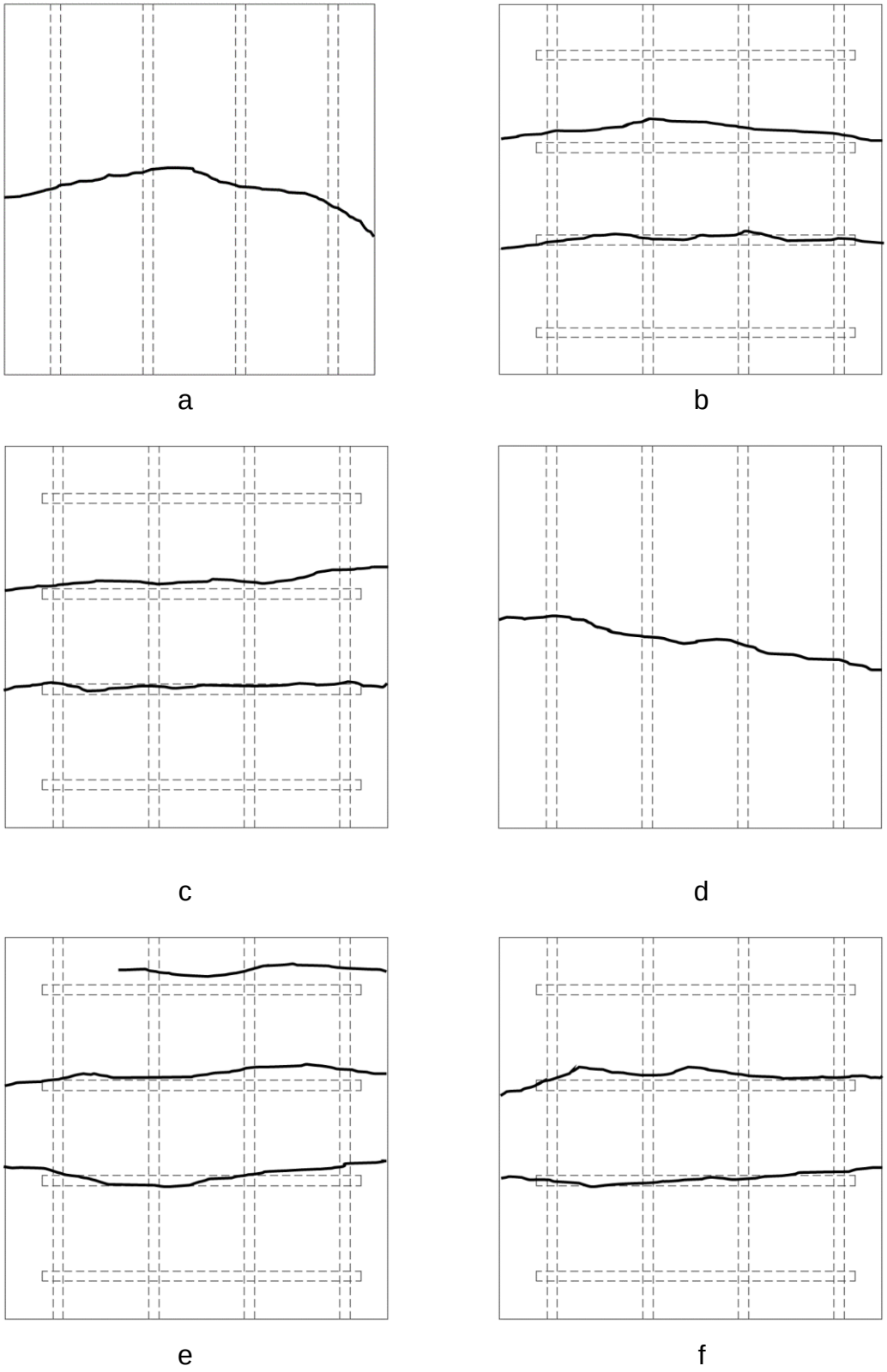

Figure 5.5. Cracking patterns in different specimens: (a) 1S1; (b) 1D1; (c) 1D2; (d) 2S1; (e) 2D1; (f) 2D2.

A possible explanation for this is that when the concrete is subjected to tensile stresses, the transverse reinforcement bears against the surrounding concrete and augments the tensile force generated in the concrete through its bond with the steel bars. This bearing force is proportional to the applied tensile stress in the concrete and the size of the transverse reinforcement bars. It is this additional tensile force which causes the concrete section to crack prematurely and at a lower load than that of the specimens without the transverse reinforcement. The additional tensile force due to the transverse reinforcement is maximum at the location of steel reinforcement and reduces away from the bar. The location of the cracks, which is almost at the same position as the transverse bars further supports this observation. This phenomenon is further illustrated in Figure 5.6 where the additional force caused by the transverse steel reinforcement has been depicted.

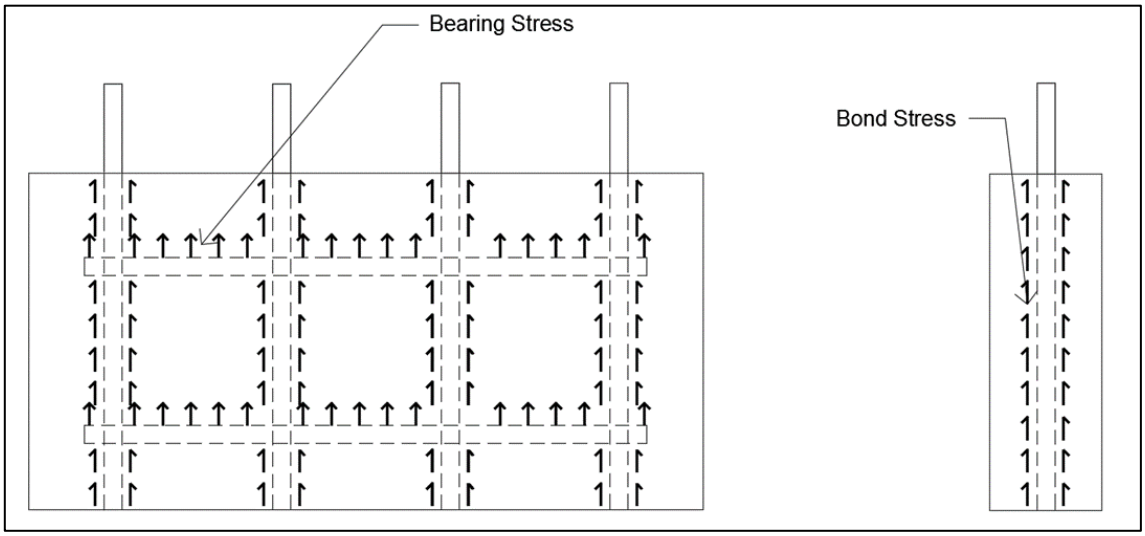

Figure 5.6. Depiction of the bearing force due to transverse steel bars.

The cracks occurred across the entire section of the specimen and were brittle in nature; there was a slight reduction in the load immediately upon cracking. A few of the cracked specimens are shown in Figure 5.7. Based on the above results, it is concluded that the cracking load in members having transverse reinforcement and subjected to uniaxial tension cannot, therefore, be realistically predicted using the existing expressions.

Figure 5.7. Cracked Specimens

5.3.3 Crack Widths

Once the cracks had formed, the crack widths were measured at each load step; the width of the cracks increased with an increase in the load. The strains measured in the steel reinforcement perpendicular to the direction of the crack increased significantly when each crack formed. This confirms that the load is transferred from the concrete to the steel reinforcement when a crack is formed. For each crack, readings at ten different points were taken to find out the maximum crack width; these are given in Table 5.2 for each specimen. The crack widths were also calculated according to Equations 5.3, 5.4 and 5.5; these are also given in Table 5.2.

Table 5.2. Comparison of predicted and measured crack widths

Crack Widths (mm)						
Specimen	ACI	Model Code	Eurocode 2	1st Crack	2nd Crack	3rd Crack
1S1	0.19	0.13	0.21	0.28	-	-
1D1				0.3	0.36	-
1D2				0.25	0.3	-
2S1	0.23	0.16	0.26	0.22	-	-
2D1				0.26	0.18	0.06
2D2				0.28	0.2	-

The predicted values are different for each of the design codes, however, it is obvious that the crack width increases with an increase in the concrete tensile strength. From Table 5.2 it can be seen that the specimens with transverse reinforcement exhibited wider cracks compared to those without transverse steel. Moreover, the measured crack widths were more than those predicted in almost all cases. Since the size of the specimens was limited due to the available space in the UTM rig, it is difficult to comment on the crack spacing in specimens without transverse

reinforcement, however, it is evident that the crack spacing in the presence of transverse reinforcement is significantly influenced by the location, size and spacing of the transverse bars.

5.3.4 Concrete Surface Strain

Surface strains on both sides of tested specimens (as indicated in Figure 5.3) were recorded after every load increment using the DEMEC gauges. The average gross strain at the surface due to the applied loads, including the concrete contribution within the transfer length, was then computed from the measured values. Predicted values of the surface strain were also calculated according to the expressions proposed by Leonhardt (1977), Beeby (1979) and Rizkalla et al. (1983a). A comparison of the predicted and experimentally obtained surface strains is shown in Figure 5.8, where it can be seen that the predictions appear to be close to the experimentally obtained values in the case of specimens without transverse reinforcement. However, where there exists the presence of transverse reinforcement the surface strains are higher than those predicted.

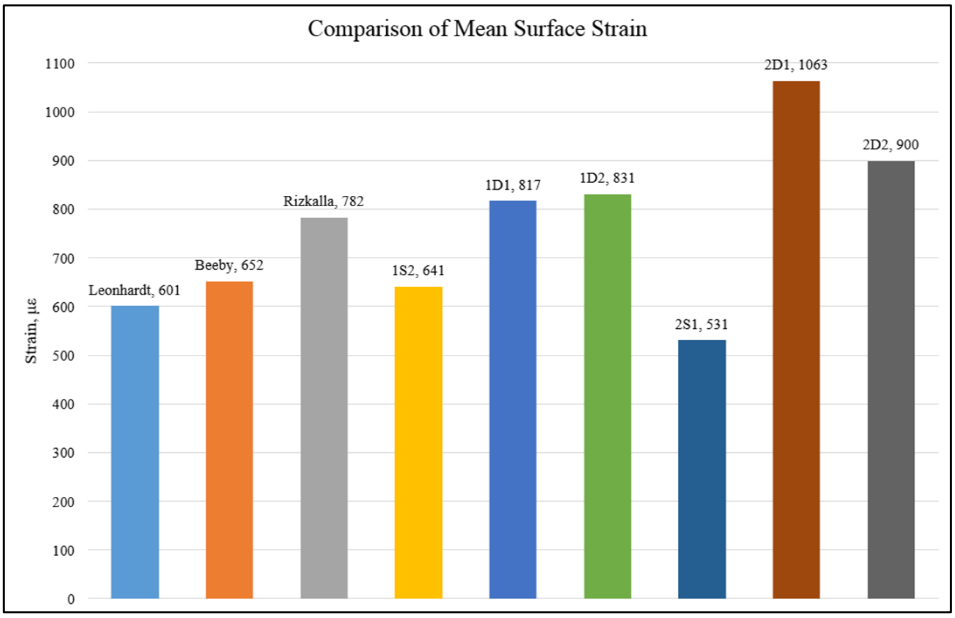

Figure 5.8. Comparison of the average surface strains in concrete after cracking

5.4 Finite Element Analysis and Results

5.4.1 Finite Element Modelling

The tested specimens were also modelled using MIDAS FEA in order to simulate the behaviour under experimental conditions. The concrete was modelled using 20 noded three dimensional hexahedron solid elements. The finite element mesh used in the analysis is shown in Figure 5.9. In order to model the concrete, a total strain based cracking model involving the rotating crack model was used. The tensile behaviour of the concrete was modelled using the nonlinear function proposed by Hordijk (1991), which provides a nonlinear softening curve for predicting the post cracking tensile behaviour of concrete assuming that the stress gradually reduces to zero at an ultimate strain, $\varepsilon_{ult} = 5.136\,(G_f^I/f_{ct}h_e)$, where (G_f^I) is the mode 1 fracture energy of concrete, (h_e) is the element size and (f_{ct}) is the concrete tensile strength. The fracture energy of the concrete was calculated according to the Model Code (2010). The reinforcement bars were modelled using solid elements, and the concrete – steel reinforcement bond was modelled through the interface elements. Material properties obtained from the experimental tests were used as input data in the models. The load was applied to one end of the exposed steel bars while the nodes on the opposite ends were restrained from translation in all directions. The Newton Raphson iteration scheme was employed for obtaining the nonlinear solution in which the energy and displacement norms for a convergence tolerance of 0.00001 were satisfied.

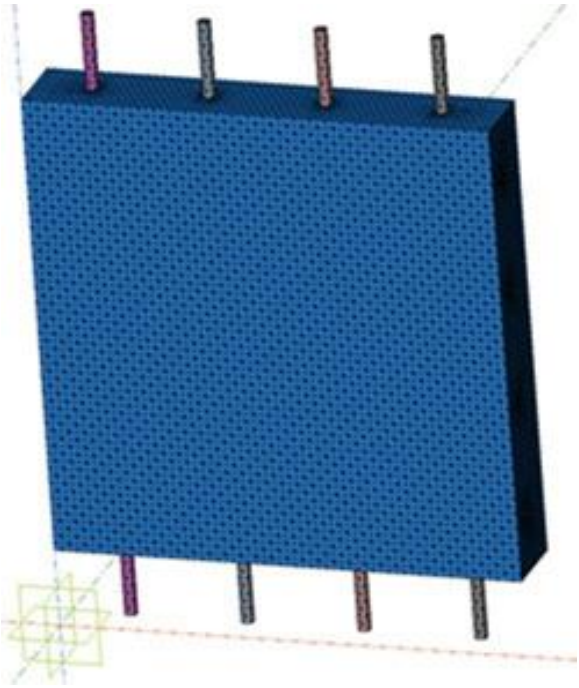

Figure 5.9. Finite element mesh used in the analysis of reinforced concrete panels

The cracking pattern for both types of specimen obtained from the finite element analysis is shown in Figure 5.10. From Figure 5.10 it can be seen that the cracking behaviour of the members obtained from the finite element analysis displayed a close resemblance to that witnessed during the experimental investigation. An analysis of the stress generated in the concrete at the location of the transverse reinforcement reveals that the concrete stress in the model with transverse steel bars was approximately 20% more than the one without the transverse bars (and is in-line with the measured reduction in cracking load observed during the tests).

Although this analysis confirms the introduction of additional tensile force in the concrete due to presence of the transverse steels bars, further work is required to more accurately quantify the influence of the transverse steel reinforcement on the cracking load.

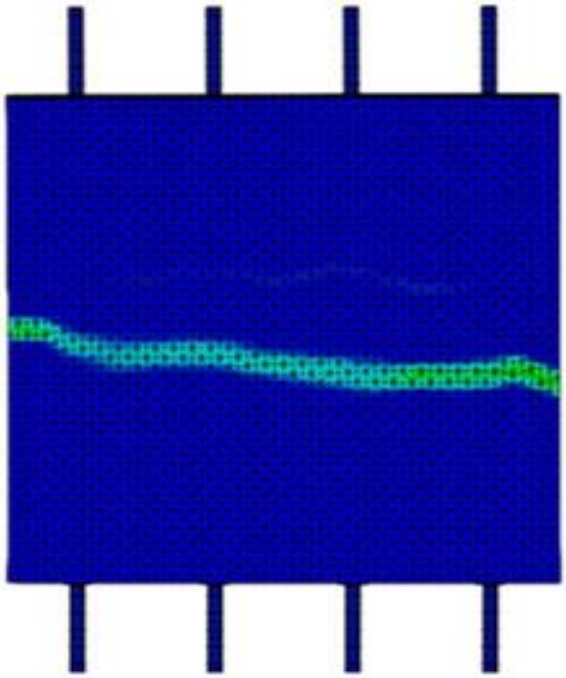

(a)

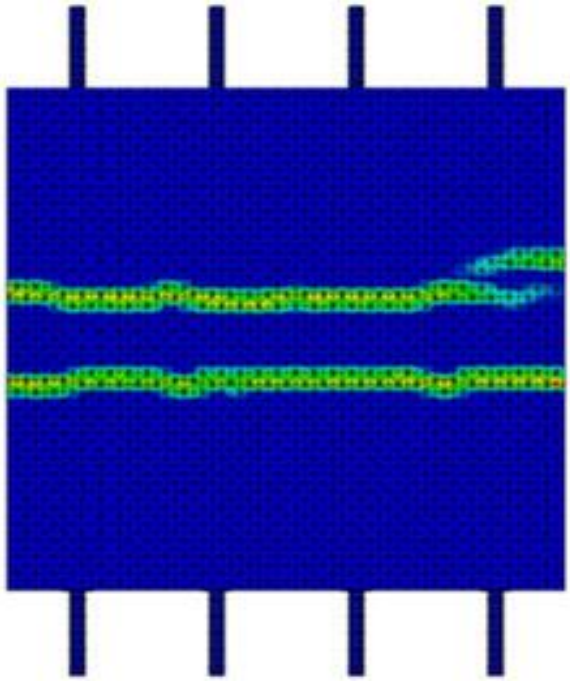

(b)

Figure 5.10. Cracking pattern obtained from the finite element analysis; (a) Model without transverse reinforcement; (b) Model with transverse reinforcement

5.5 Summary

The methodology adopted and the results obtained from tests on six reinforced concrete panels (600 x 600 x 100) mm have been discussed in the chapter. The panels were subjected to uniaxial tensile load using specially designed load distribution assembly. Cracking load, cracking pattern, crack widths and concrete surface strains were monitored during the tests and were compared to the existing guidance available in the codes and other literature. Cracking load was seen to decrease significantly in the presence of transverse steel bars. Number of cracks increased due to the presence of transverse bars and the location of the cracks was influenced by the location of transverse bars. The panels with transverse reinforcement exhibited wider cracks compared to those without these bars. Finite element models of the tested specimens are also presented; the results obtained from these models closely matched the experimental findings. The results presented here confirm the significance of the transverse reinforcement and the influence it has on the cracking behaviour of reinforced concrete walls and slabs. Further work is still required to more accurately ascertain this influence.

Chapter 6

Finite Element Modelling

6.1 Introduction

The details of the experimental program carried out as part of this study have been mentioned in the previous chapters. It is obvious that the scope of tests conducted in the laboratory remains confined and restrictions are imposed by the limited timeframe, financial expenditure incurred on the tests and limitations on the size of the specimens tested in the laboratory. As a result of this, it is not possible to study all of the important parameters influencing the cracking behaviour of reinforced concrete walls subjected to different types of restraint. In such scenarios, the finite element analysis appears to be a useful technique for evaluating the influence of different parameters involved. Few of the important influencing parameters in this regard are the height and length to height ratio of the walls, types of restraint and the boundary conditions.

For the finite element analysis, MIDAS FEA – a finite element based software was used in this study. Three dimensional linear and nonlinear static analysis were performed. Initially the models of the experimentally tested walls were created, analysed and validated in the light of the experimental findings. Later on the parametric study was conducted to evaluate the influence of wall height and aspect ratios on the cracking behaviour under edge and combined restraint. The influence of the curvature development in the base slab on the cracking behaviour was also analysed.

In this chapter the limitations and challenges involved in the modelling of concrete elements are also described. The methodology adopted for creation of the finite element models is presented. The results obtained from the finite element analysis have been compared and validated in the light of the experimental findings. This chapter also includes the cracking patterns obtained for walls of different aspect ratios subjected to edge and combined restraint.

6.2 Challenges and Limitations

Although the finite element analysis can be employed as a substitute for large scale experimental investigations, yet it is important to realize the limitations involved and the challenges posed by the modelling procedures. Modelling of the reinforced concrete structures is a complex phenomenon and certain simplifications and assumptions are required to be made. The challenges faced and the limitations encountered in this work are given below.

6.2.1 Development of Material Properties

The tensile strength, compressive strength and the modulus of elasticity of the concrete start to develop soon after casting. The strength development continues with time and needs to be incorporated in the modelling. However, in MIDAS FEA only the time independent material properties can be specified. Moreover, the phenomenon of creep and shrinkage cannot be directly incorporated in the nonlinear static analysis. In order to deal with this issue, the material properties for the wall concrete elements were specified as those calculated at the age of three days. The base elements were assigned the properties for the 28 days age of concrete.

6.2.2 Variation of Temperature with Time

Concrete temperature rises due to hydration and then starts to drop gradually reaching the ambient value as discussed in Chapter 4. This implies the thermal contraction is applied to the wall gradually. Thermal drop varies along the height and length of the wall. Moreover, the shrinkage strain is also occurring in the concrete with time. MIDAS allows for the spatial variation of the applied thermal loads however, the non-spatial or the variation of the temperature with time cannot be applied to the elements. To deal with this limitation, the applied thermal drop was linearly varied along the height and length of the wall elements (presented in Section 6.5.3). The shrinkage strain at 3 day age of concrete was calculated and using the value of coefficient of thermal expansion, an equivalent temperature drop was ascertained and added to the applied thermal loading.

6.2.3 Numerical Convergence Problems

In the nonlinear static analysis, the development of a crack introduces convergence issues in a finite element solution. This is attributed to the local softening of the concrete material after occurrence of crack. This problem can be resolved by selecting an appropriate model for the tensile behaviour of concrete which more realistically depicts the post cracking tensile behaviour. Accordingly, in this case the model presented by Hordijk (1991) was selected and used in the analysis since it provides a nonlinear post cracking response (details about the model are given in Section 6.3.2). Moreover, another solution to deal with the problem of convergence is to increase the number of load steps in the analysis so that the load is applied in small increments.

6.2.4 Modelling of Steel Reinforcement

In reinforced concrete members, the bond between the steel reinforcement and surrounding concrete exists. The bond mechanism is complex and depends on various factors. In the finite element analysis of reinforced concrete members, the bond between steel reinforcement and concrete can be modelled using the interface elements. However, the analysis presented here involved large scale members equipped with significant amount of steel reinforcement. Modelling of the bond behaviour using interface elements in such cases becomes a problem as it tremendously increases the number of elements. Therefore, for simplicity a perfect bond condition between the steel reinforcement and concrete had to be assumed and the steel reinforcement was modelled as one dimensional bar elements.

6.3 Finite Element Models for the Experimentally Tested Walls

6.3.1 Mesh Generation

The geometric dimensions of the wall and base slab were the same as used in the experimental work (given in Chapter 3). Taking advantage of the symmetry of dimensions, reinforcement, loads and boundary conditions, only a quarter of the wall was modelled in order to economize the computational effort. Correct discretization of the model is of significant importance in obtaining accurate model response and avoiding numerical distortion. In three dimensional analysis of voluminous structures

like concrete walls and slabs, solid elements are used. In MIDAS FEA, tetrahedron, pentahedron and hexahedron solid elements are available. The hexahedron elements generally provide more accurate results as compared to the tetrahedron or pentahedron elements. In order to model the concrete and the laboratory strong floor, 20 noded three dimensional quadratic hexahedron solid elements (as shown in Figure 6.1), 50 mm in size were used.

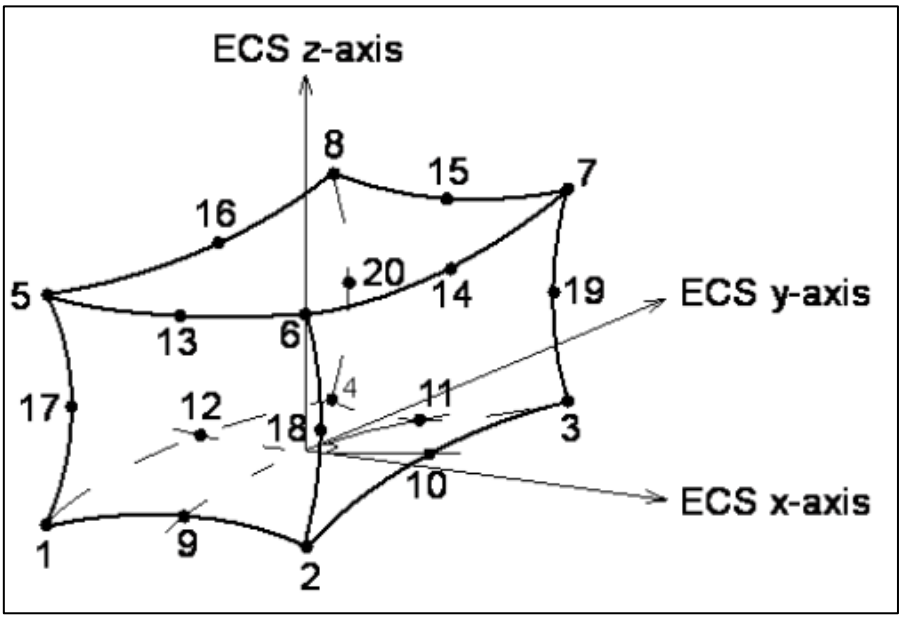

Figure 6.1. Hexahedron solid element used in the finite element modelling

Steel reinforcement was modelled using the ‘bar in solid’ elements. In MIDAS FEA, the reinforcement bar can be modelled by a geometrical line and by using the auto mesh function the bar is divided into sections. The section properties and location of the reinforcement bar are defined. During the pre-processing phase of the analysis, the reinforcement bar elements are divided into smaller elements depending on the size of the solid concrete elements. Depending on the location of the reinforcement bar elements, their contribution to the stiffness and internal forces of the mother elements are added. Mesh generation for the concrete was carried out using the map mesh function (which is suitable for regular shaped structures) and for the steel reinforcement bars, the auto mesh function was utilized. A view of the mesh used in the finite element analysis is shown in Figure 6.2.

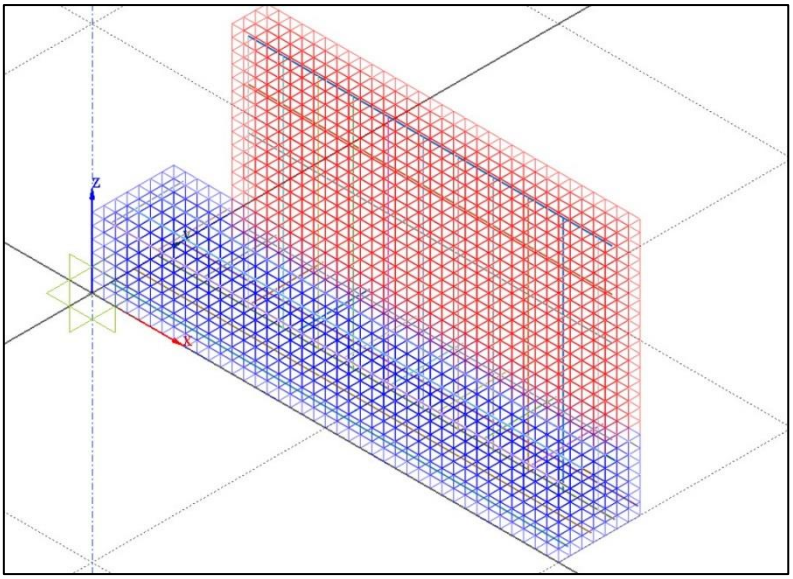

Figure 6.2. Finite element mesh for the modelled walls

6.3.2 Modelling of the Material Behaviour

Correctly modelling the material behaviour in the finite element analysis is an important and complicated task. Two approaches are available for defining the input parameters used as material properties. One is to use the empirical equations for estimating the properties like tensile strength, compressive strength and modulus of elasticity of concrete etc and the other is to obtain these properties by experimental testing in the laboratory. Moreover, sometimes appropriate assumptions are also required to be made regarding the material behaviour. In this study the behaviour of two materials i.e. concrete and steel reinforcement was required to be modelled.

In order to model different materials in MIDAS FEA, following material models are available:

- Elastic
- Rankine
- Tresca
- Von Mises
- Drucker Prager
- Mohr Coulomb
- Total Strain Crack models
- User Supplied Material

Cracking models for concrete can be classified as the discrete crack model or the discontinuum model and the smeared crack model or the continuum model. The smeared crack model is further classified into decomposed crack model and the total strain crack model depending on the numerical analysis methods. The total strain rotating crack model is a hypo elastic constitutive model where orthogonal cracks are represented by a coaxial stress-strain concept. The constitutive relationships are always evaluated in the principal directions of the strain tensor. The total strain crack model provides two methods for modelling the behaviour as shown in Figure 6.3. The fixed crack model assumes that the crack axis remain unchanged after they are defined in the analysis. However the rotating crack model assumes that the crack axis keep on rotating depending on the changes in the axis of principle strains. In this study, the total strain crack model was used for modelling the compressive, tensile and shear behaviour of concrete using the constitutive relationships. For modelling the cracking behaviour, the fixed crack model was selected. The weight density for a normal strength concrete was used as input. Modulus of elasticity values obtained through experimental testing were used. The value of coefficient of thermal expansion was specified as 10 με/°C as used in the experimental investigation.

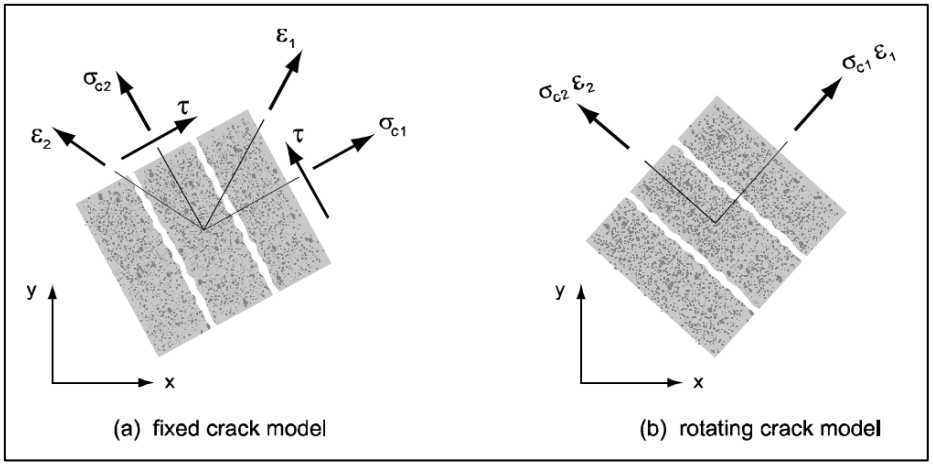

Figure 6.3. Cracking models available in the total strain crack model

- **Tensile Behaviour of Concrete**

  Accurately modelling the tensile behaviour of concrete is critical in such type of analysis. In MIDAS, various models available for predicting the post cracking tensile behaviour of concrete. As mentioned earlier in Section 6.2.3, model selected to predict the tensile behaviour is critical in satisfying the convergence criteria in the analysis. In this study the model presented by

Hordijk (1991) as shown in Figure 6.4 was used. The Hordijk model provides a nonlinear softening curve for predicting the post cracking tensile behaviour of concrete assuming that the stress gradually reduces to zero at an ultimate strain, $\varepsilon_{ult} = 5.136\,(G_f^I/f_t h_e)$; where G_f^I is the mode 1 fracture energy of concrete, h_e is the element size and f_t is the concrete tensile strength. Experimentally obtained values for the tensile strength of concrete were used as input. The fracture energy of the concrete was calculated according to the following equation given in Model Code (2010).

$$G_f = 73 f_{cm}^{0.18}$$

where f_{cm} is the mean compressive strength of concrete.

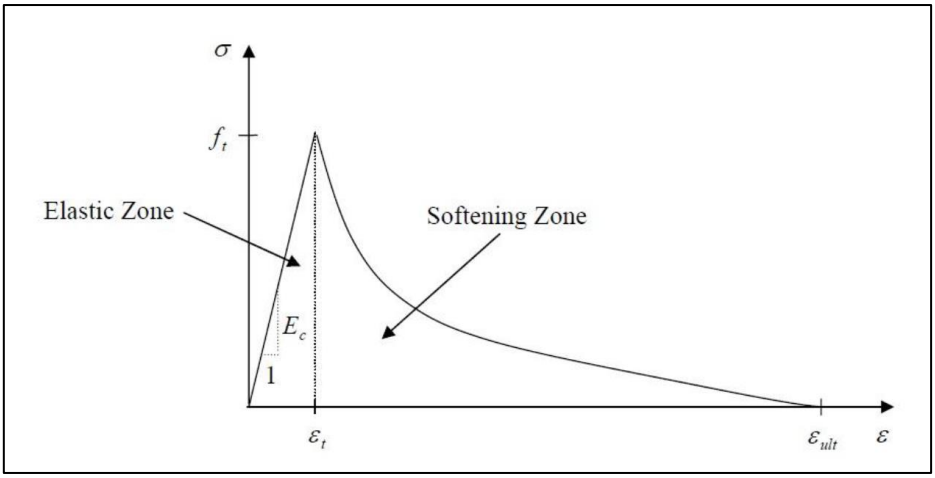

Figure 6.4. Hordijk model used for post cracking tensile behaviour of concrete (Hordijk, 1991)

- **Compressive Behaviour of Concrete**

The compressive behaviour of the concrete was also modelled using a predefined function given in MIDAS and proposed by Thorenfeldt (1987) as shown in Figure 6.5. Concrete subjected to compressive stresses displays pressure dependent behaviour. Due to the lateral confinement, the stress strain relationship is modified to incorporate the increased isotropic stresses. Moreover, the compressive behaviour is also influenced by the lateral cracking. The compressive behaviour curve can be modified internally by the software due to lateral cracking and confinement effects. It follows a nonlinear behaviour in its both zones: the ascending portion and the descending or softening portion. The input required for this model is the compressive strength of

concrete and whether the lateral confinement and cracking effects are to be incorporated or not. The experimentally obtained values of the compressive strength were used as input to model the compressive behaviour of concrete.

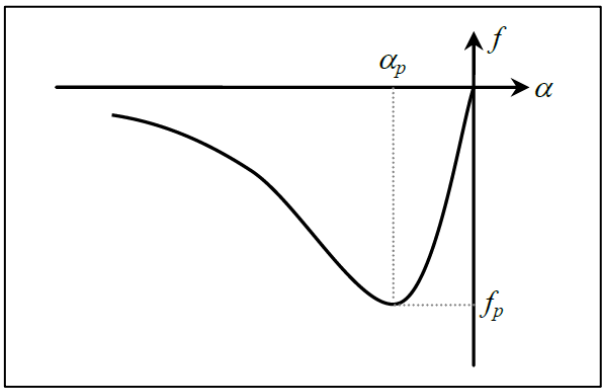

Figure 6.5. Thorenfeldt model used for compressive behaviour of concrete (Thorenfeldt et al., 1987)

- **Shear Behaviour of Concrete**

  Modelling of the shear behaviour of concrete is only required in the case of fixed crack model. This is because the shear stiffness is usually reduced after cracking. In MIDAS, a constant shear retention can be modelled by specifying a shear retention factor, β. The value of β lies between 0 and 1, however, in this work the value of 0.25 was selected based on the recommendations contained in the work by Vollum et al. (2010).

- **Behaviour of the Steel Reinforcement**

  The steel reinforcement was modelled using the Von Mises model. The value of initial yield stress for defining the hardening / softening function was obtained from the experimental tests on 16 mm diameter bars. The modulus of elasticity, weight density and the poisson ratio were selected from the material library available in the software.

6.3.3 Boundary Conditions

In order to correctly simulate the experimentally obtained behaviour of the wall, and assess the effect of restraining any curling / warping of the base, four different restraint conditions were modelled for both vertically reinforced and unreinforced walls and the results were compared to those obtained during the tests. Each wall was assigned a unique code for identification comprising a letter and a number; the letters

U and R represent the walls ‘Unreinforced’ or ‘Reinforced’ with vertical steel reinforcement and the number indicates the support conditions as explained below:

- **Support condition 1**. The first case represented a total restraint imposed on the base of the wall. The wall was modelled without the base slab and its bottom nodes were constrained from translation in all directions. The mesh and the applied boundary conditions for this case are shown in Figure 6.6.

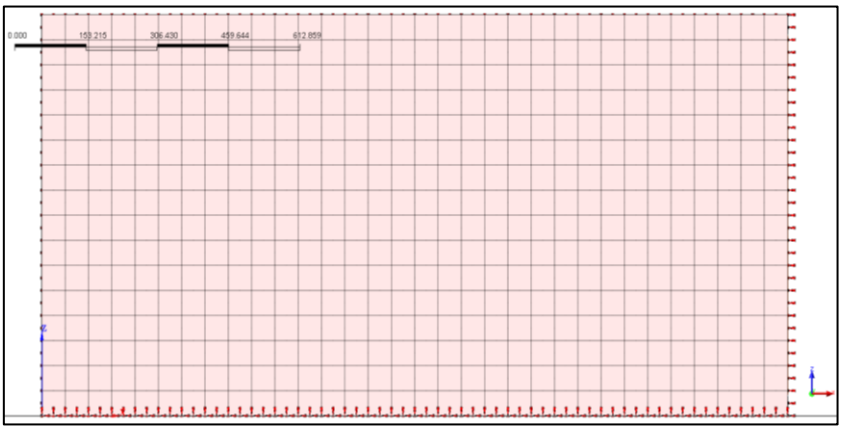

Figure 6.6. Finite element mesh and constraint applied for support condition 1

- **Support condition 2**. The second case represented the wall constructed on a base slab and a total restraint imposed on the bottom nodes of the base slab. Wall and base slab were modelled and the bottom nodes of the base slab were fixed to represent total restraint applied to the base slab. The mesh and the applied boundary conditions for this case are shown in Figure 6.7.

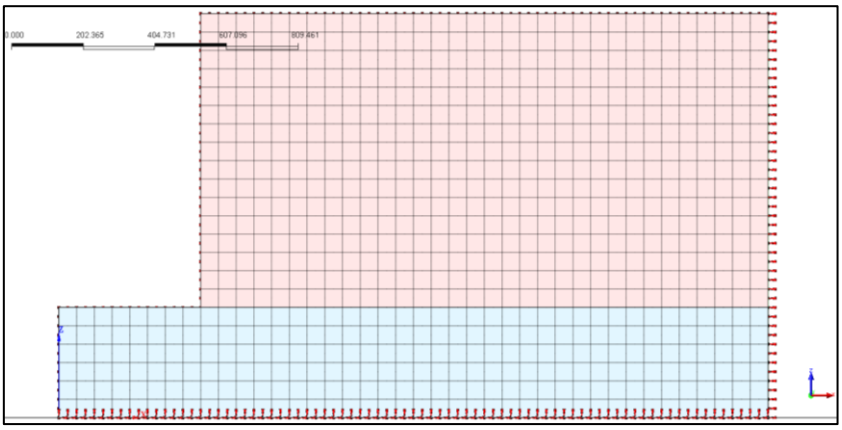

Figure 6.7. Finite element mesh and constraint applied for support condition 2

- **Support condition 3**. The third case represented the wall cast on to the base slab but the base slab was not fully restrained from movements. In this case, the wall, base slab and the floor were modelled such that the slab was connected to the floor using elastic links. This represented a partial restraint imposed on the base slab by the floor. The mesh and the applied boundary conditions for this case are shown in Figure 6.8.

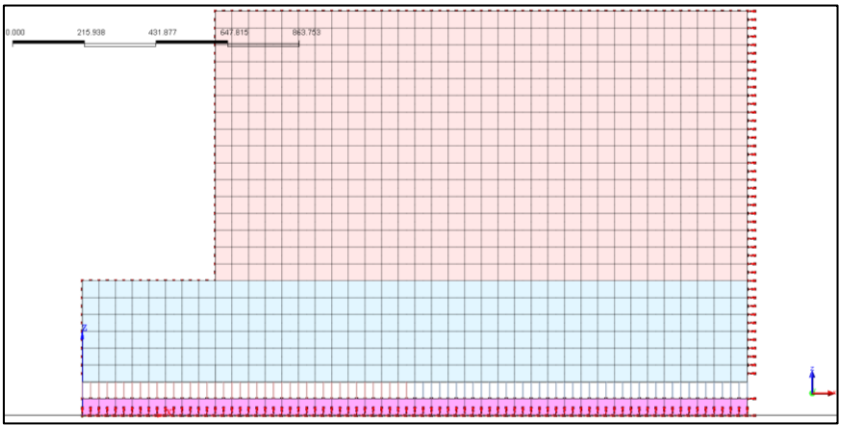

Figure 6.8. Finite element mesh and constraint applied for support condition 3

- **Support condition 4**. Fourth case was modelled to represent the case where the restraint was imposed along the edge of the wall due to the concrete base slab and its interaction with the floor. In this case, however, the base slab was not included in the model and only the wall and floor were modelled. The connection between the wall and floor was modelled using the elastic links. The stiffness for the elastic link elements was determined from the experimentally observed behaviour of the base slab. The mesh and the applied boundary conditions for this case are shown in Figure 6.9.

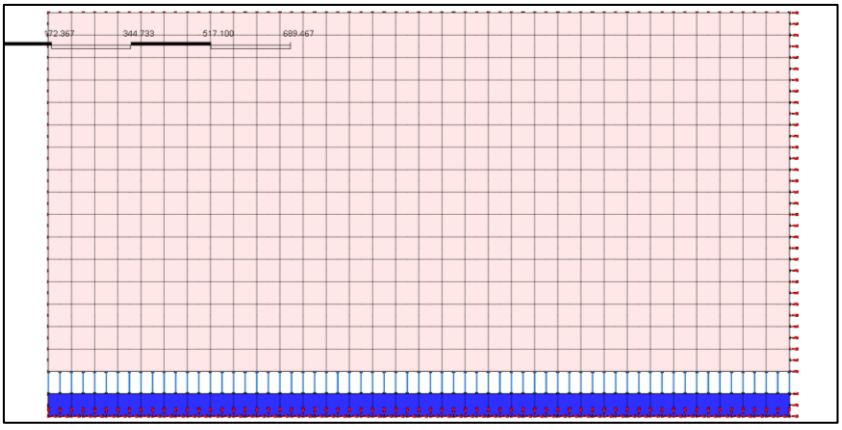

Figure 6.9. Finite element mesh and constraint applied for support condition 4

6.3.4 Loads

In reinforced concrete members subjected to restraint, the imposed loading is a combination of thermal and shrinkage strains. Thermal strain is the product of the thermal drop and the coefficient of thermal expansion of concrete. Shrinkage strain is a combination of the autogenous and drying strain. As already mentioned, the direct application of the shrinkage strain in MIDAS FEA is not available for the nonlinear static analysis. To apply the loads to the concrete elements in the models, the thermal drop (ΔT_{exp}) observed in the experiments was used. The unrestrained shrinkage strain (ε_{sh}) for the walls was calculated from the shrinkage strain experimentally observed in the concrete prisms. The shrinkage strain was then converted to the equivalent thermal drop (ΔT_{eq}) by dividing it by the coefficient of thermal expansion (α_c) as given in equation 6.1. Then the total thermal drop (ΔT_{tot}) was calculated according to equation 6.2 as the sum of thermal drop observed experimentally and the equivalent thermal drop calculated from the shrinkage strain.

$$\Delta T_{eq} = \varepsilon_{sh}/\alpha_c \tag{6.1}$$

$$\Delta T_{tot} = \Delta T_{exp} + \Delta T_{eq} \tag{6.2}$$

The thermal drop was applied as nodal temperature load to the nodes of the wall elements. It was observed in the experiments that the thermal drop was lower near the base of the wall and more in the higher regions. Similarly it reduced towards the free ends of the walls as well. Accordingly the nodal temperatures were linearly varied over the height and length in the models while applying the loads.

6.4 Analysis Results and Validation of the Models

Both linear and nonlinear static analysis were performed in MIDAS FEA. The results of the linear analysis were utilized for calculating the degree of restraint, whereas the stress variation and cracking behaviour was observed from the nonlinear analysis. The Newton Raphson iteration scheme was employed for obtaining the nonlinear solution in which the energy and displacement norms for a convergence tolerance of 0.001 were satisfied.

6.4.1 Stress Development in Walls

The applied thermal load was divided into small increments depending on the number of load steps specified in the analysis. From the analysis results, it was seen that with an increase in the thermal contraction, the stress increased in the walls. When the generated tensile stress exceeded the specified cut off value, the crack appeared. On the occurrence of a crack, the stress in the vicinity of the crack was seen to drop and with a further increase in contraction, the stress in the remaining parts of the member kept on accumulating, resulting in another crack at a different location, which also relieved the stress locally. This phenomenon is in line with the guidance provided by Bamforth (2007) with respect to the formation of cracks under edge restraint.

6.4.2 Degree of Restraint

The degree of restraint for each of the modelled cases was calculated using the obtained strain values. The degree of restraint over the height of wall obtained from the finite element analysis was compared with the values obtained experimentally. The comparison is shown in Figures 6.10 and 6.11 for test 1 and test 2 walls respectively. The variation of the restraint with height was observed in all of the modelled scenarios. The degree of restraint obtained from the finite element analysis for case 1 and 2 considerably exceeds the values obtained during the tests. The degree of restraint obtained for case 3 is important as it shows the effect of curling on the restraint profile. The profile of restraint matched the experimental values over the lower two thirds of the wall, however, near the top the software predicted less restraint as a small amount of compression will be induced at this point from the curling (compare this with the experimental values where the measured restraint tended to increase near the top due to the induced tension from not permitting curling to occur). Case 4 predicts the variation of restraint over the height reasonably well for both tests.

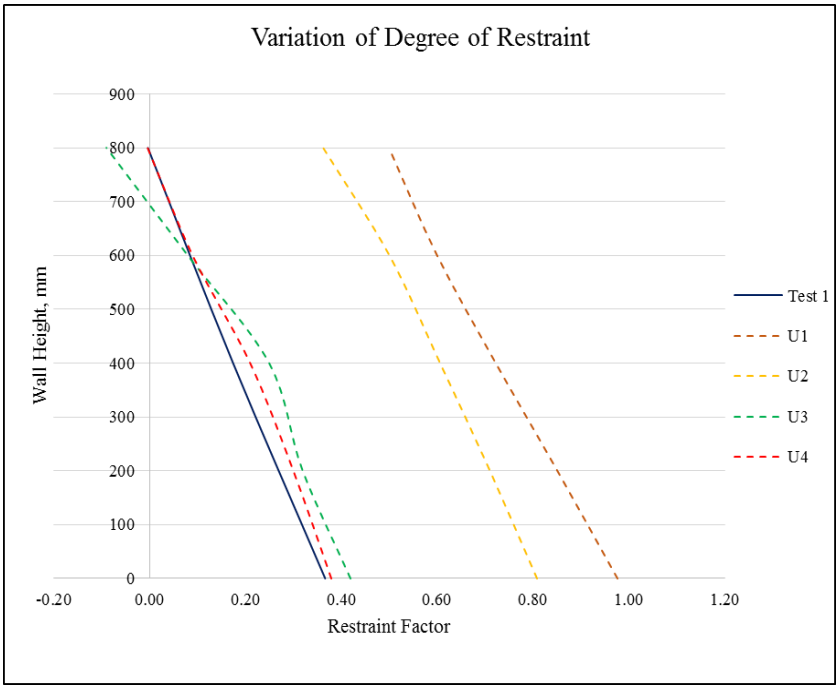

Figure 6.10. Comparison of experimentally obtained restraint factors in test 1 with those obtained using the finite element analysis

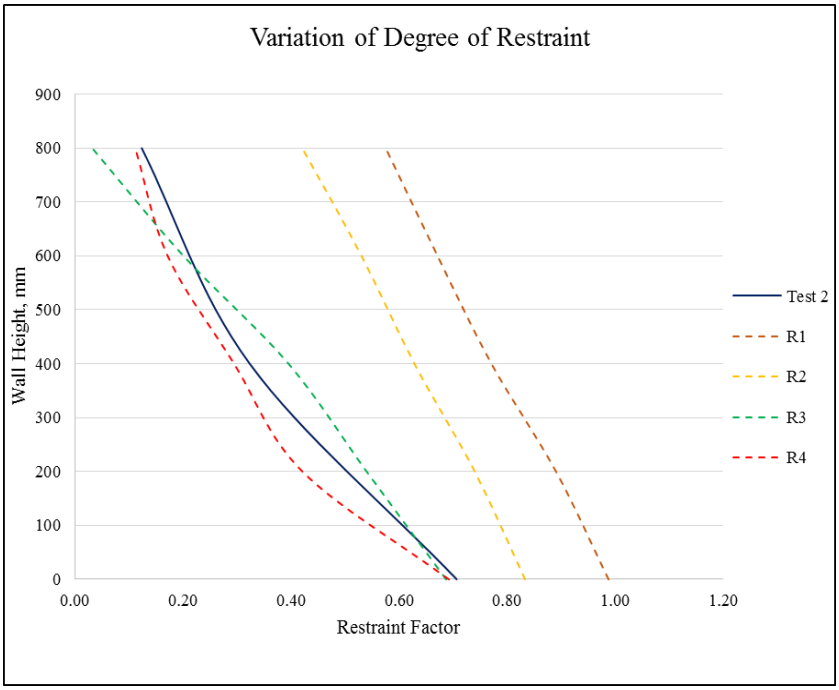

Figure 6.11. Comparison of experimentally obtained restraint factors in test 2 with those obtained using the finite element analysis

The finite element study presented in this section also, therefore, highlights the importance of correctly simulating the actual support conditions. It is not appropriate to consider the wall or the base slab edge totally restrained from movement and the mechanism supporting the base slab needs to be incorporated in the finite element

analysis. In practice, when the base slab is cast onto the soil, soil structure interaction may be modelled using the springs incorporating the modulus of subgrade reaction of the soil. However, since the tests in the present study were conducted in the laboratory and the slab was cast on the laboratory strong floor, and a special clamping mechanism was used to prevent the development of curvature in the slab, the use of elastic links for simulating the behaviour of the base slab appeared to be an appropriate option.

6.4.3 Cracking Behaviour

Owing to the different support conditions, the strain profile / cracking behaviour of each modelled wall was also different, despite having similar loading and material properties. Finite element models U3 and U4 did not develop any cracks, however, in the case of walls U1 and U2, cracks were formed as indicated in the strain profiles for each of the U-series walls in Figure 6.12. Formation of these cracks is obviously contrary to the experimental findings and is attributed to the applied boundary conditions simulating a total restraint. In the case of the R-series walls, each of the modelled walls developed cracks, as shown by the strain profiles in Figure 6.13. An unrealistic depiction of total restraint in walls R1 and R2 induced full height cracks whereas, in the case of walls R3 and R4, in which the elastic links were used, the developed cracks did not propagate over the full height of the wall. The cracks that developed in wall R4 can be related to those obtained in test 2 and 4 in which the first crack appeared close to the centre of the wall and, with an increase in the thermal contraction, the second crack appeared in between the free end and the first crack. Wall R4 predictions bear close resemblance to the cracks obtained in the experimentally tested walls except that no crack can be seen close to the free end of the modelled wall. It is anticipated that the adopted experimental methodology of clamping the base slab to the floor induces tensile stresses near the free ends of the wall which led to the crack forming close to the ends. From the cracking patterns and the restraint variations obtained using the finite element models, it can be inferred that modelling of the real time support conditions has a significant importance.

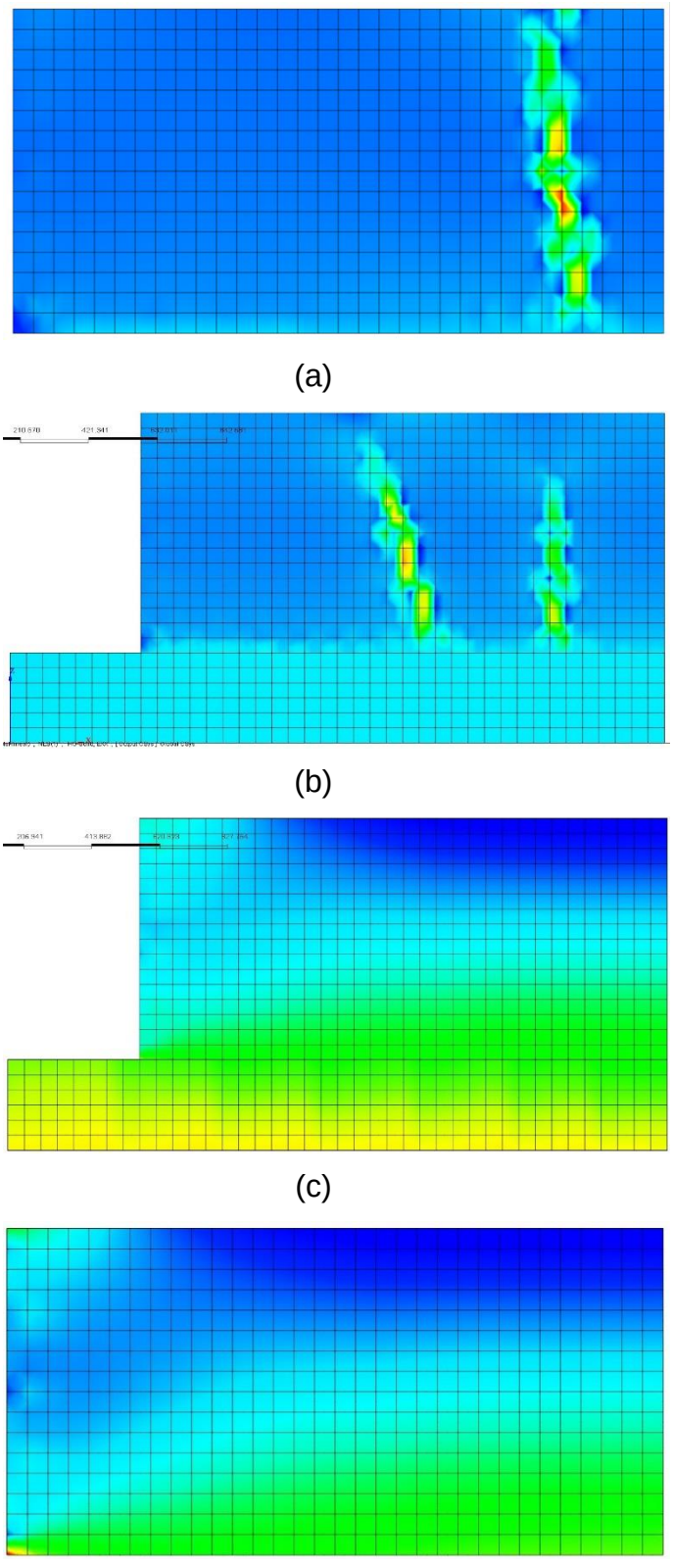

(a)

(b)

(c)

(d)

Figure 6.12. Strain profile of U-series wall obtained using the finite element analysis: (a) wall U1; (b) wall U2; (c) wall U3; (d) wall U4

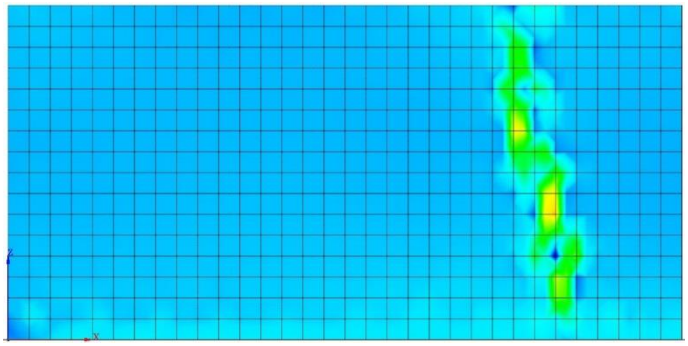

(a)

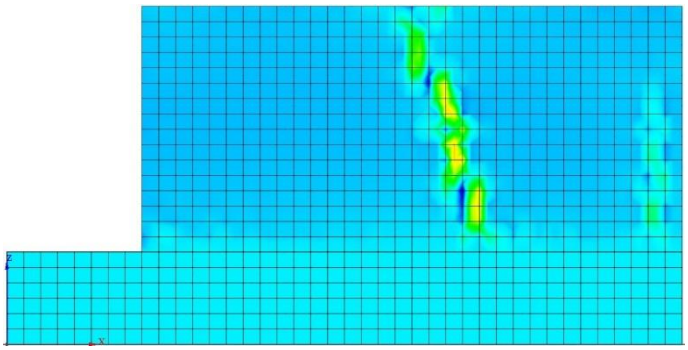

(b)

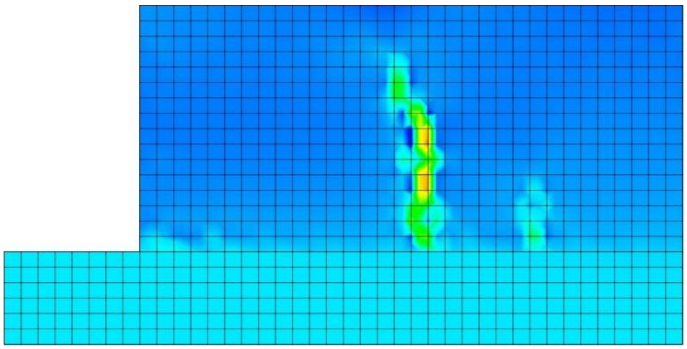

(c)

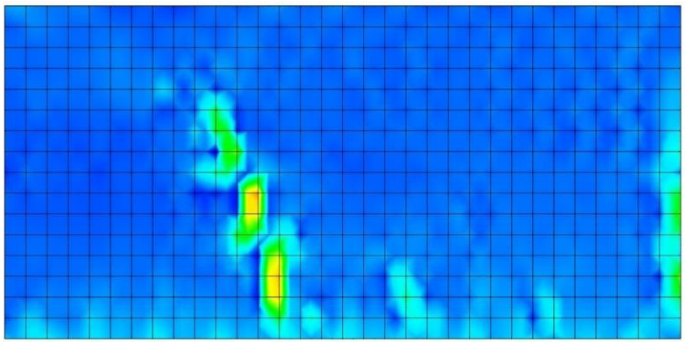

(d)

Figure 6.13. Strain profile of R-series wall obtained using the finite element analysis: (a) wall R1; (b) wall R2; (c) wall R3; (d) wall R4

6.5 The Parametric Study

In this section the parametric study based on the finite element analysis is presented. The parametric study was carried out to evaluate the influence of different parameters on the cracking behaviour of reinforced concrete walls which could not be experimentally ascertained.

6.5.1 Parameters Considered

The reinforced concrete members affected by restraint of imposed loading can be subjected to different types of external restraint. The cracking pattern and behaviour of members is influenced by the type of restraint. Moreover, the type of boundary conditions applied to the restraining members is also important factor in assessing the response of restrained members. The parameters evaluated in this analysis are as under:

- The aspect ratios of the walls.
- Types of restraint; walls subjected to edge and combined restraint were modelled.
- Support conditions of the restraining members.

Cracking patterns, crack widths and crack spacing in the walls are influenced by the wall height and the length to height ratios. Walls with aspect ratios of 1, 2, 4, 6 and 12 were modelled and following three types of restraint were applied for each wall:

- **Case 1** – Edge Restraint along the base.
- **Case 2** – Combination of Edge Restraint along the base and End Restraint on one side.
- **Case 3** – Combination of Edge Restraint along the base and End Restraint on both sides.

As highlighted from the analysis presented in the previous section, the support conditions can significantly influence the behaviour of restrained walls. To evaluate this phenomenon for the modelled walls, two types of constraints or the boundary conditions were applied for the restraining elements. The support conditions considered are as under:

- **Support Condition 1** – This condition was modelled to depict total fixity of the restraining members. Such scenario is encountered when a part of the reinforced concrete wall is cast against the parts already cast and hardened. Nodes of the restraining members were fully constrained from movement in all three directions.
- **Support Condition 2** – This condition represented the case when the restraining members are resting on the ground e.g. the foundation slab in the case of a cantilever retaining wall. In such scenario, the interaction between the soil and the concrete member is required to be modelled using the surface springs. Stiffness of the modelled soil springs can be estimated from the modulus of subgrade reaction of the soil.

6.5.2 Geometry and Material Properties

Dimensions of the restraining concrete members and the restrained walls are given in Table 6.1. Taking advantage of the symmetry of dimensions, reinforcement, loading and boundary conditions, a quarter of the wall and restraining elements were modelled for case 1 and 3. However, for case 2, symmetry along thickness only was modelled.

Table 6.1. Geometric dimensions of restrained and restraining members

	Edge Restraining Member	**End Restraining Member**	**Restrained Wall**
Length (m)	15	1.5	12
Thickness (m)	1	1	0.4
Height (m)	0.5	1, 2, 3, 6, 12	1, 2, 3, 6, 12

Material properties for concrete and steel were obtained from the experimental study and are given in Table 6.2. Concrete was modelled using the total strain crack model available in MIDAS as explained in detail in Section 6.3. The mesh size for the concrete elements was kept as 100 mm. The wall was reinforced with 12 mm bars spaced at 200 mm in the horizontal direction, along both faces. In the vertical direction, 16 mm bars spaced at 150 mm were provided. Thus making the area of steel provided

as 1130 mm^2/meter and 2680 mm^2/meter in horizontal and vertical directions respectively. The reinforcement was modelled as embedded bar in solid as explained in Section 6.3 above.

Table 6.2. Material properties of concrete and steel

Material Properties	**Restraining Members**	**Restrained Wall**
Concrete		
Compressive Strength (MPa)	43.3	31.0
Tensile Strength (MPa)	3.4	2.4
Modulus of Elasticity (MPa)	31000	24500
Coefficient of thermal expansion (με /℃)	10	10
Poisson Ratio	0.18	0.16
Fracture Energy (N/mm)	0.098	0.073
Thermal Conductivity (W/m)	1.76	2.03
Specific Heat (KJ/Kg C)	0.95	0.74
Steel		
Yield Strength (MPa)	500	500

6.5.3 Analysis Procedure

The finite element meshes for the modelled walls with support condition 1 and 2 are given in Figures 6.14 and 6.15, respectively. Suitable constraints were also applied along the symmetrical faces of the models.

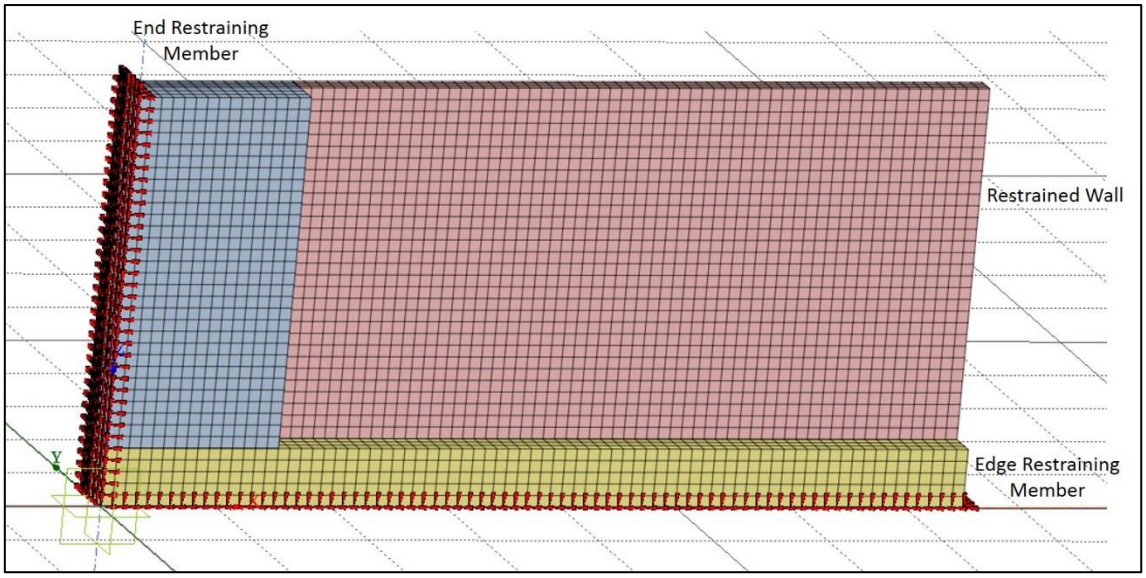

Figure 6.14. Finite element mesh and support condition 1 applied for the walls

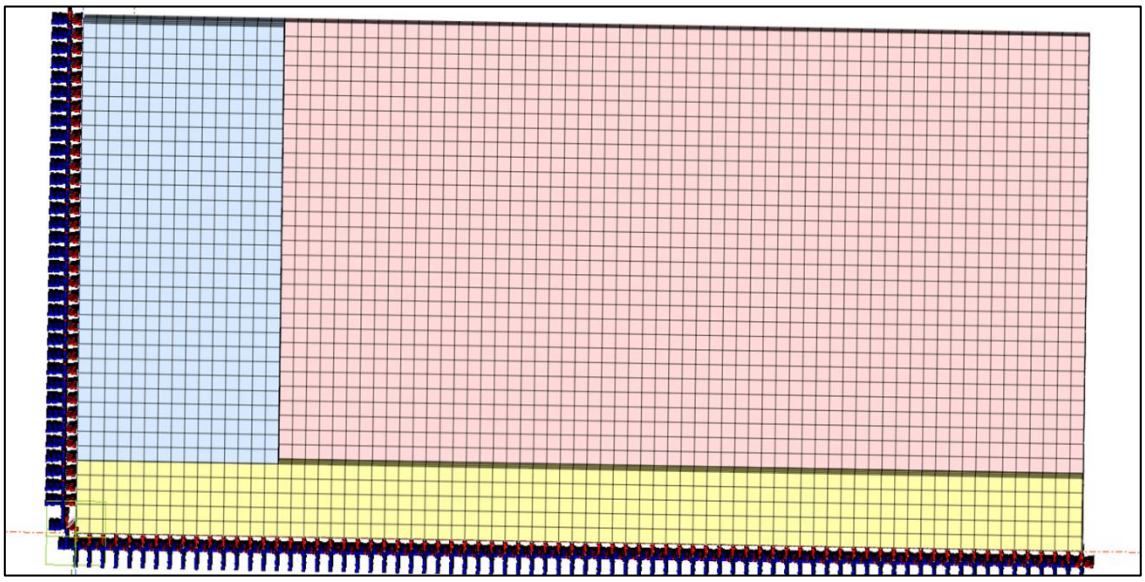

Figure 6.15. Finite element mesh and support condition 2 applied for the walls

Thermal and shrinkage load effect was simulated by applying the thermal contraction to the wall elements. As experienced in the experimental investigation, considerable amount of heat is transferred from the wall to the restraining members and thus the thermal drop is lesser close to the restraining elements and the free edges of the member and more in the centre. Correspondingly, the applied thermal load was varied along the length and height of the wall. Variation of the applied thermal loads is graphically represented in Figure 6.16. The nonlinear static analysis was performed using the Newton Raphson solution techniques. Force and energy norms for the convergence criteria with a tolerance of 0.001 were satisfied in the iterative process.

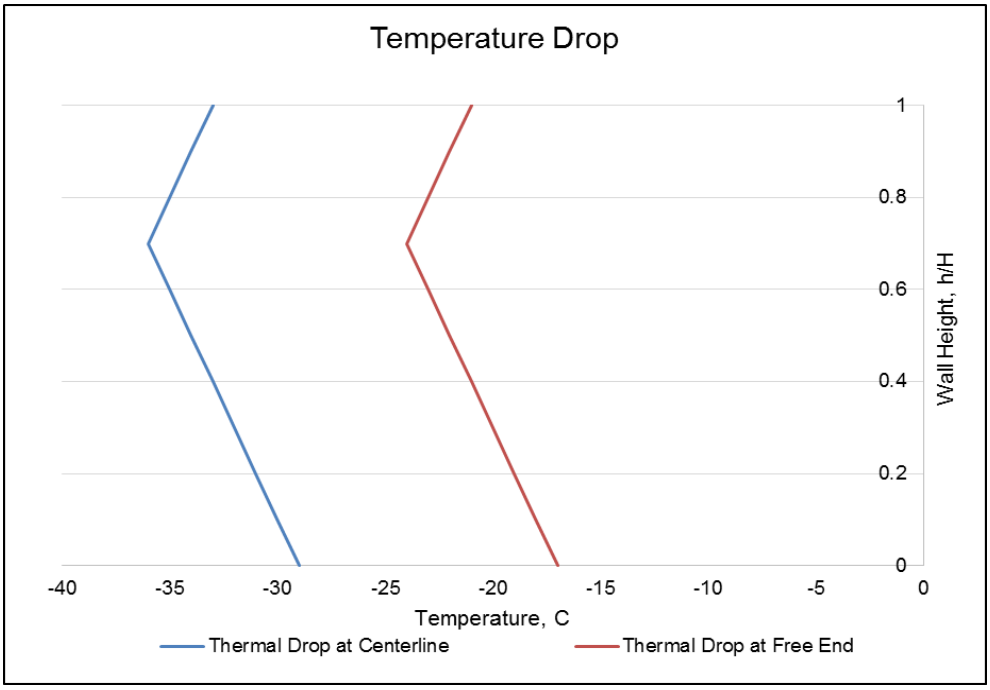

Figure 6.16. Thermal load applied to the walls

6.5.4 Influence of Restraint Type on Stress Distribution

From the analysis results, it was observed that with the increase in thermal contraction, the stress keeps on increasing in the restrained member. On occurrence of a crack in the edge restrained member, the stress relief is local in nature as explained in Section 6.4 above as well. With the introduction of end restraint at one or both ends, the stress rises in the member with an increase in thermal contraction and then drops in almost entire member with the appearance of first crack, which in the case of stiffer boundary conditions (support condition 1) appears at the joint between the wall and end restraining member. Thereafter, the stress again increases in the member and is relieved locally with the onset of each crack. It is also seen that with the increase in wall height, less stress is generated close to the free edges because of the absence of restraint. This phenomenon prevents propagation of the cracks to the wall height and to the free ends, however, it is only seen in walls with aspect ratio of less than 2. In the case of more flexible boundary conditions (support condition 2), the restraint offered to the wall reduces and so does the stress generated in the wall.

6.5.5 Influence of Wall Aspect Ratio

Cracking patterns in the walls were seen to vary with different aspect ratios. Since the modelling the rigid boundary conditions imposed a more severe degree of

restraint onto the wall, therefore in this section only the influence of aspect ratio of the modelled walls with support condition 1 is discussed. The influence of each of the support conditions is further discussed in subsequent sections. The strain profiles generated from the finite element models clearly indicate the location and orientation of the cracks. The sequence in which the cracks appeared were also noticed and marked adjacent to each crack. The behaviour of walls under three different cases of restraint are explained in detail in the succeeding paragraphs. Cracking behaviour and location of maximum crack width in the wall acquired from the strain profiles are illustrated in Figures 6.17 – 6.21 for each aspect ratio. The location of maximum crack width has been marked using a red rectangle in each picture.

- **L/H - 12**. First crack appeared close to the centre line of the wall in case 1 and case 2, however, in case 3 it appeared at the joint between the end restraining member and the wall. Cracking patterns indicate that all the cracks propagate in the vertical direction and reach the full height of the wall. Location of the maximum crack width in the wall varied with each type of restraint as indicated in the pictures. The maximum crack width, however, occurred at some height above the base. In all cases the cracks initiated at the base and propagate upwards.

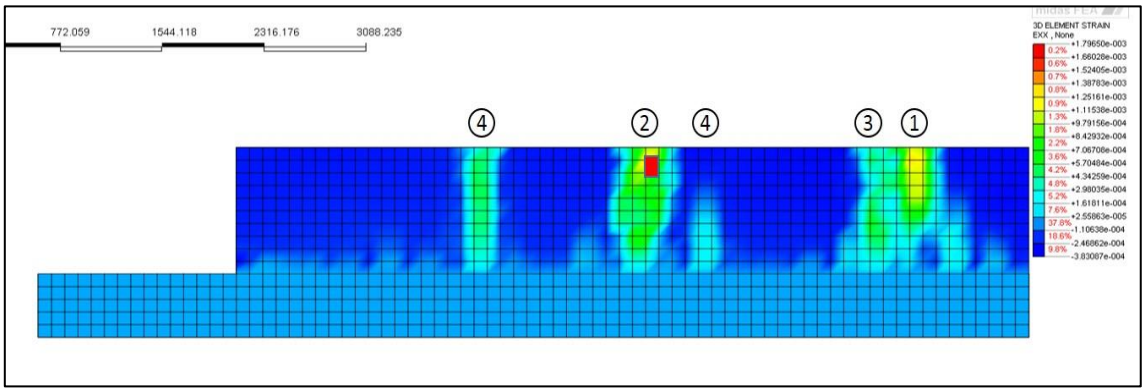

(a)

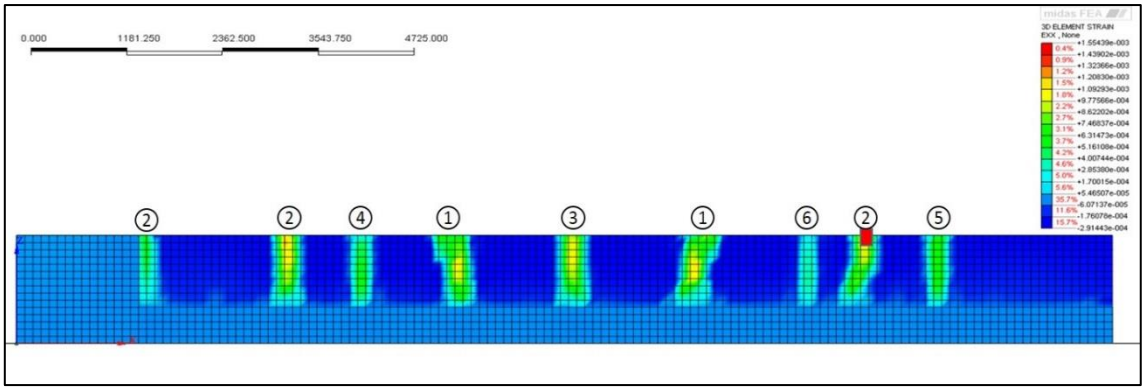

(b)

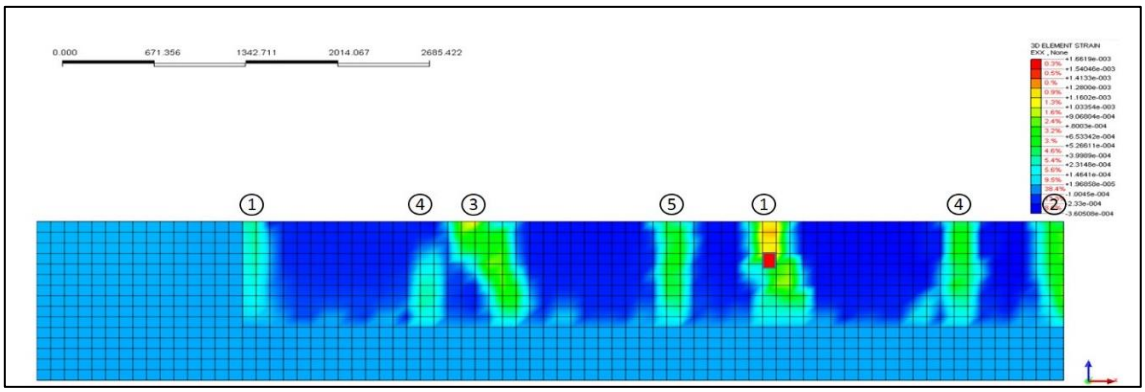

(c)

Figure 6.17. Cracking patterns for walls with aspect ratio of 12; (a) Case 1, (b) Case 2, (c) Case 3

- **L/H - 6**. In case of edge restraint, the first crack appeared close to the centre of the wall and most of the cracks reached the full height. Number of cracks were less than those in the edge restrained wall with aspect ratio of 12. With the introduction of end restraint (case 2 and 3), number of cracks increased and mostly reached the full height of the wall. All cracks initiated at the base and propagated upwards mostly remaining vertical. No significant cracking was seen in these walls within the zone of no cracking described in BS EN 1992-1-1 (2004). First crack, in case 2 and 3, appeared at the joint between end restraining member and the wall. Location of the maximum crack width varied in each case within the wall, however, it occurred at some height above the base of the wall.

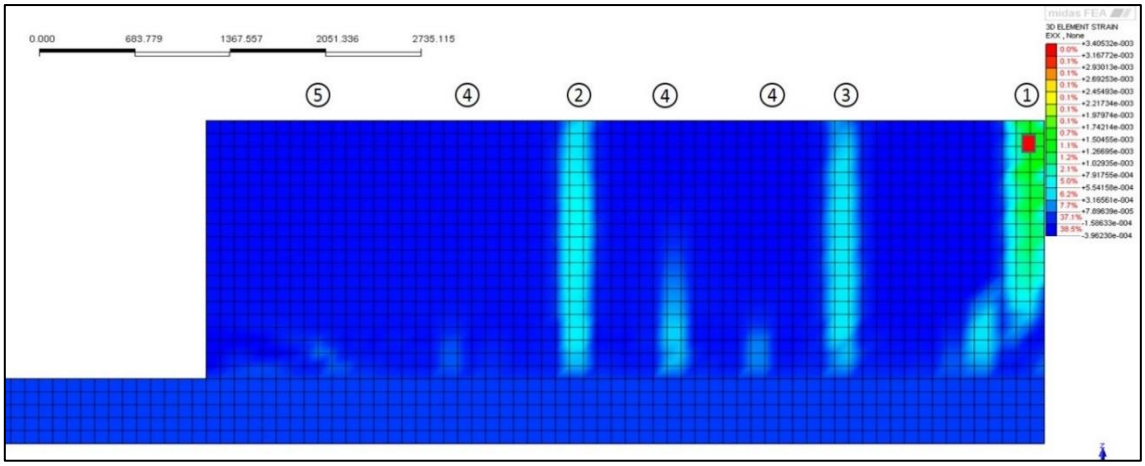

(a)

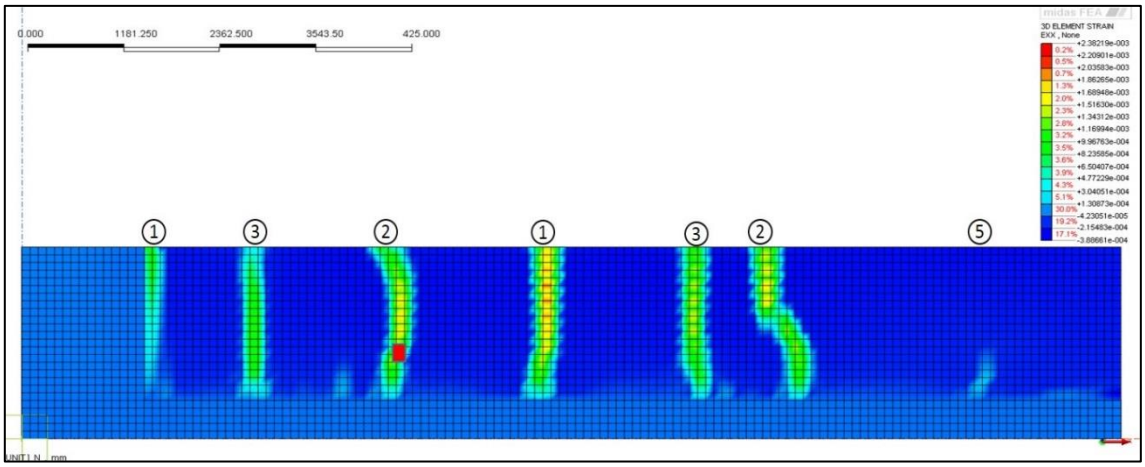

(b)

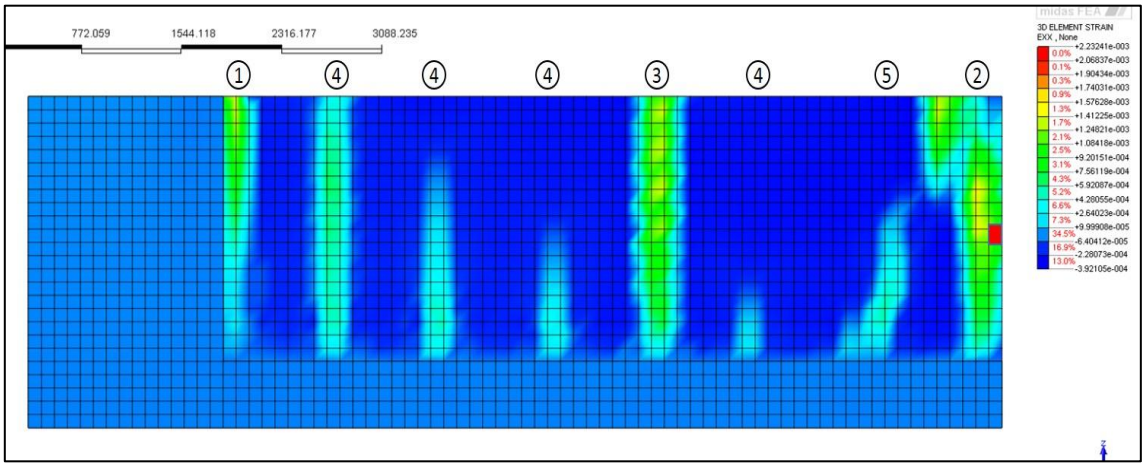

(c)

Figure 6.18. Cracking patterns for walls with aspect ratio of 6; (a) Case 1, (b) Case 2, (c) Case 3

- **L/H - 4**. In the case of edge restraint, the first crack still appeared close to the centre of the wall and reached the full height. None of the other cracks

appearing later crossed the entire height of the wall. Cracks appearing in the outer one third part of the wall length were inclined towards the free ends and prominent cracking is seen close to the end contrary to the specification of Eurocode 2. Like the walls with other aspect ratios, with the introduction of end restraint, the number of cracks in the wall increased and most of them reached the full height of wall. Cracks close to the free end in case 2 were inclined whereas all cracks in case 3 maintained their vertical orientation. Maximum crack width in the wall was seen to occur at different locations in each case. In case 3, the maximum crack width occurred at the top most point along the joint with the end restraining member.

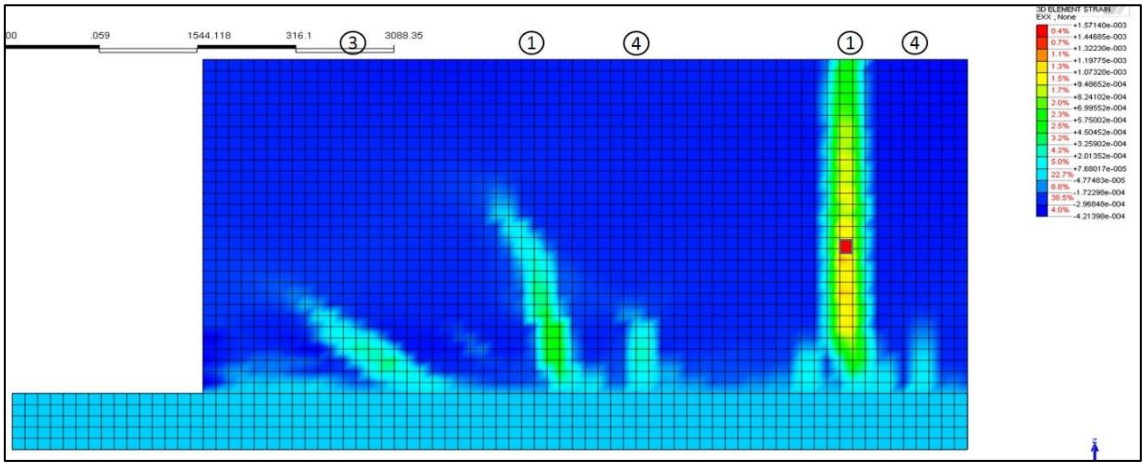

(a)

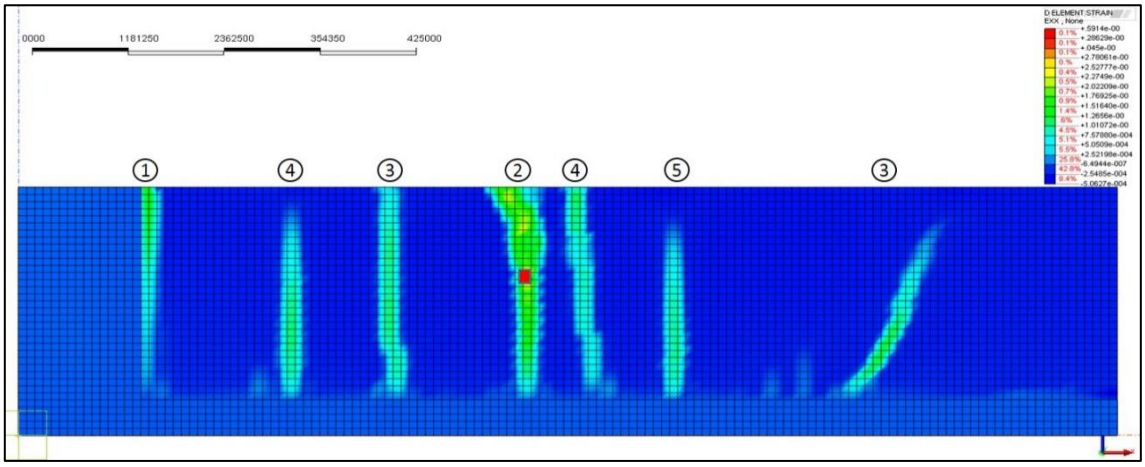

(b)

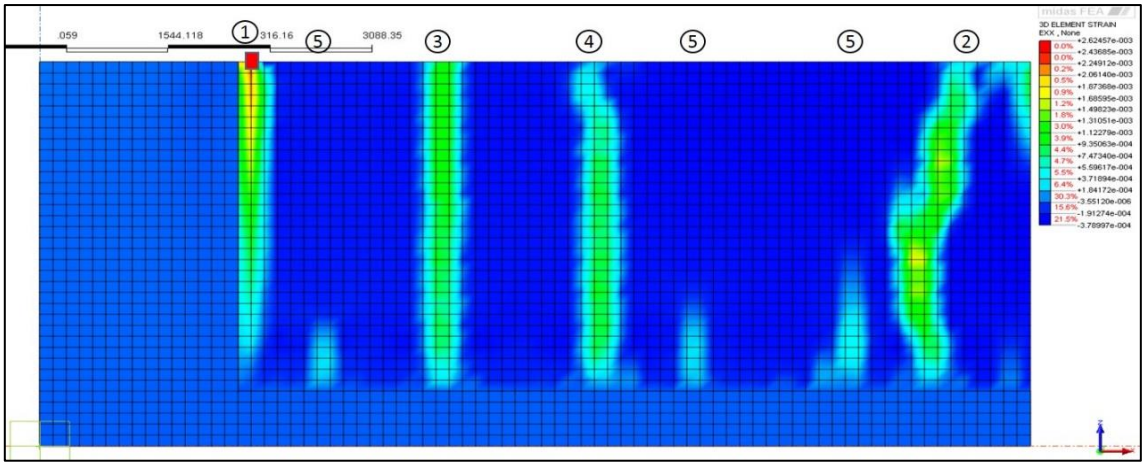

(c)

Figure 6.19. Cracking patterns for walls with aspect ratio of 4; (a) Case 1, (b) Case 2, (c) Case 3

- **L/H - 2**. Results indicated that when the aspect ratio of the wall was dropped to 2, the cracking patterns showed considerable variation from those with higher aspect ratios. The first crack in edge restrained wall appeared close to the centre like other walls and attained the maximum height among all other cracks, however, no crack reached the full height of the wall. Cracks propagated at some inclination from the vertical and noticeable cracking close to the free edge was also seen. When the influence of end restraint was analysed in case 2 and 3, the cracks increased in number and propagated higher compared to the edge restraint alone. The first crack in case 2 and 3 appeared at the joint location and the maximum crack width was also seen to occur along the joint at the top most point. Almost all the cracks in case 2 had an inclined orientation. Their inclination from the vertical axis was lesser close to the end restraint and more as the free end was reached. In case 3, the combined effect of end and edge restraints kept the cracks orientation nearly vertical. Height of the cracks in this case is more close to the end restraining members and lesser in the centre. This indicated the domination of end restraint and loss of edge restraint in the higher parts of the wall away from base. First crack in both case 2 and 3 appeared at the joint location and so did the maximum crack width.

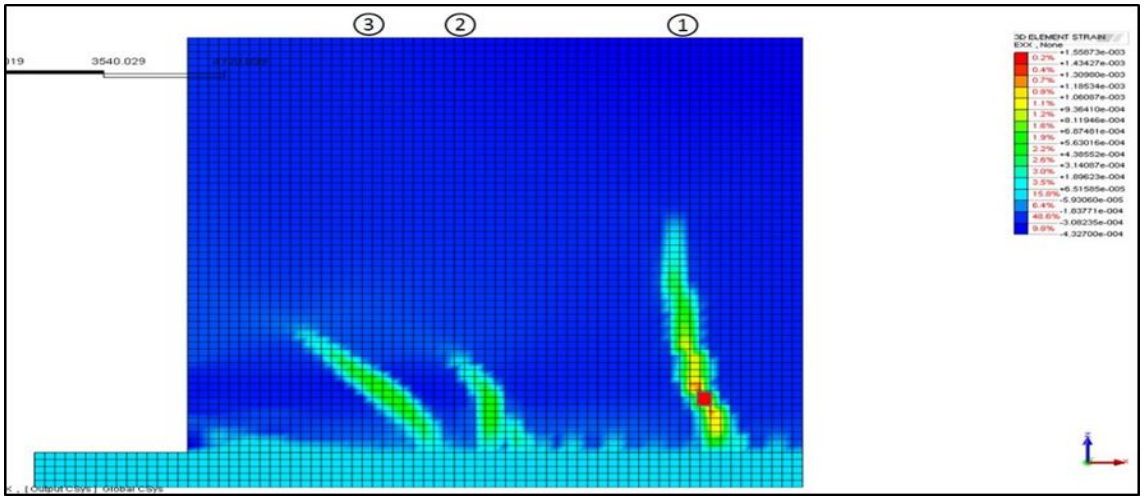

(a)

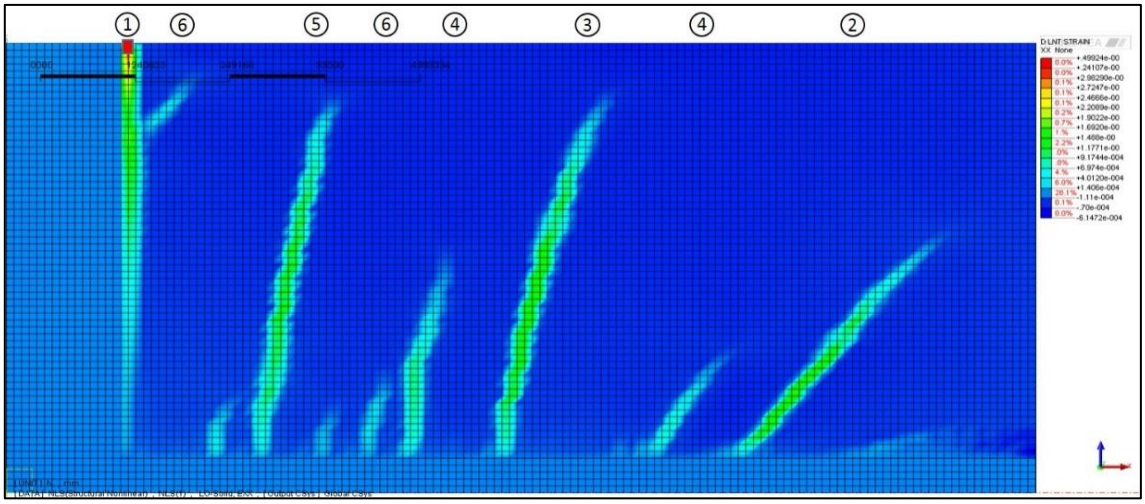

(b)

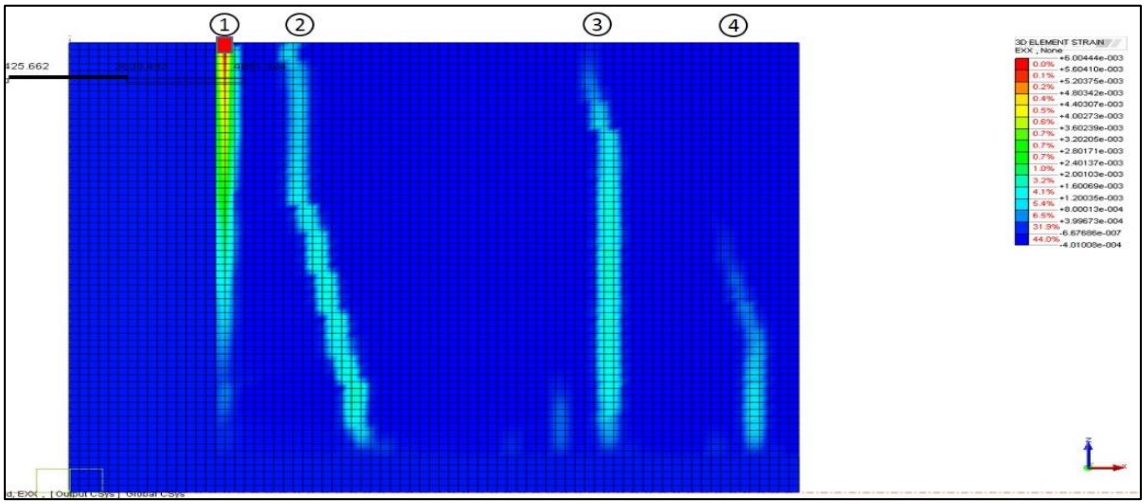

(c)

Figure 6.20. Cracking patterns for walls with aspect ratio of 2; (a) Case 1, (b) Case 2, (c) Case 3

- **L/H - 1**. The cracking behaviour of these walls was significantly different from the walls with higher aspect ratios. First crack, in case 1, appeared at the centre of the wall and propagated to approximately one third of the wall height. Subsequent cracks attained a lesser height comparatively and did not propagate vertically but were rather inclined at some angle. Maximum crack width appeared at some height above the base. In case 2 and 3, first crack appeared at the joint location and so did the maximum crack width. Cracks in case 3 were higher near the ends and changed their inclination during propagation along the height. Cracks in the middle part of the wall attained lesser height. In case 2, distinct influence of end and edge restraint was witnessed since some of the cracks initiated from the end restraint face and they propagated in the wall towards the free edges. Although a large number of cracks appeared, however, none of the cracks crossed the entire length or height of the wall.

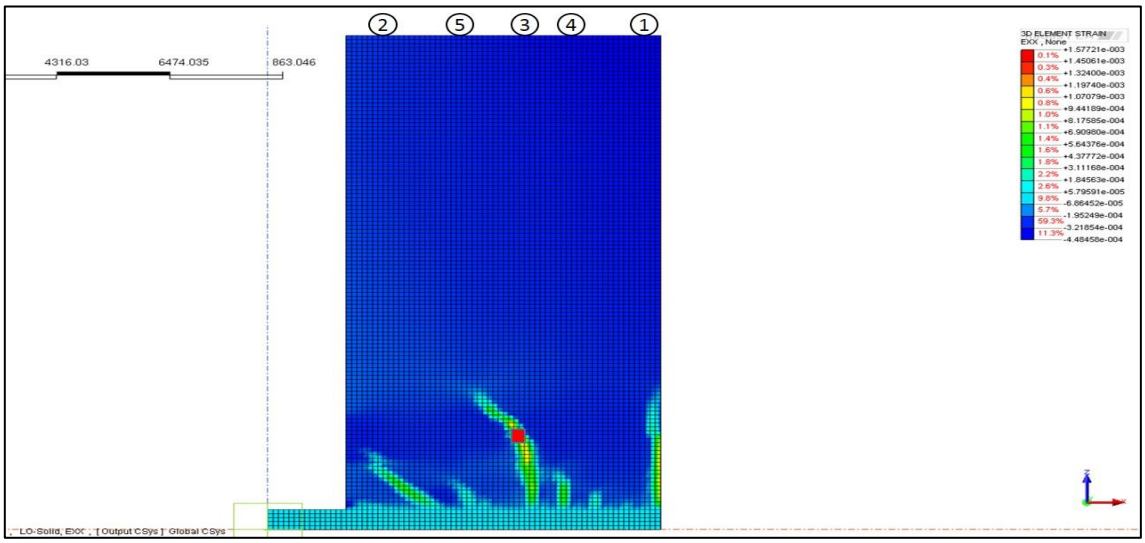

(a)

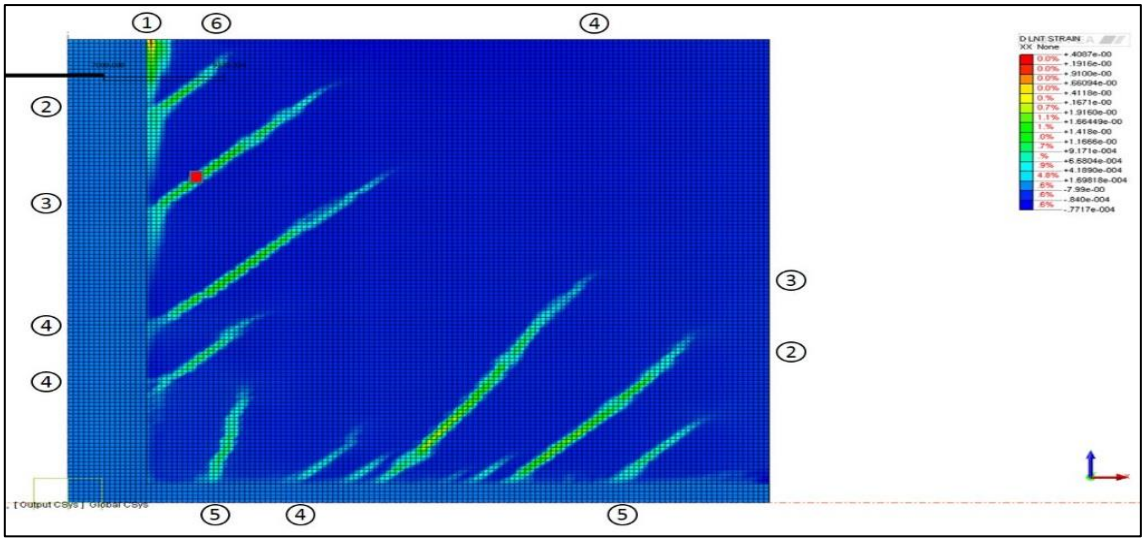

(b)

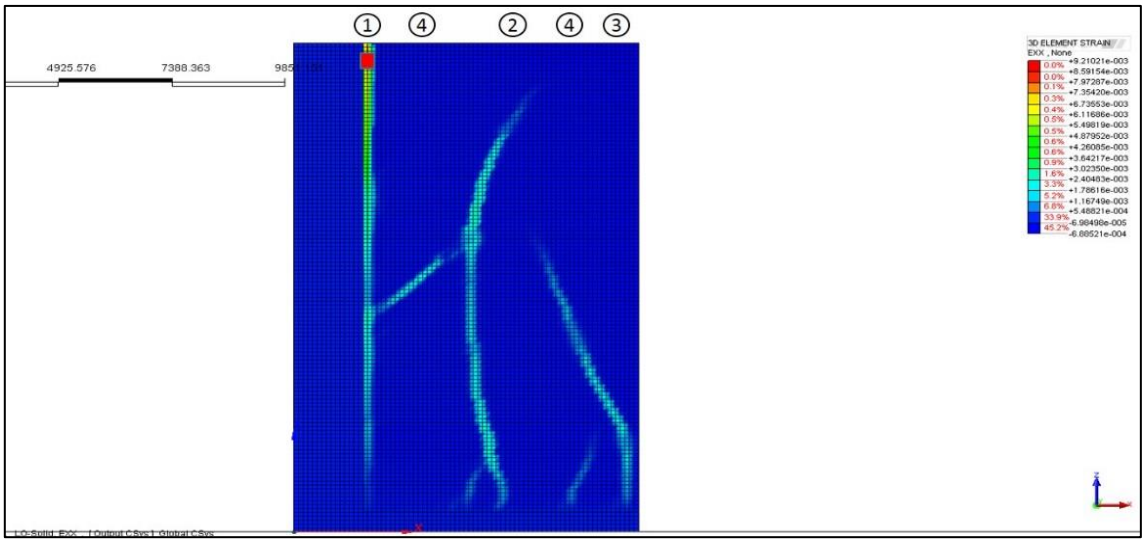

(c)

Figure 6.21. Cracking patterns for walls with aspect ratio of 1; (a) Case 1, (b) Case 2, (c) Case 3

From the above results it is obvious that the combined restraint poses a more complex challenge compared to the edge restraint considered alone. In the presence of combined restraint the domination of both edge and end restraint in different parts of the wall was observed. This endorses the hypothetical distribution of the restraint domination presented by Forth (2008) for members subjected to a combination of edge and end restraint. However, further experimental and analytical work is essential to understand the restraint distribution in the case of combined restraint.

6.5.6 Influence of Wall Aspect Ratio on Crack Widths

Comparison of the variation of maximum crack width for different aspect ratios in each of the restraint case considered is shown in Figure 6.22. The maximum crack width was lesser in the case of edge restraint alone and more in the case of combined restraint for walls with aspect ratio of 4 or less. The influence of end restraint on the maximum crack width became insignificant in walls having aspect ratio of 6 and 12. The introduction of end restraint at both ends increased the crack width more than that at one end only. From the comparison it is evident that the influence of combined restraint is more pronounced in walls with smaller aspect ratio. As the wall height is increased, the influence of edge restraint starts to diminish and the end restraint starts to affect the behaviour of the wall in the higher region of the walls. Moreover, the analysis also confirmed that in edge restrained walls, maximum crack width is located some point higher in the walls and not at the location maximum restraint (which occurs at the base of the wall). This was observed in the experimental investigation as well and is attributed to the closing action of the base as well as lesser thermal drop near base.

The results of the analysis also indicated that the location of the maximum crack width may not remain fixed rather it can change with the increase in restrained contraction. When a new crack was formed, the width of already existing cracks, at some instances, decreased as well. In the case of walls subjected to a combination of edge and end restraint, the first crack mostly occurred at the joint between the wall and the end restraining member and, in some cases, the maximum crack width was also found to occur along the same crack. Micallef et al. (2017) also observed in an experimental investigation that the first crack in the case of combined restraint always formed at the joint between the wall and the end restraining member. However, the analysis of the influence of the support conditions (given in Section 6.5.7 below) revealed that this may not be the case when the restraining member has relatively flexible boundary conditions.

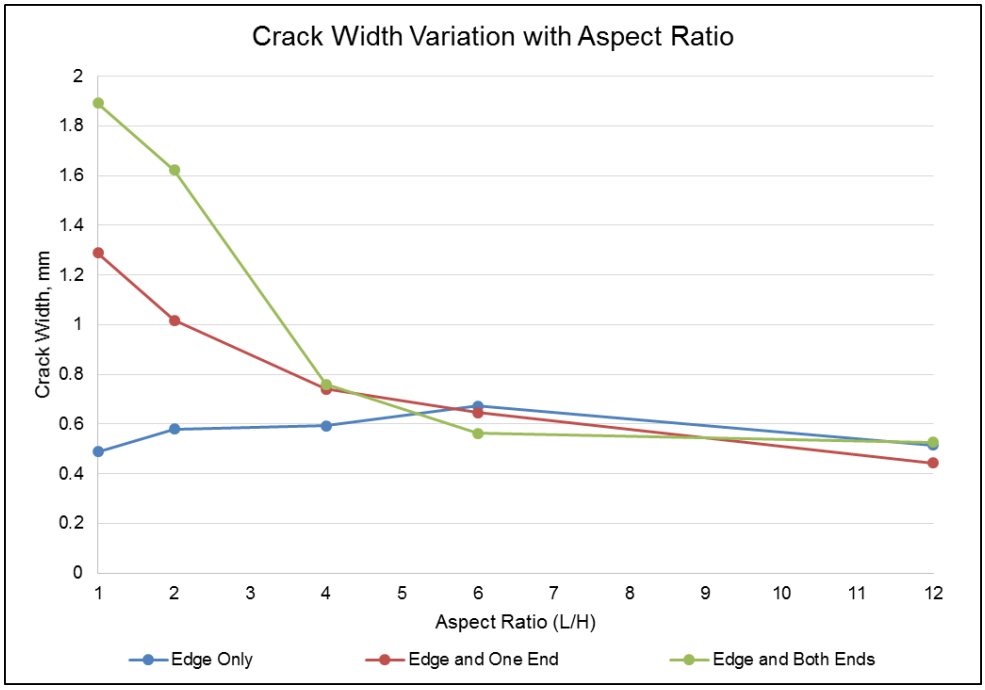

Figure 6.22. Variation of crack widths with aspect ratio under different types of restraint

6.5.7 Influence of Support Conditions on the Cracking Pattern

Two different scenarios likely to be encountered in the case of members subjected to restraint, based on the external boundary conditions of the restraining elements, were analysed. One scenario considered is when the restraining elements are rigidly connected to the surrounding members. These case can be encountered in the construction of long tunnels and large water reservoirs etc. Second scenario applies to the restraining members which are not rigidly connected; for example in the case of the foundation slab resting on the ground. While modelling such members the consideration of the appropriate boundary conditions gains significance. In this study, for modelling relatively flexible support conditions, the restraining members were assumed to be resting on a sandy soil. The modulus of subgrade reaction for such soils ranges between 20 - 50 MN/mm^3 and thus the maximum value of 50 MN/m^3 was specified in the analysis. In order to model the soil behaviour, surface springs were assigned to the end nodes of restraining members and the spring stiffness was automatically worked out by the software basing on the modulus of subgrade reaction of the soil. The analysis results indicate that the risk and extent of cracking is more in the case of restraining member with rigid boundary conditions (Support condition 1). When the restraining element is not totally fixed (Support condition 2), it has the

flexibility to undergo volume changes imposed due to contraction in the wall and thus the restraint imposed on the wall is reduced and so is the cracking. The cracking patterns obtained in the case of both support conditions for the walls having aspect ratios of 2 and 6 and subjected to edge and combined restraint are given in Figures 6. 23 to 6.26.

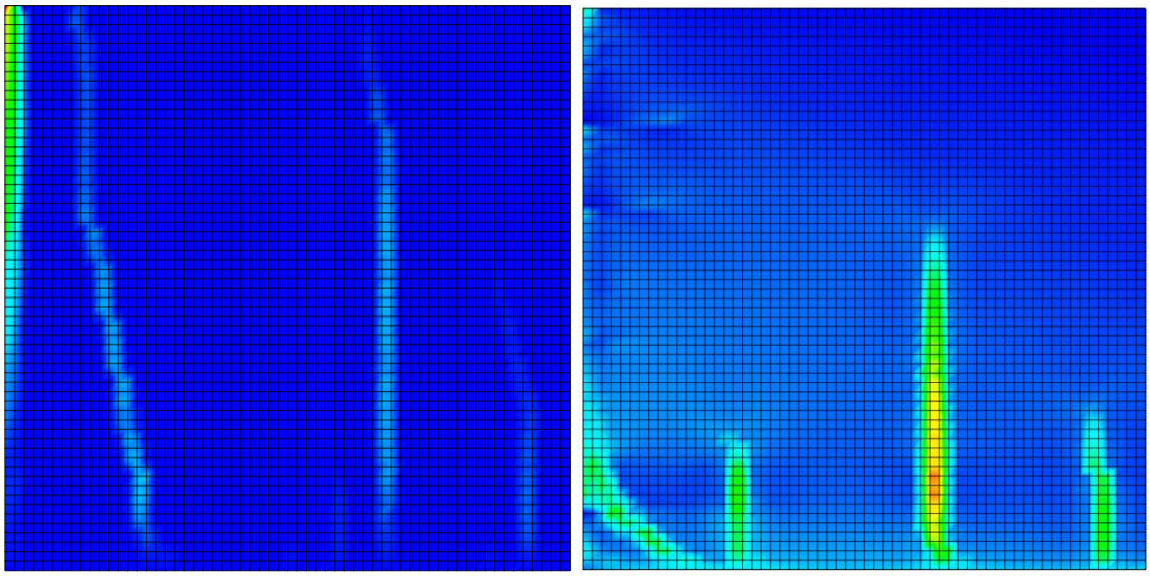

(a) (b)

Figure 6.23. Cracking pattern for wall with aspect ratio 2 subjected to combined restraint: (a) Support condition 1; (b) Support condition 2

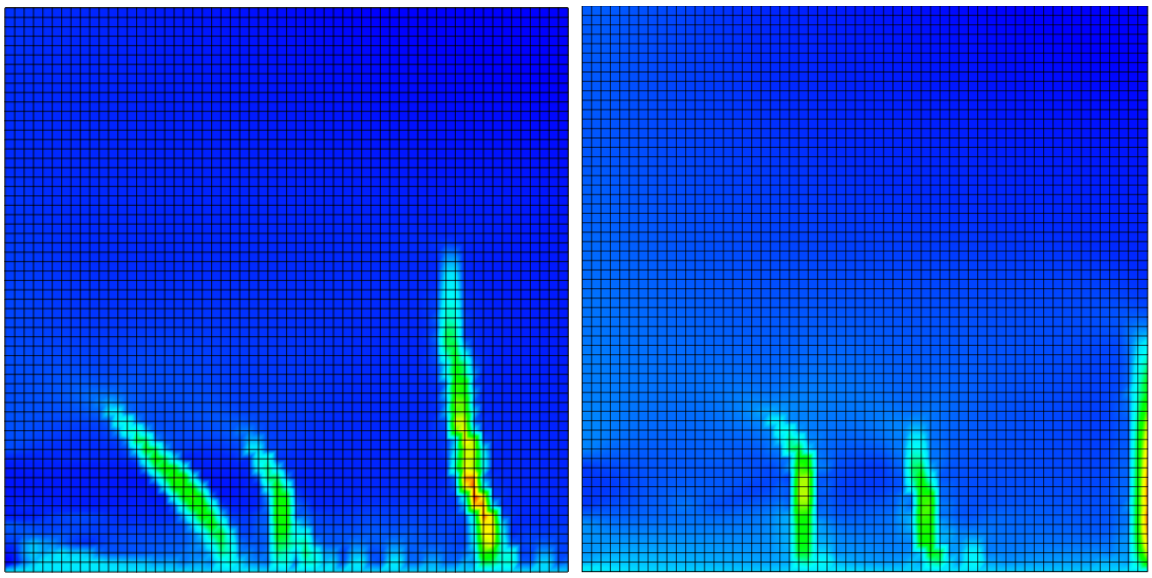

(a) (b)

Figure 6.24. Cracking pattern for wall with aspect ratio 2 subjected to edge restraint: (a) Support condition 1; (b) Support condition 2

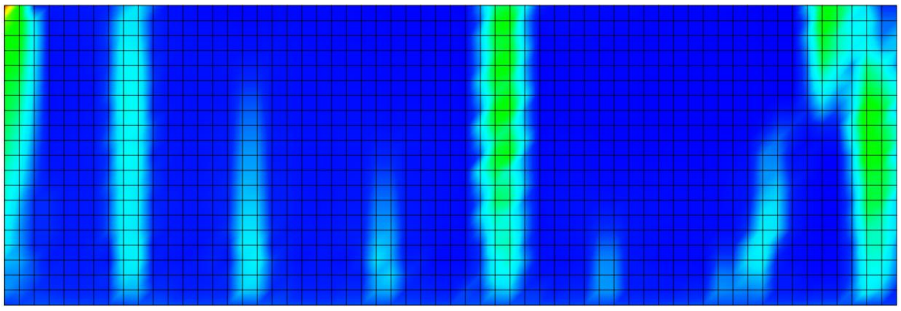

(a)

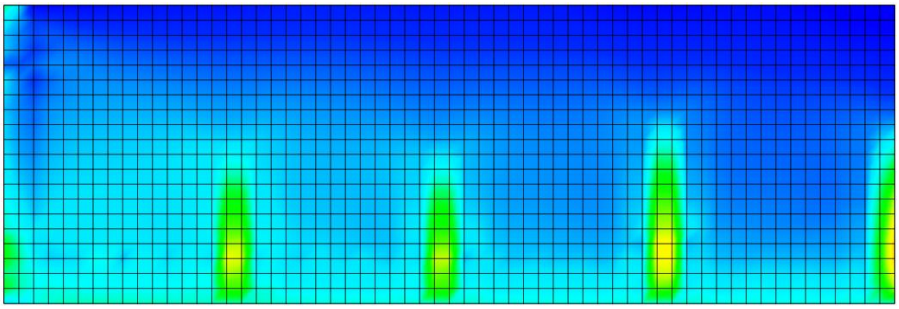

(b)

Figure 6.25. Cracking pattern for wall with aspect ratio 6 subjected to combined restraint: (a) Support condition 1; (b) Support condition 2

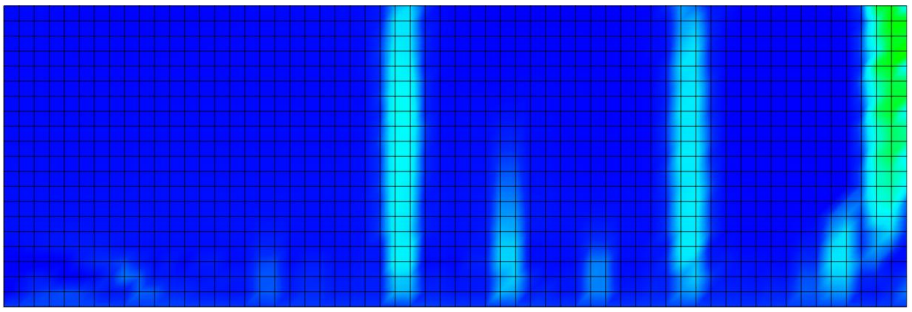

(a)

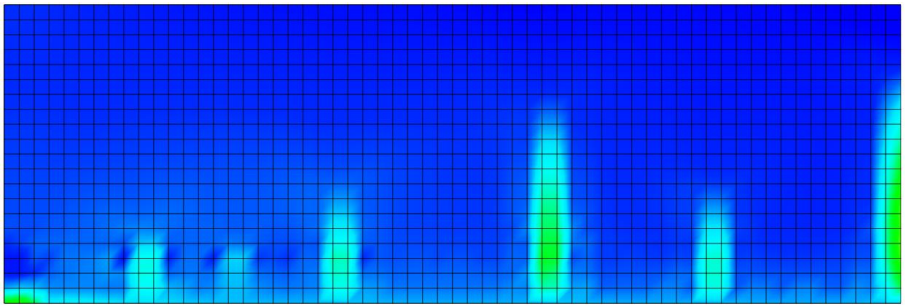

(b)

Figure 6.26. Cracking pattern for wall with aspect ratio 6 subjected to edge restraint: (a) Support condition 1; (b) Support condition 2

6.6 Summary

In this chapter the procedure adopted for performing finite element analysis to simulate the response of reinforced concrete members subjected to different forms of restraint during early age has been presented. Details of the constitutive models used for both concrete and steel, simulation of the thermal contraction in restrained members and the analysis procedure were provided. From comparison of the modelled walls with the results obtained during experimental investigation, a reasonable correlation was established between the two. After validation, the modelling was performed to analyse the influence of edge and combined restraint on walls with different aspect ratios. The number, size, location and orientation of cracks under edge restraint were found to be different that those under combined restraint. It was shown that under combined restraint, the crack widths are greater in walls having aspect ratio less than 4. Above this ratio, the crack widths remained independent of the type of restraint. This indicates that the influence of end restraint becomes more pronounced in relatively higher walls. The influence of different boundary conditions for the restraining members was also studied which revealed that the cracking and degree of restraint is more in the case where restraining members had more rigidly connected boundary conditions.

Chapter 7

Conclusions and Recommendations

7.1. Conclusions

Conclusions from the experimental investigation and finite element analysis are separately described in the following paragraphs.

7.1.1 Conclusions Based on the Experimental Investigations

From the experimental investigations carried out as part of this study, sufficient evidence has been provided to conclude following;

- The vertical steel reinforcement present at the joint between the restraining base and the edge restrained wall has a significant impact on the degree of restraint to imposed strains. In the presence of vertical steel reinforcement, the degree of restraint significantly increases for a wall which suggests that the current guidance is flawed.
- In the presence of vertical steel dowels, the degree of restraint increases with time whereas in their absence it slightly decreases. Increase in degree of restraint with time is not included in the current design guidance / methods of restraint estimation.
- Degree of restraint in the central part of the wall is comparatively higher than that near the free ends. Restraint reduces along the height of the wall. Vertical steel reinforcement influences the restraint variation along the height as well. Loss of restraint is lesser in the presence of vertical steel reinforcement.
- Variation in relative geometries of the wall and base slab (by reducing the wall thickness from 300 to 200 mm in walls where no vertical reinforcement was present), the degree of restraint did not change. It can be concluded that the vertical steel dowels are the major contributing factor in restraint mechanism.
- Experimentally obtained restraint profiles significantly differ from those calculated using the existing methods of restraint estimation. This clearly indicates that the current guidance needs improvement by incorporating major influencing factors.

- A comparison of the crack control steel reinforcement required for a wall having aspect ratio of 4 and subjected to edge restraint was carried out using the restraint factors provided by Eurocode, ACI, CIRIA C660 and those obtained in this research. The results indicate that the Eurocode requires a constant amount of steel reinforcement provided in the wall throughout the height whereas it can be reduced along the height of the wall according to other three approaches since the degree of restraint does not remain constant. The steel reinforcement required in the top, middle and bottom parts of a 3 meter high wall was 23%, 53% and 94% respectively of that required according to the Eurocode. This highlights the fact that correct estimation of the degree of restraint at various locations within a wall can prove to be economical in terms of steel reinforcement used.
- Comparison of the steel reinforcement required for the wall mentioned above also indicates that since the ACI method of restraint estimation does not incorporate the steel reinforcement dowels effect, the steel required in the top, middle and bottom parts of the wall was 30%, 40% and 52% less that that required according to the restraint factors obtained in this study. Thus a design based on the ACI approach would still lead to development or excessive width of cracks despite provision of requisite amount of steel reinforcement.
- Model Code (2010) quite accurately predicts the development of shrinkage in concrete. Eurocode model slightly overestimates whereas ACI and Bazant-Baweja B3 models underestimate the shrinkage.
- With the increase in wall temperature due to hydration, considerable amount of heat is transferred from the wall to the adjoining base. Thermal flow to the restraining base induces additional volume change.
- As recommended by Bamforth (2007), the stresses induced due to early age thermal and shrinkage effects represent sustained loads and under these loads the tensile strain capacity of the concrete increases.
- Prediction of tensile strain capacity of concrete on the basis of guidance available in CIRIA C660 (2007) very closely resembles the experimentally observed cracking behaviour. Estimation of tensile strain capacity as a ratio between tensile strength and modulus of elasticity is not suitable for members subjected to sustained loading due to restraint of imposed loads.

- The current guidance still potentially underestimates the thermal drop likely to occur due to hydration process. However, it could be viewed that the CIRIA C660 (2007) value is still conservative as if the temperature heating and cooling profile is compared directly with the time-dependent change of compression to tension in the section, the stage that the section theoretically goes into tension is at a temperature below peak temperature, so it is logical not to measure temperature drop from peak temperature.
- BS EN 1992-1-1 (2004) indicates that the direct tensile strength can be taken as 90% of the splitting tensile strength. Direct tension tests carried out in this study provided the axial tensile strength which is a much lower fraction of the splitting tensile strength than that stated in the Eurocode.
- To fully understand the mechanism of edge restraint it is necessary to quantify the thermal exchanges between the wall and the base. This can only be done when using a concrete base; experimental investigations using steel bases are misleading and inappropriate.
- Contraction in wall imposes additional volume change on the restraining base. In the absence of steel dowels, the ongoing shrinkage in base slab is further augmented due to this while when the dowels are present, they act to restrain the ongoing shrinkage in the base slab. The strain restrained from occurring in the base is additional to the restrained strain in the wall and resultantly the degree of restraint increases.
- Phenomenon of cracking under restraint of volume changes is not merely an early age problem. Onset of cracking in the tested walls at a timeframe beyond early age indicates that the drying shrinkage can also play a significant role in the development of cracks.
- In edge restrained walls, the cracks can initiate at some height above the joint location and then propagate upwards and downwards. Non initiation of the cracks from the joint is a consequence of the closing action of the base slab.
- Maximum crack width does not occur at the location of maximum restraint; this occurs at some height above the joint location with cracks propagating both upwards and downwards.

- Crack widths increase with time due to increase in the amount of restrained strain. BS EN 1992-1-1 (2004) underestimates the crack widths for edge restrained members.
- Presence of transverse reinforcement in concrete members subjected to uniaxial tension reduces the cracking load by 25 – 30%. Transverse reinforcement provides additional tensile force by bearing against the surface of surrounding concrete.
- In the presence of transverse reinforcement, crack spacing decreases and is influenced by the location of transverse bars. Crack widths and the concrete surface strain increase.

7.1.2 Conclusions Based on Finite Element Analysis

- When modelling the edge restraint and estimating the degree of restraint imposed on the wall, it is important to correctly simulate the actual support conditions for the base slab.
- In edge restrained walls, occurrence of a crack relieves the stress locally in the vicinity of crack. Stress in other parts of the member continues to grow until another crack forms elsewhere.
- When the wall is subjected to combined restraint by rigidly connected members, the first crack in most cases occurs at the connection of the wall with end restraining member. Occurrence of such cracks relieves the stress in the entire member, however, stress relief with formation of each subsequent crack is of local nature.
- In walls with aspect ratios less than 4, maximum crack width is more in the case of combined restraint and lesser in edge restraint. Crack widths remain unaffected by the type of restraint in walls with higher aspect ratios (greater than 6).
- In walls of lower aspect ratios subjected to combined restraint, edge restraint is dominant near the base of the wall and in the higher parts, influence of end restraint is more pronounced.
- The scenario where the restraining members are rigid enough not to undergo additional volume change imposed due to contraction in the wall imposes more

severe restraint than the one where they have the flexibility to accommodate these changes. Extent of cracking is also more in the case of former.

7.2 Recommendations for Further Research

This study has attempted to highlight few important factors which contribute towards development of restraint and are currently not part of the available methods. It has also evolved an experimental procedure for testing of edge restrained walls. Findings of this study can form the basis for undertaking further research on aspects mentioned below;

- During this study, the influence of vertical steel reinforcement on degree of restraint in walls with aspect ratio of 4 was investigated. Having established that the vertical steel dowels play a significant role in restraint formation, there is a need to evolve data so as to suggest and quantify the relationship between the degree of restraint and steel reinforcement ratio for walls of different length and height.
- A technique to prevent curvature development was adopted in this study which appeared to be effective to a certain degree and it influenced the restraint variation in the wall particularly in the higher parts. Further investigations for identifying the influence of boundary conditions of the restraining members on degree of restraint should be undertaken to evaluate this factor for incorporation in the design guidance.
- Tests on concrete panels subjected to direct tension revealed that the transverse reinforcement reduces the cracking load and also influences the crack spacing and width. These tests simulate the limiting cases of end restraint scenarios and should be developed further by increasing the applied loads, size of specimens and varying the steel reinforcement and concrete cover. Understanding of end restraint can be improved further by developing this test procedure as these can be easily undertaken in the laboratory.
- Combined restraint was seen to aggravate the problem of cracking due to restraint of imposed loading particularly in walls with lower aspect ratios. Experimental investigations on combined restraint are necessary to confirm and crystallize the theoretical distribution of restraint zones proposed by Forth (2014).

- From the findings of above mentioned works, analytical models should be developed to devise a method of restraint estimation which incorporates the major contributory parameters.

References

ACI 207.2R-73. 1973. Effect of restraint, volume change, and reinforcement on cracking of massive concrete. *Journal of ACI.* pp.445-470.

ACI 209.2R-08. 2008. *Guide for modeling and calculating shrinkage and creep in hardened concrete*.

ACI Committee 207. 2007. Effect of restraint, volume change, and reinforcement on cracking of mass concrete. *ACI Materials Journal.* **87**(3).

ACI Committee 224.2R. 1997. Cracking of Concrete Members in Direct Tension. *Journal Proceedings.* **83**(1).

Al-Gburi, M. 2014. *Restraint in structures with young concrete: Tools and estimations for practical use*. thesis, Luleå tekniska universitet.

Al-Gburi, M.A., Jonasson, J.E., Nilsson, M., Hedlund, H. and Hösthagen, A. 2012. Simplified metho ds for crack risk analyses of early age concrete part 1: Development of equivalent restraint method. *Nord. Concr. Res.* **46**(2), pp.17-38.

Bamforth, P. 1982. *Early age thermal cracking in concrete.* Institute of Concrete Technology.

Bamforth, P. 2007. *Early-age thermal crack control in concrete.* CIRIA.

Bamforth, P., Denton, S, Shave, J. 2010. The development of a revised unified approach for the design of reinforcement to control cracking in concrete resulting from restrained contraction. *ICE Research project.* **706**.

Base, G.D., Read J Bs, Beeby, A. and Taylor, H. 1966. *An investigation of the crack control characteristics of various types of bar in reinforced concrete beams.* Cement and Concrete Association Wexham Springs, Slough England.

Bažant, Z.P. and Baweja, S. 1995. Justification and refinements of model B3 for concrete creep and shrinkage 1. Statistics and sensitivity. *Materials and structures.* **28**(7), pp.415-430.

Beeby, A. 1979. Prediction of Crack Widths in Hardened Concrete. *STRUCTURAL ENGINEER-PART A.* **57**(1), pp.9-17.

Beeby, A. 1990. *FIXINGS IN CRACKED CONCRETE. THE PROBABILITY OF COINCIDENT OCCURENCE AND LIKELY CRACK WIDTH.*

Beeby and Forth. 2005. Control of cracking in walls restrained along their base against early thermal movements. *Concrete for Transportation Infrastructure.*

Beeby, A.W. 2005. The influence of the parameter ϕ/ρ_{eff} on crack widths. *Structural Concrete.* **6**(4), pp.155-165.

Bosnjak, D. 2000. *Self-induced cracking problems in hardening concrete structures.* Fakultet for ingeniørvitenskap og teknologi.

Branson, D.E. and Christiason, M. 1971. Time Dependent Concrete Properties Related To Design-Strength and Elastic Properties, Creep, and Shrinkage. *Special Publication.* **27**, pp.257-278.

Breugel, K.V. 1998. Prediction of temperature development in hardening concrete. *RILEM REPORT.* pp.51-75.

Brown, T. and Javaid, M. 1970. The thermal conductivity of fresh concrete. *Matériaux et Construction.* **3**(6), pp.411-416.

Browne, R. 1972. Thermal movement of concrete. *Concrete.* **6**(11), pp.51-53.

BS 8007. 1987. Code of practice for Design of concrete structures for retaining aqueous liquids. BS 8007. *British Standards Institute, London.*

BS EN 197-1. 2011. BS EN 197-1: 2011. *Cement, Composition, Specifications and Conformity Criteria for Common Cements. London, England: British Standard Institution (BSI).*

BS EN 206, A. 2013. Concrete: Specification, performance, production and conformity.

BS EN 1992-1-1. 2004. *Eurocode 2: Design of Concrete Structures: Part 1-1: General Rules and Rules for Buildings.* British Standards Institution.

BS EN 1992-3. 2006. *Eurocode 2: Design of Concrete Structures: Part 3: Liquid retaining and containment structures.* British Standards Institution.

BS EN 12350−2: 2009. 2009. 12350-2," Testing fresh concrete.,". *Slump-test., ed. London: British Standards Institution.*

BS EN 12390-3. 2009. 12390-3: 2009, 2009. Testing Hardened Concrete. Compressive Strength of Test Specimens. *British Standards Institution.*

BS EN 12390-6. 2009. 12390-6 (2009)"Testing Hardened Concrete. Tensile Splitting Strength of Test Specimens". *British Standard Institution, London.*

Byfors, J. 1980. *Plain concrete at early ages.* Cement-och betonginst.

Carino, N.J. 1995. *Prediction of cracking in reinforced concrete structures.* US Department of Commerce, National Institute of Standards and Technology.

Carlson, R.W. 1937. Drying shrinkage of large concrete members. In: *Journal Proceedings*, pp.327-336.

Carlson, R.W. and Reading, T.J. 1988. Model Study of Shrinkage Cracking in Concrete Building Walls. *Structural Journal.* **85**(4).

Concrete Society Technical Report. 2008. *Concrete Society Technical Report.*

Dawood, N. and Marzouk, H. 2010. An analytical model for crack spacing of thick reinforced concrete plates. *Engineering structures.* **32**(2), pp.472-482.

De Larrard, F., Acker, P. and Le Roy, R. 1994. *Shrinkage, Creep and Thermal Properties.* McGraw-Hill, New York, NY.

De Schutter, G. and Taerwe, L. 1995. Specific heat and thermal diffusivity of hardening concrete. *Magazine of Concrete Research.* **47**(172), pp.203-208.

Deacon, R.C. 1973. *Watertight concrete construction.*

Desayi, P. and Kulkarni, A. 1976. DETERMINATION OF MAXIMUM CRACK WIDTH IN TWO-WAY REINFORCED CONCRETE SLABS. *Proceedings of the Institution of Civil Engineers.* **61**(2), pp.343-349.

Dunstan, M. 1981. *Rolled Concrete for Dams--a Laboratory Study of the Properties of High Flyash Content Concrete.* Construction Industry Research and Information Association.

Emborg, M. 1989. *Thermal stresses in concrete structures at early ages*. thesis, Luleå tekniska universitet.

Emborg, M. and Bernander, S. 1994. Assessment of risk of thermal cracking in hardening concrete. *Journal of Structural Engineering.* **120**(10), pp.2893-2912.

Evans, E. and Hughes, B. 1968. SHRINKAGE AND THERMAL CRACKING IN A REINFORCED CONCRETE RETAINING WALL. In: *ICE Proceedings*: Thomas Telford, pp.111-125.

Forth, J.P. 2008. *Chapter 7 Edge Restraint, The Concrete Society Technical Report No 67.*

Forth, J.P., A.J. Martin. 2014. *Design of Liquid Retaining Concrete Structures.* Third ed. UK: Whittles Publishing.

Gardner, N. 2004. Comparison of prediction provisions for drying shrinkage and creep of normal-strength concretes. *Canadian Journal of Civil Engineering.* **31**(5), pp.767-775.

Gardner, N. and Lockman, M. 2001. Design provisions for drying shrinkage and creep of normal-strength concrete. *Materials journal.* **98**(2), pp.159-167.

Gedam, B.A., Upadhyay, A. and Bhandari, N. 2010. An apt material model to predict creep and shrinkage behavior of HPC concrete. In.

Gergely, P. and Lutz, L.A. 1968. Maximum crack width in reinforced concrete flexural members. *ACI Special Publication.* **20**.

Gilbert, R.I. 1992. Shrinkage cracking in fully restrained concrete members. *ACI Structural Journal.* **89**(2).

Gutsch, A. 1998. Stoffeigenschaften jungen Betons-Versuche und Modelle (in German)(Ph. D. thesis). *Technical University of Braunschweig, Germany.*

Hordijk, D.A. 1991. *Local approach to fatigue of concrete.* TU Delft, Delft University of Technology.

Houghton, D.L. 1976. Determining tensile strain capacity of mass concrete. In: *Journal Proceedings*, pp.691-700.

Houk, I.E., Paxton, J.A. and Houghton, D.L. 1970. Prediction of thermal stress and strain capacity of concrete by tests on small beams. In: *Journal Proceedings*, pp.253-261.

Hughes, B. and Chapman, G. 1965. Direct tensile test for concrete using modern adhesives. *Rilem Bulletin.* **26**, pp.77-80.

Hughes, B.P. and Mahmood, A. 1988. An investigation of early thermal cracking in concrete and the recommendations in BS 8007. *Structural Engineer.* **66**(4).

Hunt, J. 1971. *A laboratory study of early-age thermal cracking of concrete.*

Kanstad, T., Hammer, T., Bjřntegaard, Ř. and Sellevold, E. 1999. *Mechanical Properties of Young Concrete-Evaluation of Test Methods for Tensile Strength and Modulus of Elasticity-Determination of Models Parameters. NOR-IPACS Report STF22 A99762.* ISBN 82-14-01062-4, Trondheim.

Kanstad, T., Hammer, T.A., Bjøntegaard, Ø. and Sellevold, E.J. 2003. Mechanical properties of young concrete: Part II: Determination of model parameters and test program proposals. *Materials and Structures.* **36**(4), pp.226-230.

Khan, A.A., Cook, W.D. and Mitchell, D. 1998. Thermal properties and transient thermal analysis of structural members during hydration. *Materials Journal.* **95**(3), pp.293-303.

Kheder, G. 1997. A new look at the control of volume change cracking of base restrained concrete walls. *ACI structural journal.* **94**(3), pp.262-271.

Kheder, G., Al-Rawi, R. and Al-Dhahi, J. 1994. A study of the behaviour of volume change cracking in base restrained concrete walls. *Materials and Structures.* **27**(7), pp.383-392.

Kheder, G. and Al Rawi, R. 1990. Control of cracking due to volume change in base-restrained concrete members. *ACI Structural Journal.* **87**(4).

Kianoush, M., Acarcan, M. and Ziari, A. 2008. Behavior of base restrained reinforced concrete walls under volumetric change. *Engineering Structures.* **30**(6), pp.1526-1534.

Kim, K.-H., Jeon, S.-E., Kim, J.-K. and Yang, S. 2003. An experimental study on thermal conductivity of concrete. *Cement and Concrete Research.* **33**(3), pp.363-371.

Klemczak, B. and Knoppik-Wróbel, A. 2013. Comparison of analytical methods for estimation of early-age thermal-shrinkage stresses in RC walls. *Archives of Civil Engineering.* **59**(1), pp.97--117.

Leonhardt, F. 1977. Crack control in concrete structures. In: International Association for Bridge and Structural Engineering.

Meyers, B., Branson, D.E. and Schumann, C. 1972. Prediction of Creep and Shrinkage Behavior for Design from Short Term Tests. *PCI Journal.* **17**(3), pp.29-45.

Miao, B., Aitcin, P.-C., Cook, W.D. and Mitchell, D. 1993. Influence of concrete strength on in situ properties of large columns. *Materials Journal.* **90**(3), pp.214-219.

Micallef, M., Vollum, R.L. and Izzuddin, B.A. 2017. Cracking in walls with combined base and end restraint. *Magazine of Concrete Research.* **69**(22), pp.1170-1188.

Micallef, M., Vollum, RL, Izzuddin, BA. 2017. Crack development in transverse loaded base-restrained reinforced concrete walls. *Engineering Structures.* **143**, pp.522-539.

Mindess, S. 1981. and Young, JF, Concrete, Printice-Hall. *INC. New Jersey.*

Mitchell, L.J. 1953. Thermal Expansion Tests on Aggregates, Neat Cements, and Concretes. In: *PROCEEDINGS-AMERICAN SOCIETY FOR TESTING AND MATERIALS*: AMER SOC TESTING MATERIALS 100 BARR HARBOR DR, W CONSHOHOCKEN, PA 19428-2959, pp.963-977.

Model Code, C.F. 2010. *Fib model code for concrete structures 2010.*

Nejadi, S. and Gilbert, I. 2004. Shrinkage cracking and crack control in restrained reinforced concrete members. *Structural Journal.* **101**(6), pp.840-845.

Neville, A.M. 1995. *Properties of concrete.* Longman London.

Nianxiang, X. and Wenyan, L. 1989. Determining tensile properties of mass concrete by direct tensile test. *Materials Journal.* **86**(3), pp.214-219.

Nilsson, M. 2003. *Restraint factors and partial coefficients for crack risk analyses of early age concrete structures.* Luleå University of Technology.

Ojdrovic, R.P. and Zarghamee, M.S. 1996. Concrete creep and shrinkage prediction from short-term tests. *Materials Journal.* **93**(2), pp.169-177.

Pettersson, D. and Thelandersson, S. 2001a. Crack development in concrete structures due to imposed strains—Part I: Modelling. *Materials and Structures.* **34**(1), pp.7-13.

Pettersson, D. and Thelandersson, S. 2001b. Crack development in concrete structures due to imposed strains—Part II: Parametric study of a wall fully restrained at the base. *Materials and Structures.* **34**(1), pp.14-20.

Pigeon, M., Bissonnette, B., Marchand, J., Boily, D. and Barcelo, L. 2005. Stress Relaxation of Concrete Under Autogenous Early-Age Restrained Shrinkage. *Special Publication.* **227**, pp.337-348.

Rizkalla and Hwang. 1983a. Crack Prediction for Members in Uniaxial Tension. *Journal Proceedings.* **81**(6).

Rizkalla, S. and Hwang, L. 1983b. Effective tensile stress-strain characteristics for reinforced concrete. *Proceedings of the Canadian Society of Civil Engineering.* pp.129-147.

Rizkalla, S. and Hwang, L. 1983c. Transverse reinforcement effect on cracking behaviour of RC members. *Canadian Journal of Civil Engineering.* **10**(4), pp.566-581.

Ross, C.A. and Tedesco, J. 1989. Split-Hopkinson pressure-bar tests on concrete and mortar in tension and compression. *Materials Journal.* **86**(5), pp.475-481.

Saliger, R. 1936. High grade steel in reinforced concrete. In: *Preliminary Publication, 2nd Congress of IABSE. Berlin-Munich: IABSE Publications*.

Schleeh, W. 1962. Imposed stresses in the walls one-side restrained. *Beton- Und Stahlbetonbau.* **57**(3), pp.64-72.

Stoffers, H. 1978. *Cracking due to shrinkage and temperature variation in walls.* Stevin Laboratory, Department of Civil Engineering, Delft University of Technology and IBBC Institute TNO for Building Materials and Building Structures.

Tasdemir, M. 1996. The tensile strain capacity of concrete. *Magazine of Concrete Research.* **48**(176), pp.211-218.

Tazawa, E.-i. 2014. *Autogenous shrinkage of concrete.* CRC Press.

Thomas, M., Mukherjee, P., Sato, J. and Everitt, M. 1995. Effect of fly ash composition on thermal cracking in concrete. *Special Publication.* **153**, pp.81-98.

Thorenfeldt, E., Tomaszewicz, A. and Jensen, J. 1987. Mechanical properties of high-strength concrete and application in design. In: *Proceedings of the Symposium "Utilization of High Strength Concrete*, pp.149-159.

Townsend, C. 1965. Control of Cracking in Mass Concrete Structures. Engineering Monograph No. 34. *Water Resources Technical Publication. US Department of the Interior. Bureau of Reclamation.*

Vollum, R., Eder, M., Elghazouli, A. and Abdel-Fattah, T. 2010. Modelling and experimental assessment of punching shear in flat slabs with shearheads. *Engineering Structures.* **32**(12), pp.3911-3924.

Walker, S., Bloem, D. and Mullen, W. 1952. Effects of temperature changes on concrete as influenced by aggregates. In: *Journal Proceedings*, pp.661-679.

Wee, T., Lu, H. and Swaddiwudhipong, S. 2000. Tensile strain capacity of concrete under various states of stress. *Magazine of concrete research.* **52**(3), pp.185-193.